KfK 4908
Dezember 1991

Status Report
KfK Contribution to the Development of

DEMO-relevant Test Blankets for NET/ITER

Part 1:
Self-cooled Liquid Metal Breeder
Blanket
Volume 2:
Detailed Version

Compiled by: H. John, S. Malang, H. Sebening
Contributors: L. Barleon, E. Bogusch, E. Bojarsky,
H. U. Borgstedt, L. Bühler, V. Casal, H. Deckers,
H. Feuerstein, U. Fischer, G. Frees, H. Gräbner, H. John,
Th. Jordan, W. Kramer, R. Krieg, L. Lenhart, S. Malang,
R. Meyder, P. Norajitra, H. Reiser, J. Reimann,
A. Schwenk-Ferrero, H. Schnauder, R. Stieglitz, J. Oschinski,
E. Wiegner

Association KfK-Euratom
Projekt Kernfusion

Kernforschungszentrum Karlsruhe

KERNFORSCHUNGSZENTRUM KARLSRUHE

Association KfK-EURATOM
Projekt Kernfusion

KfK 4908

Status Report
KfK Contribution to the Development of
DEMO-relevant Test Blankets for NET/ITER
Part 1: Self-cooled Liquid Metal Breeder Blanket
Volume 2: Detailed Version

Compiled by: H. John, S. Malang, H. Sebening
Contributors: L. Barleon, E. Bogusch*, E. Bojarsky, H.U. Borgstedt, L. Bühler,
V. Casal, H. Deckers, H. Feuerstein, U. Fischer, G. Frees, H. Gräbner, H. John,
Th. Jordan, W. Kramer, R. Krieg, L. Lenhart, S. Malang, R. Meyder, P. Norajitra,
H. Reiser, J. Reimann, A. Schwenk-Ferrero, H. Schnauder, R. Stieglitz,
J. Oschinski, E. Wiegner

* Interatom GmbH, 5060 Bergisch Gladbach

Abstract

A self-cooled liquid metal breeder blanket for a fusion DEMO-reactor and the status of the development programme is described as a part of the European development programme of DEMO relevant test blankets for NET/ITER. Volume 1 (KfK 4907) contains a summary, Volume 2 (KfK 4908) a more detailed version of the report.

Both volumes contain sections on previous studies on self-cooled liquid metal breeder blankets, the reference blanket design for a DEMO-reactor, a typical test blanket design including the ancillary loop system and the building requirements for NET/ITER together with the present status of the associated R&D-programme in the fields of neutronics, magnetohydrodynamics, tritium removal and recovery, liquid metal compatibility and purification, ancillary loop system, safety and reliability.

An outlook is given regarding the required R&D-programme for the self-cooled liquid metal breeder blanket prior to tests in NET/ITER and the relevant test programme to be performed in NET/ITER.

Zusammenfassung

KfK-Beitrag zur Entwicklung von DEMO-relevanten Testblankets für NET/ITER

Ein selbstgekühltes Flüssigmetall-Brutblanket für einen DEMO Fusionsreaktor und der Stand der Entwicklungsarbeiten, als Teil des Europäischen Entwicklungsprogramms für ein DEMO-relevantes Testblanket für NET/ITER werden beschrieben. Band 1 (KfK 4907) enthält die Zusammenfassung und Band 2 (KfK 4708) den detaillierten Bericht.

In den beiden Berichten werden bisher durchgeführte Untersuchungen für selbstgekühlte Flüssigmetallbrutblankets beschrieben. Es werden der Referenzentwurf für das DEMO-Reaktorblanket und ein tpyischer Entwurf für ein Testblanket in NET/ITER mit den dazugehörigen externen Kreisläufen und einem Komponentenaufstellungsplan vorgestellt. Der augenblickliche Stand der Forschungs- und Entwicklungsarbeiten bezüglich: Neutronenrechnungen, Magnetohydrodynamik (MHD), Tritiumgewinnung, Beständigkeit im Flüssigmetall, Flüssigmetallreinigung und Sicherheit und Zuverlässigkeit der Kreisläufe wird aufgezeigt.

Es wird ein Ausblick gegeben auf die noch vor dem NET/ITER Test notwendigen F+E-Arbeiten für das selbstgekühlte Flüssigmetallblanket und das zugehörige Testprogramm, das in NET/ITER durchgeführt werden soll.

TABLE OF CONTENTS

1. PREVIOUS STUDIES ON SELF-COOLED LIQUID METAL BLANKET CONCEPT AND REASONS FOR THE SELECTED DESIGN

1.1 Overview

The breeding blankets in a thermo-nuclear power reactor employing the Deuterium-Tritium fusion reaction

$$D + T \rightarrow n(14.1\,\text{MeV}) + \text{He}\,(3.52\,\text{MeV})$$

have to

- generate the tritium for the fueling of the machine
- convert the energy of the neutrons from the fusion reaction into heat usable for electricity production
- shield the superconducting magnets from neutrons and gamma-radiation.

Tritium is generated from Lithium by the following reactions:

$$^{6}\text{Li} + n \rightarrow T + \text{He} + 4.8\,\text{MeV}$$
$$^{7}\text{Li} + n \rightarrow T + \text{He} + n' - 2.87\,\text{MeV}$$
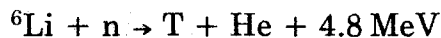
Lithium can be supplied as a liquid metal (Li, Pb-17 Li), as a ceramic (LiO_2, $LiAlO_2$, Li_4SiO_4, Li_2ZrO_3), as a molten salt (FLIBE, a mixture of LiF and BeF_2) or as an aqueous lithium salt solution (LiOH, $LiNO_3$).

Liquid metal breeder materials have a number of inherent advantages [1] over solid breeder materials such as the possibility to bring the breeder material outside the blanket for tritium extraction, a practical immunity to irradiation damage and a high thermal conductivity. These features facilitate a relatively simple blanket design. Therefore liquid metal breeders are selected in a number of reactor- and blanket studies

The family of liquid-metal breeder materials is comprised of pure lithium, the Pb-17 Li eutectic alloy, and low melting point ternary Li-Pb-X alloys. Two major design classes for liquid metal blankets are under consideration. Separately-cooled blankets use stagnant or slowly flowing liquid-metal breeder with helium, water, or another liquid metal as coolant. In self-cooled blanket concepts, the

liquid-metal breeder serves as coolant as well and is circulated for heat extraction. In this report, the main technical aspects of self-cooled designs will be examined.

From the beginning of fusion research lithium has been used in blanket concepts as breeder and coolant. However, the Pb-17Li eutectic alloy as proposed in the WITAMIR-study [2] is an interesting alternative (see Fig. 1.-1). Compared to pure lithium, the main advantage of Pb-17Li is its much lower chemical reactivity with air and water which allows for example even water cooling of the liquid breeder. In the case of self-cooled Pb-17Li blankets, water-cooled components such as divertors or limiters adjacent to the blanket segments are acceptable and simpler steam generator designs are possible in contrast to lithium loops.

A self-cooled Pb-17Li blanket concept similar to the WITAMIR-design has been proposed in the MARS-study [3]. Both machines are of the mirror type with a small surface heat flux to the first wall and a considerably reduced magnetic field strength compared to the one encountered in tokamaks. In addition, the flow path length in the blanket segments of a mirror machine is less than half of the one in a tokamak blanket. These three features of the mirror blanket allow for a much simpler blanket design without excessively high magneto-hydrodynamic (MHD) pressure drop in comparison to a self-cooled blanket concept for tokamaks.

Two different self-cooled Pb-17Li blanket concepts have been proposed in the Blanket Comparison and Selection Study, BCSS [4]. One design, shown in Fig. 1.-2, is very similar for the lithium blanket and the Pb-17Li blanket. Breeding blankets are arranged at the outboard and the inboard region of the torus. In the first wall, the coolant flows in toroidal channels. The same cooling principle is used in the outboard region of the second BCSS self-cooled Pb-17Li concept which is a dual coolant concept. The inboard region in this concept is cooled by high temperature helium. However, both self-cooled concepts using Pb-17Li have been ranked lower for tokamak reactors in the BCSS compared to the concepts using lithium. In the European blanket development program, however, lithium has been excluded because of safety reasons.

A design of a self-cooled Pb-17Li blanket for the Next European Torus (NET) is described in ref. [5]. and shown in Fig. 1.-3. The design is based on the same flow concept as considered in the BCSS but has been adjusted to the boundary conditions of NET. This blanket concept served as basis for a design of a DEMO-relevant blanket [6,7]. In this design, shown in Fig. 1.-4, a 300 mm thick layer of

2

beryllium in the front region of the outboard blanket serves as neutron multiplier, providing tritium self-sufficiency without breeding blankets at the inboard side of the torus.

A new specification of a DEMO-reactor which provides the basis for the blanket development in the European Community enables the additional arrangement of self-cooled liquid metal blankets at the inboard side of the torus, avoiding the need for a beryllium multiplier at all. This led to the reference concept described in this report.

1.2 Tokamak design features, geometrical boundary conditions

The tokamak geometry and other boundary conditions have a strong impact on the overall blanket design philosophy, objectives, and requirements. The arrangement of coolant access tubes at the blanket segments and the method employed for the exchange of blanket segments, i.e. vertical or horizontal maintenance are of special importance in the case of self-cooled liquid-metal blankets.

The arrangement of supply lines at both the top and bottom end of the blanket segments is preferable for liquid-metal cooled blankets because it allows the coolant to enter the blankets at one end and leave at the other one. Such a configuration is especially suitable for horizontal blanket maintenance. This overall geometry has been proposed in a number of reactor studies as well as in the BCSS. Contrary to this design, vertical maintenance is proposed for NET and the International Tokamak Experimental Reactor (ITER) [8]. In these designs, the arrangement of both coolant inlet and outlet tubes at the top end of the blanket segments is anticipated.

This arrangement of cooling lines allows a viable self-cooled blanket concept for the outboard region only. At the inboard side, however, the magnetic field strength is higher by roughly 50% and the space available for the blanket segments is more limited compared to the outboard region. Both differences together make the design of inboard segments with coolant supply lines from the top only nearly impossible.

The new EC-DEMO-specification, however, allows, to split the inboard segments into an upper and a lower half with separate coolant supply from the top

3

(upper half) and bottom (lower halfes), leading to acceptable low MHD pressure drop. This solution has been selected as reference concept.

1.3 Flow channel geometry

The design of a self-cooled tokamak blanket is governed primarily by magneto-hydro-dynamics (MHD) effects in the liquid metal flowing through the magnetic field, which cause by orders-of-magnitude higher pressure drops than viscous forces, govern the velocity profiles in the coolant channels, and are believed to reduce the heat transfer through laminarization of the flow. High MHD pressure drops result in high mechanical stresses in the coolant ducts, which raise major technical feasibility questions for the development of self-cooled blankets. In the following, these issues will be discussed on the basis of the geometrically simplest blanket design, the poloidal-flow concept.

A schematic of the poloidal-flow design is shown in Fig. 1.-5 which is taken from ref. [9]. For an uninsulated single straight coolant duct in which the liquid metal flows perpendicular to the magnetic field, the MHD pressure drop is approximately given by:

$$\Delta P = L \cdot B^2 \, v \cdot \sigma_w \cdot \frac{t_w}{a} \tag{1}$$

where

L   = length of the channel,
t_w = wall thickness perpendicular to the magnetic field B,
a   = half width of the channel in direction of B,
σ_w = electrical conductivity of the wall material,
v   = mean velocity of the liquid metal flow,
B   = magnetic field strength.

This approximation indicates that the MHD pressure drop is proportional to the thickness of the walls perpendicular to the magnetic field. The walls parallel to the field have no influence on the pressure drop and can be made as thick as necessary to stay within specified stress limits. Mechanical stresses in walls perpendicular to the magnetic field, however, cannot be reduced by increasing the wall thickness because thicker walls mean larger pressure drop, and, as a conse-

4

quence, higher internal pressure. An effective way to reduce stresses is to keep the coolant velocity low. The lower limit of the velocity, however, is determined by the allowable maximum temperature at the coolant-to-structure interfaces as dictated by corrosion considerations. This interface temperature is considerably higher than the coolant bulk temperature at the exit, since the heat transport perpendicular to the flow direction is basically by conduction only.

Simple calculations for the poloidal-flow concept for a realistic geometrical configuration, power density and material properties do not lead to promising results. It can be shown [10] that

- low velocities cause high interface temperatures,
- high velocities result in an excessively high MHD pressure drop and a very low bulk temperature rise through the blanket which is not attractive for electric power generation.

A way to overcome these problems is to keep the flow path along the first wall short and to divert the coolant flow to cooler zones of the blanket segment. In order to accomplish this, two alternative designs were considered in the BCSS [9]. The first design shown in Fig. 1.-6 represents a helical-flow concept. The basic idea was to provide enough cooling for the first wall by placing helical vanes inside the individual coolant ducts. This design offers the possibility of bringing the cold bulk fluid to the first wall and vice versa. A second design shown in Fig. 1.-7 depicts a radial/poloidal flow blanket. It consists of poloidal-flow channels which are connected with radial-flow modules exposed to the plasma. The entire coolant flow is forced through the radial modules to cool the first wall efficiently.

In the BCSS, these two flow concepts were not investigated in detail because the poloidal/toroidal/poloidal-flow concept was believed to offer the greatest potential.The ANL reference design [4] shown in Fig. 1.-2 represent such a flow concept in which the flow is diverted at the front part of the blanket to the toroidal direction, i.e. parallel to the magnetic field in order to cool the first wall properly by providing a relatively high velocity in the short channels without a significant increase in pressure drop. The flow diversion is achieved by slightly slanted walls of the poloidal coolant ducts. The mean velocity can be kept low here because power density and coolant temperature rise are considerably lower. In this way, the MHD pressure drop is reduced substantially in the poloidal ducts.

For the BCSS, the MHD analysis was carried out on the basis of a single flow channel and yielded a pressure drop associated with the poloidal/toroidal/poloidal bends of 0.26 MPa. For the toroidal channel, a value of 0.15 MPa was estimated. In the FINESSE study [11], H. Madarame draws attention to additional high pressure drops caused by electrical currents flowing normal to parallel flow ducts. Applying a multi-channel bend model for the ANL design, a pressure drop of 3.5 MPa was estimated for the uninsulated case, and a one-order-of-magnitude reduction of the pressure drop if insulators are inserted in the slots between the poloidal and toroidal coolant channels.

A poloidal/radial/toroidal flow concept similar to the BCSS-design has been selected as a basis of the reference concept described in section 2.

1.4 Electrical insulation of the flow channels

The optimized coolant flow path concept described in BCSS is an important measure to improve the viability of liquid-metal cooling for blankets, but the MHD pressure drop in electrically uninsulated ducts perpendicular to the magnetic field is still high. Even without taking in consideration the multi-channel-effects, it was difficult to keep the primary stresses induced by coolant presssure differences within allowable limits. Therefore, it was necessary to adjust the wall thickness of the coolant channels to the pressure distribution along the flow path which resulted in a decrease in wall thickness in the flow direction.

A better way to reduce the pressure drop decisively would be to decouple electrically the coolant flow from the load-carrying walls. From an MHD point of view, it would be ideal to provide an insulation layer at all duct walls. This layer, however, has to be compatible with the liquid metal during the total lifetime of a blanket without cracking, peeling off, and wearing down in order to avoid direct contact between the liquid metal and steel. Such layers have been proposed for a long time and were taken into consideration in BCSS. So far, however, no experimental results which indicate the feasibility of this method have been reported.

In the MARS study [5] a so called "laminated wall" design has been suggested which consists of a steel sheet liner supported by the load-carrying walls via an electrically insulating ceramic layer. Since contacts between the liquid metal and the ceramic layer are avoided, the requirements on the insulation are not as stringent. The fabrication, however, must be of high quality because at insuffi-

ciently supported places, e.g. corners, the stresses in the liners may reach unacceptable values.

Novel flow channel inserts (FCI) proposed for the self-cooled liquid-metal blanket [12], [13] offer several engineering advantages over the laminated wall design. The principle of the FCI is described in section 4.3.1 and shown in Fig. 4.3-1. FCIs are made by sandwiching a thin ceramic layer between two steel sheets. The claddings are welded at all edges to insure against any contact of the liquid metal with the insulator. This laminated material is then formed to the shape of the individual flow channels. By this arrangement of FCIs, the load carrying walls are electrically decoupled from the voltage induced in the flowing liquid-metal by the magnetic field.

1.5 Comparison of breeder materials

Compared with lead-lithium, lithium is a breeder material characterized by a

- lower melting point,
- better thermal conductivity,
- flatter gradient of volumetric heat generation,
- higher allowable maximum interfacial temperature, and
- lower hydrostatic pressure due to a lower density.

Considering the MHD, heat transport, and corrosion features which result from these properties, lithium is superior to lead-lithium as breeder material.

With regard to tritium inventories and permeation losses, the two breeder materials behave very differently. Due to the high tritium solubility in Li, the tritium inventory can reach very large values unless a very efficient tritium extraction method is provided. On the other hand, the high tritium solubility favours small permeation losses through structural materials to the water loop. For Pb-17Li, both tendencies are reversed due to the very low tritium solubility. Here, tritium inventory is not the critical issue, but the reduction of the permeation losses to acceptable values. The method to achieve this for the self-cooled Pb-17Li blanket is described briefly in section 2.4. In contrast to lithium, the tritium inventory is significantly smaller.

Lithium and lead-lithium are strikingly different in their chemical reactivity with air and water [14]. Lithium being the more reactive metal was from the beginning excluded from all liquid-metal breeder blankets in the European Community. US concepts refrain from using it whenever there are other water-cooled components (e.g. divertor plates) involved in a design.

1.6 Selection of structural material

BCSS considered austenitic steels, ferritic steels, and vanadium alloys as candidate structural materials. In a fusion power reactor, the damaging effects of radiation on austenitic stainless steel cause probably a too short lifetime of the blanket. Furthermore, the compatibility of austenitic stainless steels with the Pb-17Li eutectic alloy is limited [1]. Therefore, austenitic steels are not suitable for fusion power reactors. On the other hand, vanadium alloys are capable to allow for higher temperatures, and are, therefore, superior to ferritic steels with regard to corrosion resistance [4] but are excluded at this time from European DEMO-reactor designs because of the limited knowledge about these alloys. MANET is a martensitic steel which was finally selected for DEMO-reactor blankets. It allows for temperatures up to about 550°C. The allowable maximum Pb-17Li interfacial temperature is in the range of 450-470°C [15].

The ductile-brittle-transition temperature (DBTT) sets a lower limit to the suitability and use of some metals. This critical temperature for martensitic steel not exposed to radiation is below 0°C. DBTT increases considerably as soon as neutron irradiation causes a few dpa (displacement per atom). The shift in DBTT up to 150 K has been measured with a relatively large uncertainty. Conservatively, a value of 250 K is assumed at the moment [16].

References to section 1. - 1.6

[1]   H. Tas, S. Malang, F. Reiter, J. Sannier, Liquid Breeder Materials, J.Nucl.Mater. 155-157 (1988), 178-187.

[2]   B. Badger et al., WITAMIR-1: A Tandem Mirror Fusion Power Plant, University of Wisconsin at Madison, UWFDM-400 (1980).

[3]   G. Logan et al., Mirror Advanced Study (MARS) - Final Design Report, Lawrence Livermore National Laboratory, UCRL-53480 (September 1984).

[4]   D. L. Smith et al., Blanket Comparison and Selection Study (Final Report), Argonne National Laboratory, ANL/FPP-84-1, Vols. 1, 2, and 3 (September 1984).

[5]   S. Malang et al., Self-cooled Liquid-metal Blanket Concept, Fusion Technol., 14 (November 1988), pp. 1343-1356.

[6]   S. Malang, K. Arheidt and U. Fischer, Test Module in NET for a Self-cooled Liquid-metal Blanket Concept, in: Proc. 15th Symp. on Fusion Technol., Utrecht, The Netherlands, September 1988, Vol. 2, ed. A.M. van Ingen (Elsevier Sc. Pub., Amsterdam, 1989), pp. 1223-1228.

[7]   S. Malang et al., Self-Cooled Blanket Concept Using Pb17-Li as Liquid Breeder and Coolant, Fusion Engng. Des. 14 (1991) 373-399.

[8]   ITER, Conceptual Design Report, ITER Document Series, No. 18, International Atomic Energy Agency, Vienna 1991.

[9]   M. Abdou et al., Blanket Comparison and Selection Study (Interim Report), Argonne National Laboratory, ANL/FPP/TM-177 (September 1983).

[10] L. Barleon, Kernforschungszentrum Karlsruhe, unpublished report (June 1990).

[11] M. Abdou et al., FINESSE: A Study of the Issues, Experiments, and Facilities for Nuclear Research and Development (Interim Report), University of California at Los Angeles, PPB-821, UCLA-ENG-89-30, Vol. III, (October 1984).

[12] S. Malang, Einrichtung zur Verringerung des MHD-Druckverlustes in dickwandigen Kanälen, DE-PS 36 00 645, (14. Juli 1987).

[13] S. Malang et al., Liquid-metal Cooled Blanket Concept for NET, in Proc. 14th Symp. Fusion Technol., Avignon, France September 1986, Vol. 2, ed. Assoc. EURATOM/CEA-CEN Cadarache (Pergamon Press Oxford, 1986) pp. 1273-1280.

[14] S. J. Piet, D. W. Jeppson, L. D. Muhlestein, M.S. Kazimi, Liquid Metal Chemical Reaction Safety in Fusion Facilities, Fusion Eng. Design 5 (1987), 273-298.

[15] H.U. Borgstedt et al., Corrosion and Mechanical Properties of the Martensitic Steel X18CrMoVNb 12 1 in Flowing Pb-17Li, Fusion Engrg. Des., 13 (in print).

[16] M. Küchle, Kernforschungszentrum Karlsruhe, unpublished report (November 1988).

TUBE SHEET

MANIFOLD

LiPb INLET

EXTRUDED
SEAMLESS
HT-9 TUBES

PLASMA

LiPb OUTLET

BLANKET

REFLECTOR

SHIELD

COIL

BLANKET SUPPORT
& GUIDE RAIL

0   1   2   3   4   5 Meters

PLASMA

JUNCTION BETWEEN ADJACENT
BLANKET MODULES
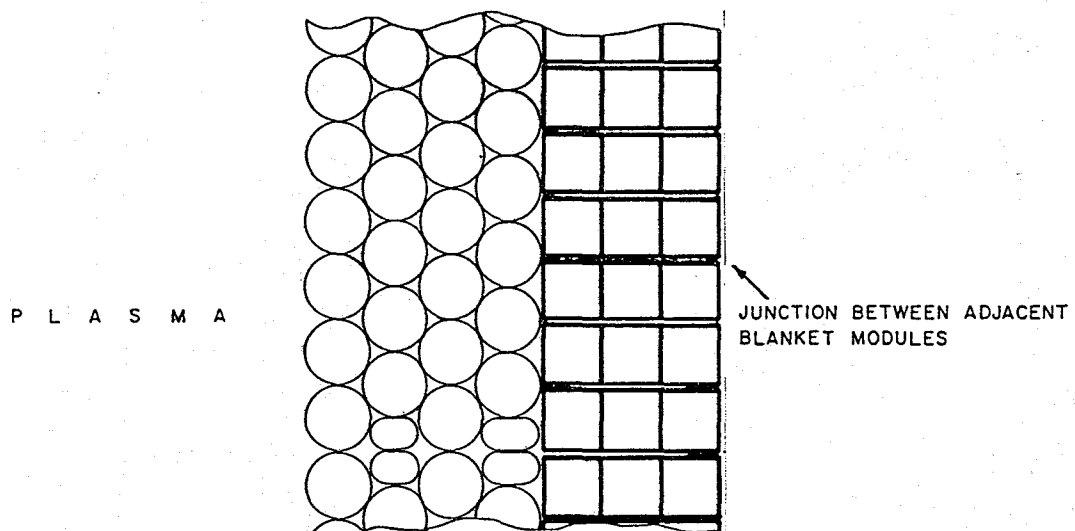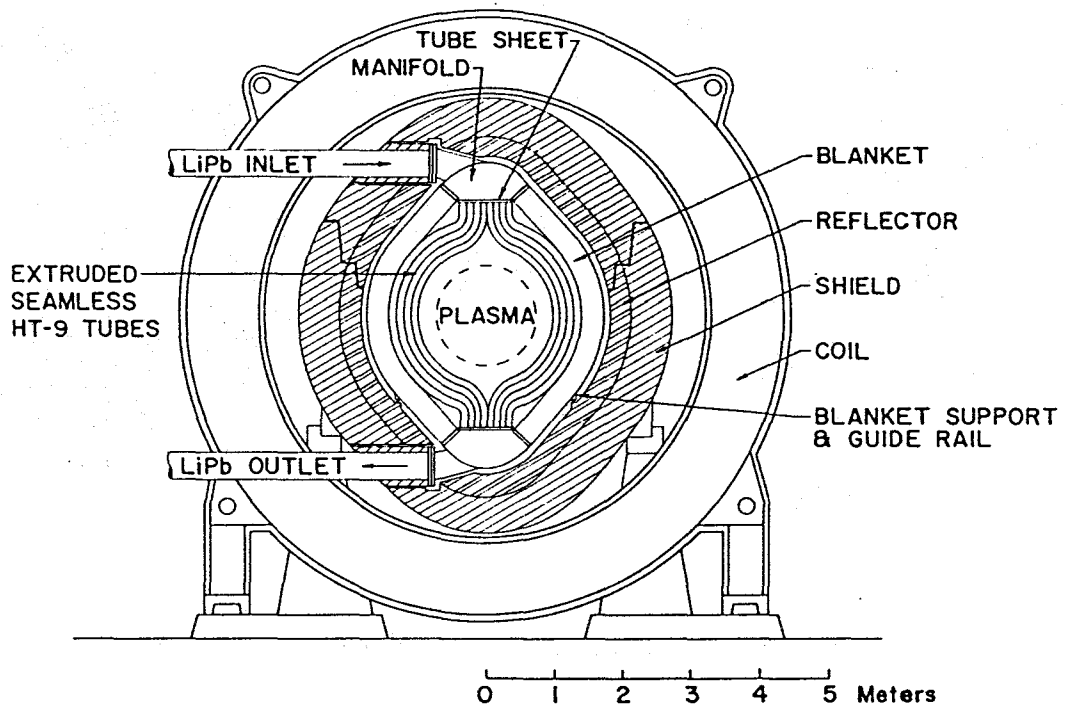
Fig. 1-1   Self-cooled liquid metal blanket for a mirror reactor [2]
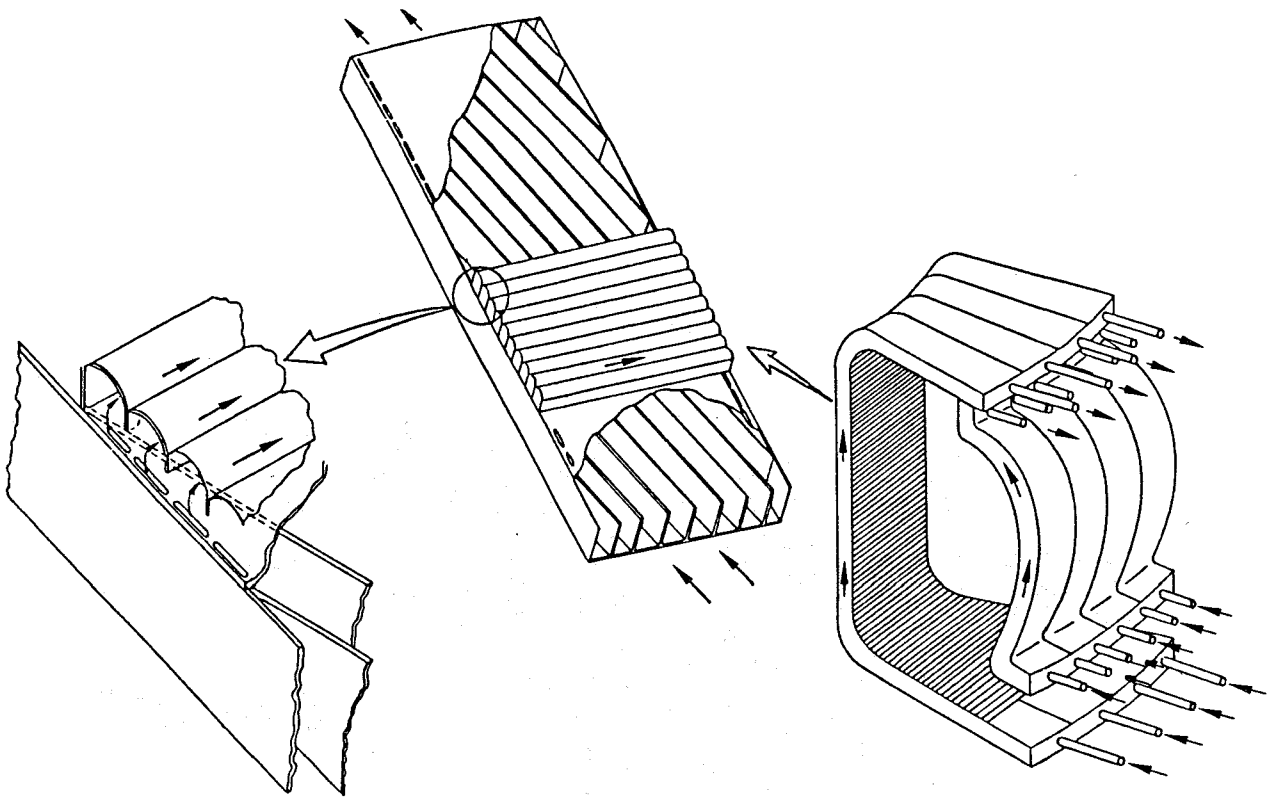
Fig. 1.-2   Self-cooled liquid metal blanket (BCSS) [4]
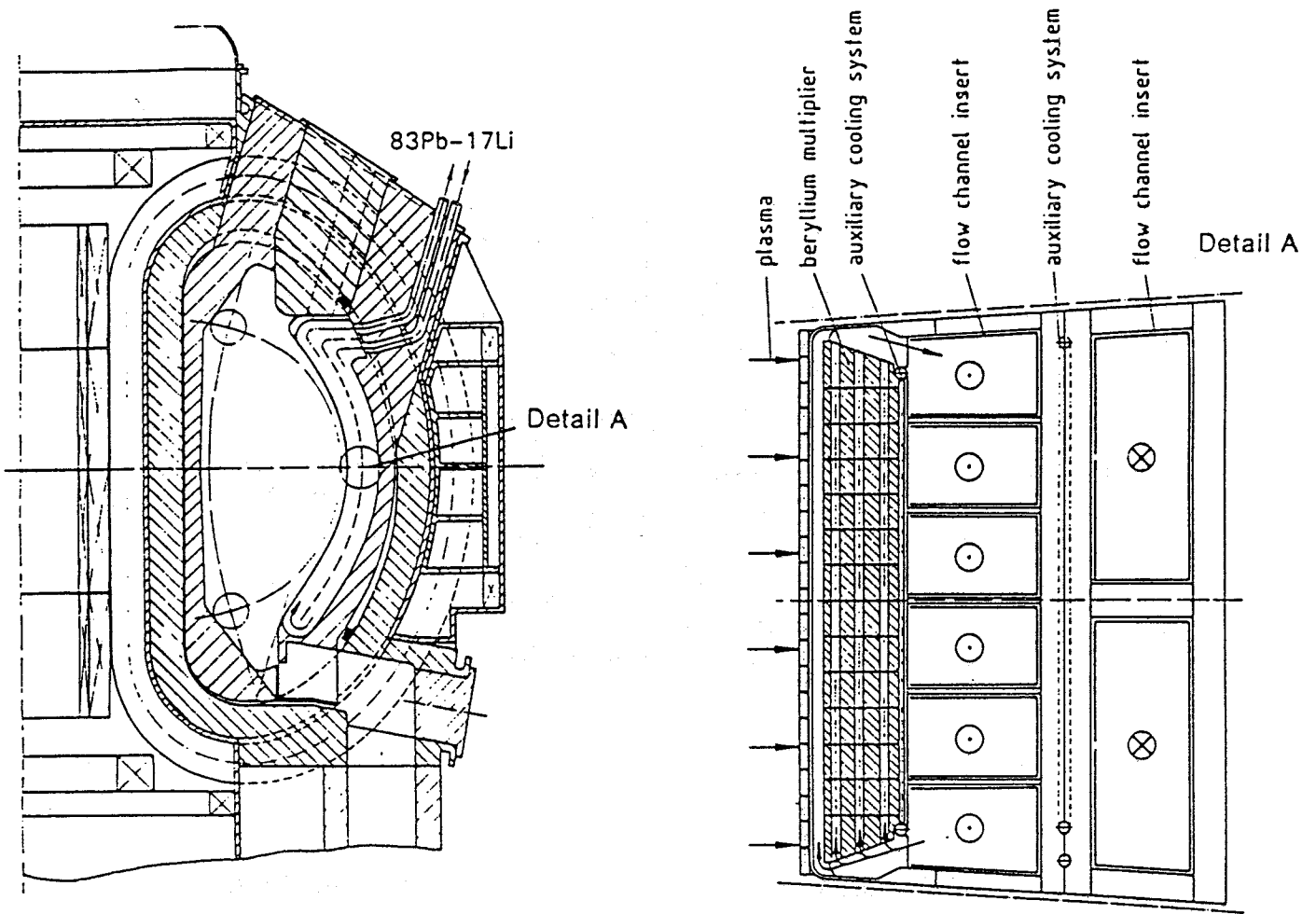
Fig. 1.-3   Self-cooled liquid metal blanket for NET

Detail X

NaK - System I ⎫ Preheating and
NaK - System II ⎭ Auxiliary Cooling

First Wall Supporting Plates

Pb - 17 Li

X

Flow Channel
Inserts

Corrugated First Wall

Beryllium
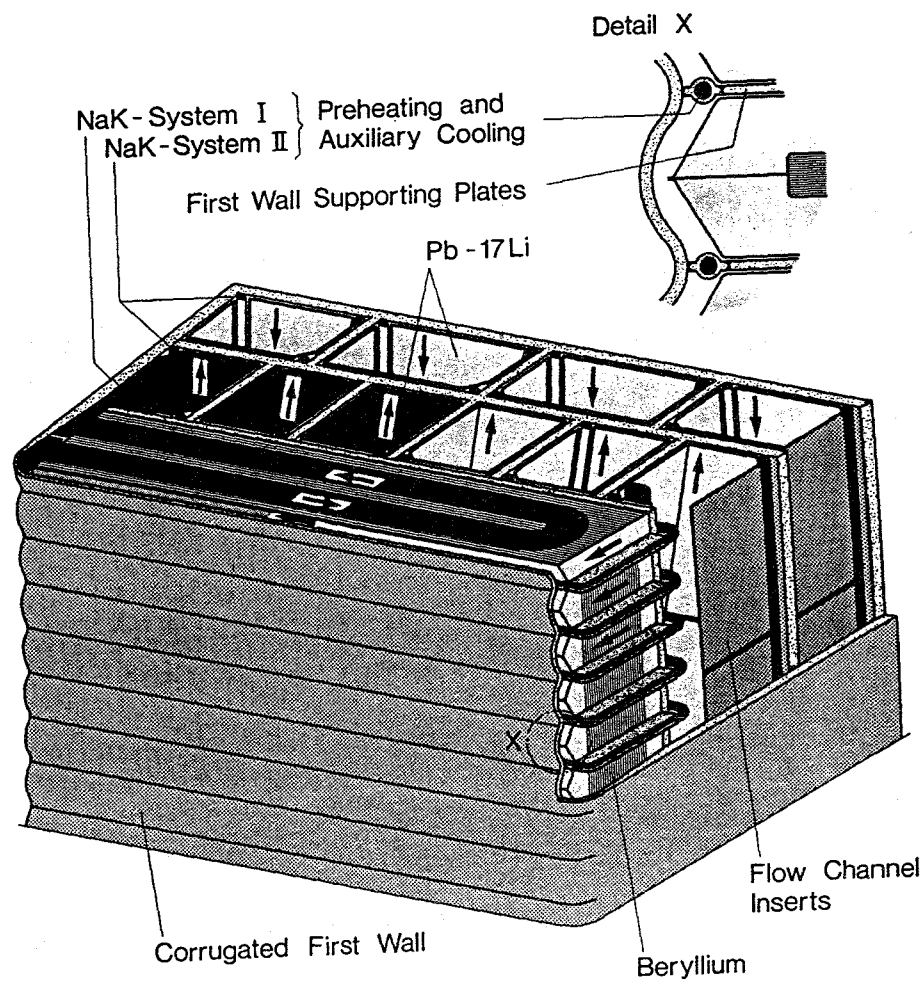
Fig. 1-4   Cross section of a self-cooled Pb-17Li blanket segment for DEMO

~30 cm

MANIFOLDS

REACTOR SECTOR
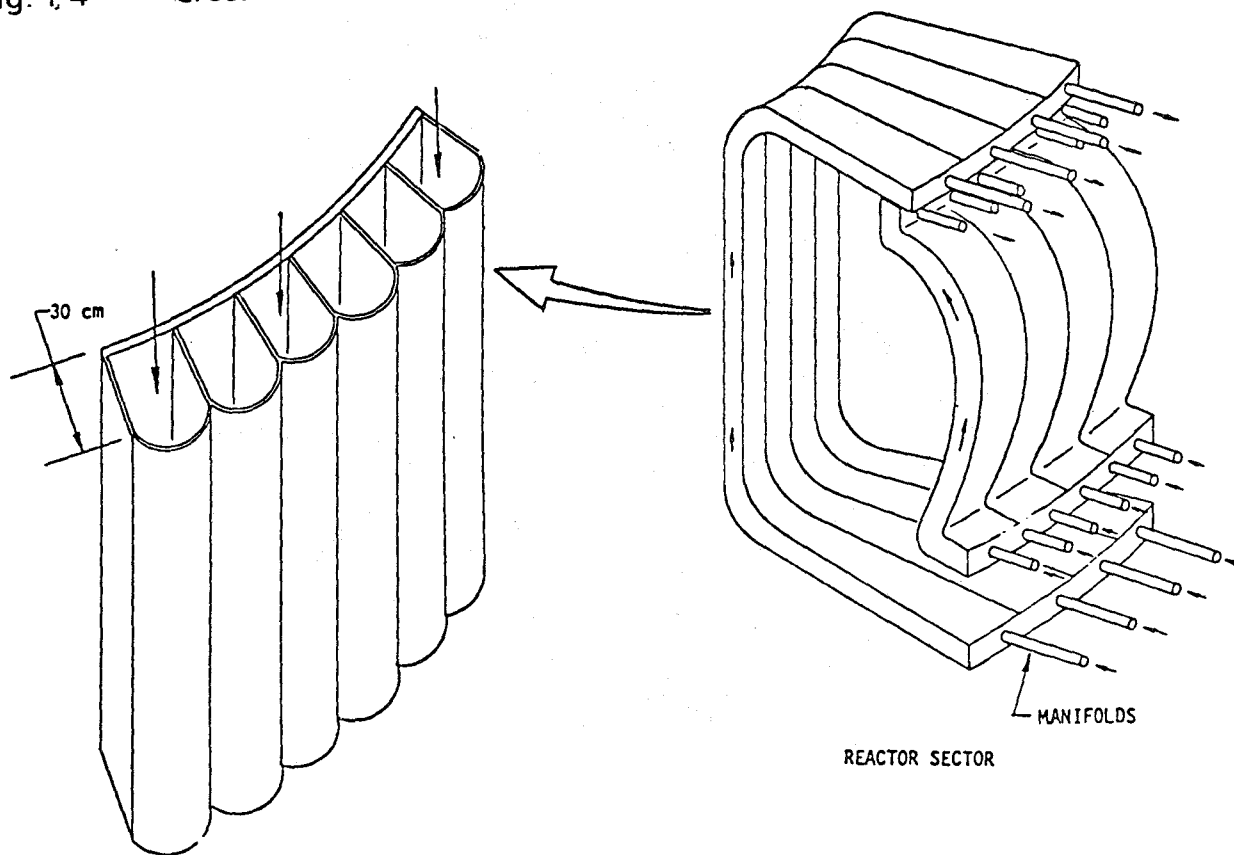
Fig. 1-5   Poloidal flow concept in a self-cooled liquid metal blanket (BCSS) [9]

13
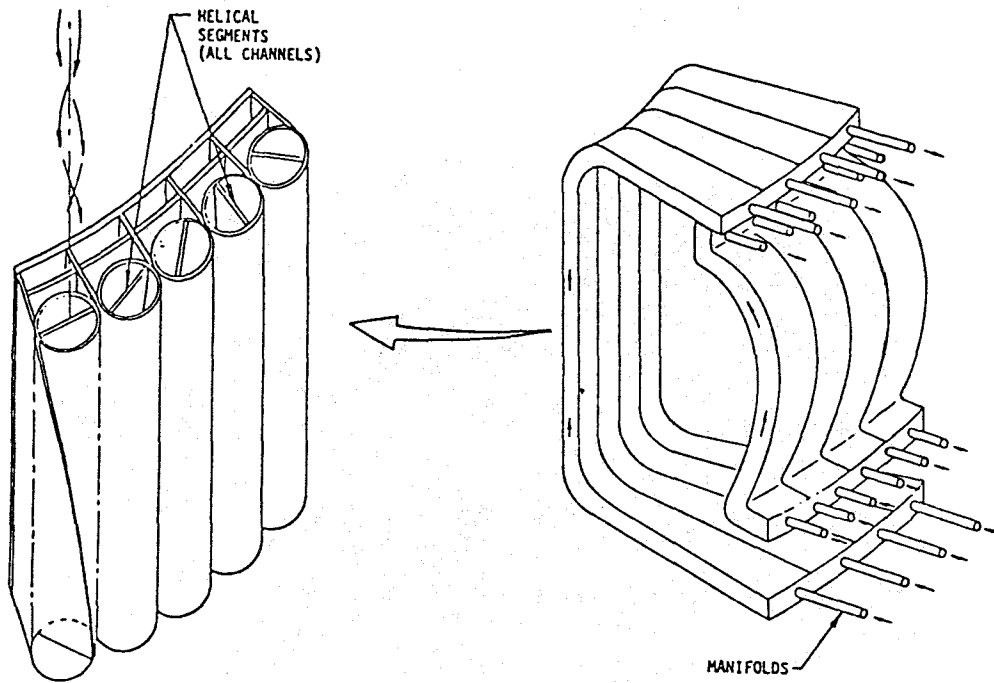
Fig. 1-6   Helical flow concept in a self-cooled liquid metal blanket (BCSS) [9]
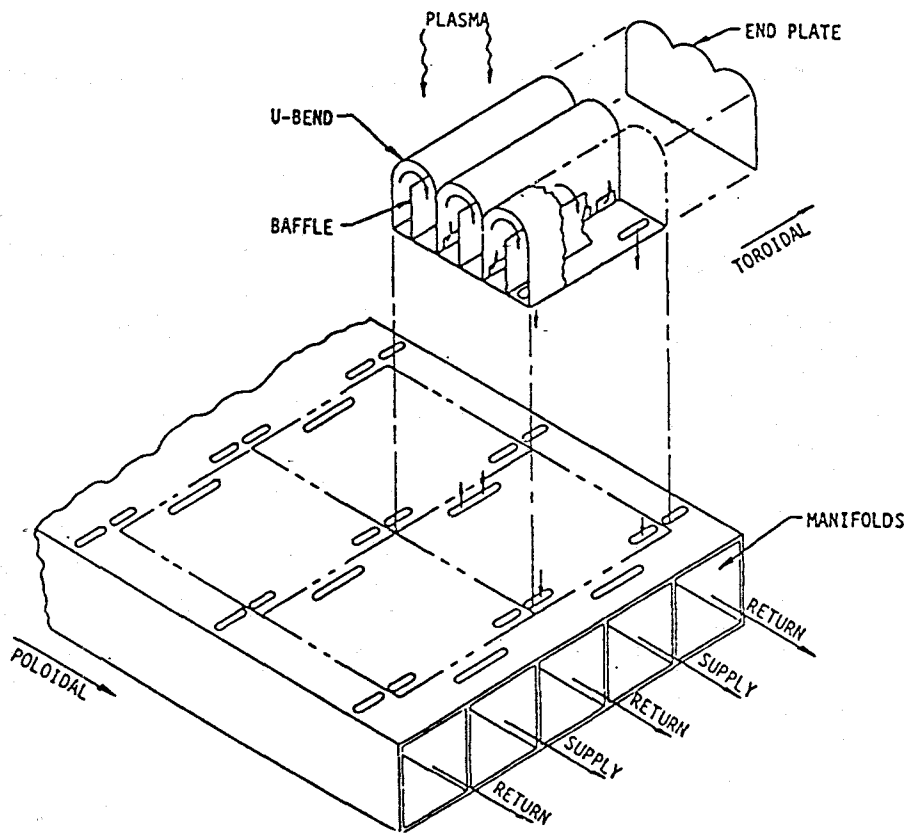
Fig. 1-7   Radial/poloidal flow concept in a self-cooled liquid metal blanket
(BCSS) [9]

2. BLANKET DESIGN FOR A DEMO-REACTOR

The goal of the blanket development programme is to select, develop and test a small number of blanket concepts suitable for power reactors. The strategy in the European Community is to develop two solid breeder and two liquid breeder blanket concepts until 1995 and select than one concept out of each group for further development and testing in NET/ITER. The common basis for this selection process is a DEMO-reactor spezified by the Test blanket Advisory Group (TAG). This DEMO-reactor is not a result of a detailed reactor study but a specification of the boundary conditions and minimum requirements for breeding blankets.

A cross section of the DEMO-reactor which provides the geometrical boundary conditions for the breeding blankets is shown in Fig. 2.-1.

The minimum requirements for DEMO-relevant blankets are:

- Tritium self-sufficiency, i.e. tritium breeding ratio (TBR) > 1,
- Average neutron wall load of 2.2 MW/m^2 which in case of a specific neutron energy of 14.1 MeV corresponds to a flux of 9.74×10^{17} neutrons/(m$^2 \cdot$s) at the first wall,
- Full power life-time of 20.000 h resulting in a maximum first wall damage of 70 dpa,
- Coolant conditions sufficient for an electric power generation with an efficiency equal to that one of a pressurized water reactor (PWR).

For each concept it has to be shown, that it is feasible, meets the minimum requirements and is attractive in comparison with other concepts. No detailed design is required for this purpose but the conceptual design and the accompanying R and D work should provide the basis for a meaningful selection.

The following section 2.1 describes the reference design of a selfcooled Pb-17Li blanket segment and the present status of the analysis work.

2.1 Blanket segment
2.1.1 Design description

The principle arrangement of the blanket segments is identical to the one proposed for ITER [8, section 1.-1.6]. There are 48 outboard segments, with both coolant inlet and outlet tubes attached at the top end of the segments.
At the inboard side the torus is divided into 32 segments. The inboard segments are split into upper and lower halves. At the upper half the coolant inlet and outlet tubes are connected to the top end of the segment, at the lower half to the bottom end. This arrangement can be seen in Fig. 2.1-1 which shows a vertical cross section of the torus.

The arrangement of inlet and outlet tubes at the same end of a segment requires a double pass of the coolant through the segment. The flow path is identical for the outboard segments and the upper half of the inboard segments. Coolant enters the blanket at the top end, flows downward in the rear channels, turns 180 deg at the bottom end and flows upward. This flow perpendicular to the magnetic field does not allow velocities high enough for sufficient first wall cooling. Therefore, the total coolant flow in upward direction is diverted into the relatively small toroidal channels (parallel to the main magnetic field) of the blanket front region. This coolant diversion is achieved by a slight inclination of the walls in the return ducts. The liquid metal flows with relatively high velocity in the toroidal channels between the plasma facing first wall and the second wall. Passing two meander shaped cooling channels in toroidal direction, the coolant is heated up further before it flows back in the return channels to the exit at the top end of the blanket.

This flow path used in the front part of the blanket can be seen in Fig. 2.1-2 which shows a cross section of an outboard segment.

Compared to a single toroidal channel for first wall cooling the arrangement of meander-shaped channels leads to a mechanically stiff region in the front of the segment and to lower liquid metal temperatures in the first wall cooling channel because this liquid metal is coming from a zone characterized by a low power density due to the steep gradient in volumetric heat generation.

The first wall separating the toroidal cooling channels from the plasma chamber is considered to be the most critical part of the blanket segment. It is thermally loaded by a rather high heat flux caused by radiation and a particle flux at the plas-

ma facing surface. To avoid excessive thermal stresses, the wall thickness must not exceed 6 mm. The stiffness of the first wall is increased by giving it a corrugated shape with webs welded in between to support it (Fig. 2.1-2). This mechanical coupling between the corrugated first wall and the remaining part of the front region results in a stiff structure.

In the blanket segment, the coolant flows with velocities between 0.5 m/s (in the inlet channels perpendicular to the magnetic field) and 2 m/s (along the first wall, parallel to the magnetic field). In spite of this optimum flow and velocity distribution, failure to decouple electrically the load-carrying walls from the liquid metal would result in excessively high MHD pressure drops due to the voltage induced by the magnetic field.

In the present blanket design, all coolant channels except the first wall cooling channel are equipped with FCIs described in section 4.3. Mechanical stresses in the FCI become insignificant when a longitudinal slot or holes are made for pressure equalization between the inner flow region and the outer gap. The voltage induced in the liquid metal flowing through the FCI is short-circuited only over the inner liner. Even the longitudinal slot does not give the voltage an additional short-circuit path. The FCI covers the total surface of a flow channel or only parts of it. The thickness of the inner liner can be reduced to a minimum value necessary for sufficient corrosion resistance ($\simeq$ 0.5 mm) in order to minimize the MHD pressure drop. An additional advantage of the FCI is its function as thermal sleeve in the case of cyclic power generation. A change in the liquid-metal temperature will arrive at the load-carrying wall with a time delay, dampened by the FCI itself and the stagnant liquid metal in the gap. The flow in the three toroidal channels is basically in parallel to the main magnetic field. This direction is usually not accompanied by a large MHD pressure drop. Nevertheless, FCI's are used in nearly all channels in order to avoid excessively large currents flowing perpendicular to the plates which would cause the multi-channel problem as explained in section 2.1.3.

Under normal conditions, the breeder material is kept liquid and the afterheat is removed by circulating it in the primary loop, providing cooling or heating outside of the blanket segment. If for some reasons the breeder material in the segment solidifies or if afterheat removal by forced or natural convection is not possible (for example during blanket exchange), an indepenent auxiliary heat transport system to be housed in the segment is necessary. NaK serves as the heat transfer

17

medium. It is a 22% natrium/78% potassium alloy melting at -11°C. One of the circuits of the cooling/heating system supplies the first wall region (see Fig. 2.1-2). The second NaK cooling system is responsible for the outer part of the blanket. Its pipes are loosely arranged, and run in the liquid metal along the walls. The NaK system allows for the afterheat removal during or subsequent to emptying the blanket segment.

2.1.2   Neutronics

From a neutronic point of view the self-cooled liquid metal blanket is characterized by the use of the breeding material Pb-17Li and the absence of any neutron moderating material. The major breeding material component lead (83 atom %) shows a large elastic neutron cross-section resulting, along with its heavy mass, in a high neutron reflection, but a poor neutron slowing down power. These properties lead to enhanced neutron losses through openings and ducts with subsequent neutron absorption processes in non-breeding reactor components, and they lead to rather flat radial profiles of the neutron flux density, the tritium production rate and the power density across the blanket. To restrict the neutron outscattering losses it is beneficial to utilize any available space around the plasma surface for breeding: the conceptual design of the Demo reactor provides a high blanket coverage by arranging blanket segments at both the outboard and the inboard side of the vacuum chamber and additionally behind the divertors. The large blanket thickness of 85 cm, futhermore, assures the utilization of the whole breeding potential inherent to Pb-17Li.

The technical layout of the self-cooled liquid metal blanket mainly is dictated by magneto-hydrodynamic and thermal-hydraulic constraints. It provides large liquid metal flow channels in poloidal direction and a meander-shaped flow scheme in radial-toroidal direction for the cooling of the first wall. This blanket layout largely agrees with a neutronically optimized one and therefore a further neutronic optimization is not necessary. The main neutronic task therefore is to assess the real tritium breeding ratio, the shielding performance and to provide the power density distribution in the three-dimensional geometrical configuration of the Demo reactor; this can be achieved by means of Monte Carlo transport calculations.

For this purpose a three-dimensional torus sector model of the Demo reactor has been set up. The Demo reactor is composed of 16 torus sectors (22.5°), each consist-

ing of two inboard and three outboard segments. Due to its toroidal symmetry it is sufficient to model a torus sector of 11.25° and applying reflective boundary conditions (Fig. 2.1-3). Within this torus sector the model follows very closely the geometrical arrangement of all relevant reactor components (blanket segments, divertors, vacuum vessel, etc.), as they are given in the technical layout. The geometrical modelling of the blanket segments is illustrated by radial-toroidal cross-sections of the inboard (Fig. 2.1-5a) and outboard (Fig. 2.1-5b) segments. Their poloidal arrangement can be taken from Fig. 2.1-4.

The Monte Carlo code MCNP [1] has been used to set up the torus sector model and for performing all neutronic calculations presented here. The nuclear data used in these calculations originate from the European Fusion File EFF-1 and have been processed into a MCNP working library at PSI Würenlingen [2].

In the Monte Carlo calculation the spatial plasma source distribution is described by a probability distribution of the 14 MeV neutron source density s (a). The normalized neutron source density is given by:

$$s(a) = \left| 1 - \left(\frac{a}{A} \right)^2 \right|^4 \quad 0 \le a \le A$$

The parameter a fixes a contour line at constant neutron source density. It corresponds to a magnetic flux line which can be represented according to:

$$R = R_0 + a \cdot \cos(t + \delta \sin t) + e \left| 1 - \left(\frac{a}{A} \right)^2 \right|$$

$$z = E \cdot a \cdot \sin t$$

$$\delta = \delta_0 \cdot \frac{a}{A} \qquad 0 \le a \le A \,, \, 0 \le t \le 2\pi$$

R gives the radial distance to the torus axis and z the poloidal distance to the torus mid-plane.

This plasma source representation has been adopted from neutronic calculations for the NET-reactor [3]. For the Demo reactor the following parameters are used:

$$R_0 = 630 \, cm \qquad \text{major plasma radius}$$

19

$$A = 182\,\text{cm} \qquad \text{minor plasma radius}$$
$$E = 2.17 \qquad \text{elongation}$$
$$e = 16.2\,\text{cm} \qquad \text{excentricity}$$
$$\delta_0 = 0.57 \qquad \text{maximal triangularity}$$

Tritium breeding ratio

For the calculation of the tritium breeding ratio (TBR) about 50 000 neutron histories have been followed. Table 2.1-1 shows the neutron balance and the associated statistical errors obtained in these calculations. The rather high global breeding ratio of TBR = 1.165 obviously is due to the utilization of the divertor region for breeding. The breeding ratio would drop to TBR = 1.057 ± 0.3% in case without divertor breeding, although the neutron multiplication would not change: the neutrons being out-scattered through the divertor openings are absorbed usefully in the breeding material arranged behind the divertors. Divertor breeding therefore improves the neutron economy of the self-cooled liquid metal blanket considerably. The TBR-calculations assume a divertor composition according to the specifications of the test blanket advisory group: 5 mm tungsten, 30 mm copper and 40 mm stainless steel. Note that the in- and outlet liquid metal flow channels of the outboard blanket segments are not taken into account in the TBR-calculations; actually this would provide a further TBR-increase of about 0.05.

The tritium breeding in the actual reactor will be further reduced due to the inclusion of blanket ports for plasma heating, remote handling, pellet injection, diagnostics etc.. The Demo reactor design provides horizontal ports in a total of 10 outboard blanket segments. To assess their impact on the breeding performance a torus sector model of $4 \times 11.25° = 45°$ with 4 inboard and 6 outboard segments has been constructed [4]. It represents the whole reactor with 32 inboard and 48 outboard segments by applying reflective boundary conditions. In this model 8, 12 and 16 horizontal ports of the Demo reactor are simulated. Each port covers an area of 340 cm height times the full segment width in the centre of an outboard segment. The model relies on a simplified geometrical representation of the self-cooled liquid metal blanket. Fig. 2.1-6a shows a radial-toroidal cross-section through the 45° torus sector with $1 + 2 \times 1/2 = 2$ ports, simulating a total of $2/6 \times 48 = 16$ ports. Fig. 2.1-6b shows a radial-poloidal cross-section through a torus sector including a blanket port.

Three different port configurations are considered: a partially voided port with a steel plate at the level of the blanket back side (see Fig. 2.1-6a), a port plugged with steel, and a completely voided port (i.e. voiding also the steel structure between the blanket port and the vacuum vessel, see Fig. 2.1-6a). Fig. 2.1-7 shows the dependence of the TBR on the number of ports for all port configurations considered. Obviously the TBR decreases smoothly with the number of ports and therefore it can be interpolated linearly in this number. In the cases of the plugged port and the partially voided port ("steel plate option") the albedo of the outboard blanket segments is changed only marginally: the breeding performance of the inboard segments is not affected and the reduction of the TBR is due to the loss of breeding material in the outboard segments. For 10 ports a TBR loss of 0.06 can be taken from Fig. 2.1-7, corresponding to an 8% reduction of the outboard and a 5.5% reduction of the total TBR. In the case without any blanket port the breeding ratio amounts to TBR = 1.14 in the $4 \times 11.25°$ torus sector model. Thus it can be deduced that the global TBR of the self-cooled liquid metal blanket in the actual configuration of the Demo reactor with a total of 10 ports would decrease from TBR = 1.165 (Table 2.1-1) to about TBR = 1.10. The outboard TBR would decrease from 0.766 to about 0.70, while the inboard TBR would not change significantly.

One blanket port covers about 48% of the first wall area of an outboard blanket segment of 7.5°. Based on the reduction of the blanket coverage a TBR loss of $10 \times 0.48 \ / \ 48 = 10\%$ would be expected for the outboard segments in case of 10 ports. This would result in an estimated total breeding ratio of TBR = 1.09, which is in fairly good agreement with the above deduced value of TBR = 1.10. Thus it can be concluded that the impact of the blanket ports on the tritium breeding ratio can be estimated by the reduction of the outboard blanket coverage within sufficient accuracy. This holds for the plugged port and the "steel plate option". In case of the completely voided port, this does not hold; there the TBR loss is enhanced (Fig. 2.1-7) due to a reduced albedo of the outboard blanket segments i.e. there are out-scattering losses through the voided ports. This leads to TBR losses both in the outboard and the inboard segments. The completely voided part, however, is not a realistic option for the port configuration.

Power production

For the thermal-hydraulic blanket layout a detailed evaluation of the spatial power density distribution is needed. This is achieved by performing coupled neutron-photon Monte Carlo transport calculations with up to 150 000 source neutrons. In

these calculations the material zones of the torus sector model are appropriately segmented in radial and poloidal direction. Based on a fusion power of 2216 MW of DEMONET the calculated power production of single blanket segments and the complete reactor, equipped only with self-cooled liquid metal blanket segments, is given in Table 2.1-2. 80% of the power is produced in the front part of the blanket segments, where the meander flow scheme is applied (about 1/3 of the total blanket thickness, see Fig. 2.1-5), whereas the back part of the blanket with the liquid metal in-flow channels (with again about 1/3 of the blanket thickness) produces only 4% of the power.

Due to the inherent nuclear properties of Pb-17Li, discussed above, the radial and poloidal profiles of the power density are comparatively flat. As an example Fig. 2.1-8a shows the radial power distribution of the material components Pb-17Li and steel (MANET) in the torus mid-plane of the outboard segment, Fig. 2.1-8b shows the poloidal power distribution of the breeding material Pb-17Li in the meander-shaped part of the outboard blanket segment (meander zones I to V in Fig. 2.1-5b). The maximum power density of Pb-17Li is not more than about 23 W/cm^3 (outboard first wall cooling channel at torus mid-plane); this rather low maximum value is due to the absence of any neutron moderator in the blanket and the fact that a large volume fraction is available for the breeding material Pb-17Li. In case of a self-cooled Pb-17Li blanket variant using beryllium as additional neutron multiplier the maximum power density would be twice as high [5].

Shielding

Radiation shielding is most crucial at the inboard side of the Demo reactor: although the total thickness of the blanket/shield system amounts to 115 cm, the thickness of the vacuum vessel, acting as major shielding component, is only 30 cm, whereas the total blanket thickness is 85 cm. The shielding performance of a breeding blanket in general is poor (with the exception of aqueous salt solution blankets); especially this holds for the self-cooled Pb-17Li blanket due to the inherent nuclear properties of Pb-17Li and the absence of neutron moderating material. The total neutron flux density decreases, for instance, from $1.28 \cdot 10^{15}$ $cm^{-2} s^{-1}$ at the inboard first wall to $6.15 \cdot 10^{13}$ $cm^{-2} s^{-1}$ at the rear wall of the inboard blanket, i.e. by not more than a factor 20 across the blanket with a thickness of 85 cm.

Therefore it is questionable, if the shielding requirements can be met in the actual configuration of the Demo reactor. To clarify this question, appropriate shielding calculations have been performed in the 11.250° torus sector model of the Demo reactor. The MCNP-code has been applied for performing the shielding calculations making use of the importance sampling technique. About 150 000 neutron histories have been followed in the shielding calculations to assure a sufficient statistical accuracy in the region of the TF-coil. For the vacuum vessel the layout shown in Fig. 2.1-5 has been used: a steel layer (SS-316) of 5 cm thickness, a layer of borated water (40 g $H_2 BO_3$ per liter of water) with a thickness of 2 cm, a steel layer of 7 cm, again a layer of borated water (5 cm) and a steel layer of 11 cm. Such a material configuration shows a high shielding performance; if it is necessary, however, it can be further optimized with regard to its shielding efficiency (see below).

Various design options have been taken into account in the shielding investigations:

- the reference design option with large liquid metal inflow channels at the blanket back side

- a design option with improved shielding performance by inserting the solid metal hydride ZrH into the inflow channels ("ZrH option"). A homogeneous mixture of 20% ZrH and 80% Pb-17Li is used in this case.

- a design option with improved shielding performance of the vacuum vessel ("optimized vacuum vessel"): the average volume fraction of the borated water is increased to about 50% in this case; for the blanket the reference design is used.

All of these design options, however, neglect the effect of dividing the inboard blanket segment into two poloidal halves. In order to assess this effect on the shielding performance a separate shielding calculation has been performed by using the "ZrH-design option" for the blanket segment.

Fig. 2.1-9 shows the radial profiles of the total and the fast (E > 0.1 MeV) neutron flux densities across the inboard blanket segment and the vacuum vessel in case of the reference design option, the "ZrH-option" and the optimized vacuum vessel. Obviously the inclusion of the solid neutron moderator ZrH greatly reduces the penetrating neutron radiation: the total neutron flux density at the front of the

23

vacuum vessel decreases by nearly one order of magnitude. On the other hand, an improved vacuum vessel design is even more efficient for minimizing the penetrating neutron radiation. In any case it is obvious that a well moderated neutron spectrum is a precondition for a high shielding efficiency: the emerging neutron radiation easily is absorbed in the structural components of the blanket segment, or, subsequently, in the vacuum vessel.

With regard to the radiation loads on the inboard TF-coils it is observed that the radiation design limits for the Demo reactor (2216 MW fusion power and 20 000 h integral operation time) can be met in case of neglecting the division of the inboard blanket segment. The inclusion of the blanket division increases the radiation loads at the torus mid-plane by about a factor 3 and the radiation design limits are exceeded by a factor 2 in this case. This factor can be eliminated easily by increasing the ZrH-fraction in the inflow liquid metal channels to about 40%, or, by optimizing the vacuum vessel for shielding, or, simply by increasing the thickness of the vacuum vessel by about 5 cm.

Table 2.1-1: Neutron balance for the liquid metal blanket in the Demo reactor configuration

neutron multiplication M	1.620 ± 0.1 %
tritium breeding ratio TBR	
outboard segment	0.766 ± 0.4 %
inboard segment	0.285 ± 0.7 %
divertor region	0.113 ± 1.2 %
total TBR	1.165 ± 0.3 %

Table 2.1-2: Power production [MW] in single blanket
             segments and in the complete reactor
             based on a fusion power of 2216 MW

inboard segment (11.25^0)	
central part	13.5
divertor breeding region	3.74
total inboard	17.2
outboard segment (7.5^0)	25.7
total power production	1783

Table 2.1-3: Radiation loads on the inboard TF-coil for various design options (20 000 h integral operation time)

	Radiation design limits	Reference design	Optimized vacuum vessel	"ZrH-option" (0.2 ZrH / 0.8 Pb-17Li)	
				reference	inboard blanket divided
Epoxy radiation dose [rad]	$\sim 5 \cdot 10^9$				
torus mid-plane		$1.02 \cdot 10^{10}$	$3.61 \cdot 10^9$	$3.34 \cdot 10^9$	$9.55 \cdot 10^9$
poloidal average		$5.67 \cdot 10^9$	$2.26 \cdot 10^9$	$1.88 \cdot 10^9$	$2.63 \cdot 10^9$
Fast neutron fluence [cm^{-2}]	$\sim 10^{18}$				
torus mid-plane		$2.73 \cdot 10^{18}$	$8.78 \cdot 10^{17}$	$1.37 \cdot 10^{18}$	$2.86 \cdot 10^{18}$
poloidal average		$1.50 \cdot 10^{18}$	$5.92 \cdot 10^{17}$	$7.24 \cdot 10^{17}$	$8.97 \cdot 10^{17}$
Maximum power density [mW/cm^3]	~ 1.0				
torus mid-plane		2.52	0.891	0.822	2.35
poloidal average		1.40	0.557	0.464	0.650
Total power production in the TF-coil [kW]	~ 20	18.90	12.25	6.67	8.48

26

2.1.3   MHD Analysis

The design of the liquid metal cooled blanket is dominated by MHD considerations, which are considered in more detail in section 4.2.

Liquid metal flow within the strong magnetic field of a tokamak is accompanied by a high MHD presssure drop which can be a feasibility issue because it may result in mechanical stresses beyond the allowable limits of the structural material. Additionally the magnetic field may also influence the velocity in the cooling channels and herewith the heat transfer. The later is considered in more detail also in section 4.2.

The MHD-pressure drop and flow distribution of the reference concept is very difficlt to calculate. In the present state only assessments can be made. This is caused by the fact that the concept contains flow channels with three flow directions. One type of channel is very often arranged perpendicular to the adjacent channels. Therefore, the electrical potential of one channel is short-circuited in the adjacents.

The MHD pressure drop of the liquid metal (Pb-17Li) flowing through the in- and outboard blanket of the reference concept (Fig. 2.1-10) is calculated using mainly simple analytical models based on the well established slug flow model for liquid metal channel flow [6].

In this model a constant velocity over the cross section of the cooling channels is assumed, an assumption which is also taken for the thermal-mechanical analysis in this report.

This model may be applied mainly for straight or slightly bended channels which are perpendicular to the magnetic field. Channel flow in bends in plains perpendicular to the magnetic field are treated similarly using an equivalent mean length.

The pressure drop in expansions and contractions is calculated using simple analytical correlations, which are based on experiments and numerical calculations.

The flow of the liquid metal in and out of the magnetic field is calculated numerically using the Core Flow Solution. The radial to toroidal bend, this means the

change of the flow direction from the radial feeding to the toroidal front channels (position 8a in Table 2.1-5) as well as the meander shaped flow (position 8c) are also calculated with simple expressions based on experiments [7,8]. Additionally the meander shaped flow was numerically analysed (see also section 4.2) with a generalized version of the Core Flow Solution.

The pressure drop resulting from MHD interaction of channel flow, which is the most critical issue of the reference concept, was calculated using an electrical network method.

The pressure drop in the in- and outboard blanket is calculated following the flow path from the entrance to the outlet shown schematically in Fig. 2.1-10. In the Tables 2.1-5 and 2.1-6 the different stations along the flow path are labled in sequence by a number and characterized by a sketch. The pressure drop calculations, whose results are listed in these tables too, are conducted using the following types of correlations.

MHD pressure drop correlations:

Nomenclature:

$\bar{v}$	mean velocity of the liquid metal in the channel
$B_\perp$	magnetic field component perpendicular to $\bar{v}$
$B_\perp = B_T \cdot \alpha$	
B_T	magnetic field in toroidal direction
α	angle between $\bar{v}$ and B_T
L	length of the considered channel section
a	the half width of the channel in direction of $B_\perp$
b	the half height of the channel perpendicular to $B_\perp$
$\beta = a/b$	the aspect ratio of the channel
$\sigma = f_1(T)$	electrical conductivity of the liquid metal
$\sigma_w = f_2(T)$	electrical conductivity of the channel wall
t_w	the MHD effective wall thickness
$C = \sigma_w \cdot t_w / \sigma \cdot a$	the wall conduction ratio

28

2.1.3.1 Pressure drop in channel flow perpendicular or inclined to the magnetic field direction

For fully developed flow and MHD conditions relevant for the reference concept a simplified version of the pressure drop correlation (4.2.1.4) can be used.

(Type 1)

$$\Delta p = \bar{v} \cdot B_{\perp}^2 \cdot L \frac{\sigma_w \cdot t_w}{a}$$

As shown in section 4.2 the assumption of fully developed flow is questionable due to the low wall conduction ratios involved ($C = 10^{-3} - 10^{-4}$) and the resulting large developing length of the flow. In the sections where the MHD flow profile is not fully developed the MHD pressure drop is higher. There are some indications from MHD-experiments in a round channel with a flow channel insert with a wall conduction ratio $C = 0.004$, that the measured pressure drop is about 15-20% higher than calculated.

Therefore we increased all the pressure drops calculated with the Type 1 correlation by 20%.

2.1.3.2 3-dimensional pressure drop in a bend with flow changing from perpendicular to parallel to the field direction B_T

(Type 2)

$$\Delta p_{3D} = K(C^*,\beta) \cdot b\, \beta^{-1} C^* \sigma\, v\, B_{\perp}^2$$

In this correlation $C^* = \sigma_w \cdot t_w / \sigma \cdot b$ is the wall conduction ratio based on the channel half height b. The factor K, which is a function of the wall conduction ratio C^* and the aspect ratio β, is taken from [7].

2.1.3.3 Pressure drop at the transition from the poloidal distribution channels to the radial channels

This problem can be treated similar to the manifold problem, where the liquid metal enters out of a large pool into a small channel perpendicular to the field. From the model shown in Fig. 2.1-11 a simple analytical correlation was derived, which has to be considered as a first rough approximation.

(Type 3)

$$\Delta p_{3D} = \frac{3}{4} \bar{v}\, \sigma\, B_{\perp}^2 \cdot L$$

Within the frame of the model the following values of the velocity $\bar{v}$ and the length L has to be used:

$$\bar{v} = \bar{v}_{Channel} \quad \text{the mean velocity in the channel perpendicular to the field}$$
$$L = 2\,a \qquad \text{the width of the channel}$$

2.1.3.4 Pressure drop in the U-bends of the meander flow in the front channels

This kind of pressure drop is calculated using an experimental correlation as shown in [8]. This correlation was transformed for our calculation purposes in the following form:

(Type 4)
$$\Delta p_{3D} = \frac{1}{2}\,a\ o\ v\,B^2\cdot\ f(N)$$

where f(N) is an experiementally determined function of the interaction parameter N
with

$$N = \frac{o\cdot\ a\cdot\ B^2}{\rho\cdot\ \bar{v}}$$

In the Tables 2.1-5 and 2.1-6 the calculated pressure drops along the flow path from the inlet to the outlet of the outboard- and the inboard blanket respectively are listed together with all the data needed to evaluate the application limits of the used correlation and to conduct the pressure drop calculations for the in- and outboard blanket, like the mean velocity $\bar{v}$, the field strength B_T, the angle α between the field and the flow direction, the conductivities o of the liquid metal and o_w of the wall, the length L, the half width a and the half height b of the channel in the respective section, and the wall thickness t_w. The velocities and the temperatures are taken from the thermo-mechanical analysis, the temperature dependent electrical conductivity of the liquid metal o from Jauch, Karcher and Schulz [9].

2.1.3.5 Pressure drop caused by multichannel effects

The first wall of the blanket of the reference concept is cooled by liquid metal flowing parallel in 96 channels in toroidal direction. These channels are roughly 1 m long and have a cross section of about 1200 mm^2 each. The basic problem of the concept considered are MHD-pressure-drop and flow distribution in these parallel

30

channels together with the inlet and outlet channels. The toroidal front channels are in electrical contact. The radially arranged inlet- and outlet-channels have countercurrent flow. This counterflow will create countercurrent induced voltage in the fluid. The latter will find an electrical short circuit in the first wall and the adjacent front channels; the electrical power of this short circuit creates additional MHD-pressure losses and possibly non-uniform flow distribution through the front channels. Both effects are difficult to predict. For a first approach the MHD pressure losses by flow channel interaction were calculated with the computer programme SCEPTRE. This programme enables to calculate electrical circuits. In our case the flow channels of the blanket were described by voltage sources (equivalent to fluid velocities (slug flow model)) and by electric resistances (equivalent to the resistance of the fluid in the flow channels and the resistance of the channel structures). The calculated electric currencies can be transformed into MHD pressure losses.

For a first assessment of the pressure losses detailed calculations were conducted using an electric network model. In this model plausible assumptions of the electrical resistances are made. For the calculations the geometry and the flow velocities of the previous outboard blanket concept were used. These results have been scaled to the conditions of the present design resulting in a pressure drop caused by multichannel interaction of $\Delta p = 0.78$ MPa for the outboard blanket. An extrapolation for the inboard blanket gives a value of $\Delta p = 1.0$ MPa.

The total pressure drop, including the pressure drop caused by multichannel interaction, amounts to

Outboard: $\Delta p = 3.4$ MPa

Inboard: $\Delta p = 3.1$ MPa

In Table 2.1-4 the pressure losses of the outboard and inboard blanket are splitted into five characteristic groups. From this table it is evident that a better knowledge of the multichannel MHD-effects which contribute with 23 respectively 32% to the total pressure loss is an ongoing key issue of this concept, especially because these effects have a strong influence on the partioning of the flow on the parallel arranged front channels.

Table 2.1-4   MHD Pressure Losses

Category	Δp [MPa] Outboard Segment	Δp [MPa] Inboard Segment
① Pressure drop in ducts perpendicular to the magnetic field	1.744	1.379
② Pressure drop in bends between flow directions perpendicular and parallel to the magnetic field	0.012	0.025
③ Pressure drop in the transition zone between poloidal distribution channels and radial ducts	0.641	0.509
④ Pressure drop in the meander flow region	0.220	0.230
⑤ Pressure drop caused by multi channel effects	0.78	1.00

Tab. 2.1-5: MHD-Pressure Drop (Outboard-Blanket)

Channel section	Geometry	Field direction	Channel length [m]	mean velocity [m/s]	Temp. [°C]	σ_W 10^6 [A/Vm]	t_W [mm]	characteristic length [m]	Field strength B[T]	Type	$\sigma_{PbLi}(T)$ 10^5 [A/Vm]	M	Δp [Pa]
1. Inlet													
a) Radial-toroidal 3D-effect		$v\perp B$ $\rightarrow u\|\|B$	0,25		300 °C	1,24	0,5		1	2	7,892	-	1163
b) Field inclination effect	see 8b	$vB\sin\alpha$	5,0	0,67	300 °C	1,24	0,5	pipe r = 0,25	1	1	7,892	914	402
c) $v\perp B$ in radial channel		$v\perp B$	2,9		300 °C	1,24	0,5		1-5 = 3	1	7,892	15850	52163
2. Manifold		$v\perp B$	0,7	0,67	300 °C	1,24	0,5	0,25	5	1	7,892	26416	35200
3. Rear Poloidal channels		$v\perp B$	8,68	0,5	300 °C	1,24	0,5	0,13	4,5	1	7,892	12363	506674
4. Hairpin Bend		$v\perp B$	0,5	0,5	300 °C	1,24	0,5	0,13	5	1	7,892	12363	36032
5. Poloidal Distributor		$v\perp B$	8,68	0,5	300 °C	1,24	0,5	0,08	4,5	1	7,892	7608	820317
6. Poloidal-Radial Transition		$v\perp B$	0.074	0,3	350 °C	1,19	0,5	0,037	5	3	7,762	-	323052
7. Radial Channel		$v\perp B$	0,275	0,3	350 °C	1,19	0,5	0,037	5	1	7,762	3877	41090
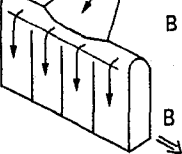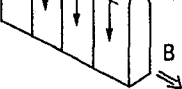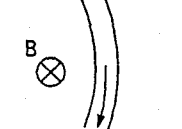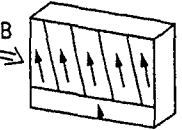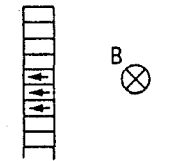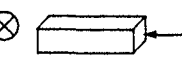
33

Tab. 2.1-5: MHD-Pressure Drop (Outboard-Blanket), cont.

Channel section	Geometry	Field direction	Channel length [m]	mean velocity [m/s]	Temp. [°C]	σ_w 10^6 [A/Vm]	t_w [mm]	characteristic length [m]	Field strength B[T]	Type	$\sigma_{PbLi}(T)$ 10^5 [A/Vm]	M	Δp [Pa]
8. Toroidal Channel													
a) 3D effect		$v \perp B$	0,0425	0,3	350 °C	1,19	3 mm	0,0425	5	2	7,762	-	9206
b) Field inclination effect in tor. channels		$v\,B\,\sin\alpha$	1,069	1,4	350 °C	1,19	3 mm	0,0425	0,868	1	7,762	773	137131
c) Meander-Flow in the front part		$v\,\|\,B$	1,069	1,4 0,3	350 °C	1,19	3 mm	0,0425	5	4	7,762	-	219551
9. Radial Channel analogue to 7		$v \perp B$	0,275	0,3	400 °C	1,14	0,5 mm	0,037	5	1	7,635	4168	40391
10. Radial-Poloidal Transition analogue to 6		$v \perp B$	0,074	0,3	400 °C	1,14	0,5 mm	0,074	5	3	7,635	-	317821
11. Manifold with poloidal-radial Bend		$v \perp B$	0,7	0,5	400 °C	1,14	0,5 mm	0,25	5	1	7,635	28164	24153
12. Outlet analogue to 1		$v \perp B$	5 2,9	0,67	400 °C	1,14	0,5 mm	0,25	1-5 Tesla ~3	1,2	7,635	16899	50944

Tab. 2.1-6: MHD-Pressure Drop (Inboard-Blanket)

Channel section	Geometry	Field direction	Channel length [m]		Temp. [°C]	σ_W 10^6 (A/VM)	t_w [mm]	characteristic length [m]	Field strength B[T]	Type	$\sigma_{PbLi}(T)$ 10^5 [A/Vm]	M	Δp [Pa]
1. Inlet													
a) Radial-toroidal 3D-effect		$v \perp B$ $\rightarrow v \parallel B$	0,25	0,46	300	1.24	0,5	0,25	1	2	7,892	-	799
b) effect of field inclination	see 8b	$v \perp B$	5				0,5	0,25	1	1			276
c) $v \perp B$ in radial channel		$v \perp B$	2,05				0,5	0,25	1→7.3,5	1		18491	34862
2. Manifold		$v \perp B$ $\rightarrow v \parallel B$	2,23	0,46	300	1.24	0,5	0,25	7	1	7,892	36982	150404
3. Rear Poloidal channels		$v \perp B$	4,05	0,3	300	1.24	0,5	0,11	7	1	7,892	16272	403290
4. Hairpin Bend		$v \perp B$	0,5	0,3	300	1.24	0,5	0,11	7	1	7,892	16272	49789
5. Poloidal Distributor		$v \perp B$	8,68	0,5	300	1.24	0,5	0,079	7	1	7,892	11686	373164
6. Poloidal-Radial Transition			0.045	0,2	350	1.19	0,5	0,045	7	3	7,761	-	256695
7. Radial Channel			0,260	0,2	350	1.19	0,5	0,0225	7	1	7,761	3301	78970

Tab. 2.1-6: MHD-Pressure Drop (Inboard-Blanket), cont.

Channel section	Geometry	Field direction	Channel length [m]		Temp. [°C]	σ_w 10^6 (A/VM)	t_w [mm]	characteristic length [m]	Field strength B[T]	Type	$\sigma_{PbLi}(T)$ 10^5 [A/Vm]	M	Δp [Pa]
8. Toroidal Channel													
a) Rad.-tor. bend 3D-effect		$v \perp B$ $\to v \| B$	0,0225		350	1.19	3	0,025	7	2	7,761	-	22669
b) field inclination effect in tor. channel		$v \perp B$	0,863	1,4	350	1.19	3	0,0425	7	1	7,761	1083	113058
c) Meander-Flow		B	-	1,4 0,3						4	7,761	-	230330
9. Radial channel analogue to 7		$v \perp B$	0,260		400	1.14	0,5	0,0225	7	1	7,63535	3943	68282
10. Radial-Poloidal Transition analogue to 6		$v \perp B$	0,045		400	1.14	0,5	0,045		3	7,63535	-	252539
11. Manifold with poloidal-radial bend		$v \perp B$	2,73		400	1.14	0,5	0,25		1	7,63535	39430	73340
12. Outlet analogue to 1			0,255	0,46	400	1.14	0,5	0,25	7 1→7 3,5	1,2	7,63535	19715	34923

2.1.4 Thermal-mechanical analysis

The thermal-hydraulic analysis receives input from a neutronic analysis. The spatial distribution of the power density in the liquid metal (Pb-17Li) and the steel structure (MANET) has been determined by means of a three-dimensional Monte Carlo calculation (cf. section 2.1.2) and is shown in Fig. 2.1-8a and 2.1-8b. The volumetric heat generation in a single blanket segment caused by the neutron flux results in a heat input of about 17.2 MW and 25.7 MW for the inboard and outboard blanket segment respectively. Taking into account a conservatively high mean value for the surface heat flux of 0.4 MW/m^2, the total heat input amounts to 20.1 MW and 29.2 MW for the inboard and outboard blanket segment respectively. The total coolant mass flow rate is determined by the allowable temperature rise of the liquid-metal flow between the blanket inlet and outlet. This temperature rise is limited by the allowable maximum temperature at the coolant-to-wall interfaces as dictated by corrosion considerations. A mean exit bulk temperatur of 400°C has been selected to keep the maximum temperature at the interface of coolant and martensitic steel well below 470°C with respect to corrosion of the structural material. The blanket inlet temperature is governed by the melting temperature, which has a value of 235°C for the Pb-17Li eutectic alloy. Therefore, the inlet temperature has been set at 275°C, a temperature which is well above the ductile-brittle-transition temperature for irradiated martensitic steel. This results in an overall temperature rise of 125 K and a total mass flow rate of 850 kg/s and 1236 kg/s through the inboard and outboard blanket segment respectively. Since the inboard segment is divided into an upper and a lower half of equal size, the mass flow rate through each half is 425 kg/s. There is one more constraint which determines the thermal-hydraulic design, i.e. the first wall temperature limit of 550°C is based on data of material strength.

For the computation of the temperature distribution in the meander region, the following assumptions have been made:

- The coolant temperature is uniform over the entire cross-section at the inlet side of the toroidal flow path.
- The coolant flow is fully developed and the velocity is uniform (slug flows) as a result of the MHD effects.
- Perpendicular to the flow direction, heat is transported by conduction only.

Steady-state temperature calculations have been carried out for the front zone with meander-shaped coolant channels at the torus midplane. Because of the higher thermal load of the outboard blanket it is sufficient to calculate this part only. The computations have been performed by using the finite-element code ABAQUS [10]. Because of the lack of more sophisticated computer programs for the combined application to solids and fluids, the method of a moving coordinate system has been utilized for the computation. Quasi nonsteady-state calculations have been carried out within the calculated residence time of the fluid in the toroidal coolant channels and setting the specific heat of the solid materials equal to zero. The different flow directions require in addition that the temperatures of some subregions are computed separately in an inital step. For nodes at the intersection lines, the resulting temperatures have to be averaged and serve as input for a rerun. The same method has to be applied to the connection with the rear part of the blanket segment containing the poloidal coolant inlet channels. Figure 2.1-12 shows a radial-poloidal cross-section of the first wall and the meander region at the torus midplane. This geometry has been determined by optimizing calculations performed in parallel to the thermal-hydraulic analysis. The figure represents the main dimensions of the geometrical model and its nodalization used in the computation. For better illustrating the mesh of the coolant channels has been hidden. For the computation of the temperature field, a maximum surface heat flux of 50 W/cm^2 has been assumed, which is considered as a peak value of DEMO. The radial distribution of the material dependent power density has been provided by neutronic calculations. The heat generation in the steel structure decreases with radial distance from the first wall. In the first wall, the volumetric heat generation amounts to 20 W/cm^3. The power density in the coolant itself takes a maximum value of 23 W/cm^3 in the first wall cooling channel.

The most important design requirement is now the determination of the minimum average velocity needed to provide enough cooling for the highly loaded first wall. An optimum design is achieved if the same temperature rise is set in all toroidal front channels of the blanket segment. Based on the poloidal power distribution, a coolant mass flow of 15 kg/s must pass through the first wall channel at the blanket midplane and a value of 7.5 kg/s at the upper and lower end of the segment, respectively. This results have been obtained by taking into account a total of 114 cells in which the blanket height has been subdivided. The material data have been taken from refs. [11,12].

Figure 2.1-13 shows the temperature field at the exit side of the first wall channel (I). It can be seen that there is a boundary layer near the first wall where the temperature rises sharply primarily due to the effect of the surface heat flux. The maximum temperature of 415°C is at the first wall-to-coolant interface. Accross the first wall of 6 mm thickness a large temperature difference of $\Delta T = 126$ K occurs which results in a maximum first wall temperature of 541°C at the plasma facing surface. Figures 2.1-14 and 2.1-15 illustrate the temperature field in the coolant at the exit of channel II and III respectively where the temperature at the interface between the flowing coolant and the steel sheet reaches value of 412°C in the channel III. Figure 2.1-16 shows in the upper part again the radial-poloidal cross-section of the investigated geometry. The lower part of the graph respresents the radial temperature profile at the coolant outlet plane along the cross-section X-X as calculated for the torus midplane.

The coolant temperature rise amounts to 32 K for the first wall coolant channel. This corresponds to a heat removal of 91 kW, from which 53 kW (about 58%) are generated in the first wall (surface power plus volumetric power). The ratio of surface power to volumetric power of the first wall is roughly 4:1. The power contribution by the lead-lithium coolant in the meander region amounts to about 63% of the total power.

In Table 2.1-12 coolant temperatures at three blanket levels are summarized. The temperatures at the blanket bottom and top ends have been estimated on the basis of the power density distribution.

The meander-shaped coolant flow in the multiplier region proves to be ideal from the thermal point of view. A parallel flow through the cooling channels would lead to unacceptable high first wall temperatures at the coolant exit side.

The stress analysis [13] which has been previously carried out for the first version of the self-cooled DEMO-blanket with respect to the ASME Boiler and Pressure vessel code [14] has shown that a considerable amount of safety margin exists for the stresses. The limit for the internal pressure loading has been found at 6.5 MPa.

Compared with the results for that version using a beryllium multiplier the maximum first wall temperature is only a little higher. With the unchanged temperature difference in the first wall the secondary stress should not be higher, and the-

re are considerable reserves in strength. Because of the removal of the beryllium the maximum temperature of steel structure is at 420°C much lower than for previous versions. Therefore, the limit on the internal pressure in the first wall cooling channel at the torus midplane will be at least 6.5 MPa, the value determined for the previous design.

Table 2.1-7: Coolant temperatures and pressures at three different blanket levels

	bottom end	midplane	top end
coolant inlet temperature [°C]	287	296	306
liquid-metal mass flow [kg/s]	7.5	15.1	7.5
maximum first wall temperature [°C]			
- inside	400	415	419
- outside	517	541	537

References to section 2.1:

[1]   J.F. Briesmeister (Ed.): MCNP - A General Monte Carlo Code for Neutron and Photon Transport, Version 3A, Report LA-7396-M, Rev. 2, Sept. 1986

[2]   P. Vontobel: Generation of an EFF-1 Based Monte Carlo Neutron Library for MCNP, Paul Scherrer Institut, Villigen, Switzerland, 1990

[3]   U. Fischer: Die neutronenphysikalische Behandlung eines (d,t)-Fusionsreaktors nach dem Tokamakprinzip (NET), KfK-4790, Oktober 1990

[4]   U. Fischer: Impact of Ports on the Breeding Performance of Liquid Metal and Solid Breeder Blankets in the DEMONET-configuration, contribution to 2. Int. Symp. on Fusion Nuclear Technology, June 2 - 7, 1991, Karlsruhe, F.R. Germany

[5]   S. Malang, H. Deckers, U. Fischer, H. John, R. Meyder, P. Norajitra, J. Reimann, H. Reiser and K. Rust: Self-cooled Blanket Concepts Using Pb-17Li as Liquid Breeder and Coolant, Fusion Engineering and Design 14 (1991), 373-399

[6]   Hoffmann, M.A., Carlson, G.A.: "Calculation Techniques for Estimating the Pressure Losses for Conducting Fluid Flows in Magnetic Fields". UCRL-51010, Lawrence Livermore Laboratory (1971)

[7]   Hua, T.Q., Walker, J.S.: "MHD Considerations for Poloidal-Toroidal Coolant Ducts of Self-Cooled Blankets". Proc. Ninth Topical Meeting on the Techn. of Fusion Energy, Oct. 7-11, 1990, Oak Brook, IL

[8]   Grinberg, G.K., Kaudze, M.Z., Lielausis, O.A.: "Local MHD Resistances on a Liquid Sodium Circuit with a Superconducting Magnet". Magnituaya Gidrodinamika, No. 1, Januar-March 1985, pp. 121-126

[9]   Jauch, U.; Karcher, V.; Schulz, B.: "Thermophysical Properties in the System Li-Pb". KfK 4144, Sept. 1986

[10]   HIBBIT, KARLSSON and SORENSON, "ABAQUS User's Manual, Version 4.8, 1989," Providence, Rhode Islands, USA

[11]   M. KÜCHLE, "unpublished report," November 1988

[12]   U. JAUCH, et al., "Thermophysical Properties in the System Li-Pb,"KfK-3133, Kernforschungszentrum Karlsruhe (1986)

[13]   P. NORAJITRA, "Temperature and Stress Analysis of the Self-cooled Demo Liquid-metal Blanket (Option A)," KfK-4657, Kernforschungszentrum Karlsruhe (1990)

[14]   American Society of Mechanical Engineers Boiler and Pressure Vessels Code II, 1986
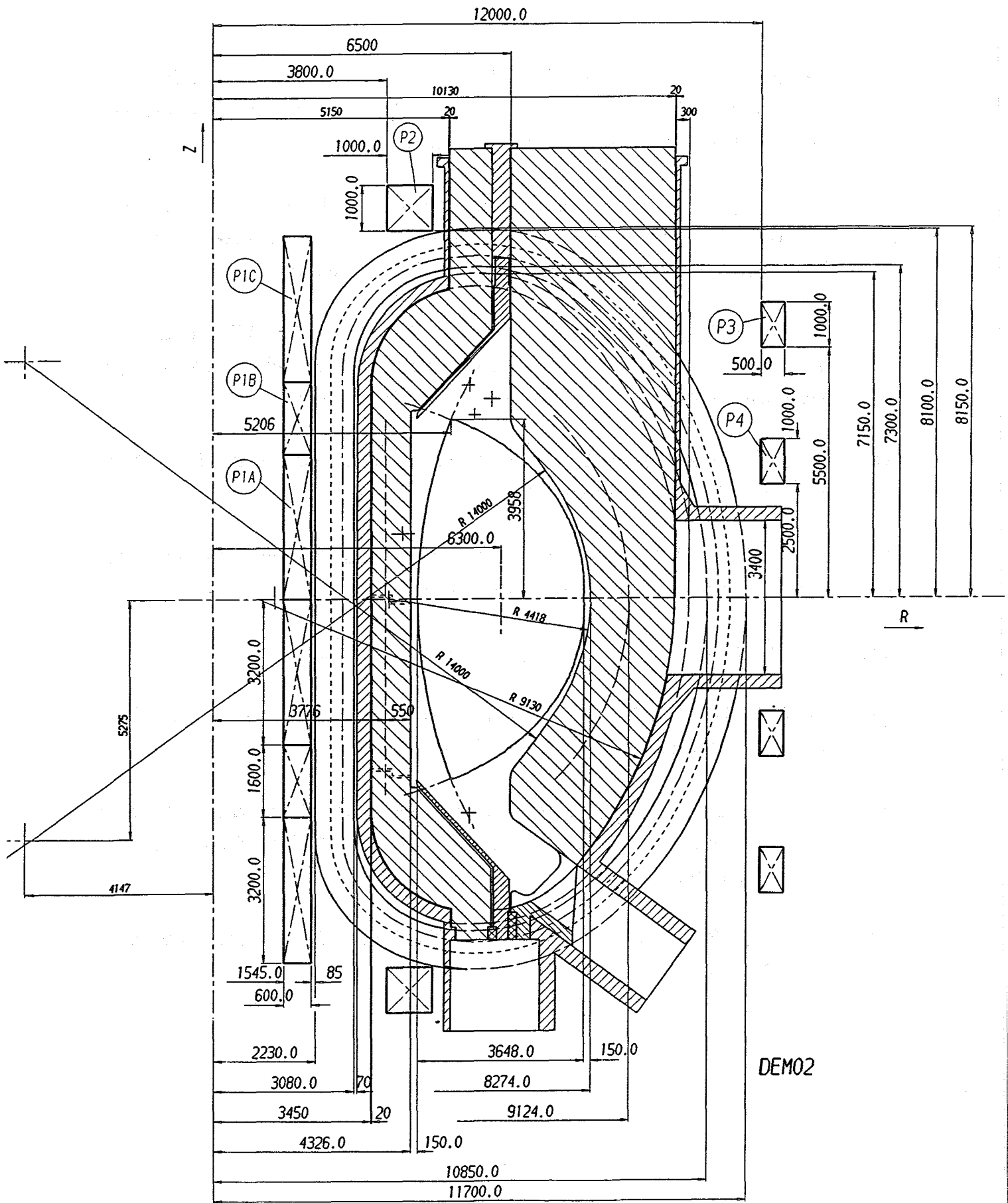
Fig. 2.1   Torus cross section of the DEMO-reactor

Upper
Inboard
Blanket Segment

Upper
Divertor

Breeding
PbLi Blanket

Shielding
Structure

Lower
Divertor

Lower
Inboard
Blanket Segment

Outboard
Blanket Segment

Breeding
PbLi Blanket
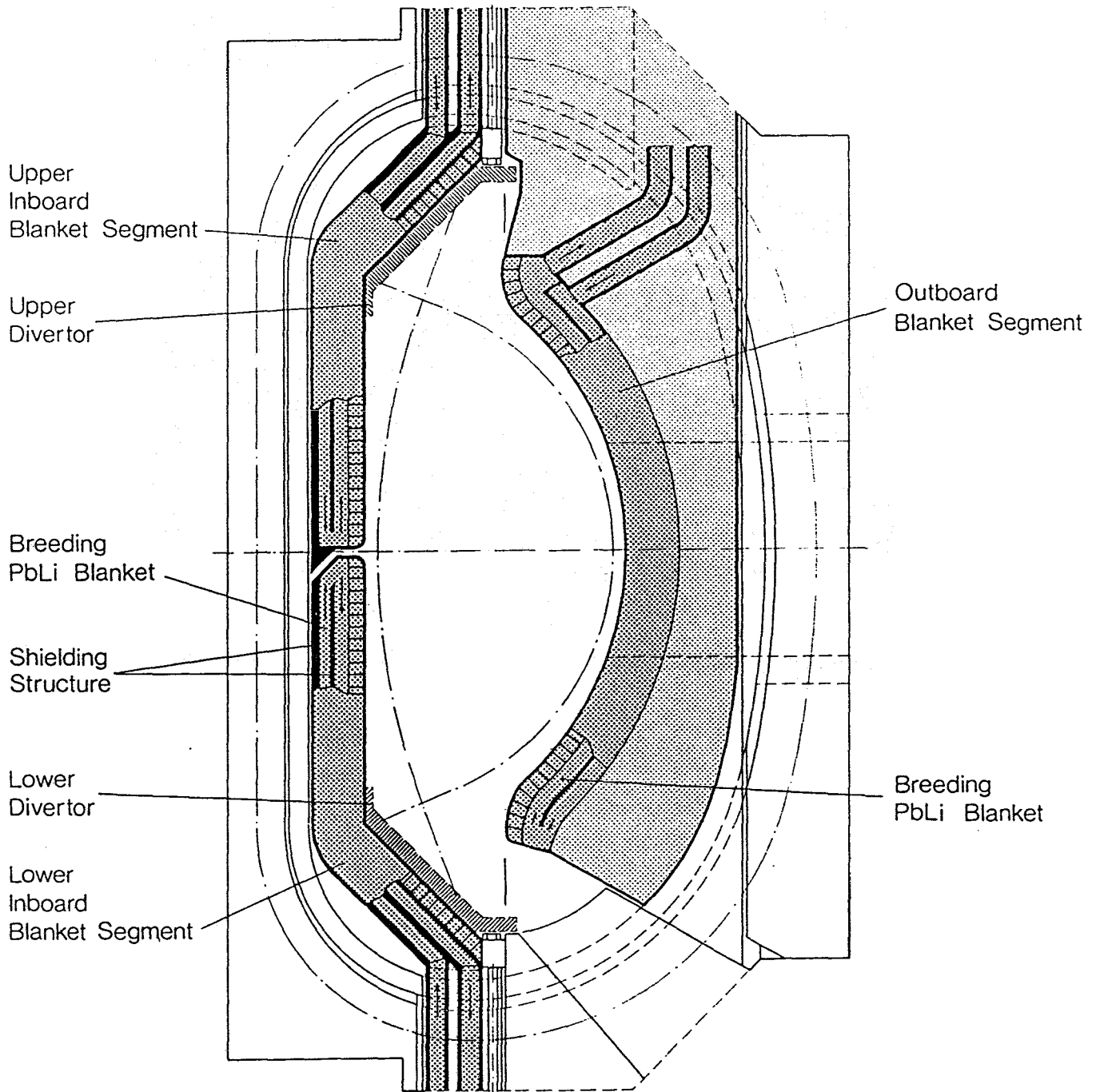
Fig. 2.1-1   Arrangement of the blanket segments

First Wall

Flow Channel Insert

Pb-17Li
Outlet   Inlet

Auxiliary
NaK-System

Corrugated First Wall

Steel
Structure
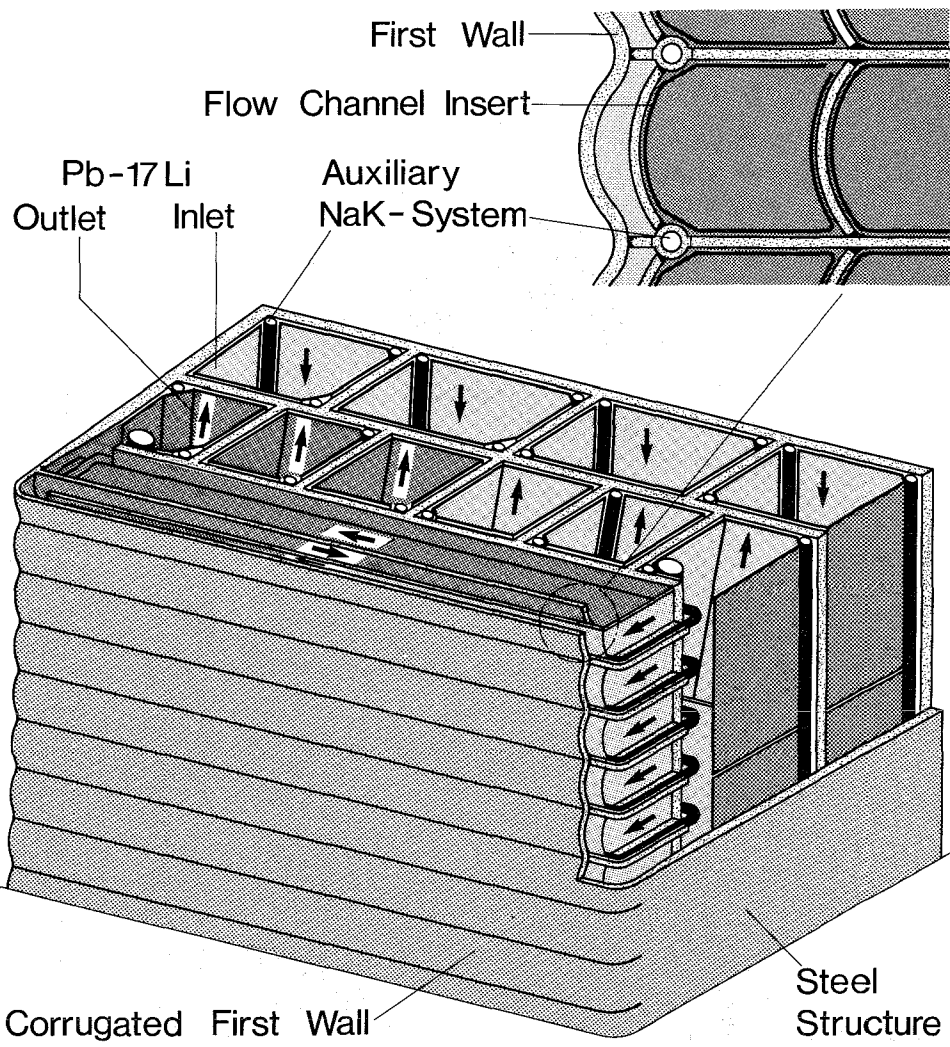
Fig. 2.1-2   Cross section of an outboard blanket segment

Fig. 2.1-3   Radial-toroidal cross-section of the 11.25° torus sector model

upper divertor

vacuum vessel

structure (MANET)

poloidal

radial

outboard blanket segment

inboard blanket segment

lower divertor

vacuum chamber
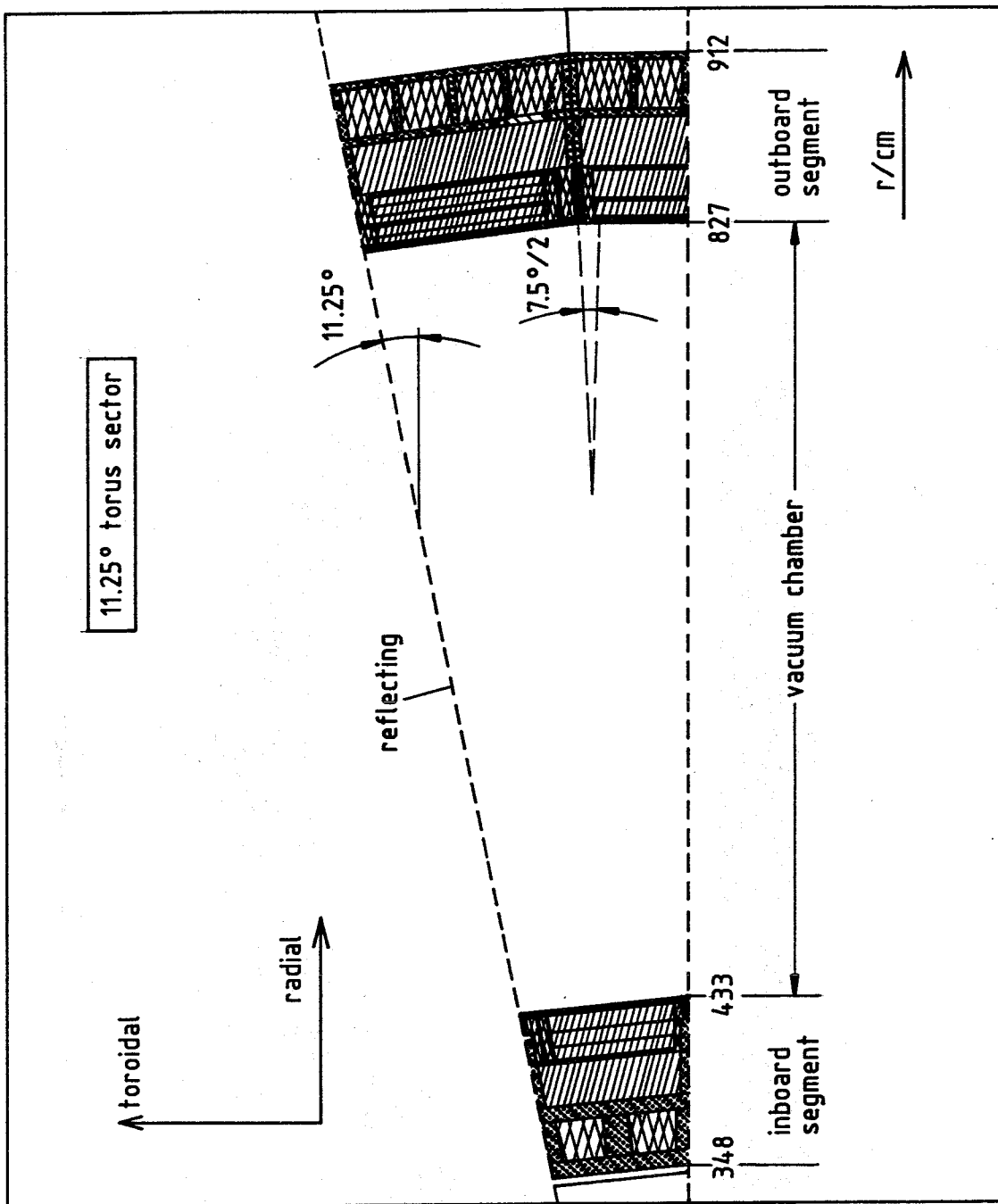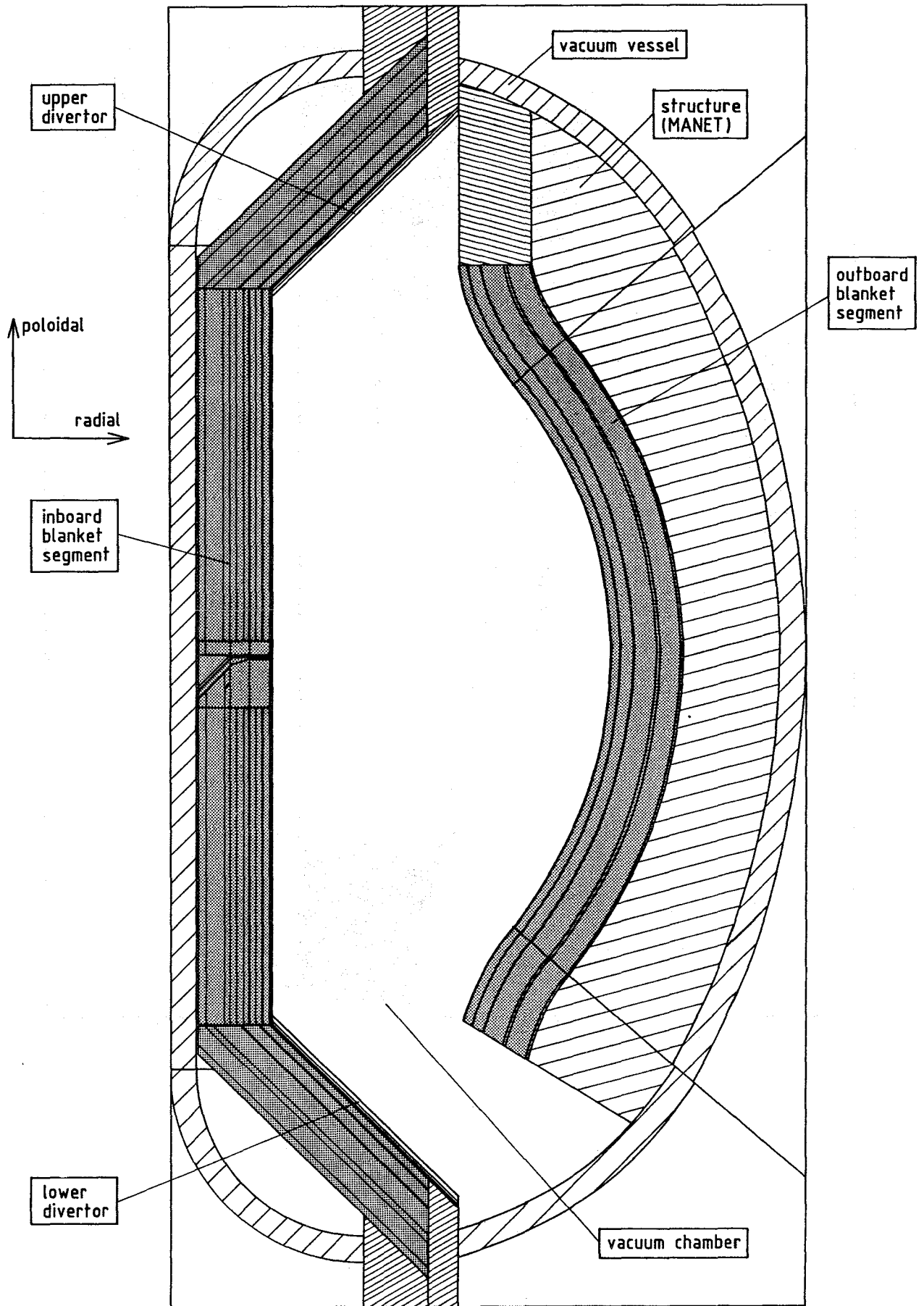
Fig. 2.1-4   Radial-poloidal cross-section of the 11.25° torus sector model

46

a) inboard segment

inboard segment

toroidal

radial

reflecting

11.25°

305 310 315   345 348   433

TF-coil — casing — gap — gap — vacuum vessel — gap — blanket segment

r/cm

steel SS 316   0.91Pb-17Li/0.04 NaK/ 0.05 MANET   1.0 Pb-17 Li

MANET steel   borated water   0.9 Pb-17 Li/0.1 MANET
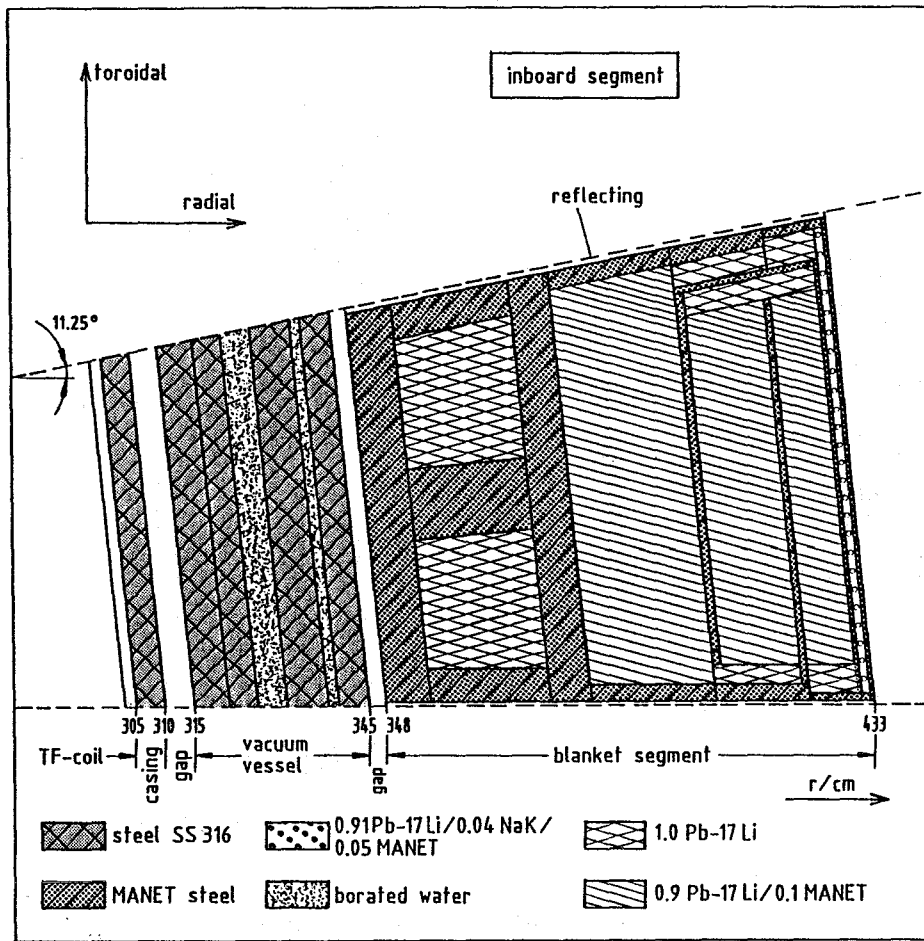
a) inboard segment

b) outboard segment

outboard segments

reflecting

toroidal

radial

meander II
meander III
meander IV
meander V

vacuum chamber

827   912

r/cm
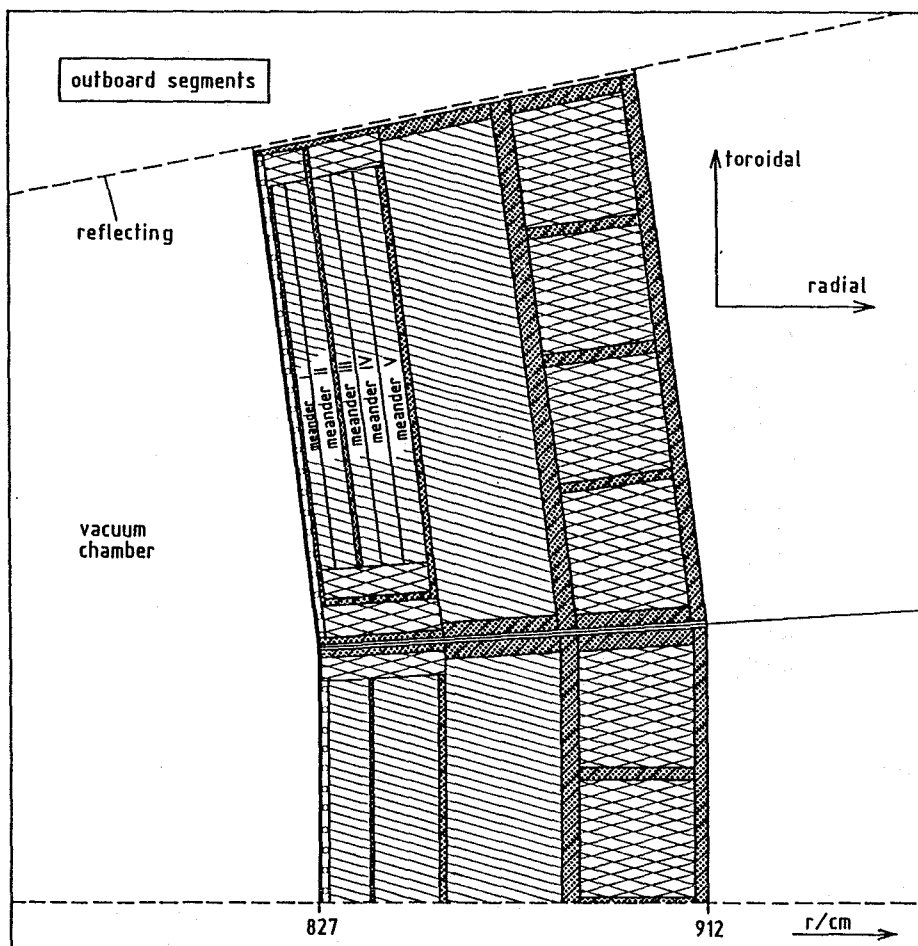
b) outboard segment

Fig. 2.1-5   Material composition in the blanket-segments (radial-toroidal cross-section)

47
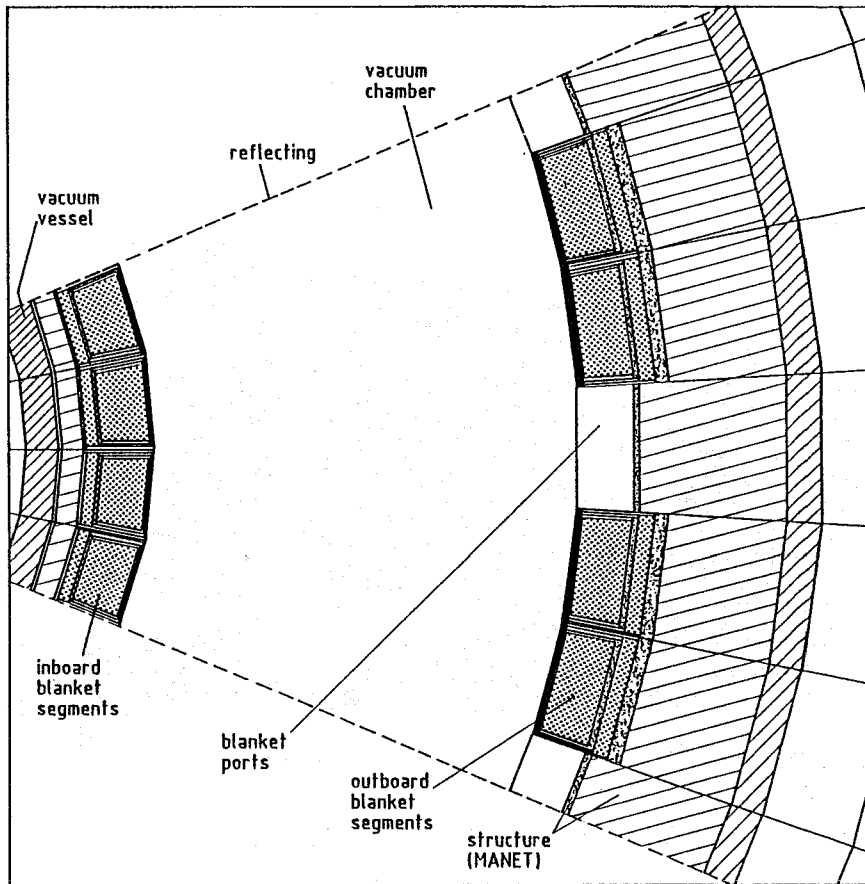
a) Radial-toroidal cross-section at torus mid-plane
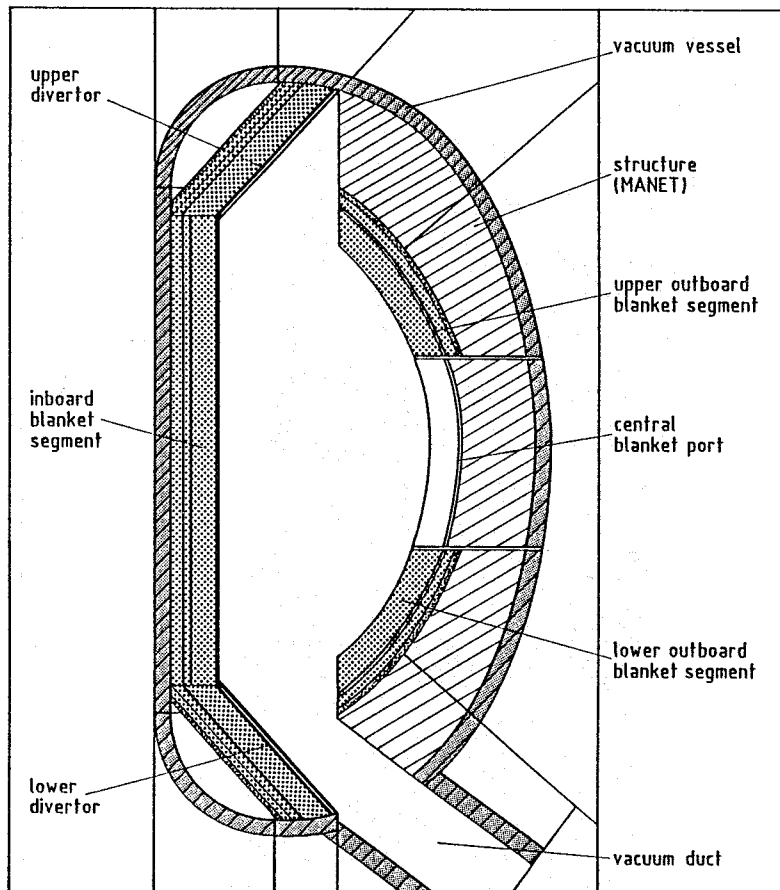
b) Radial-poloidal cross-section at the centre of the torus sector

Fig. 2.1-6   4 x 11.25° torus sector model for analyzing the port effect
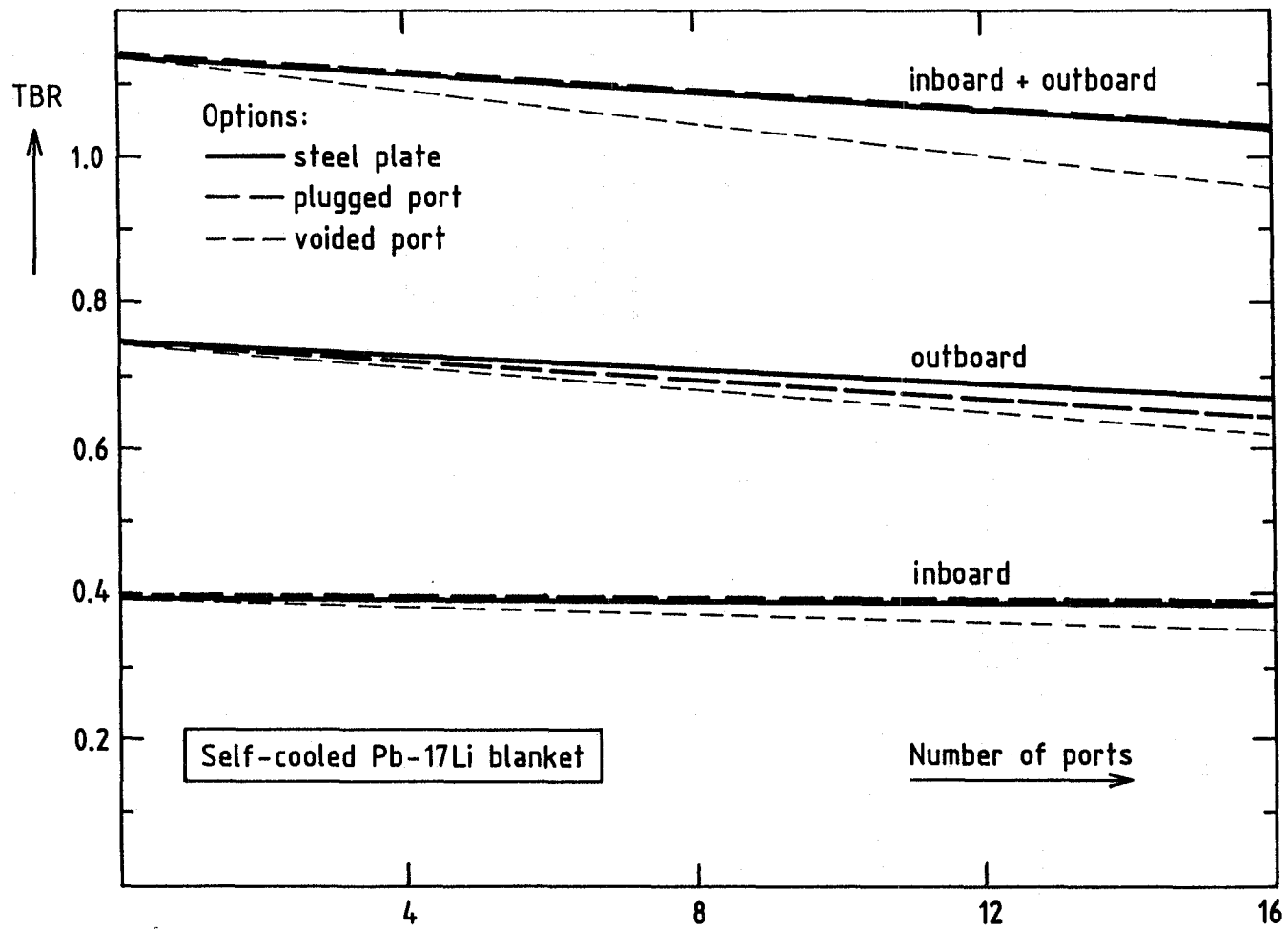
Fig. 2.1-7   Dependence of the tritium breeding ratio (TBR) on the number of outboard blanket ports
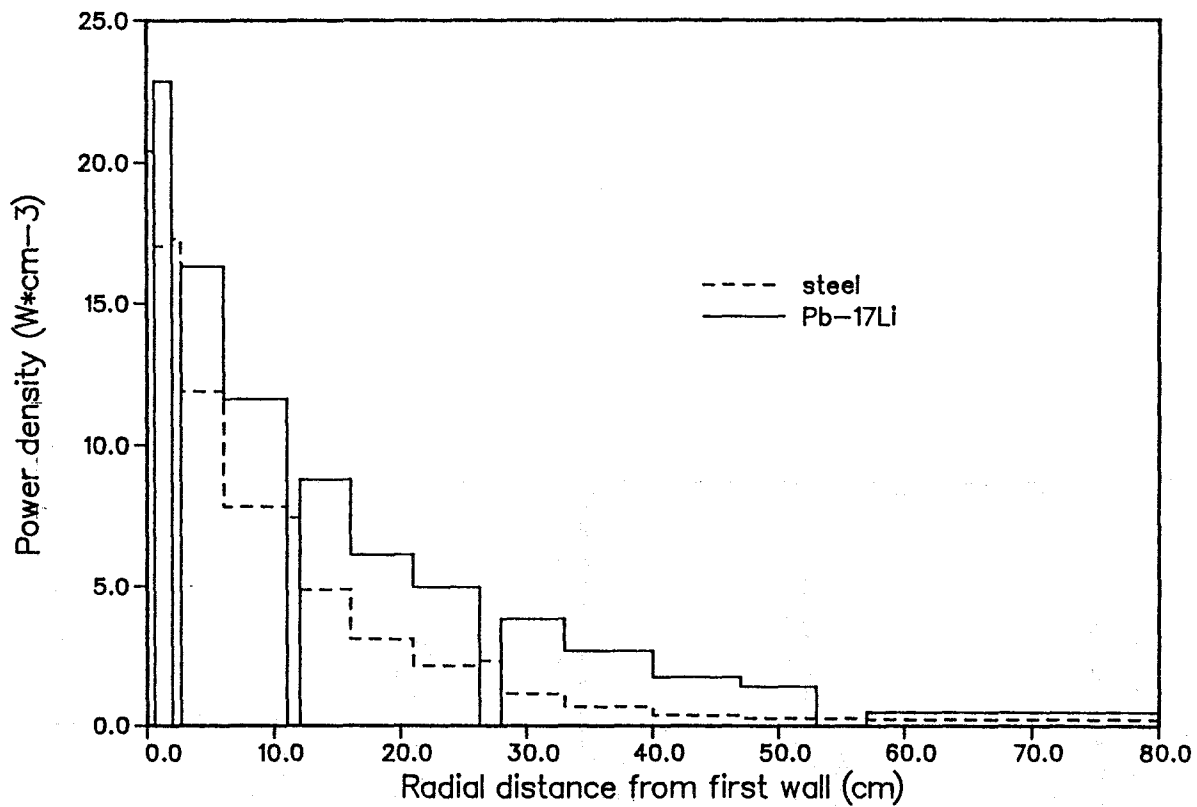
Fig. 2.1-8a)   Radial profiles of the power density at the torus mid-plane

DEMONET/outboard : poloidal profile of Pb—17Li power density
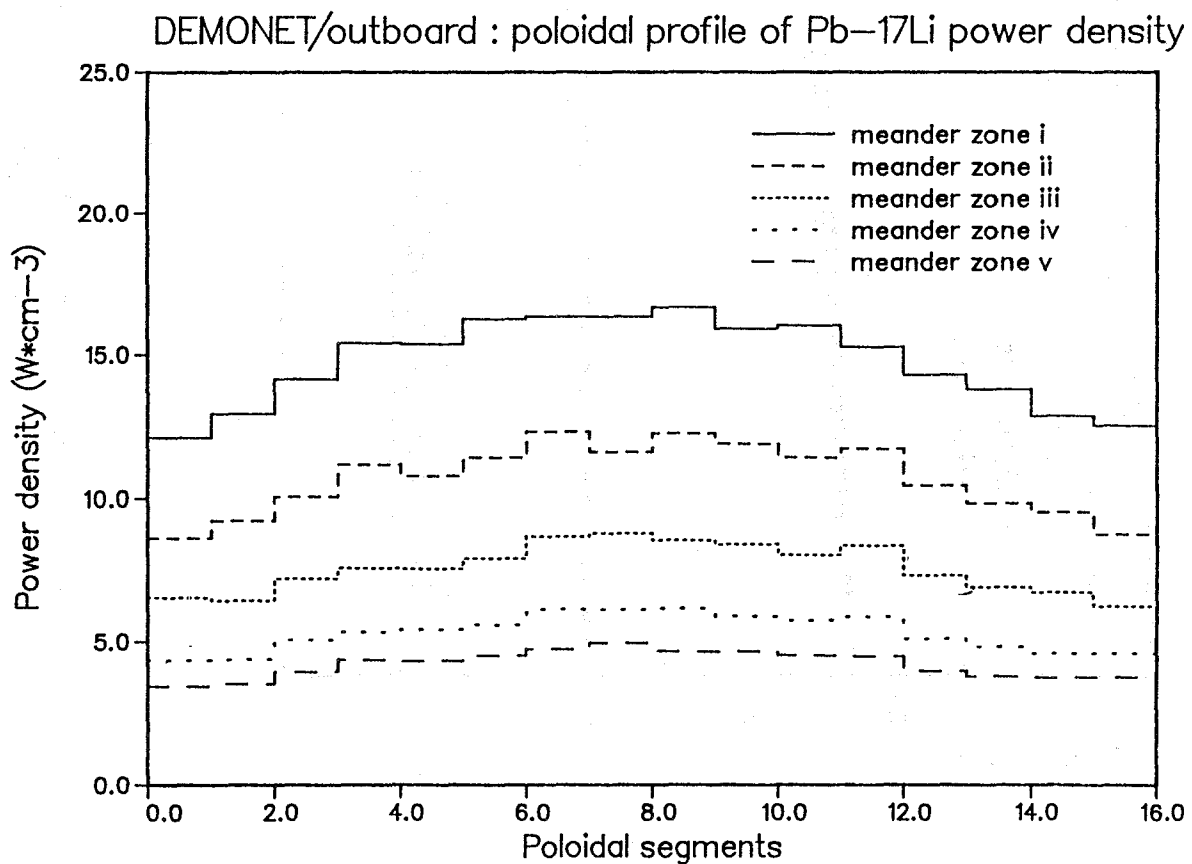
Fig. 2.1-8b)   Poloidal profiles of the Pb-17Li power density in the outboard
blanket segment

DEMONET/inboard : poloidally averaged neutron flux density
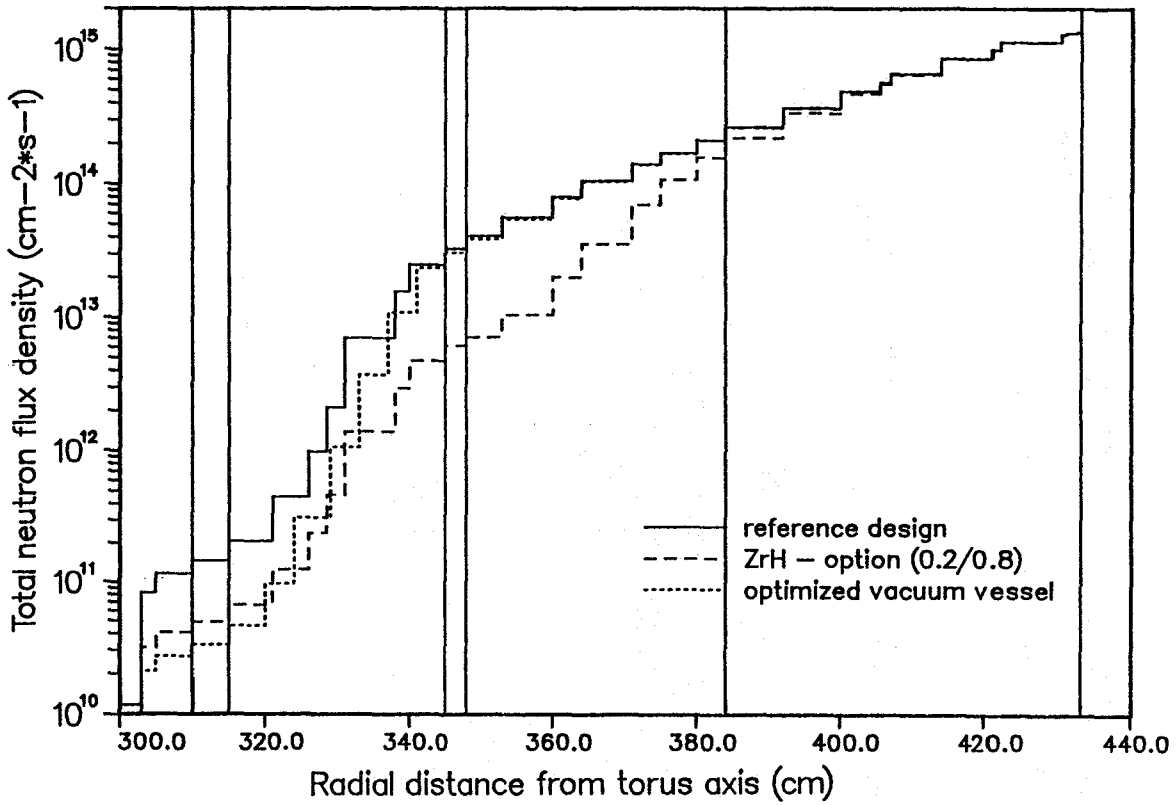
a) total neutron flux density

DEMONET/inboard : poloidally averaged neutron flux density
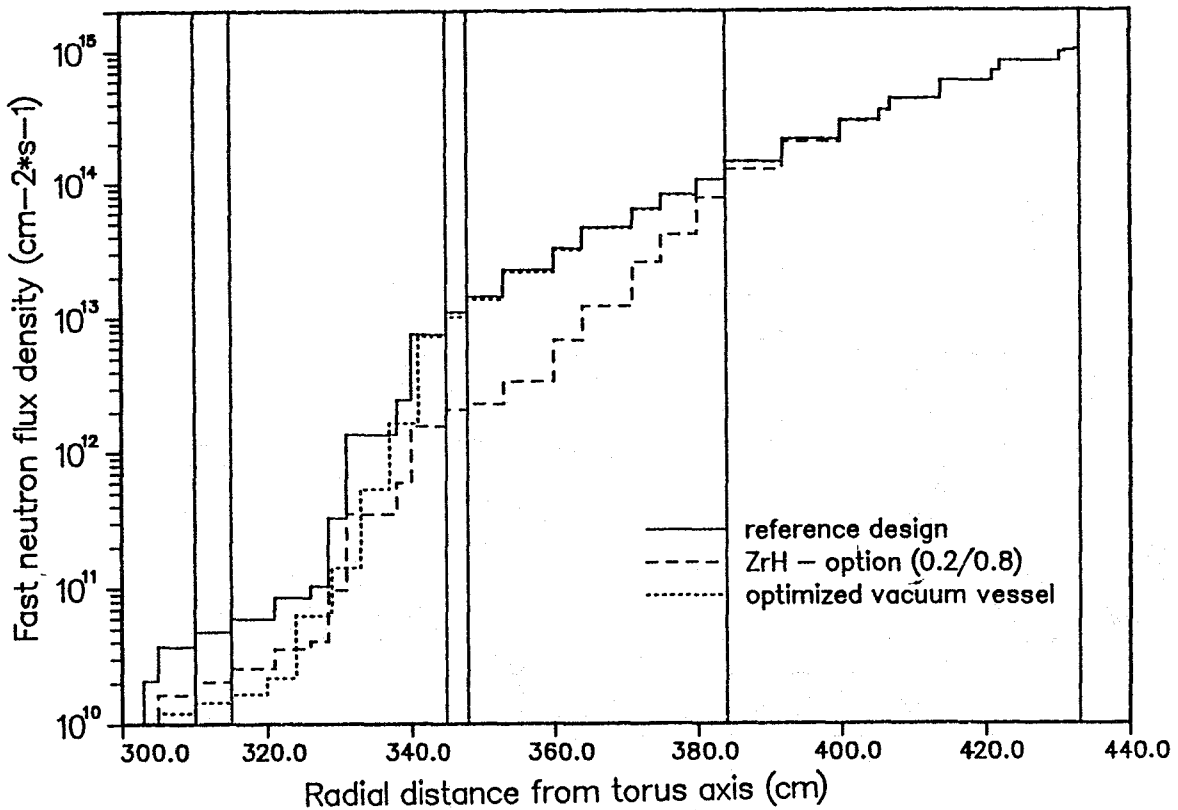
b) fast (E > 1.0 MeV) neutron flux density

Fig. 2.1-9   Radial profiles of the neutron flux density across the inboard
blanket segment and the vacuum vessel (poloidally averaged)

51
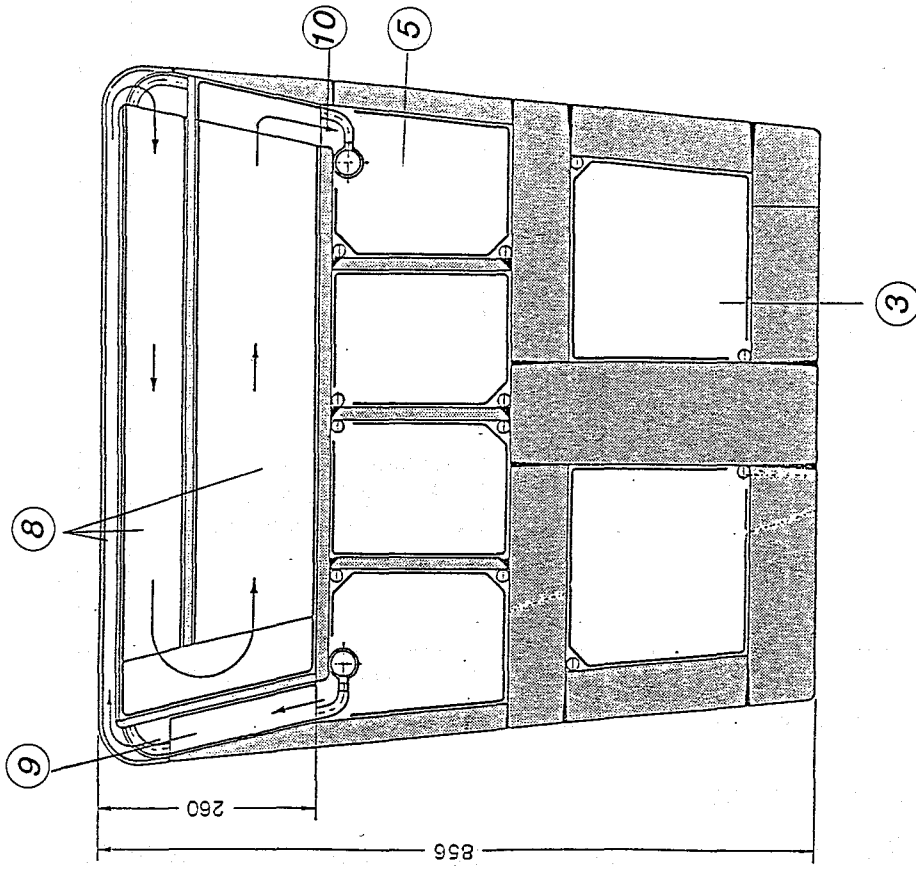
Cross section of a PbLi-Inboard blanket
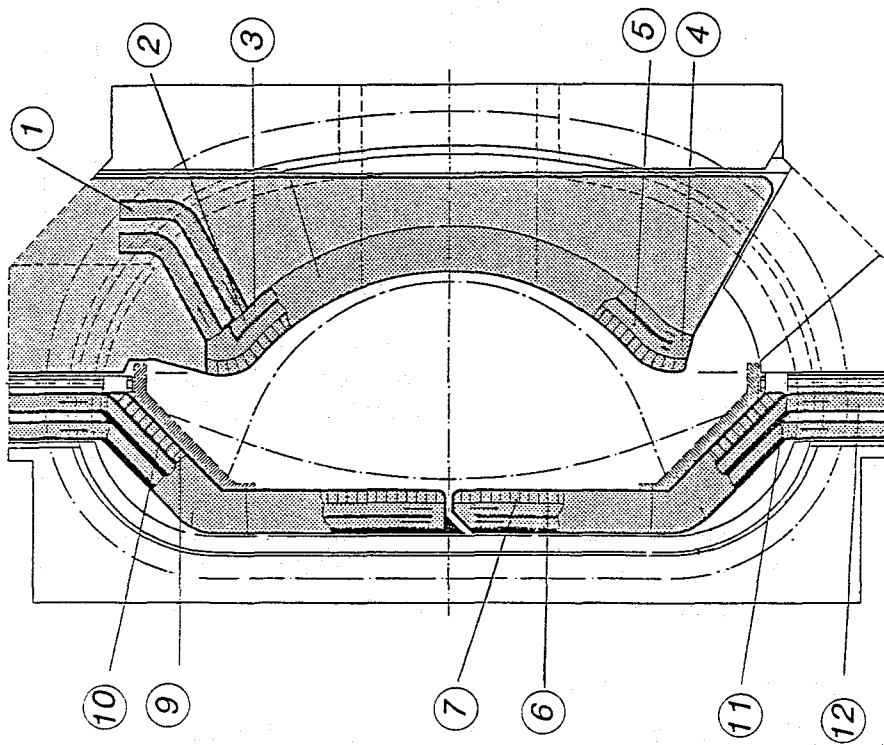
Scheme of a PbLi-Inboard and
outboard blanket

Fig. 2.1-10

52
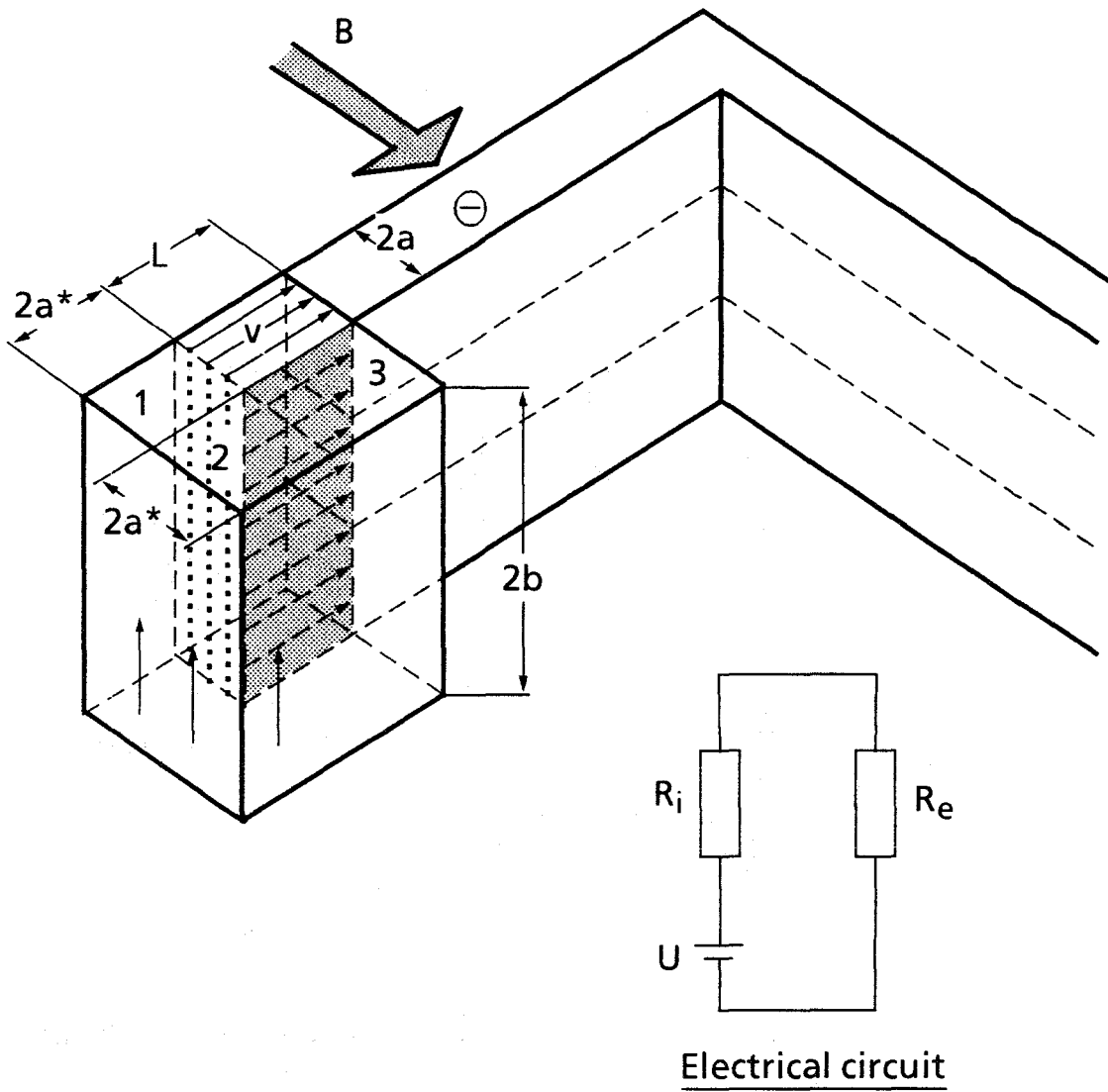
Induced voltage: $\quad U = 2b \cdot v \cdot B_\perp$

Current: $\quad I = \dfrac{U}{R_i + R_e}$ $\qquad R_i = \dfrac{2b}{2a\,L\,\sigma}$

Lorentz force: $\quad F_L = 2b \cdot I \cdot B_\perp$ $\qquad R_e = \dfrac{2b}{3(2a^* \cdot L) \cdot \sigma}$

Pressure drop: $\quad \Delta p = \dfrac{3}{4} \cdot L \cdot v \cdot \sigma \cdot B_\perp^2$ $\qquad$ with $a^* = a$; $L = 2a$

Fig. 2.1-11   Model of the poloidal-radial transition
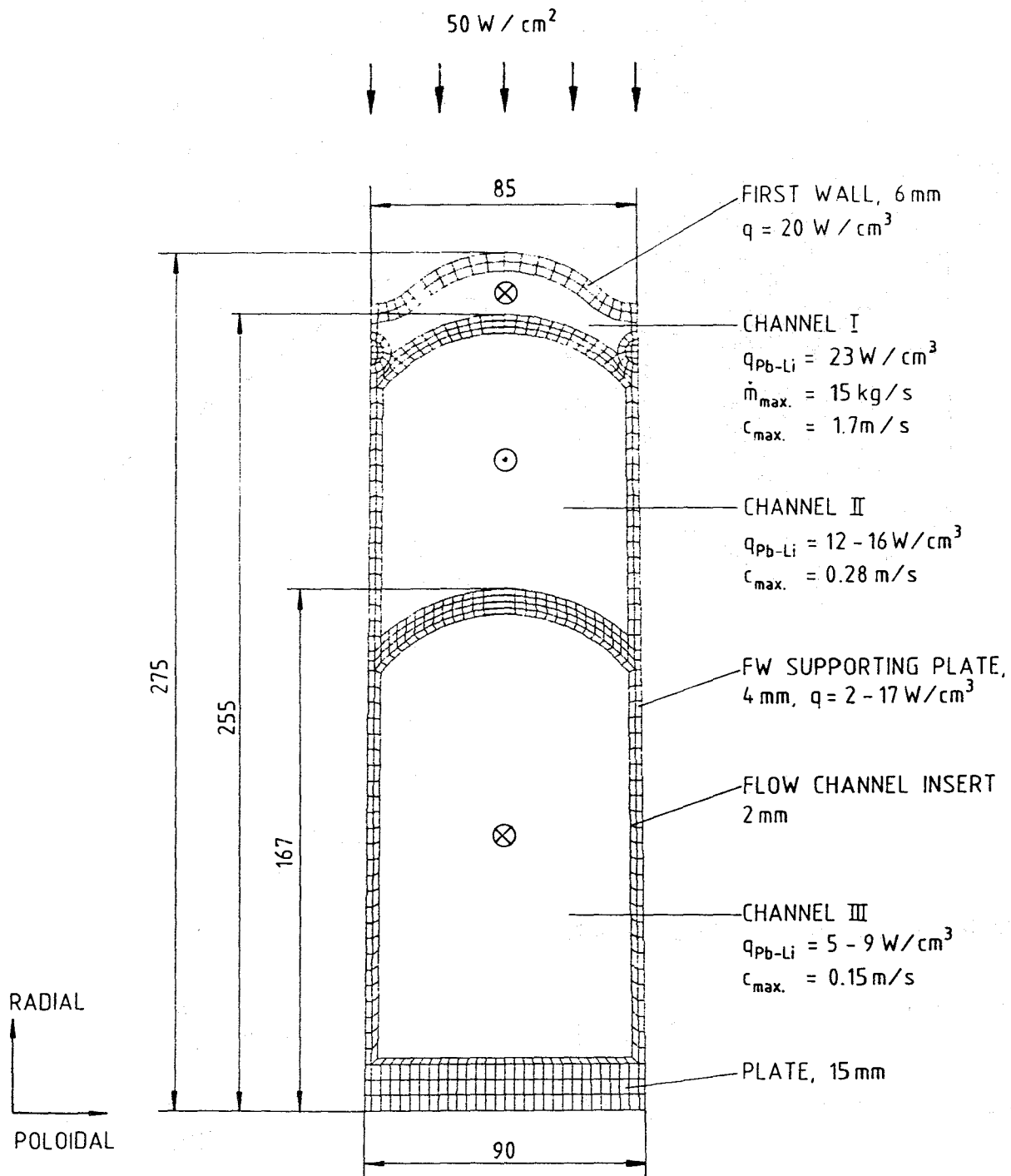
Fig. 2.1-12　Cross-section of the front region with meander-shaped coolant channels

The following labels and values appear in the figure:

$50\ W/cm^2$

85

FIRST WALL, 6 mm
$q = 20\ W/cm^3$

CHANNEL I
$q_{Pb-Li} = 23\ W/cm^3$
$\dot{m}_{max.} = 15\ kg/s$
$c_{max.} = 1.7\ m/s$

CHANNEL II
$q_{Pb-Li} = 12 - 16\ W/cm^3$
$c_{max.} = 0.28\ m/s$

FW SUPPORTING PLATE,
4 mm, $q = 2 - 17\ W/cm^3$

FLOW CHANNEL INSERT
2 mm

CHANNEL III
$q_{Pb-Li} = 5 - 9\ W/cm^3$
$c_{max.} = 0.15\ m/s$

PLATE, 15 mm

275

255

167

90

RADIAL

POLOIDAL

$q = 50 \, W / cm^2$

FIRST WALL, 6 mm
$q = 20 W / cm^3$

541°
532°
415°
532°
409°
409°
493°
493°
395°
323°
395°
329°

347°
347°

358°
358°
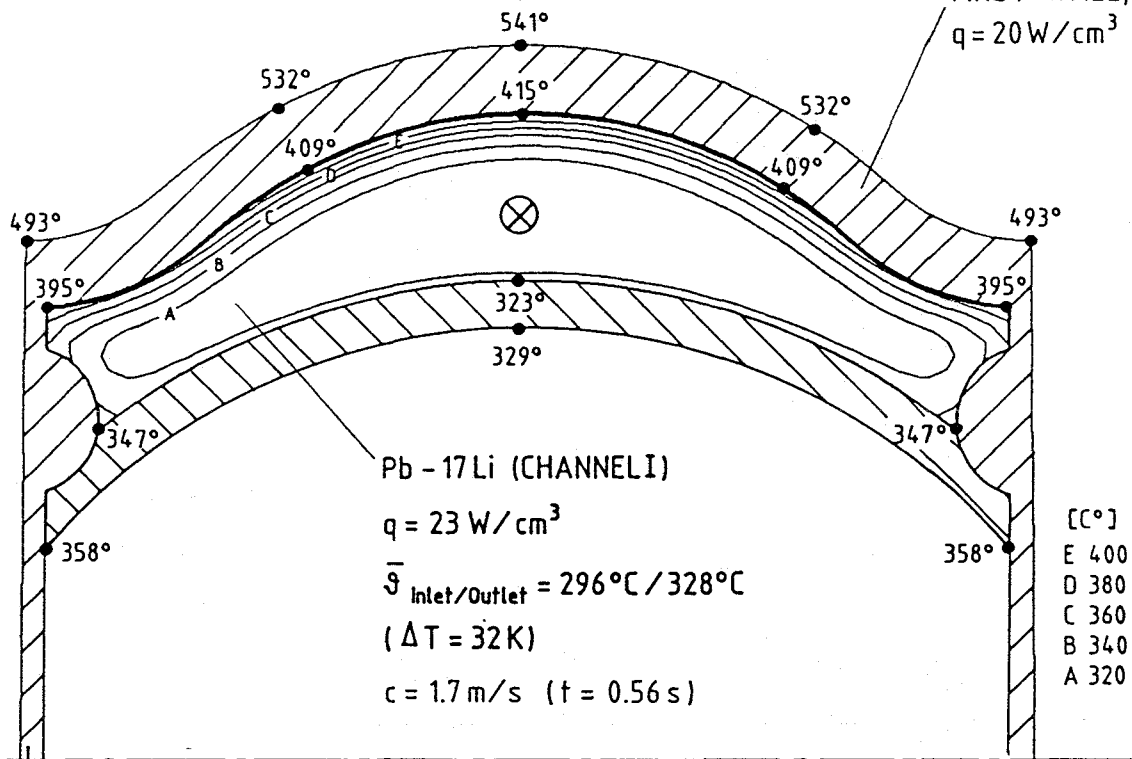
Pb – 17 Li (CHANNEL I)

$q = 23 \, W / cm^3$

$\bar{\vartheta}_{Inlet/Outlet} = 296°C / 328°C$

$(\Delta T = 32 \, K)$

$c = 1.7 \, m / s \quad (t = 0.56 \, s)$

RADIAL

POLOIDAL

[C°]
E 400
D 380
C 360
B 340
A 320

FW SUPPORTING PLATE, 4 mm
$q = 2 - 17 \, W / cm^3$

Fig. 2.1-13   Temperature distribution at the exit of the first wall cooling channel

[°C]

J 384
I 380
H 376
G 372
F 368
E 364
D 360
C 356
B 352
A 348

RADIAL

POLOIDAL

Pb – 17 Li (COOLANT CHANNEL II)

$q = 12 - 16$ W / cm³

$\bar{\vartheta}_{Inlet/Outlet} = 331°C / 366°C$

$(\Delta T = 35 K)$

$c = 0.28$ m/s $(t = 3.5 s)$

MAX. 385 °C
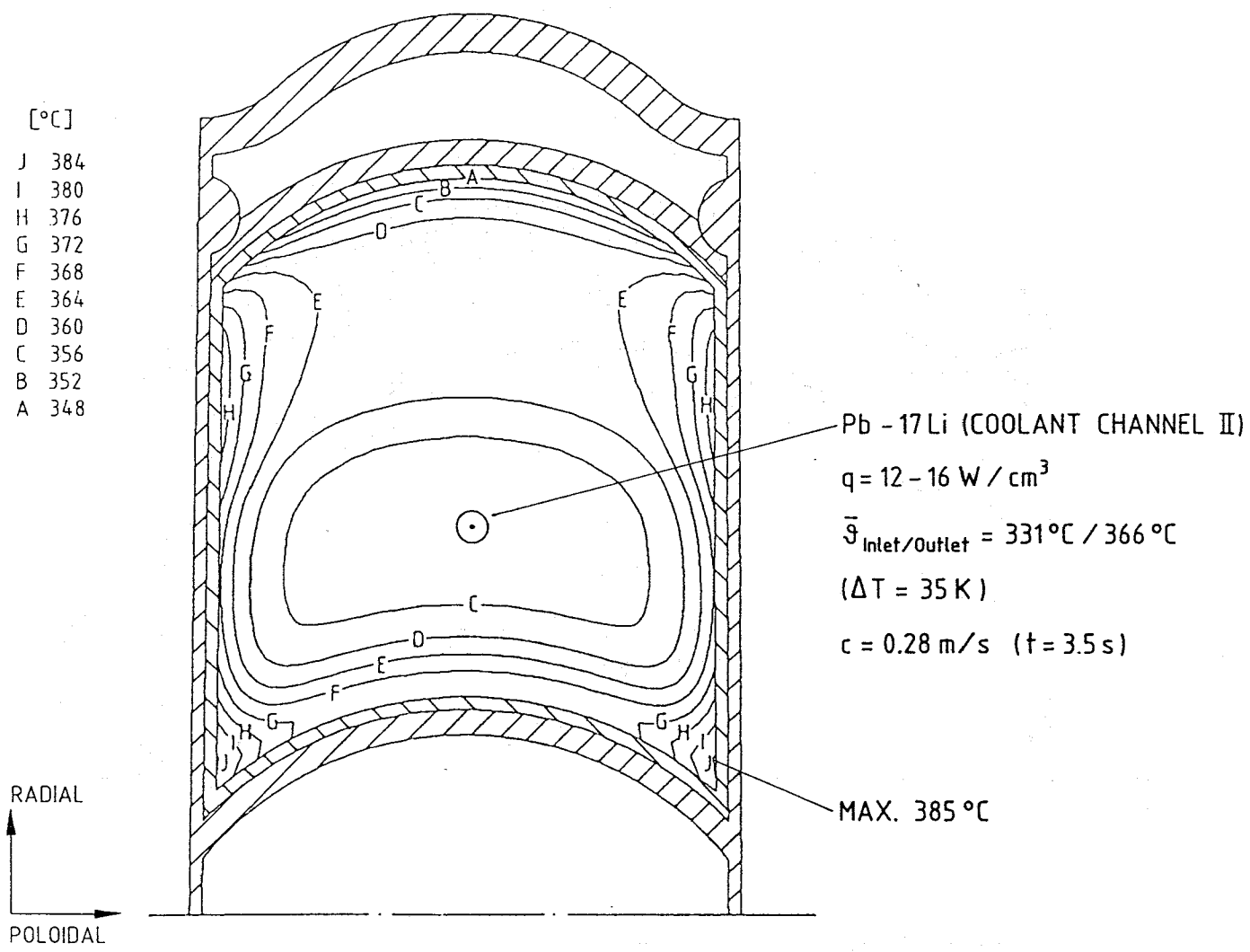
Fig. 2.1-14   Temperature field at the exit of cooling channel II

MAX. 411 °C

Pb – 17 Li (COOLANT CHANNEL III)

$q = 5 - 9 \, W/cm^3$

$\bar{\vartheta}_{Inlet/Outlet} = 370\,°C / 396\,°C$

$(\Delta T = 26 \, K)$

$c = 0.15 m/s \, (t = 6.6 \, s)$

[°C]
F 410
E 406
D 402
C 398
B 394
A 390

RADIAL

POLOIDAL
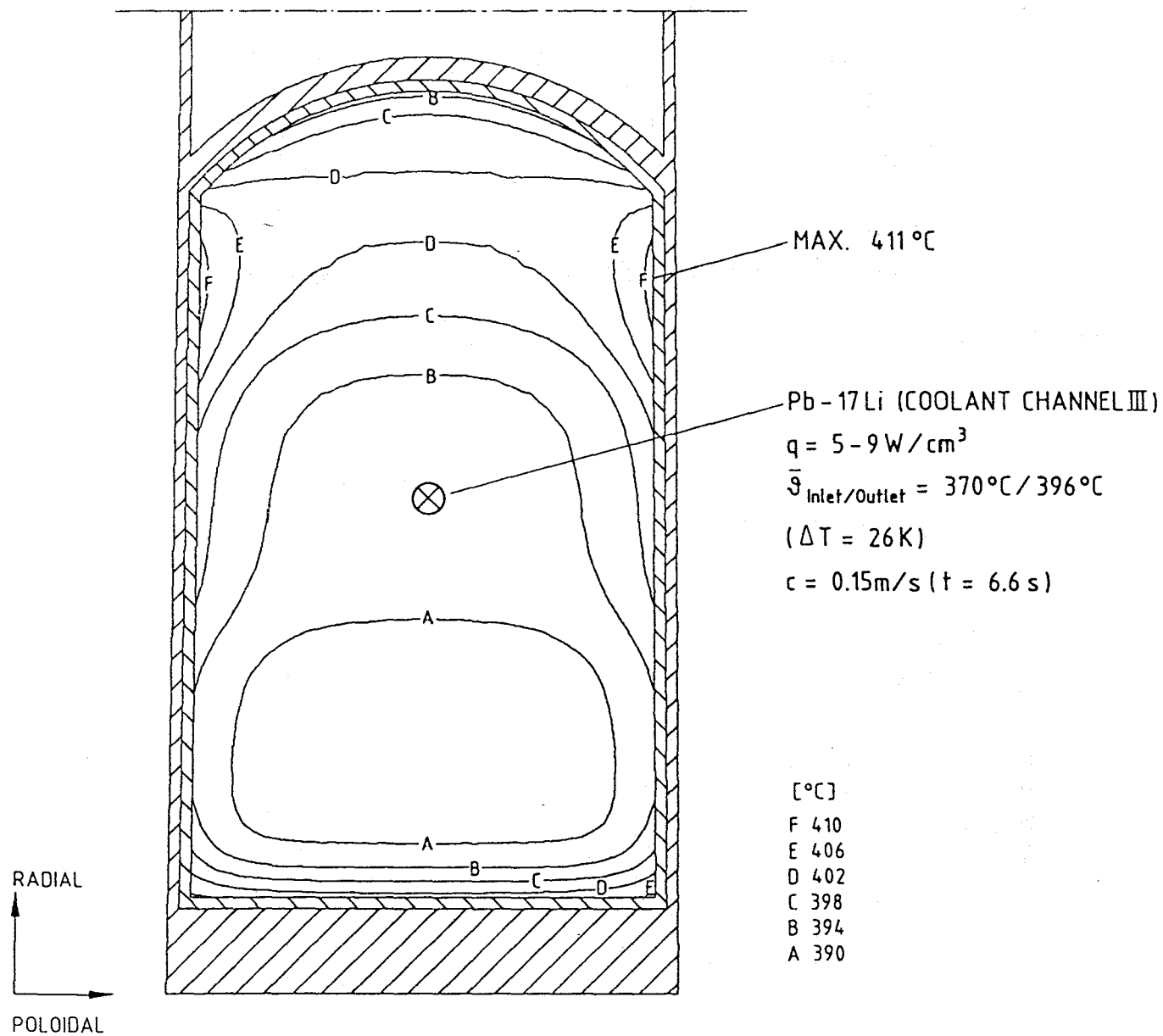
Fig. 2.1-15   Temperature field at the exit of cooling channel III
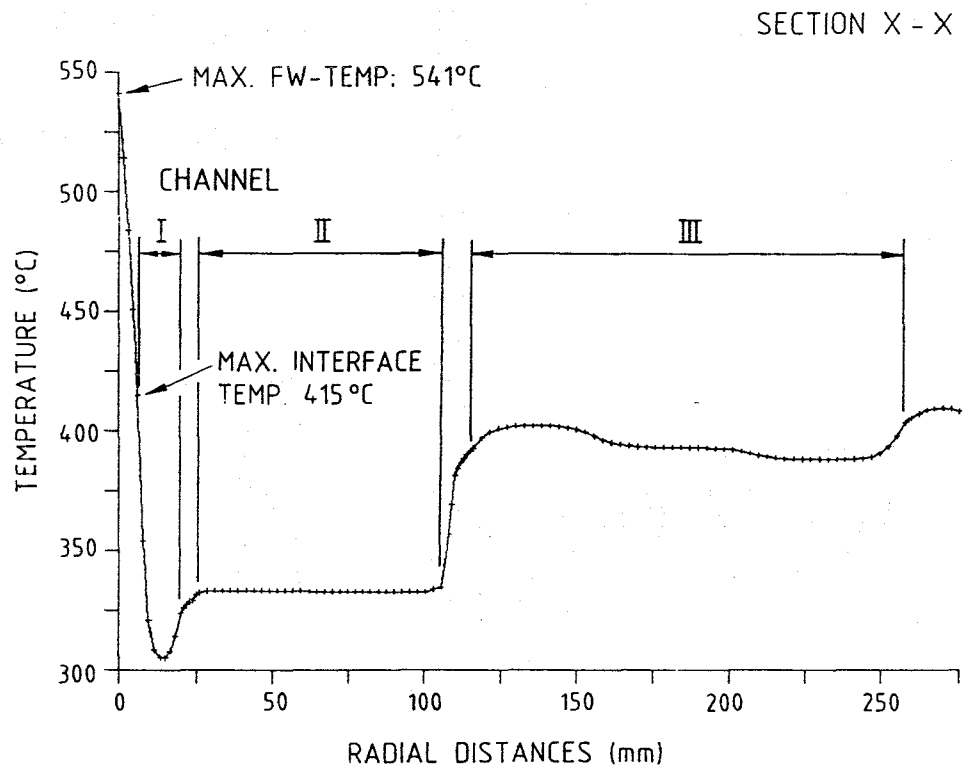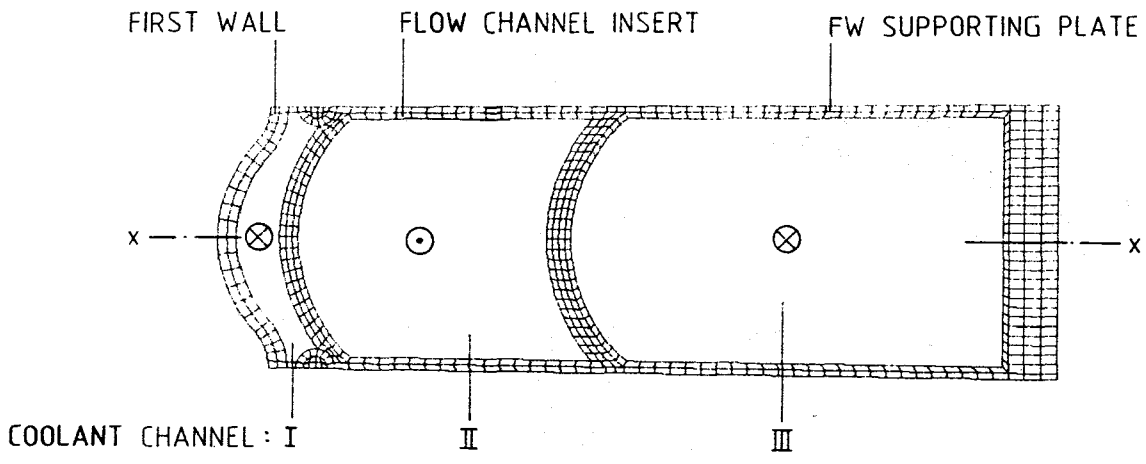
Fig. 2.1-16   Radial temperature profile in the front region with meander-shaped cooling channels

2.2 Alternative blanket designs

Self-cooled liquid metal blankets are especially difficult to design for the inboard
region of the torus. In this region the strength of the magnetic field is roughly 50%
higher than in the outboard region and the space available for the blanket is more
limited. The resulting MHD pressure drop is therefore really critical. One possibil-
ity to avoid this problem is to use a thick layer of beryllium in the front part of the
outboard blanket. The neutron multiplication in this material increases tritium
breeding so much that tritium self-sufficiency can be achieved without the use of
breeding blankets at the inboard side of the torus. This design is described in [1]
and shown in Fig. 2.2-1 and 2.2-2. There are water-cooled steel reflectors arranged
at the inboard region. The flow principle in the outboard segments is identical to
the one employed in the reference design with first wall cooling in toroidal direc-
tion and meander-shaped channels in the front region. The beryllium plates with
a thickness of roughly 80 mm are fabricated in two halves, both are canned with a
0.5 mm thick steel sheet after oxidizing the entire beryllium surface. Beryllium
oxide is an excellent electrical insulator, therefore, it decouples the liner from the
beryllium plates. This insulation is necessary to avoid excessively large currents
flowing perpendicular to the plates which would cause the multi-channel problem
as explained in section 2.1.3.

A neutronics analysis has shown [2] that a 300 mm thick beryllium multiplier in
the outboard blanket together with a steel reflector at the inboard side leads to
roughly the same tritium breeding ratio as breeding blankets without beryllium
at both the outboard and inboard side. The alternative for self-cooled Pb-17Li
blankets is therefore either to find solutions for the MHD-problems encountered in
designing inboard systems (for example split the inboard segment into two halves,
see reference design) or to use beryllium in the order of 200 tons for a DEMO-
reactor (alternative design).

A completely different approach is to combine helium-cooling of the first wall with
self-cooling of the breeding zone of a Pb-17Li blanket. A segment cross-section of
such a dual-coolant concept is shown in Fig. 2.2-3. This concept is characterized by
a stiff first wall box with rectangular cooling channels in toroidal direction. Con-
nected to this box is a grid of steel plates forming large ducts for liquid metal cool-
ing in poloidal direction. This is a very novel design not yet analysed in details.
The main advantages are a real double containment of the liquid metal, a more
simple geometry and much less problems with liquid metal cooling. Most of the

MHD-problems in self-cooled liquid metal blankets are caused by the surface heat flux to the first wall requiring relatively high liquid metal velocities. This is avoided here by using gas-cooling which results in much lower temperatures at the steel/liquid metal interface and decisively lower liquid metal velocities. First estimates indicate that this concept is feasible even without splitting the inboard segment into two halves and that the breeding ratio will be roughly the same as for the reference design. The disadvantage is the need for a second coolant with separate ancillary systems. On the other hand, there is no auxiliary cooling system required for after heat removal since this is possible either with the helium cooling of the first wall or with the liquid metal cooling of the breeding zone.

References to section 2.2

[1]   S. Malang, et al., Self-Cooled Blanket Concept Using Pb17-Li as Liquid Breeder and Coolant, Fusion Engng.Des. 14 (1991) 373-399.

[2]   S. Malang, K. Arheidt and U. Fischer, Test Module in NET for a Self-cooled Liquid-metal Blanket Concept, in: Proc. 15th Symp. on Fusion Technol, Utrecht, The Netherlands, September 1988, Vol. 2, ed. A.M. van Ingen (Elsevier Sc. Pub., Amsterdam, 1989), pp. 1223-1228.

NaK - System

Pb-17Li-System

Liquid Metal
Inlet
Outlet

Beryllium
Neutron Multiplier

First Wall
Supporting Plates

Corrugated
First Wall

Pb-17Li
Flow Scheme
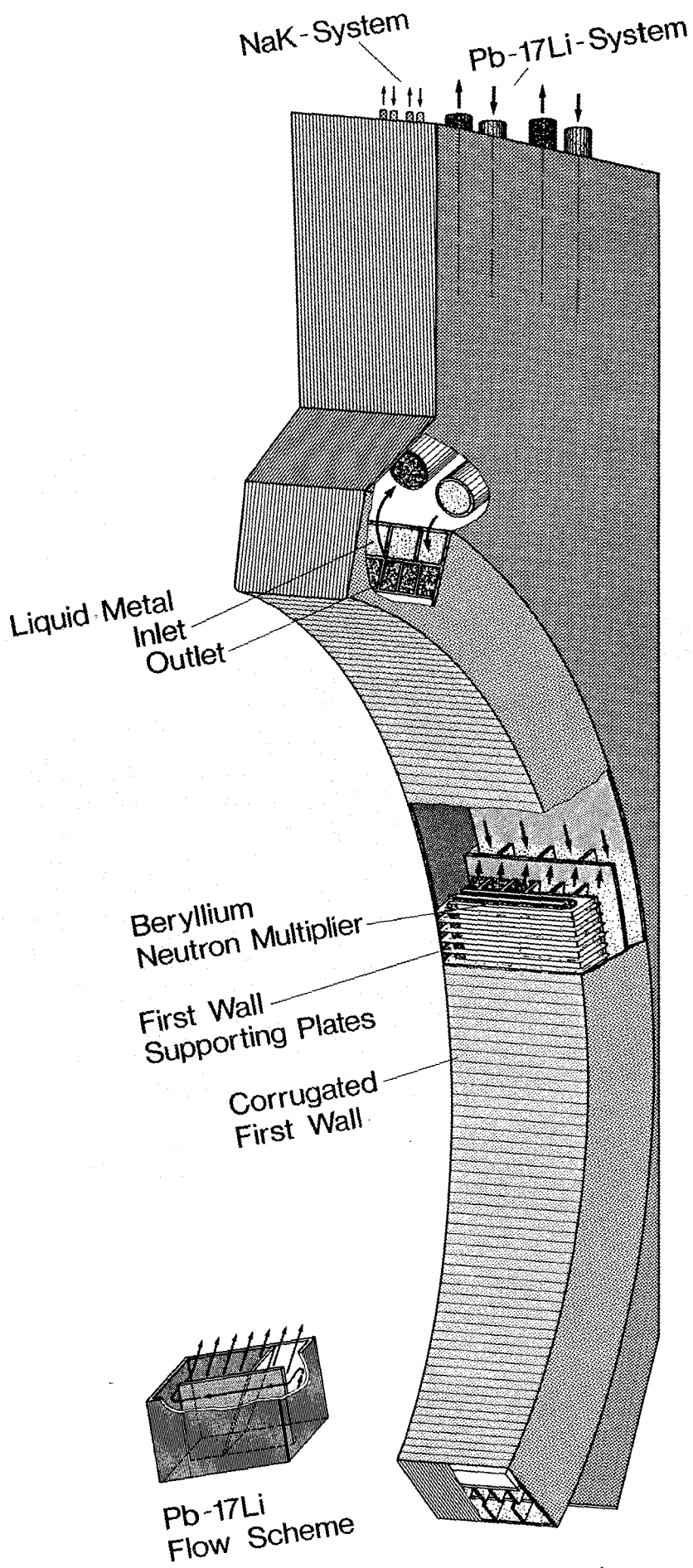
Fig. 2.2-1   Outboard blanket segment

Detail X

First Wall Supporting Plates

Pb-17Li

Corrugated First Wall

Flow Channel
Inserts

Beryllium
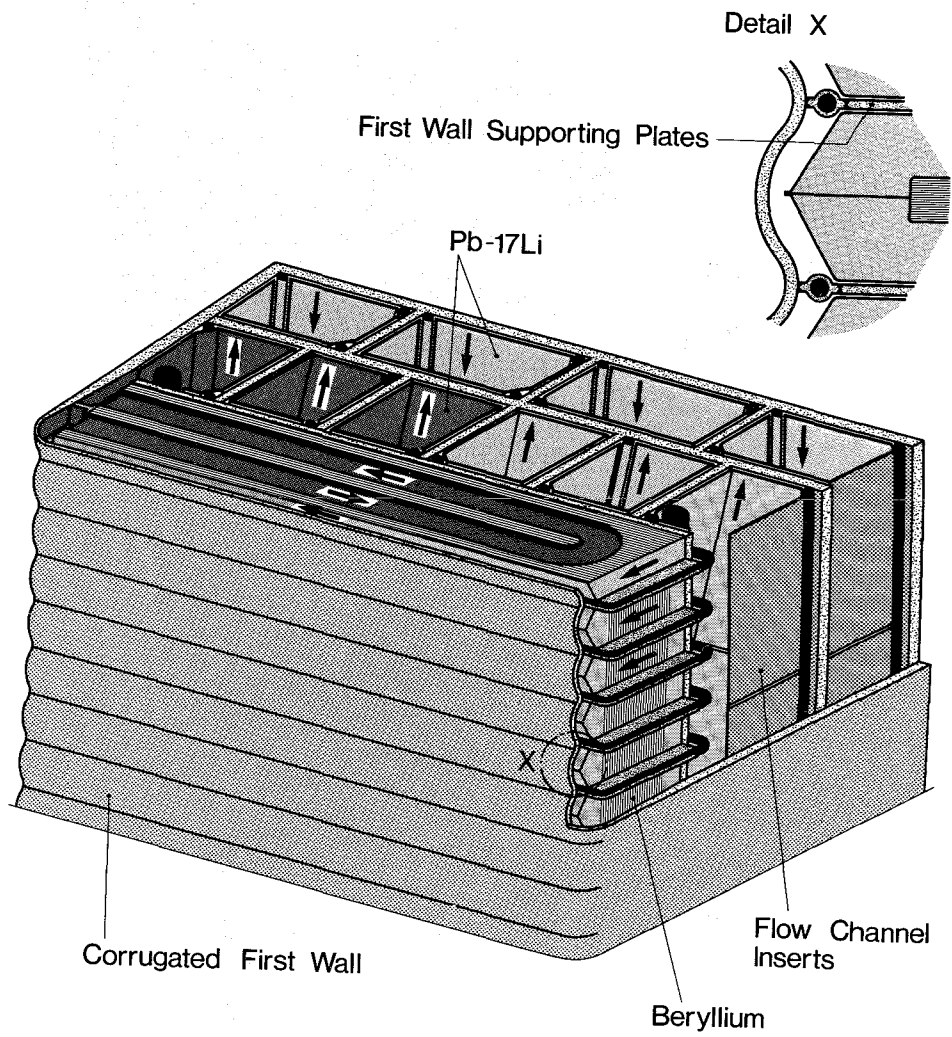
Fig. 2.2-2   Cross section of an outboard blanket segment and the first wall
cooling channels
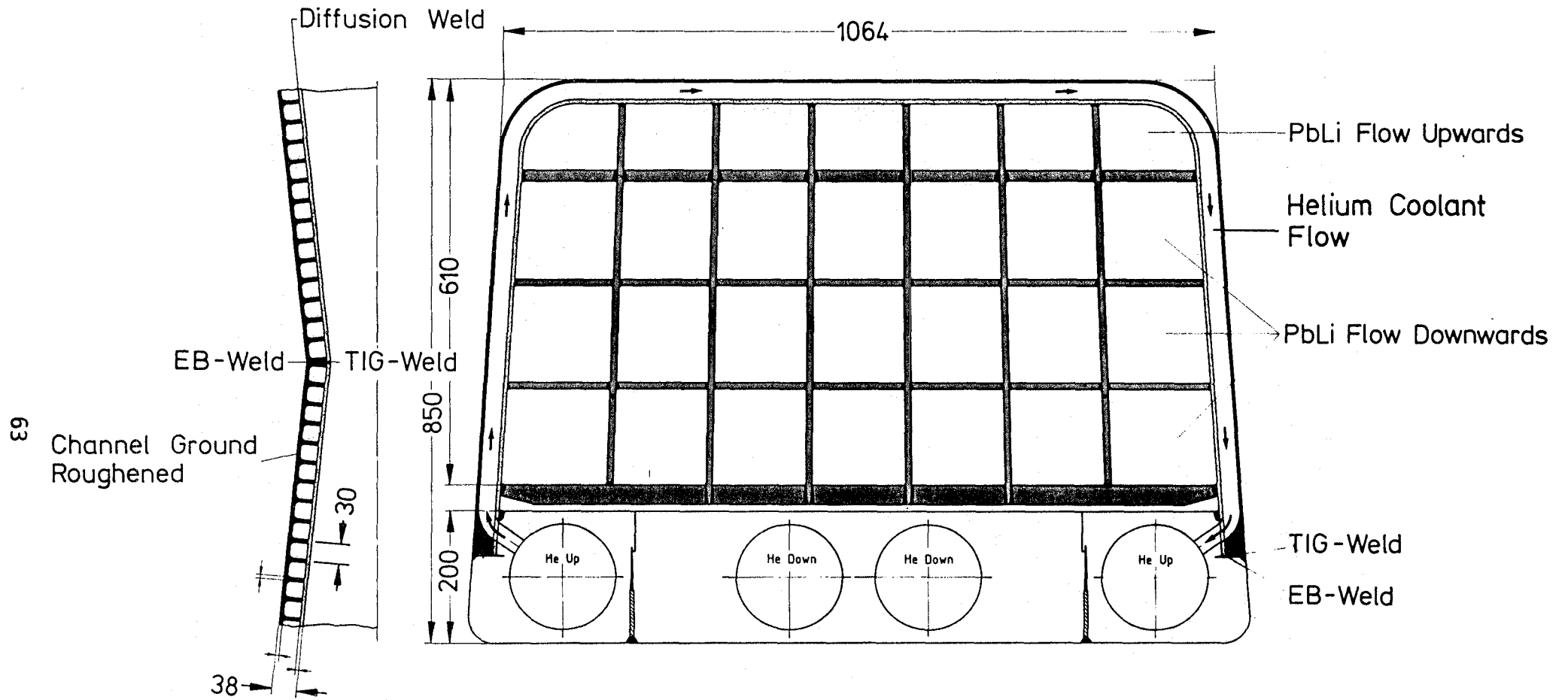
Fig. 2.2-3   Self-cooled liquid metal breeder blanket with helium-cooled first wall

Diffusion Weld

1064

PbLi Flow Upwards

Helium Coolant Flow

PbLi Flow Downwards

610

850

200

30

38

EB-Weld — TIG-Weld

Channel Ground Roughened

TIG-Weld

EB-Weld

He Up   He Down   He Down   He Up

63

2.3 Ancillary loop system
2.3.1 Loop concept

The ancillary loops are necessary for the heat and tritium transport from the blanket to the power conversion system and to the fuel cleaning system respectively. 80 loop systems are proposed for DEMO, 48 for the outboard blankets and 32 for the inboard blankets. The principle operation of an ancillary loop system for the selfcooled Pb-17Li blanket is as follows:

The liquid Pb-17Li which is both cooling fluid and tritium breeder is revolved by a circulation pump via pipes through the blanket, the steam generator and a purification system. Fig. 2.3-1 shows a very simplified schematic of the loop system. The steam generator has two functions, first the cooling of the Pb-17Li in order to produce steam for the electrical power production and secondly the extraction of the bred tritium from the Pb-17Li using NaK as a secondary fluid. The tubes in the steam generator are double walled having water (steam) in the inner tube, Pb-17Li around the outer tubes and NaK in the gaps between both walls. While the heat flows from the Pb-17Li through both walls and the NaK gap to the water, producing steam, the tritium penetrates only the outer wall and is solved in the NaK. Due to the high solubility of tritium in NaK compared with the extremly low solubility in Pb-17Li the partial tritium pressure in the NaK gap can be kept at such a low level that the tritium losses to the water system by penetrating the inner wall can be tolerated.

The steam conditions are proposed to be saturated steam at 7 MPa. This has been found to be optimal concerning the thermal efficiency, the thermal stresses in the steam generator bundles and the possibility of operating a steam accumulator to bridge the interruptions in the steam flow to the power station in case of pulsed operation of the plasma [1]. (More details in section 2.3.2.4).

The steam separators of the 80 steam generators are connected by a pipe system collecting the saturated steam for the central power station.

The liquid NaK flowing through the tube gaps with a low velocity is circulated with a magnetic pump from the steam generator through an economiser to one of the cold traps and back to the steam generator. The temperature of the NaK is cooled down in the economiser first and than in the cold traps below the saturation temperature for NaK-tritide.

In the cold traps the tritide is precipitating. After a precipitation period of about 1 day this trap is drained and the tritium is recovered by heating up and evacuating. Two cold traps are alternatively operated: one for collecting and one for recovering of tritium. This is described in detail in section 2.4.

The three outboard loops and the two inboard loops of the 16 sectors are connected on the Pb-17Li side by pipes to increase the availability of the whole reactor system (see section 2.3.3 and 2.5.3 for more details). Further connections are not allowed due to electrical reasons. Fig. 2.3-2 shows the scheme of the 5 connected loop systems.

The details of one ancillary loop system are outlined schematicly by Fig. 2.3.-3

2.3.2 Conceptual design

The most important design details of the Pb-17Li loop, the auxiliary blanket cooling system, the NaK-tritium system and the power conversion system are described in the following sections.

2.3.2.1 Main blanket cooling system (Pb-17Li loop)

The most important components of the main cooling loop are the steam generator, the Pb-17Li pumps, the purification system and the pipes. A dump tank, two expansion tanks and a covergas system as shown in Fig. 2.3-3 are necessary for the operation of the liquid metal loop.

The steam generator, which is shown in Fig. 2.3.-4, is of the straight double walled tube type.It has been choosen out of several types of heat exchangers which are known from liquid metal operated sides, as a result of extended investigations (described in section 4.6.1). The outer tubes and the inner tubes are welded on two pairs of tube plates. They are forming together with the tubes and the shell the lead lithium room , the NaK room and the water (steam) room. To match the different thermal extension of the inner and outer tubes two compensators are installed in the shell between the tube plates. The data of the steam generator are outlined in Table 2.3-1.

The Pb-17Li is flowing down between the pipes, boiling water is flowing up in the inner pipes and NaK is flowing up in the narrow gaps (1 mm) between the walls of

the concentric pipes. The steam generator must be located at least 5 m (distance of the midle points) above the blanket to initiate natural convection flow in case of a pump outage (section 2.3.3.). The outer pipe wall serving as the separation between the Nak- and the Pb-17Li chamber is continued into the NaK collection chambers to protect the inner pipes against damage in case of water leakage in this region (section 4.6.2).

The lead lithium pump is a one flow single stage circulation pump with a vertical shaft. The function is to overcome the hydraulic pressure losses of the loop mainly caused by the MHD pressure loss in the magnetic field in the blanket. To protect the shell of the steam generator with their pressure sensitive compensators from the high pressure of the pump outlet, the pump is situated downflow of the steam generator behind the purification-system in the cold line. Similar to the pumps well known from sodium cooled reactors this pump is of the free surface type with a double slide ring sealing on the shaft between the liquid metal surface and the pump motor. The room below the sealing is filled with covergas. Shaft sealing problems with liquid metal are eliminated by this design but a quick acting level control is necessary because the liquid level in the pump is below the highest level in the loop. A parallel expansion tank is easing the level control.

The purification system has the function of removing the corrosion products, oxides or other contaminants of the liquid lead lithium in order to reduce radioactive contamination of the loop components by activated corrosion products or even to prevent plugging of the pipes. It is situated like the steam generator at the low pressure side of the pump. The operation principle of the purification system is still in development. Further details are reported in section 5.5.2.

In the pipe system the main pipe has a nominal diameter of 400 mm. It is leading the liquid lead lithium from the blanket outlet to the steam generator and then via the pump and the purification system back to the blanket. Due to the extremely high density ($\sim 10\,g/cm^3$) and the relativ high melting point of the fluid this pipe can not be conventional. An analysis was made (section 4.6.2) to check whether such a pipe is selfsupporting with a practicable distance of the supports. The encouraging result is that such a pipe a pipe is selfsupporting with a length below 6 m between bearings. These pipes are carrying electrical heaters and leak detection sensors in the thermal insulation layer. The connection of the pipes with the blanket in - and outlet on top of the blanket must be removable by a remote controlled facility.

Table 2.3-2 contains the important thermal data of the loops.

The cover gas system uses Helium as inert gas instead of the less expensive argon gas. The reason is the fact that the lead lithium is releasing He as a product of the breeding process. For each tritium atom one He atom is produced. Till now it is unknown how long the time of separation of the atomical distributed He from the liquid metal will be. The upper expansion tank is prepared to work as a He collector.

The covergas system of course has a pressure control system, a steam trap, filters and several valves.

2.3.2.2 Auxiliary blanket cooling system

In case circulation of the liquid metal in the primary loop is not possible or after draining the blanket in order to replace it, the auxiliary cooling system is needed to remove the after heat produced in the activated structural material of the blanket. The second function of the cooling system is heating up of the blanket before filling it with lead lithium or for maintaining the metal liquid when the plasma is not burning. It is proposed to use NaK as the heat transport medium. A small loop with all the conventional components like electromagnetic pump, heat sinks, and heat source (air cooler, heater) dump tank, expansion tank, cleaning cold trap and cover gas system is necessary. It has to be constructed small enough to guarantee the replaceability together with the blanket in case of an exchange of the blanket. A small NaK pipe is integrated in the structures of the blanket. The development of this loop is not finished till now and some alternatives (noble gas cooling system) are still in discussion.

2.3.2.3 Tritium removal and recovery system

In this section only some design features of this system are described because more details of the removal and recovery of tritium are handled in the sections 2.4 and 4.4.

This NaK loop has the goal to move the eutectic alloy NaK through the small tube gaps of the double walled steam generator and to lead it to one of the cold traps of the system. The most important parameter for this system is the average tritium partial pressure in the NaK filled pipe gaps. It must be kept low so that the tritium loss to the water-steam system by permeation through the inner tube walls is

below the tolerable level (about 20 Ci/d). Assuming a permeation barrier on the surfaces of the inner wall of a factor of 100 a NaK flow of 4 kg/s is necessary. An electromagnetic pump is circulating this mass flow from the steam generator through an economiser to one of the cold traps and again via the economiser back to the steam generator (Fig.2.3.-3). The NaK flow is cooled down in the economiser in a first step. In the cold trap it is cooled by an inert gas flow below saturation.

The two cold traps are working alternatively with about 1 day cycle, in the extracting mode or the recovering mode. The cold trap cooling and heating system is delivering alternatively a cooling or a heating flow, preferably inert gas, which is flowing through an annulus around the cold traps. In the first mode the NaK filled cold trap is cooled down to less than 54°C, in the second mode the drained and evacuated cold trap is heated up to about 400°C. This inert gas system therefore needs two blowers, a water cooler, an electrical heater, and a valve combination as shown in Fig. 2.3-3.

All pipes and ducts in the NaK system must be designed to resist pressure pulses up to 100 bar. These can occur in the case of a water leakage in the NaK system and a following NaK water reaction as has been calculated. It must further resist the pressure of the water-steam cycle of 70 bar for longer time in the case of a larger amount of water emerging into the NaK system. The water flow can be stopped by equalising the pressures in the NaK and the water system.

The volume of one cold trap is about 1.2 m^3 (s. section 2.4). This is roughly corresponding to 1 m diameter and 1.5 m length of inner dimensions.

The NaK loop of course needs a dump tank, an expansion tank, some valves and an Ar-covergas system.

2.3.2.4   Power conversion system

The production of electrical power is planned in a central steam turbine generator unit. Calculations were made to find out the optimal steam process for the thermal electrical power conversion.

Based on the Pb-17Li temperature of 400°C at the blanket outlet two candidat steam conditions were found to be optimal and are discussed shortly:

a) saturated steam at 70 bar

b) superheated steam at 350°C and 50 bar

The efficiency of the steam process a) with intermediate steam overheating at 11 bar and stepwise feedwater preheating is $\eta = 0,349$ and at the condition b) with stepwise feedwater preheating it is $\eta = 0,346$. These values are nearly equal with a small advantage for the saturated steam process. By the higher technical effort which a turbine process with saturated steam needs, like steam separator after the heat exchanger, a water circulation pump, an overheating during the expansion process and special turbine blade protection, this advantage is nearly balanced. Some other positiv features led to the decision to prefer the process a):

- The average temperature of the steam pipes in the steam generator is lower at saturated steam and therefore the tritium losses to the water are smaller.

- The temperature distribution over the cross-section of the steam generator pipe bundle is more constant and therefore the differences in thermal expansion are smaller.

- In the case of a pulsed plasma operation mode the problem of delivering a fairly constant steam flow to the turbine must be solved. A system for saturated steam has a higher storage capacity for steam, especially when a storage vessel is integrated in the loop which can be combined with the steam separator. Boiling water is producing steam by pressure reduction alone.

The 80 steam generators of the ancillary loops are proposed to produce saturated steam at 70 bar. An optimal operation with respect to the heat transfer (pinch point) is given at a steam-quality of $x = 0.4$. Therefore a circulation pump as can be seen in Fig. 2.3.-3 is necessary for recirulating the water from the steam separator which is 60% of the steam generator flow rate mixed with the feed water (191°C) which is coming from the turbine station.

The steam of the 80 steam generators is collected by a ring pipeline.

If a plasma interruption time for 100 s is assumed and an acceptable pressure drop of the turbine inlet from 70 to 52 bar corresponding to a temperature drop of 20 K is acceptable an additional storage mass of boiling water of 35 tons for each loop system is necessary for bridging the power interruption of the reactor.

2.3.3   Safety and availability aspects

Safety aspects of the ancillary loop components and the blanket are considered here only as far as the hazards of the loss of flow accident and the water leak into the NaK loop are regarded. The general safety for workers and for the environment is handled in section 2.5. Only the important results of an availability study for the ancillary loops are reported here. A more detailed description is given in section 2.5.1. After a stop of burning of the plasma a small amount of heat, the so called afterheat is produced for a considerable time by decay of activated isotopes in the blanket structure and the liquid metal. For the removal of this decay heat care must be taken.

In the case that a Pb-17Li-pump and/or the respective steam generator fails, the total ancillary loop can be disconnected from the blanket by valves. The two adjacent outboard loops or the one adjacent inboard loop resp. can overtake the cooling function in this situation, without interruption of the reactor operation for longer time. If two pumps on the inboard side of a sector are failing the reactor must be stopped and afterheat removal must be ensured. At the outboard side after heat removal is demanded if three pumps are failing, for instance, in case of an outage of the electrical auxiliary power.

The removal of afterheat by natural convection has been studied. It has been assumed that immediatly after the pump outage (the situation described in the last section) the plasma stops burning but the toroidal magnetic field further exists and that the flow velocity of the Pb-17Li-flow is zero. It has been further assumed that the heat sink ist still intact. The elevation difference H between the vertical middle point of the blanket and of the steam generator has been considered in the calculation as the unknown parameter. The cooling flow velocity by natural convection and the maximum outlet temperature of the blanket are computed. Fig. 2.3-5 [2] shows the afterheat production over the time and the calculated blanket outlet temperature and the cooling flow velocity at H = 5 m. The diagram shows that for H greater or equal 5 m natural convection is sufficient to prevent blanket overheating.

If NaK comes into contact with water which can occur in case of a leakage in the inner steam generator tube walls it will react violently and a instantanously propagation of the leak can follow. In the double-walled steam generator in the region

of the narrow NaK filled gaps such a damage propagation is not expected because the formation of hydrogen and hydroxides will probably lead to an obstruction of the gap causing a stop of the propagation. In the region of the NaK collectors at both ends of the gap the outer tube is prolongated forming a protection sleeve for the adjacent pipes. Fig. 4.6-3 shows the measures to prevent wastage by NaK water reaction. In section 4.6.2 more details are described. The NaK system including the cold traps must be designed to withstand a short reaction shock wave of 100 bar.

A study of the reliability of the ancillary loops, which is described in section 2.5.1, showed that if all 80 loop systems are working independently the outage time of the reactor would be more than 30% only concerning failures of the steam generators and Pb-17Li circulating pumps. By redundant connection of the lead lithium pipes so that the two neighbouring loops can overtake the cooling of an effected blanket in the case of an outage of one or two outboard loops (steam generators, pump) or in case of a failure of an inboard loop the one neighbouring loop can cool both inboard blankets, the availability of the loop systems can be increased to more than 98%. Fig. 2.3-2 shows the scheme of the redundantly connected 5 loops of a sector. More combinations are not allowed due to electrical insulation restrictions.

References to section 2.3:

[1]   H.J. Neitzel, personal communication

[2]   INTERATOM, contract for development of the cooling circuits for the liquid metal cooled blankets, Kernforschungszentrum 1990, unpublished.

Tab. 2.3-1　　Design data of the DEMO double-walled steam generator

Thermal design power [MW]	40
Normal operation power [MW]	
Inboard loop	20
Outboard loop	30
Anomal operation power [MW]	
(one inboard loop and/or one outboard loop are failing)	
Inboard loop	40
Outboard loop	45
Steam conditions [bar/°C]	70/286
Steam content (at 40 MW)	0,4
PbLi-temperature [°C]	
Inlet	400
Outlet	275
Heating surface [m^2]	430
Number of tubes	255
Tube dimensions [mm]	
Outer tube	30x2
Inner tube	24x2
Annular gap	1
Tube length [m]	$\approx$ 18
Total height [m]	$\approx$ 21
Vessel diameter [m]	$\sim$ 0,9
PbLi content [m^3]	$\sim$ 6
NaK content [m^3]	$\sim$ 0,9

Table 2.3-2   Thermal data of the DEMO ancillary loops

	Inboard loop		Outboard loop		Site
	normal operation 2 loop/sector	1 loop/sector	normal operation 3 loop/sector	2 loop/sector	Site
Thermal Power [MW]	20	40	30	45	2080
Number of loops operating	32		48		80 (norm.)
PbLi-loops:					
Mass flow rate [kg/s]	842	1684	1263	1895	
Temperatures [°C]:					
Blanket outlet	400	400	400	400	
Blanket inlet	275	275	275	275	
Total volume (PbLi) [m^3]	20		20		. 1600
Nom. diameter (main pipe) [mm]	400		400		
NaK-loops:					
Mass flow rate [kg/s]	4	4	4	4	
Temperatures [°C]:					
Steam generat. inlet	~265	265	265	265	
Steam generat. outlet	~325	325	325	325	
Total volume (NaK) [m^3]	~3		~3		~240
Nom. diameter (main pipe) [mm]	50		50		
Water-steam loops:					
Mass flow rate [kg/s]					
Satur. Steam	10,5	21	15,3	23	1070,4
Feed water temperature [°C]	250	250	250	250	
Steam temperature [°C]	286	286	286	286	
Steam pressure [bar]	70	70	70	70	
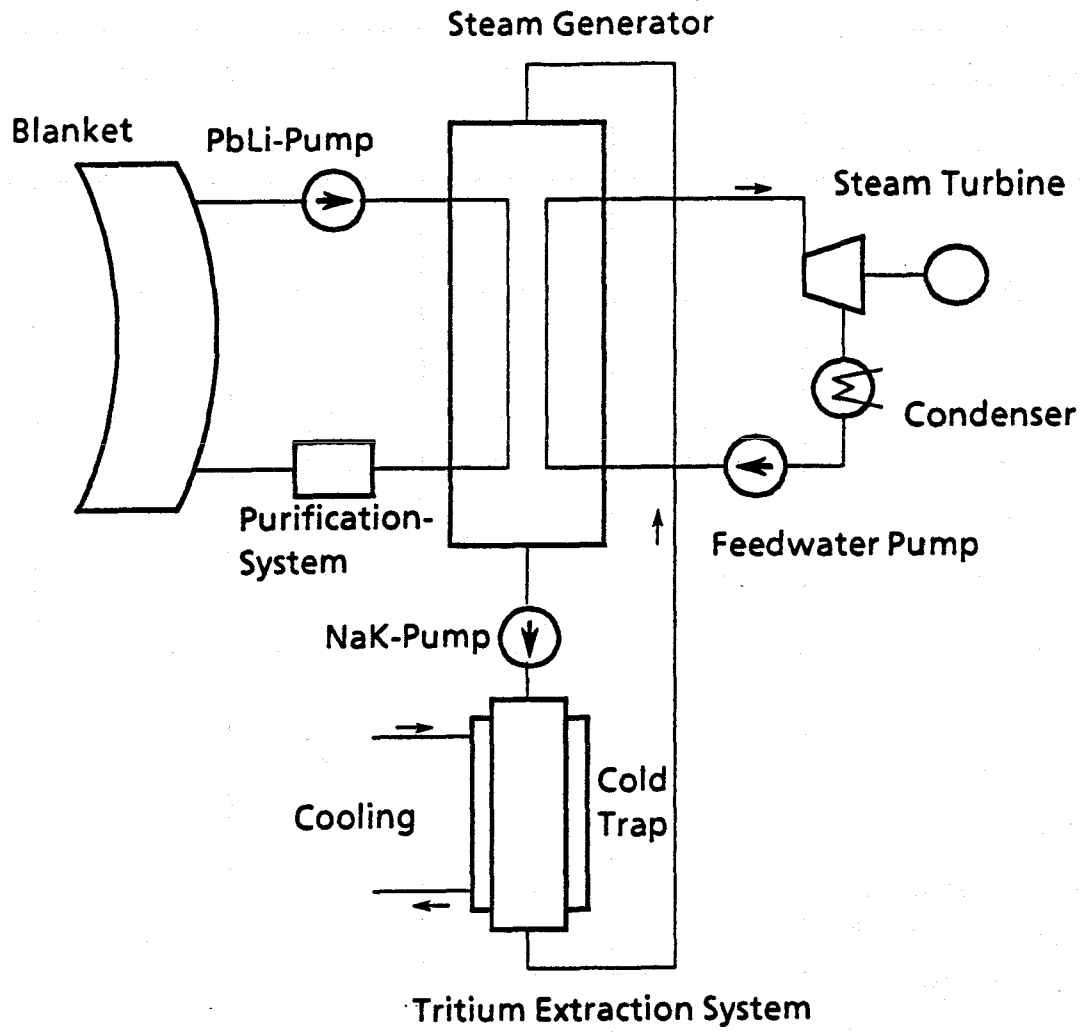
Fig. 2.3-1   DEMO-system for tritium and heat removal
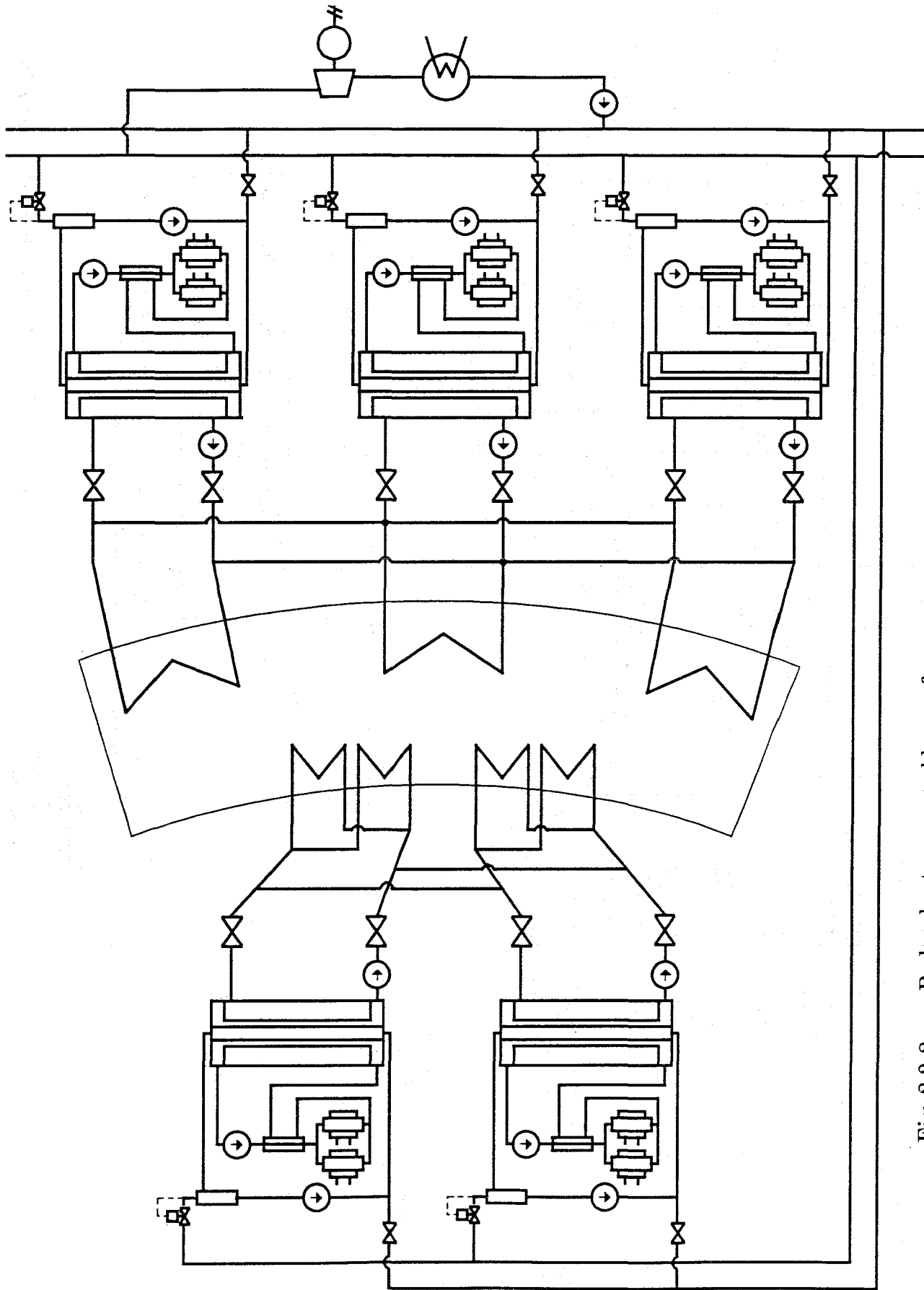
Fig. 2.3-2   Redundant connected loops of one segment

He-Inlet

NaK-expansion vessel

Steam separator (accumulator)

Central power station

Expans. vessel (degaser)

Double-walled steam generat.

Steam turbine

El. generator

Blanket

Auxil. cooler

Heater

PbLi-purificat.

Cooling tower

Fill up pump

PbLi-pump

Expansion vessel

Condenser

Coolingwater pump

He-Outlet

Filter   Steam trap

PbLi-dump tank

NaK-pump

Water circulation pump

Feed-water pump

Economiser

Ar-Inlet

Ar-Outlet

Vacuum pump

Cold trap

Heater
Cooler

Cold trap

To fuel cleaning syst.

NaK-dump tank

Fig. 2.3-3   DEMO ancillary loop system

H2O

NaK

PbLi

Approx. 21 m

17.9 m

ϕ 0,9m

PbLi

NaK

A

H2O

ϕ 30

ϕ 26

PbLi

ϕ 24

ϕ 20

NaK

H2O

Detail A   (without wastage protection)
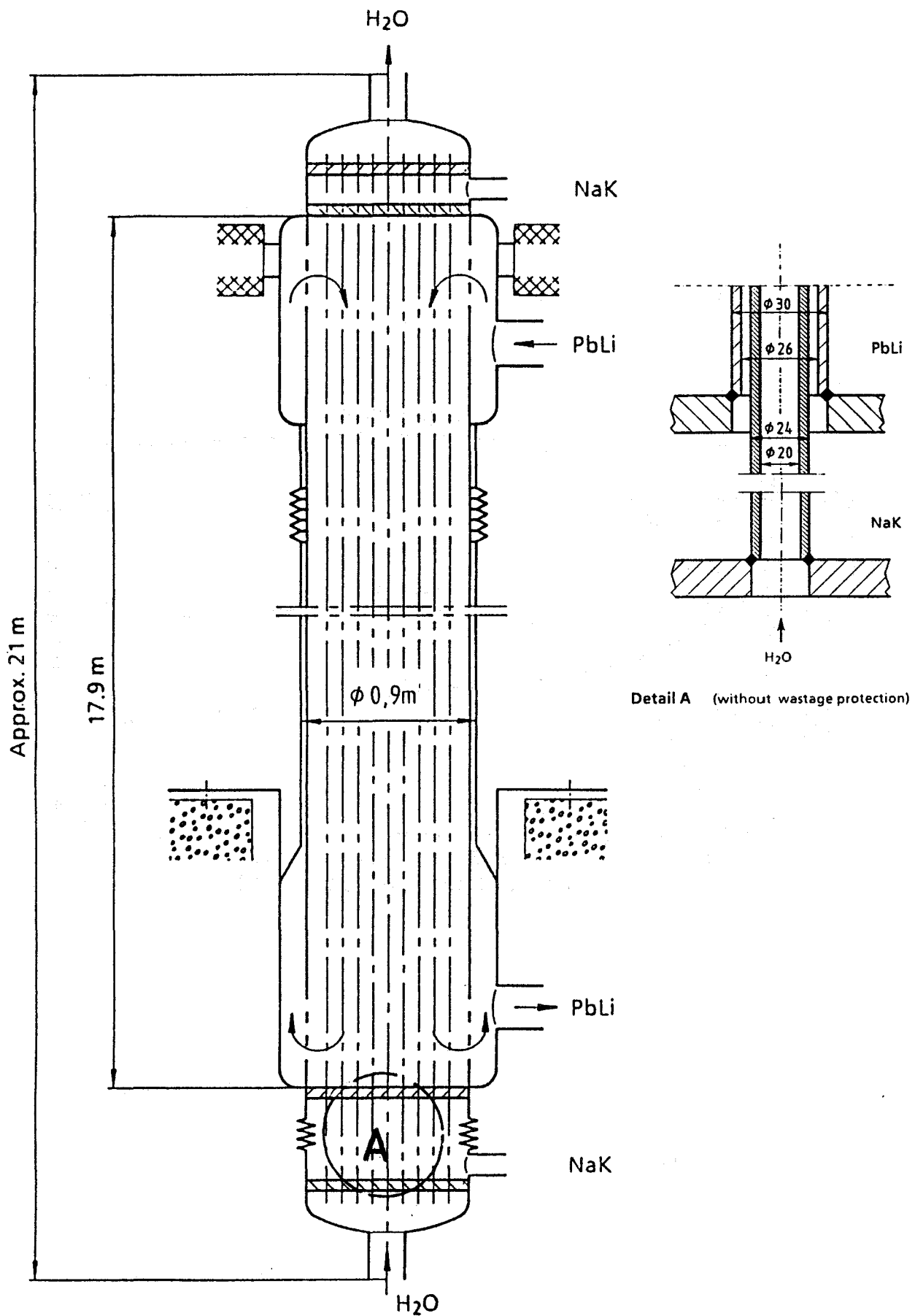
Fig. 2.3-4   DEMO straight-tube double-wall steam generator
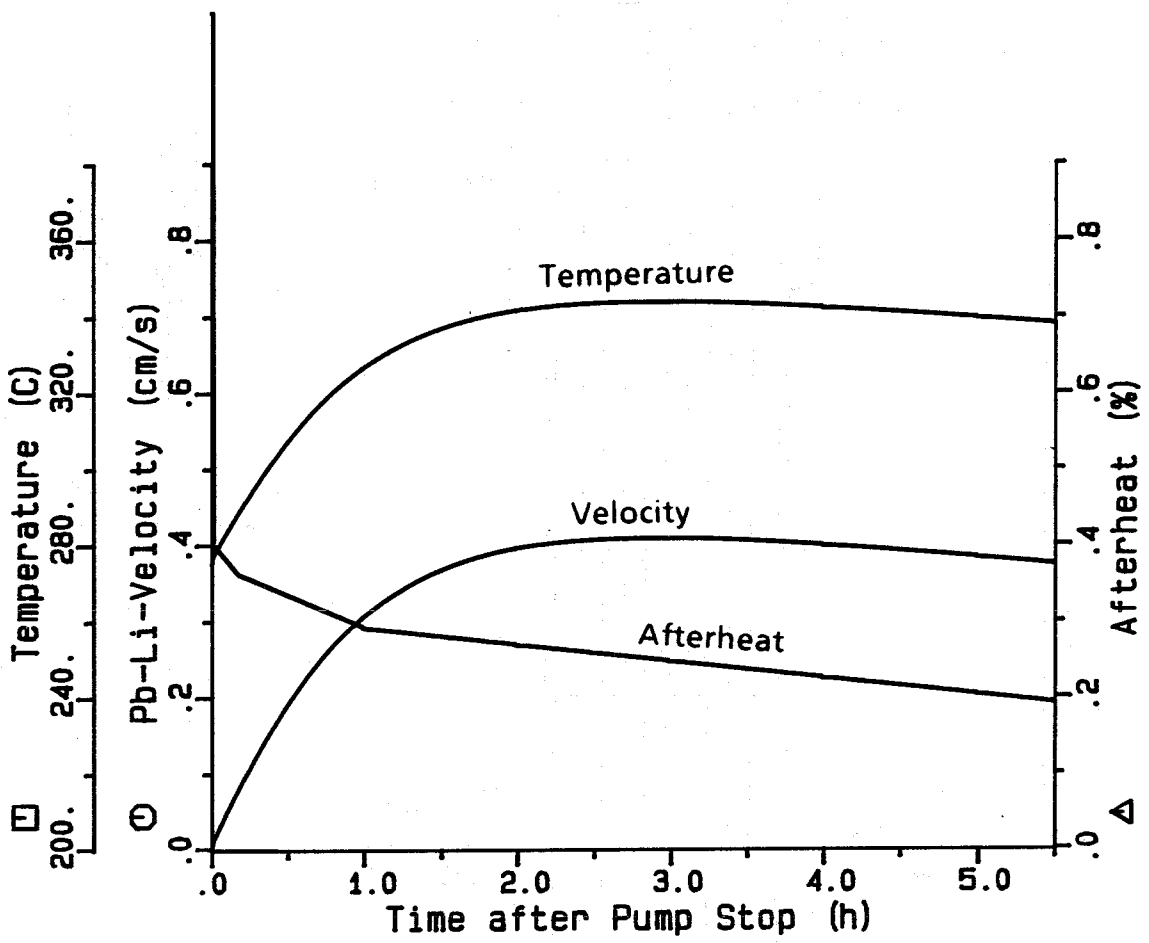
Fig. 2.3-5   Afterheat removal by natural convection (H = 5 m)

2.4 Tritium removal and recovery

The requirements on the blanket tritium recovery system are a low tritium inventory in the total blanket system and an acceptable small tritium loss through the steam generator into the water loop. The latter requirement is the crucial one for a Pb-17Li blanket due to the low tritium solubility of Pb-17Li. In the present design a tritium loss of 20 Ci/d for all reactor blankets is assumed.

The selected tritium removal and recovery technique includes the following steps (for details see Section 4.4.1):

- tritium permeation into the NaK-filled gap of the double-walled steam generator

- tritium removal from the NaK by precipitation as potassium tritide in a cold trap

- tritium recovery by thermal decomposition of the tritide and pumping off the tritium gas.

Figure 2.4-1 shows schematically the flow sheet for one blanket segment (80 identical systems are used): two cold traps are operated in parallel: one for tritium removal by circulating the tritium dissolved in the NaK to the cold trap; the other for tritium recovery. For this purpose the cold trap is decoupled from the circulation loop, drained from NaK, heated up to temperatures of about 380°C and the released tritium gas is pumped off and stored in a getter bed. In this section only a brief description of the design is given, for details see [1].

The critical design value is the tritium pressure in the NaK-filled gap which must be so small that the tritium loss does not exceed the value given above. This tritium pressure depends on the permeation barrier which preferentially occurs at the water side of the steam generator. The following numbers are valid for a permeation barrier factor of B = 100 (which means that the permeation rate is decreased by a factor of 100 compared to ideal permeation conditions). Factors between 10 and 100 are reported for natural oxide layers at the water side but taking into account the extensive work on the development of permeation barriers, compare e.g. [2], a value of B = 100 appears to be feasible for the time when the DEMO reactor will be built. In Table 2.4-1, B is considered as a parameter and results for other values are also presented.

As example an outboard blanket segment is considered (for details see Tables 2.3-1 and 2.3-2). The tritium removal system for the inboard blanket would be somewhat smaller due to the lower tritium generation rate. However, the same size is recommended for all segments. As structural material outside of the blanket a ferritic steel with the permeability according to [3] is used; the tritium solubility in Pb-17Li and NaK was determined according to [4] and [5], see also [6]. A tritium partial pressure of $p = 1.3 \cdot 10^{-5}$ Pa is then required in the NaK gap, corresponding to a mean tritium concentration of $c_{SG} = 12.8$ w_{ppb}. This results in a tritium concentration of $c_{CTo} = 5$ wppb at the cold trap outlet, which corresponds to a cold trap outlet temperature of $T_{CTo} = 29°C$ for a cold trap efficiency of one. (A value of 1 is reached if the cold trap outlet concentration is equal to the saturation concentration which belongs to the cold trap outlet temperature T_{CTo}). Cold trap efficiencies in the required low concentration range are not known presently. The operational regime of the cold trap is shifted to higher concentrations (and with this in a more favourable regime) if other hydrogen isotopes (preferentially protium) are coprecipitated (method of isotope swamping). Other hydrogen isotopes might be purposely added in a special permeator unit or they occur due to protium permeation from the steam generator. For a protium source term of $\dot{m}_p/\dot{m}_T = 3$, the required cold trap outlet temperature becomes 54 °C for an ideal cold trap. In practice, a lower cold trap outlet temperature has to be chosen in order to reach the required outlet concentration, compare Section 4.4.2. If higher cold trap inlet and outlet temperatures are selected a higher protium additon rate has to be used. The disadvantage of isotope swamping is the required isotope separation after recovering the isotopes in gaseous form. However, hydrogen separation columns are required anyway in the fuel clean-up processing system. The additional load from the blanket system should not require a significant enlargement of these columns.

The NaK circulates with a mass flow rate of 4.0 kg/s, the cold trap volume is about 1.2 m³. These values decrease drastically for larger values of B, see Table 2.4-1.

The tritium inventories in the structural materials and liquid metals were assessed taking into account the different tritium pressures and temperatures in different parts of the system. The following values were used for one blanket segment: $m_{steel} = 3.4 \cdot 10^4$ kg, $m_{PbLi} = 2.3 \cdot 10^5$ kg, $m_{NaK} = 2.5 - 5.9 \cdot 10^3$ kg, depending on the cold trap volume. For the tritium inventory in the cold traps a half day production was assumed which is approximately obtained for two removal/recovery cycles per day (see Section 4.4.1.3). Table 2.4-1 shows that the total tritium inventory is governed by the inventory in the cold traps. The residuary in-

ventory is very small and a drastic increase due to neglected effects would still result in a favourable value.

For tritium recovery the drained cold trap is heated up to temperatures between 350 and 400°C. The potassium tritide (compare Section 4.4.1.2) decomposes to metallic potassium and gaseous tritium. During vacuum pumping potassium vapour, generated in the hot zone, can be transported in cooler zones and can condense. The design of the cold trap and subsequent piping has to consider this fact to prevent plugging. Cold trap designs were proposed where the potassium vapour trap is incorporated in the cold trap vessel [8].

Table 2.4-1　Tritium recovery system for a DEMO blanket segment

permeation barrier factor B(1)	50	100	500	1000
tritium production rate m_T(g/d)	5.05	5.05	5.05	5.05
mass flow rate in m_{NaK}(kg/s)	14.0	4.0	1.0	0.5
tritium concentrations 　steam generator　　C_{SG}(wppb) 　cold trap inlet　　C_{CETi}(wppb) 　cold trap outlet　　C_{CTo}(wppb)	6.1 8.2 4.0	12.1 19.4 4.8	60.1 89.9 31.5	121 182 60.5
isotopic swamping IS = $(mol_p + mol_T)/mol_T$	10	10	1	1
cold trap inlet temp. T_{CTi}(°C)	64	81	66	79
cold trap outlet temp. T_{CTo}(°C)	<51	<54	<47	<58
cold trap dimensions 　volume　　V_{CT}(m³) 　height　　h_{CT}(m) 　diameter　D_{CT}(m) 　number　　n(1)	4.11 1.5 1.0 3	1.17 1.5 1.0 1	0.29 1.5 0.5 1	0.14 1.5 0.4 1
tritium inventory 　in steel　　　J_s(g) 　in PbLi　　　J_{PbLi}(g) 　in NaK　　　J_{NaK}(g) 　in cold traps　J_{CT}(g)	0.10 0.26 0.05 2.5	0.10 0.26 0.06 2.5	0.10 0.26 0.27 2.5	0.10 0.26 0.53 2.5
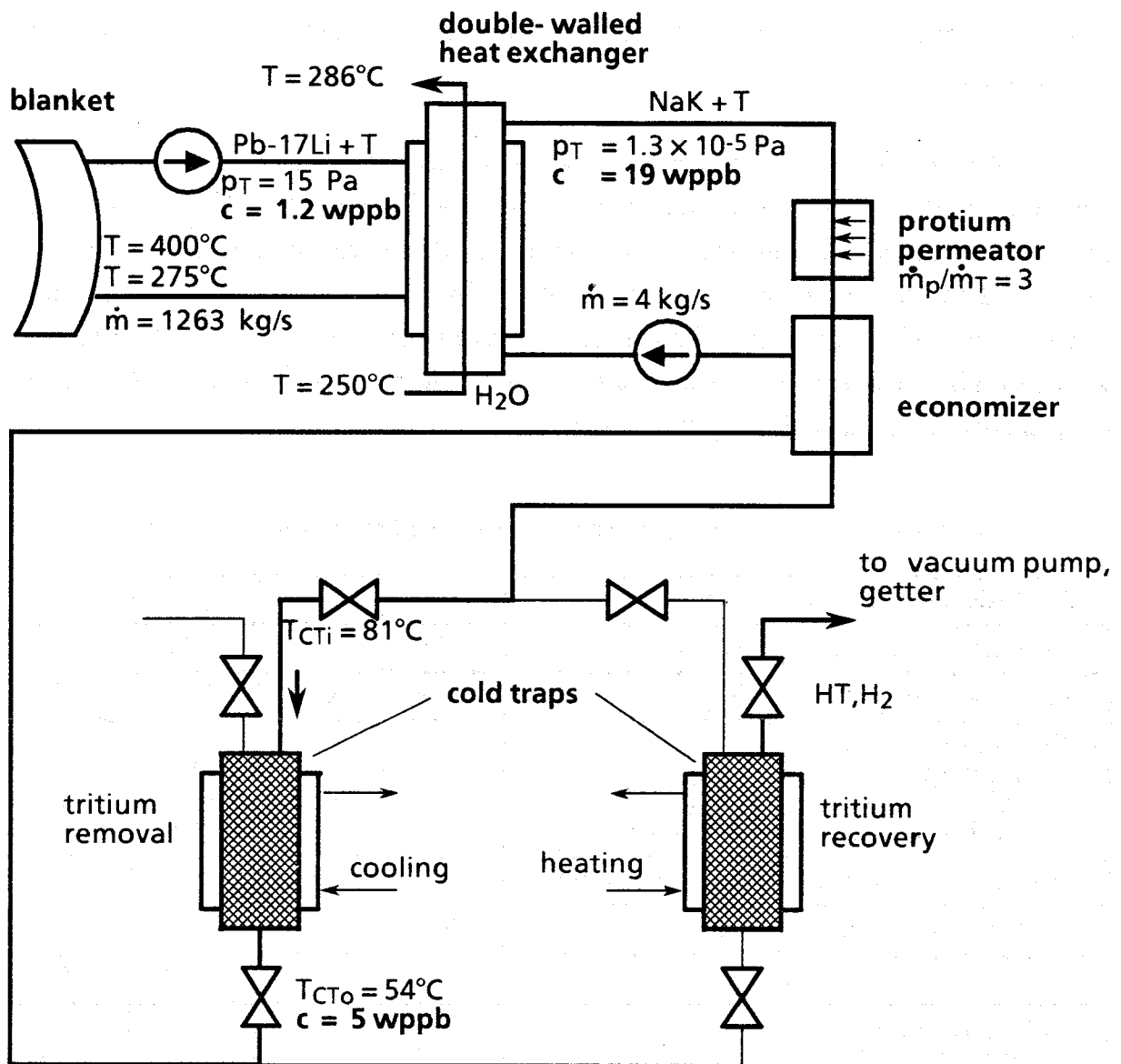
Fig. 2.4-1 Tritium Flow Sheet for a DEMO Blanket Segment ($\dot{m}_T = 5.05$ g/d) (outboard)

References to section 2.4

[1]   J. REIMANN and S. MALANG, "A study of tritium separation from LiPb by permeation into Na or NaK and cold trapping", Kernforschungszentrum Karlruhe, KfK-4105 (Oct. 1986).

[2]   K.S. FORCEY, D.K. ROSS, J.C.B. SIMPSON and A.G. WHITACKER, "The Use of Aluminising on 316L Austenitic and 1.4914 Martensitic Steels for the Reduction of Tritium Leakage from the NET Blanket", J. Nucl. Mater. 161(1989), pp. 108-116.

[3]   T.A. RENNER and D.S. RAUE, "Tritium Permeation through Fe-2 1/4 Cr-1Mo Steam Generator Material", Nuclear Technology 22(1979), 312-319.

[4]   F. REITER, J. CAMPOSILVAN, G. GERVASINI and R. ROTA, "Interaction of hydrogen isotopes with the liquid eutectic alloy 17Li83Pb", Proc. 14th SOFT, Avignon (1986), 1185-1190.

[5]   P. HUBBERSTEY, "Solutions of hydrogen in alkali metals", in: Handbook of Thermodynamic and Transport Properties of Alkali Metals, ed. R.W. Ohse (Blackwell Scientific Publications, 1984).

[6]   J. REIMANN, "Tritium inventory and recovery for a self-cooled Pb-17Li blanket", to be published in Fus. Eng. and Design.

[7]   K.S. FORCEY, D.K. ROSS, J.C.B. SIMPSON and D.S. EVANS, "Hydrogen Transport and Solubility in 316L and 1.4914 Steels for Fusion Reactor Applications", J. Nucl. Mater. 160(1988), pp. 117-121.

[8]   J. REIMANN, H. JOHN, and S. MALANG, "Tritium separation and recovery from NaK by cold traps: Results on hydrogen recovery from Na and NaK"; Fusion Technology 1988, Elsevier Science Publishers (1989), 1306-1311.

2.5 Reliability and safety
2.5.1 Reliability

This chapter deals with the reliability of the blanket cooling system. The reliability of the blanket elements itself has to be investigated when details of the design will be available.

Reliability of the blanket cooling system can be expressed by the system availability. The availability in the previous consideration is the percentage of time, where the system is operating or even able to operate. The complement of the availability to 100 % is the unavailability, where the system is down or unable to operate, respectively.

In view of the cooling medium Pb-17Li, the components used are of prototype character with the consequence, that usually operating experience is not available. This is particularly the case for the three media (Pb-17Li/NaK/H_2O) steam generator (SG). The operating experiences with components of comparable sizes and environments come from the liquid sodium technology, therefore these data have to be the basis for the previous considerations of blanket technology.

Concerning the failure rates from the SG data base, there is no influence deductible by size of units. But in general and especially in case of the three medium double tube SG-type, it is suggested to provide a dependency on size. This is done by extraction of "specific" failure rates related to the length of weldings in the tube plates and of the length of exchanger tubes, respectively, from the data source available. By this procedure λ_R [1/m · h] is the failure rate for one running meter heat exchanger tube and λ_S [1/m · h] is the failure rate for one running meter weld. The data are given in the following Tab. 2.5-1. The failure rates for pumps and valves but also the mean times to repair (MTTR) [h] as assumed are also given in the table.

A first calculation on the basis of that failure data for the cooling system without any redundancy in components, results in an availability lower than 70%. Improvements are possible by mainly three precautions:

A. Reduction of the individual component failure rates.
B. Reduction of the MTTR.

C. Design precautions by alternative design variants or transfer of component functions to other components, e.g. by redundancy.

To **point A**, improvements in the individual component availability are problematic because of the prototype character of the components and of the insufficient operating experience. Especially in case of the SG a comparison of the data assumed with the operating experience [2] shows, there is only little potential for improvements in availability.

To **point B**, improvements in availability by reduction of the MTTR, especially in case of the SG, seem to be also improbable because it is impossible yet, to answer all the questions which influence the MTTR as there are service and maintenance procedures, but also environment and operating conditions, beside others. Therefore, the values assumed according to Tab. 2.5-1 seem to be classified on the lower possible level.

To **point C**, by-passing the problems related to the points A and B, improvements in availability seem only efficient and feasible by delegation of component functions in case of component failures to other components or systems, e.g. by redundancy. But here the degree of redundancy is also restricted by the requirement of a strict electrical separation of the blanket sectors or segments, respectively. It is not possible to answer all these questions in any detail sufficiently at the present time, therefore the availability of the cooling system is determined as a function of different lay-out variations, and dependent on the SG failure rate which is varied between $1.0 \cdot 10^{-6}/h$ and $1.0 \cdot 10^{-5}/h$.

Five different cases are considered. All redundancies are in relation to a blanket sector (consisting of three outer and two inner blanket segments).

Case A   No redundancy in the cooling circuits and components. A failure of one single component results in a failure of the system, that means unavailability of the whole cooling system.

Case B   Two out of three redundancy in SG's in the outer blanket sectors. One SG out of three can fail without failure of the whole sector.

Case C   One out of two redundancy at the SG's in the inner blanket and two out of three redundancy in the outer blanket sectors. No redundancy in the pumps.

Case D   Additional to the SG's redundancy also redundancy in all of the cooling pumps, that means redundancy in all of the individual cooling circuits. One failure in a pump and/or in a SG is equal to the failure of the individual circuit. In each sector one inner and one outer individual cooling circuit may fail without failure of the whole cooling sector element.

Case E   Additional to SG's and pumps also complete redundancy in the valves is assumed. A single failure of one of the cooling components will not lead to a failure of the whole section.

The considerations made for the individual cases of sectors are transferable to the whole cooling system consisting of 16 sectors, which are assumed to be independent of each other. Therefore all the failures of different cases, with the exception of Case A, may happen 16 times simultaneously in the cooling system. On the example of Case D, 32 individual cooling circuits (16 inner from 32 and 16 outer from 48) may fail without failure of the whole cooling system.

The results as given for the different cases in the Fig. 2.5-1 are always valid for the whole blanket cooling system.

The specific failure rates as a reference according to the Tab. 2.5-1 result in a SG failure rate of about $3.0 \cdot 10^{-6}$/h for the **Case A**. The availability of the whole cooling system is lower than 70 %, as given in the Fig. 2.5-1. In this special case, which can be taken as the lowest limit for availability, the unit size of SG's is little lower than that in the residual cases including redundancies. Going vertical to the next higher curves, the SG failure rates gets little higher because of the larger units but the individual specific failure rates are kept constant. Therefore, an exact vertical move to the next curve gives the influence on availability by the changes also necessary in the design.

Going to **Case B** there is an increase in availability from < 70% to 85%, although the size of the SG's and therefore the failure rate is little higher (about 15%). The restriction for a higher increase in availability comes from the inner blanket without any redundancy.

Case C achieves a further increase up to about 90%. By redundancy the influence from the SG's failure rate is here considerably reduced. The part resulting from

the pumps and from the valves, which are not redundant, dominates here the result.

Case D shows that a further, but little, increase in availability is attainable, from 90 to about 92%, by additional redundancy also in the pumps. But one has to keep in mind, the pumps and SG's in the individual circuits are OR-connected that means, a failure of either one pump or one SG leads to a failure of the individual circuit. The change in availability is minimal because the now dominating influence from the valves, which is, in this certain case, also the restriction for further improvements. This actually means, each individual valve function is redundant. In case of an opening function the valves are arranged in parallel and in case of a close function the arrangement is in series.

Considerable improvements in availability additional to the SG and pump redundancies are possible, if also redundancy in the valve function can be realized. The result is given in **Case E**, where availability values higher than 99% can be achieved. This case can be considered as a limit value calculation, reachable by the maximum changes in design.

It must be kept in mind that the availability spectrum between < 70 to > 99% can be achieved by use of the identical individual components only by different degrees of redundancy.

The different design variants make clear that by the variety of the possibilities in design acceptable availabilities remarkably higher than 90% are achievable. Which solution finally will be used, can't be answered definitively yet. This question depends beside others on the space situation for arrangement of the components in the environment but also on the requirements given by the physics and operating conditions.

Some questions influencing the availability coming from auxiliary or even safety systems caused by service and maintenance procedures, can't be answered in this early state of the conceptual design phase.

Concerning the availability of the heat sink, behind the SG's, problems are not expected, because of the operating experiences in the commercial fission reactor technology.

2.5.2   Safety assessment
2.5.2.1   Hazard potential

The hazards associated with Pb-17Li and NaK are due primarily to their chemical reactivity with several substances, and to the induced radioactivity.

Sources for radioactivity in the liquid metals are beside the tritium inventory the lead, the sodium, and potassium, impurities, and corrosion products from the structural materials.
Whereas for Pb-17Li the radiological hazard is of special concern, for NaK its chemical reactivity is of importance.

A general review on critical safety issues of liquid metal blanket designs is given in [3].

Safety analyses for radiation protection have to distinguish between operational and environmental safety. Furthermore, there are different aspects for routine radioactivity release due to leakages under normal operation and maintenance, and for the accidental release of radioactivity.

2.5.2.1.1 Energies

As liquid metals are used for the blanket coolant and for tritium extraction the pressures involved are moderate and have no special hazard potential. For the water circuit a pressure of 60 to 70 bars is planned. Because there exists a lot of experience for such steam process systems no special effort seems to be necessary.

In terms of chemical energy we have the oxidation of lithium in Pb-17Li coolant and the oxidation of NaK. There are three different circuits per blanket segment:

Their volumes are estimated at 20 m^3 Pb-17Li for the blanket coolant, 0.01 m^3 NaK for the auxiliary cooling circuit integrated in the blanket segment, and about 3.0 m^3 NaK for the tritium removal and recovery system. More than 50% of the latter are in containers like cold trap or storage tank and therefore not as vulnerable as in a pipe.

The thermal energy of the Pb-17Li for one circuit at a temperature of 300°C is about 15 GJ. If a complete chemical reaction of 20 m^3 Pb-17Li with water is

assumed (resulting for example from the pessimistic assumption of a simultaneous leak in a blanket and a divertor segment) there is about 50 GJ of energy available. A reaction of 3 m³ NaK with oxigen theoretically can release 60 GJ. It is doubted that this amount could actually be released in an accident.

At the present stage of development it is unclear whether the tritium recovered from the cold traps is passed directly to the fuel storage system or a local storage is foreseen. In the latter case tritium getter beds will be used prepared from UO_2 powder. This powder reacts with oxygen as well as with nitrogen. This reaction is exothermic. The amount of UO_2 powder per circuit is estimated at 1 to 2 kg.

2.5.2.1.2 Radioactive inventories

The most important radioactive inventory with respect to mobilization is tritium. At the present stage of knowledge the total inventories for one loop of a DEMO are estimated as follows:

- Pb-17Li loops	0.26 g
- auxiliary coolant circuit	$<10^{-2}$
- tritium removal and recovery system except cold trap	0.06 g
- cold trap (maximum value)	2.5 g
- getter (maximum value)	2.5 g

The bulk of the neutron-induced radioactivity trapped in the solid structure of the blanket cannot be dispersed without melting and evaporization of a larger amount of the structure. Hence, this radioactivity is of concern primarily for maintenance and waste management. More hazardous with respect to a possible release are the activated corrosion/erosion products in the coolant and the activated coolant itself. The lithium-lead alloy differs from other materials used in nuclear fusion in that it generates α-emitting radionuclides, namely Pb-210, Bi-210, Bi-210 m, Po-206, Po-208, Po-209 and Po-210 [4]. From these radionuclides Po-210 is of most concern, and polonium needs special attention due to its high volatility. However, in the moment no clear picture is available on the possibility to extract it from Pb-17Li and therefore the total amount cannot be estimated. For more details about Po-210 production, activity inventories, and the impact of various bismuth impurities, see section 2.6. In terms of long-lived radioactivity of the Pb-17Li the β-emitter Pb-205 is the dominant radionuclide.

When comparing results of different radioactive inventory calculations and in particular those of Po-210 with differences in the order of magnitude of a factor 10 a revision of the cross-section data base of lead seems to be necessary [5].

2.5.2.1.3 Chemical and radiological toxins

Lead and different lead-compounds as well as some lithium and sodium reaction products are chemical toxins especially if they are evaporated and enter the respiratory tract of men. If coolant is dispersed to the environment, for instance due to a leak or chemical reaction, airborne pollution and inhalation of both chemically and radiologically toxic materials are of immediate concern. It is assumed that the necessary protection against exposure to ionizing radiation will automatically afford protection against chemical exposures.

To give an idea some industrial limits for occupational exposures are given in Table 2.5-2, having in mind that a comparison of long-term adverse effects of chemical and radiological toxins is very difficult. For chemical substances industrial threshold limit values (TLV) of the airborne concentration, and for the radio-activity the maximum permissible concentration (MPC) in air of working areas as calculated according to [6] are used. The annual limits of intake of the different nuclides as an input for the calculation are taken from [6 and 7].

Release of liquid metal into the containment atmosphere should be avoided by a multiple barrier concept because of the low permissible concentration of Po-210. The annual limit of intake by inhalation of Po-210 is $7 \cdot 10^3$ Bq in restricted access areas [6]. Referred to a stay of 2000 h per year and an inhalation rate of 1.2 m3/h the derived limit of the mean activity concentration amounts to 2.92 Bq/m3.

It should be stressed that this extremely small value is primary an issue of operational safety with the consequence of severe access restrictions.

The environmental aspects of an accidental polonium release and additionally of the release of the beta-gamma emitter Hg-203 (Half-life 46,6 d) are considered in [5]. This study indicates the following: With the assumption that a narrow limitation of the bismuth concentration is possible and, furthermore, that a total release is not realistic the radiation doses due to an accidental release could be kept below 10^{-4} Sv for Po-210 and $9 \cdot 10^{-3}$ Sv for Hg-203.

These values are much lower than the working target limit of 0.1 Sv.

Compared with the values of polonium for the self-cooled blanket it should be mentioned that the study [5] has a smaller amount of polonium since it refers to a Pb-17Li blanket cooled by water.

2.5.2.1.4 Eutectics formation
In case of an accidental mixture of Pb-17Li and NaK high melting eutectics may be formed with the hazard of plugging flow channels.

In case of the use of an intermediate tritium storage there exists a hazard in terms of eutectics formation between UO_2 powder and steel at temperatures above 700°C. The use of uranium tritide beds and protective measures against overheating are standard practice in tritium technology.

2.5.2.2 Functional analysis

In terms of safety the release of hazard potentials is important. If we consider the list of hazards above we find that as long as no containment function fails no large hazard release is to be expected. The functional analysis performed in [10] investigates different possible scenarios of failures of the containment and ranks them. The summary of the hazard potentials revealed that it should be checked whether getters are really needed to be attributed to each circuit, because a pipe connection is foreseen to pass the tritium to the tritium storage and fuel system.

Safety issues to be considered are:

- Loss of coolant accident (LOCA)
- Loss of coolant flow (LOFA)
- Loss of heat sink
- Plasma disruption
- Overheating of cold trap
- Earthquake.

For reason of uncertainty in the component and overall plant design a complete accident analysis is not yet performed. Supposed accident scenarios are well known, values to be determined in this regard are the radioactive inventory eventually released to the plant in the case of an accident, the in-plant transport of mo-

bilized material, the retention capability of filters and the different confinement barriers, and the fraction of radioactivity finally released to the environment.

2.5.2.3 Loss of coolant accidents

For this type of accident we have to consider all 3 circuits attributed to a blanket segment.

2.5.2.3.1 LOCA in Pb-17Li system

a) Consequences to other systems
We have to distinguish between a LOCA inside of the vacuum vessel and a LOCA outside. Basically a LOCA inside of the vacuum vessel should have less consequences than a LOCA outside. However, a jet of Pb-17Li may damage a divertor plate resulting in a major LOCA of the divertor cooling system. An investigation should be performed for this type of accident.

For a LOCA outside vacuum vessel the leak collecting system has to make sure that a direct contact between masses of Pb-17Li and concrete is inhibited. Then no severe consequences have to be expected here.

b) Consequences to the system
Another problem is the question of decay heat removal while the regular coolant flow path is interrupted due to a leak. It must be assured that the plasma is shut down as fast as possible. Then due to the low decay heat, the masses of steel involved, the auxiliary coolant circuit, and the fact that only one circuit i.e. 1/80 of the total cooling capacity for the torus is lost no big hazard is expected. If the shut down of the plasma fails then the LOCA will run into a superimposed LOCA for the defected segment due to a thermal failure of the first wall. Then, however, a plasma shutdown will occur.

2.5.2.3.2 LOCA in the auxiliary cooling system

a) Consequences for other systems
Also here we have to differentiate between a leak inside the blanket module or outside. If the leak is inside the blanket and the pressure in the Pb-17Li system is higher than in the auxiliary system no big problems are expected, because the mass loss for the Pb-17Li system is negligible. If the leak is outside the main con-

cern would be the interaction of the NaK with the atmosphere in the environment. If we assume that there is an inert gas and a reliable leak collecting system to prevent an interaction of NaK with concrete then the problem reduces to the release of tritium from large surfaces. This question has to be investigated.

b) Consequences for the system itself
If the leak is in the blanket module Pb-17Li will enter the NaK system with the hazard of formation of high melting alloys which may lead to a blockage of cooling channels. Since, however, the cooling system does not really remove a significant amount of heat such a problem as well as a leak outside will pose no hazard as long as the function of the system is not required.

2.5.2.3.3 LOCA in Tritium separation and removal system

This system probably will be installed in two different compartments one being large and having air atmosphere and a low content of liquid metals and another small one where the NaK storage tank, the cold traps, and the tritium getters are installed. The latter compartment has an inert atmosphere.

a) Consequences to other systems
A leak in the large compartment may lead to a NaK fire and possibly damage other systems. It has to be asserted that the smaller inert compartment containing most of the NaK and tritium is not affected by such a fire.

b) Consequences to the system
For any problem in this system it is forseen that the NaK is drained into the NaK storage tank. This is in principle equivalent to a LOCA. Therefore no new problem is expected.

2.5.2.4 Loss of coolant flow

This type of accident covers several other initiators, e.g. local blockages, pump failures, valve malfunctions. To summarize, their final consequence will end in the worst case in a LOCA which is considered above. So a loss of flow is a question of availability of the plant which is not of primary concern in terms of safety.

2.5.2.5 Loss of heat sink

This event poses a problem because heat removal is always necessary due to decay heat. However, again the time constants are in the order of days until structural failure has to be assumed. Nevertheless, emergency storage tanks for an emergency coolant should be foreseen.

2.5.2.6 Plasma disruption

The consequences of a plasma disruption is an excess load on a blanket module. As DEMO is assumed to undergo only few disruptions it must be shown that this accident does not lead to a LOCA for Pb-17Li and that the blanket module can be removed. For further details see section 4.8 and 5.7.

2.5.2.7 Overheat of cold trap

There are two pathes to overheat the cold trap. One is a leak in the cold trap superimposed by some oxigen content in the atmosphere around. This oxigen can react with residual NaK on the walls and release heat. The other path is a failure in the heating system. Both pathes may lead to unexpected tritium decomposition rates and so to overpressure in the cold trap.

2.5.2.8 Earthquake

To avoid the initiation of a LOCA by an earthquake - induced pipe break the general guidelines for a seismic design should be observed, especially for the piping, the associated equipment, and their supports. The seismic classification and loading conditions have to be determined according to site specific regulatory details.

References to section 2.5:

[1]   INTERATOM, Contract for development of the cooling circuits for liquid metal cooled blankets, Kernforschungszentrum Karlsruhe 1990, unpublished.

[2]   IAEA, Survey of ranges of component reliability data for use in probabilistic safety assessment, IAEA-TEDOC-508, 1989

[3]   S. Malang et al., Crucial Issues on Liquid Metal Blanket Design, ISFNT2, Karlsruhe, June 2-7, 1991

[4,] G.J. Butterworth, Activation characteristics and waste management options for some candidate tritium breeders,
AEA FUS Vol. 82 (Jan. 1991)

[5] G. Casini, P. Rocco, M. Zucchetti, Radioactivity Effects of Pb-17Li in Fusion Power Reactors, ISFNT2, Karlsruhe, June 2-7, 1991

[6] Neufassung der Strahlenschutzverordnung vom 30. Juni 1989, Bundes-gesetzblatt, Teil 1, Z5702A, Nr. 34, (12. Juli 1989)

[7] Bekanntmachung der Tabelle IV 1: Freigrenzen und abgeleitete Grenzwerte der Jahres-Aktivitätszufuhr für Inhalation und Ingestion einzelner Radio-nuklide, Bundesanzeiger G1990A, Nr. 185a, (30.9.89)

[8] MAK-Werte 1987, TRGS 900, Senatskommission zur Prüfung gesundheit-sschädlicher Arbeitsstoffe der deutschen Forschungsgemeinschaft

[9] W.E. Kastenberg, D. Ohrent, Some Safety Considerations for Conceptional TOKAMAK Fusion Power Reactors,
ER-546, UCLA (July 1978)

[10] Functional Analysis for Blanket and Cooling System of a DEMO-Reactor based on the KfK-PbLi Self-cooled Blanket, INTERATOM, Final Report (March 1991)

Table 2.5-1: Failure rates for tubes, pumps and valves

Failure mode	Failure rate	Symbol	Dim.	MTTR [h]	Reference
SG tube welding failure	$3.3 \cdot 10^{-8}$	λ_S	$[1/m \cdot h]$	1440	[1]
SG tube failure	$6.9 \cdot 10^{-11}$	λ_R	$[1/m \cdot h]$	1440	[1]
pump fail to run mechanics	$5.6 \cdot 10^{-6}$		1/h	50	[1]
pump fail function control	$2.6 \cdot 10^{-5}$		1/h	10	[1]
valve fail to change position	$7.0 \cdot 10^{-3}$		1/d	30	[2]

Table 2.5-2: Relative toxic hazard potential

Substance	Type of radiation	Half-life	TLV mg/m³ air (chemical toxin)	MPC mg/m³ air (radiological toxin)	Ref.
Lead			0,1 (as lead)		[8]
Lithium			2 (as LiOH) 0,025 (as LiH)		[9] [8, 9]
Sodium			2 (as NaOH) 0,2 (as N₃Na)		[8] [8]
Na-22	β^+, γ	2,6 a		$1,80 \cdot 10^{-8}$	
Na-24	β^-, γ	15,03 h		$1,30 \cdot 10^{-8}$	
K-40	β^+, γ	$1,28 \cdot 10^9$ a		32,22[1]	
K-42	β^-, γ	12,36 h		$1,31 \cdot 10^{-10}$	
Pb-205	ε	$1,4 \cdot 10^7$ a		0,904	
Pb-210	β^-, γ, α	22,3 a		$7,34 \cdot 10^{-10}$	
Po-210	α, γ	138,38 d		$1,75 \cdot 10^{-11}$	
Bi-210	α, β^-, γ	5,01 d		$3,63 \cdot 10^{-11}$	

[1] For the naturally occurring isotope there is no limitation!
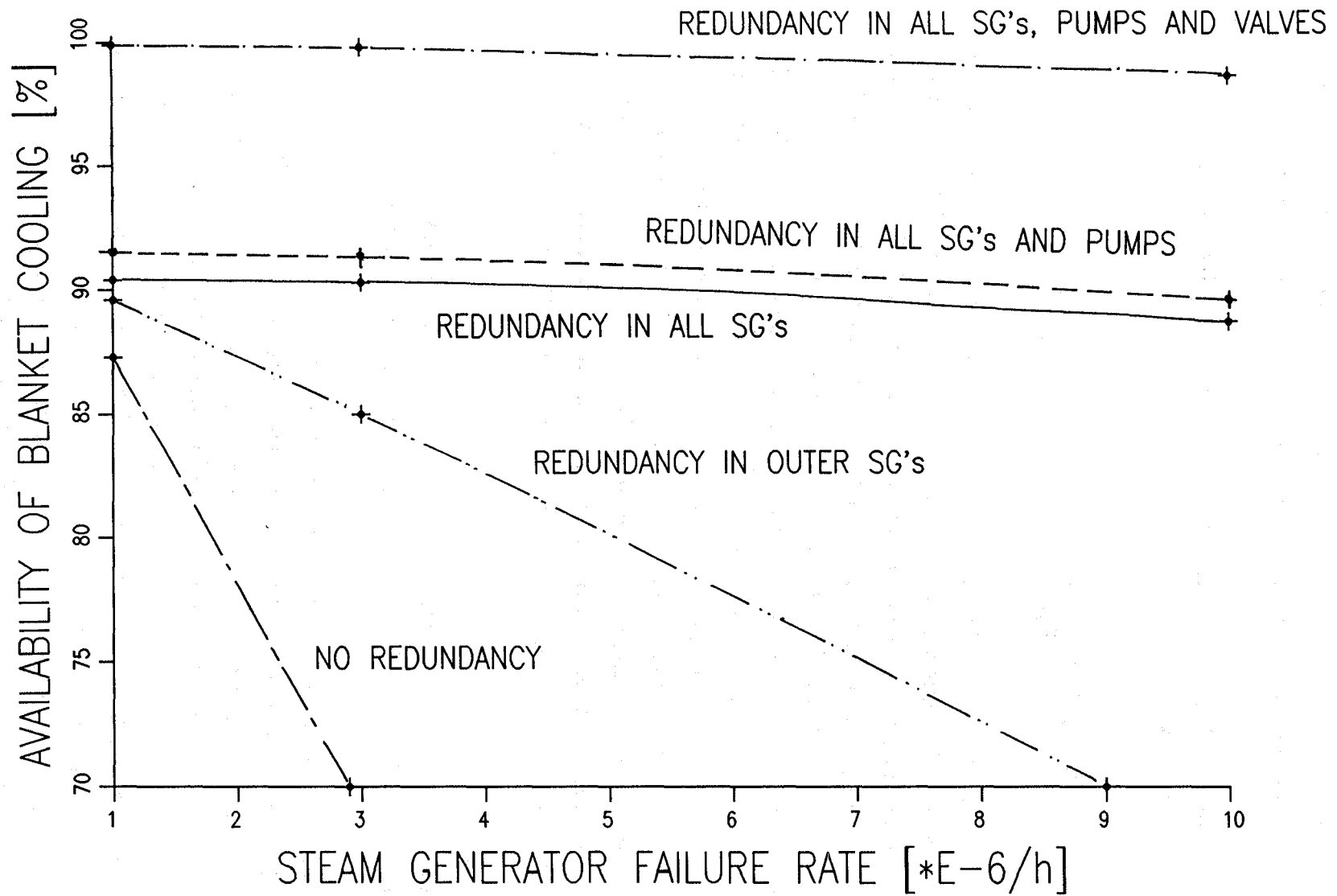
Fig. 2.5-1 Availability of the blanket cooling system dependent on the failure rate
of steam generators

2.6 210Po-production in the Pb-17Li liquid metal blanket

The 210Po-production in a liquid metal blanket with Pb-17Li as breeding material may be a concern for the safety of a fusion reactor facility due to the high evaporation pressure and the very high radiotoxity of 210Po [1] (see also section 2.5).

In the eutectic alloy Pb-17Li the α-emitter 210Po ($T_{1/2}$ = 138,38 d) is produced according to the following scheme:

$$(1) \qquad {}^{208}Pb\,(n,\gamma)\,{}^{209}Pb\,\xrightarrow[\;T_{1/2}=3.5\,h\;]{\beta^-}\,{}^{209}Bi\,(n,\gamma)\,{}^{210}Bi\,\xrightarrow[\;T_{1/2}=5.0\,d\;]{\beta^-}\,{}^{210}Po$$
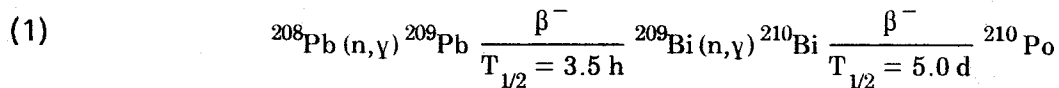
Lead usually contains 209Bi as impurity in the ppm-range and the production of 210Po therefore may be sensitive to the initial bismuth content. The fact that 210Po is produced via two subsequent (n,γ)-transitions from 208Pb, on the other hand, results in a square dependence of the 210Po-inventory on the neutron flux density. For a reliable evaluation of the 210Po-production it is therefore necessary to know the spatial and energetic distribution of the neutron flux density throughout the liquid metal blanket. Actually this only can be achieved in correlation with a three-dimensional transport calculation taking into account the geometrical arrangement of the liquid metal blanket in the real configuration of the Demo reactor. One-dimensional transport calculations give an incorrect radial profile of the neutron flux density with a strong overestimation in the front region of the liquid metal blanket [2] and are therefore inadequate for the calculation of the 210Po-production from 208Pb.

For this reason the following procedure has been applied to assess the 210Po-production in the self-cooled liquid metal blanket of the Demo reactor.

(i)   A three-dimensional Monte Carlo transport calculation with the MCNP-code [3] is performed to obtain the spatial and energetic neutron flux distribution. For this purpose a 7.5°/2 torus sector model is used with a simplified layout of the self-cooled liquid metal blanket (see section 2.1.2). The neutron spectra are calculated in the 100 energy groups of the GAM-II structure. In order to obtain a sufficient statistical accuracy for the calculated neutron spectra about 200000 neutron histories are followed. Fig. 2.6-1 shows typical examples of the neutron spectra in the first wall cooling channel, the front (meander zone), the middle (diverting flow channel) and the

back region (inflow channel) of the outboard blanket. Note that the neutron flux density is normalized according to the fusion power of the DEMO reactor, which is $P_{fus} = 2216$ MW.

(ii)   The ^{208}Pb- and ^{209}Bi-activation cross sections are taken from the very recent UKACT1-library [4]. They are given in the 100 GAM-II group structure and are condensed to one energy group using the specific 100 group spectra of each liquid metal zone. In this way zone-dependent one-group activation cross-sections are produced, which are appropriate for the use in the subsequent activation calculations.

(iii)   The activation calculations make use of the analytical solutions of the coupled system of linear first-order differential equations describing the generation and depletion of ^{209}Bi and ^{210}Po according to the production scheme (1) shown above. The activation calculations are performed in each liquid metal zone using the specific one-group activation cross-sections, neutron flux densities and, of course, atomic number densities.

The liquid metal in the blanket segments is circulated in primary loops, leading to both an increased liquid metal inventory and a complete mixing of breeder material from front and back regions. Both effects are not considered here and would lead to a reduced polonium production rate.

Table 2.6-1 shows the calculated ^{210}Po activities along with the total neutron flux densities and the spectrum-averaged (n,γ)-cross-sections of ^{208}Pb and ^{209}Bi in each liquid metal zone. These calculations are based on a total irradiation time of 2.28 a (20000 h) without any initial Bi-impurity. Obviously there is a strong dependence of the ^{210}Po inventory on the neutron flux density, whereas the impact of the spatially varying neutron energy spectrum, expressed in the zone-dependent spectrum-averaged (n,γ)-cross-sections $<\sigma_{n,\gamma}>$ of ^{208}Pb and ^{209}Bi, is rather moderate.

For practical purposes it is beneficial to have a quick estimation of the ^{210}Po-production rate. Actually the specific activity of ^{210}Po A_{Po} (given in Bq/cm^3) can be approximated according to:

(2)
$$A_{P_0} = N_{Pb} \cdot <\sigma_{n,\gamma}^{Pb}> \cdot <\sigma_{n,\gamma}^{Bi}> \cdot \Phi^2 \cdot t$$

where N_{Pb} is the atomic number density of 208Pb, Φ is the total neutron flux density, t the irradiation time, $< \sigma_{n,\gamma}^{Pb}>$ and $< \sigma_{n,\gamma}^{Bi}>$ are the spectrum-averaged (n,γ)-cross sections of 208Pb and 209Bi, respectively. As shown in Table 2.6-1 this approximation overestimates the exact calculation by not more than about 25%. As the spatial variation of $<\sigma_{n,\gamma}^{Pb}>$ and $<\sigma_{n,\gamma}^{Bi}>$ is rather low, it is sufficient to know the total neutron flux density Φ to obtain an approximative estimation of the 210Po-activity inventory produced according to equ. (2).

The impact of Bi-impurities on the 210Po-production rate is shown in Table 2.6-2. In a good approximation the increase of the total 210Po-activity inventory is proportional to the initial bismuth content: it increases by about $4.3 \cdot 10^4$ Ci per 10 appm Bi. Due to the square dependence on the neutron flux density (eq. 2), the increase is rather moderate in the blanket front region (high neutron flux density) but stronger in the middle and the back part of the blanket. Thus there is an outward radial shift of the 210Po-production rate depending on the amount of the bismuth impurity.

The 210Po-production rate depends crucially on the (n,γ)-cross-sections of 208Pb and 209Bi, which are the main sources of uncertainties imposed on the calculation of the activation inventory. Especially this holds for the isomeric branching ratio 209Bi (n,γ) 210gBi versus 209Bi (n,γ) 210mBi. The ground state 210gBi decays to 210Po by a β^--transition, whereas the isomeric state 210mBi decays to 206Tl by an α-transition. Actually the isomeric branching ratio m/g is not well known. It is scaled in the UKACT1 data file according to m/g = 1:100, but in the REAC-ECN-2 data library [5] it is estimated as m/g = 1:1. Obviously there is a strong need for improving the knowledge on the isomeric branching ratio of 209Bi (n,γ) 210Bi. With regard to the 210Po-production, however, it is clear that the UKACT1-library provides conservative estimates of the activation inventory.

References to section 2.6:

[1] N.J. Hoffman, K.A. Murray, J.A. Blink, W.R. Meier, W.F. Vogelsang: "Polonium Aspects Associated with the Use of Lead-Lithium Blankets in Fusion Applications", Fusion Technology 8, July 1985, 1376 - 1384

[2] U. Fischer: Neutronic Characterization of Various Blanket Concepts in the Geometrical Configuration of a Tokamak Reactor, 16th Symposium on Fusion Technology, London, U.K., September 3 - 7, 1990

[3] J.F. Briesmeister (Ed.): MCNP - A General Monte Carlo Code for Neutron and Photon Transport, Version 3A, Report LA-7396-M, Rev. 2, Sept. 1986

[4] R.A. Forrest, M.G. Sowerby, B.H. Patrick, D.A.J. Endacott: The Data Library UKACT1 and the Inventory Code FISPACT, Int. Conf. on Nuclear Data for Science and Technology, Mito, Japan, May 30 - June 3, 1988

[5] H. Gruppelaar, H.A. J. van der Kamp, J. Kopecky, D. Nierop: The REAC-ECN-2 Data Library with Activation and Transmutation Cross-Sections for Use in Fusion Reactor Technology, ECN Petten, Report ECN-87-161, November 1987

Table 2.6-1: Radial distribution of the ^{210}Po-production in the self-cooled liquid metal blanket (2.28 a irradiation time in the Demo reactor with $P_{fus} = 2216$ MW, no initial bismuth content)

	Φ_{tot} [10^{14} cm^{-2} s^{-1}]	$< \sigma_{n,\gamma} >$ [mb]		specific activity [Ci/cm3]		activity inventory [Ci]
		208Pb	209Bi	approximative (equ. 2)	exact	
inboard blanket						
backward channel II	1.79	4.85	23.5	9.08-5	6.94-5	1.22 + 3
backward channel I	2.54	4.79	25.5	1.97-4	1.51-4	2.71 + 3
middle channel II	3.53	4.68	26.7	3.89-4	2.96-4	4.71 + 3
middle channel I	4.68	4.55	28.1	6.98-4	5.33-4	8.61 + 3
meander zone III	6.40	4.31	28.9	1.21-3	9.14-4	1.59 + 4
meander zone II	8.06	4.06	29.4	1.85-3	1.41-3	2.49 + 4
meander zone I	9.69	3.78	28.7	2.43-3	1.85-3	2.83 + 4
first wall cooling channel	10.5	3.60	28.1	2.81-3	2.14-3	7.67 + 3
total inboard						9.40 + 4
outboard blanket						
first wall cooling channel	12.2	3.42	27.9	3.39-3	2.57-3	1.73 + 4
meander zone I	11.6	3.57	28.1	3.22-3	2.43-3	7.10 + 4
meander zone II	10.0	3.84	28.9	2.64-3	2.01-3	5.98 + 4
meander zone III	8.28	4.08	29.4	1.96-3	1.48-3	4.49 + 4
meander zone IV	6.61	4.30	28.9	1.30-3	1.03-3	3.69 + 4
middle channel I	4.93	4.53	27.9	7.67-4	5.84-4	1.78 + 4
middle channel II	3.76	4.56	26.9	4.32-4	3.36-4	1.22 + 4
middle channel III	2.86	4.78	25.5	2.49-4	1.89-4	6.00 + 3
middle channel IV	2.15	4.90	24.3	1.37-4	1.05-4	4.55 + 3
backward channel I	0.911	5.03	23.3	2.70-5	2.06-5	1.42 + 3
backward channel II	0.527	5.0	21.6	8.37-6	6.28-6	4.89 + 2
total outboard						2.72 + 5
total inboard + outboard						3.66 + 5

Table 2.6-2: Impact of various bismuth impurities on the ^{210}Po production (activity inventory refers to the complete DEMO-reactor with $4.63 \cdot 10^9$ g lead)

	initial bismuth content in lead [appm]				
	0	1	10	50	100
specific activity					
Ci/cm^3	$6.75 \cdot 10^{-4}$	$6.85 \cdot 10^{-4}$	$7.54 \cdot 10^{-4}$	$1.07 \cdot 10^{-3}$	$1.47 \cdot 10^{-3}$
Ci/kg Pb	$7.91 \cdot 10^{-2}$	$8.03 \cdot 10^{-2}$	$8.83 \cdot 10^{-2}$	0.125	0.172
activity inventory					
Curie	$3.66 \cdot 10^5$	$3.72 \cdot 10^5$	$4.09 \cdot 10^5$	$5.80 \cdot 10^5$	$7.94 \cdot 10^5$
inventory increase					
Curie		$5.45 \cdot 10^3$	$4.26 \cdot 10^4$	$2.14 \cdot 10^5$	$4.28 \cdot 10^5$

Pb—17Li self—cooled DEMO blanket : outboard neutron spectra

Legend:
— first wall cooling channel
---- blanket front region
.... blanket middle region
— — blanket back region

Y-axis: Neutron flux density (cm−2*s−1*u−1)

X-axis: Neutron energy (MeV)
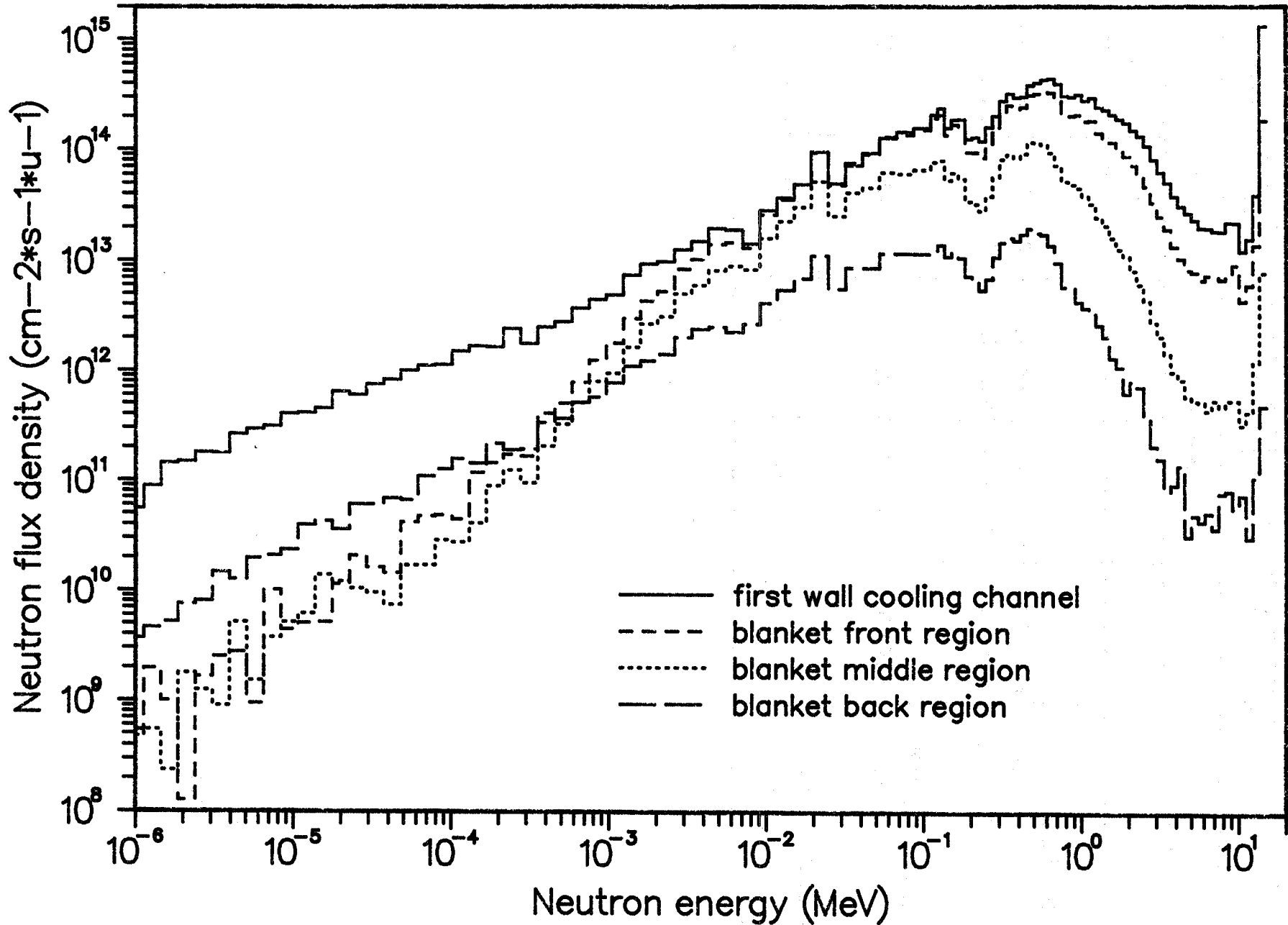
Fig. 2.6-1   Neutron spectra in the self-cooled Pb-17Li outboard blanket (DEMO reactor   with a fusion power of 2216 MW)

3.   TEST OBJECT DESIGN FOR NET/ITER

One of the major objectives of NET/ITER is to test blanket concepts relevant for a DEMO-reactor. NET/ITER offers the unique possibility to test simultaneously all aspects of such blanket concepts in the real geometrical configuration, with the real magnetic field, and with an incident neutron flux having the real neutron spectrum and spatial distribution. The main differences to DEMO are the lower wall load (1.0 MW/m^2 instead of 2.2 MW/m^2) and the shorter burn time.

In spite of the lower power density the average temperature in the blanket can be adjusted to DEMO values by flow reduction. However, the local temperature distribution and temperature gradients in the materials will be different. Furthermore, reduced flow rates influence MHD pressure drops and consequently the mechanical loading of the blanket structure. This points to the fact that fully integrated tests with look-alike test objects are not really suitable to investigate all issues of a blanket concept simultaneously. Therefore, it has been suggested in the FINESSE-study [1] to use act-alike test modules instead of look-alike test modules in order to obtain maximum benefit from testing at reduced device parameters.

One can choose to emphasize one or several blanket issues at the expense of others, which results in a "scaled test option". By performing several different scaled test options, one might hope to reconstruct most of the important blanket phenomena. Interactive, or "synergistic", issues can be easily lost with this approach. Care must be exercised to identify and eliminate the omission of important interactive effects.

There is a large number of issues involved in a blanket concept. The most critical ones for self-cooled liquid metal blankets are:

-    MHD pressure drop and flow distribution
-    electrical insulation of the flow channels either by flow channel inserts or by direct insulation
-    potential chemical reactions between the liquid metals (Pb-17Li, NaK) and air, water, or concrete
-   response of blanket segments to plasma disruptions.

All these issues either require tests in NET/ITER or have to be taken into account in designing test objects, ancillary loops and interfaces to the basic machine.

3.1 Test module design

Different test objectives require dedicated test modules. The basic machine will be designed for a frequent replacement of test modules. For this purpose a number of blanket test ports are allocated at the equatorial midplane, each of them roughly 3 m high and 1 m wide. Fig. 3.1-1 shows schematically such a test port in ITER [2,3]. In order to cope with the very limited testing time, it is anticipated to divide a test port into up to four sub-ports for a number of tests. Fig. 3.1-2 shows such a quarter-sized test module which is designed for exchanging it completely independent of the neighbouring sub-modules. The module shown in this figure is located behind a first wall provided by the basic machine. This is anticipated for all tests during the physics phase of NET/ITER operation and for the first part of the technology phase respectively in order to limit the risk to the machine caused by blanket tests. Exposure of the test modules to the plasma required for final tests of a blanket concept will be allowed only after extensive testing of the concept behind the first wall provided by the basic machine.

References to section 3.-3.1:

[1] M. Abdon et al., FINESSE: A study of the issues experiments and facilitites for nuclear research and development (Interim report), University of California at Los Angeles, PPB-821, UCLA-ENG-89-30, Vol. III (Oct. 1984).

[2] ITER, Conceptual Design Report, ITER Document Series, No. 18, International Atomic Energy Agency, Vienna 1991.

[3] M. Tillak et al., ITER Test Program, ITER Document Series, No. 24, International Atomic Energy Agency, Vienna 1990.
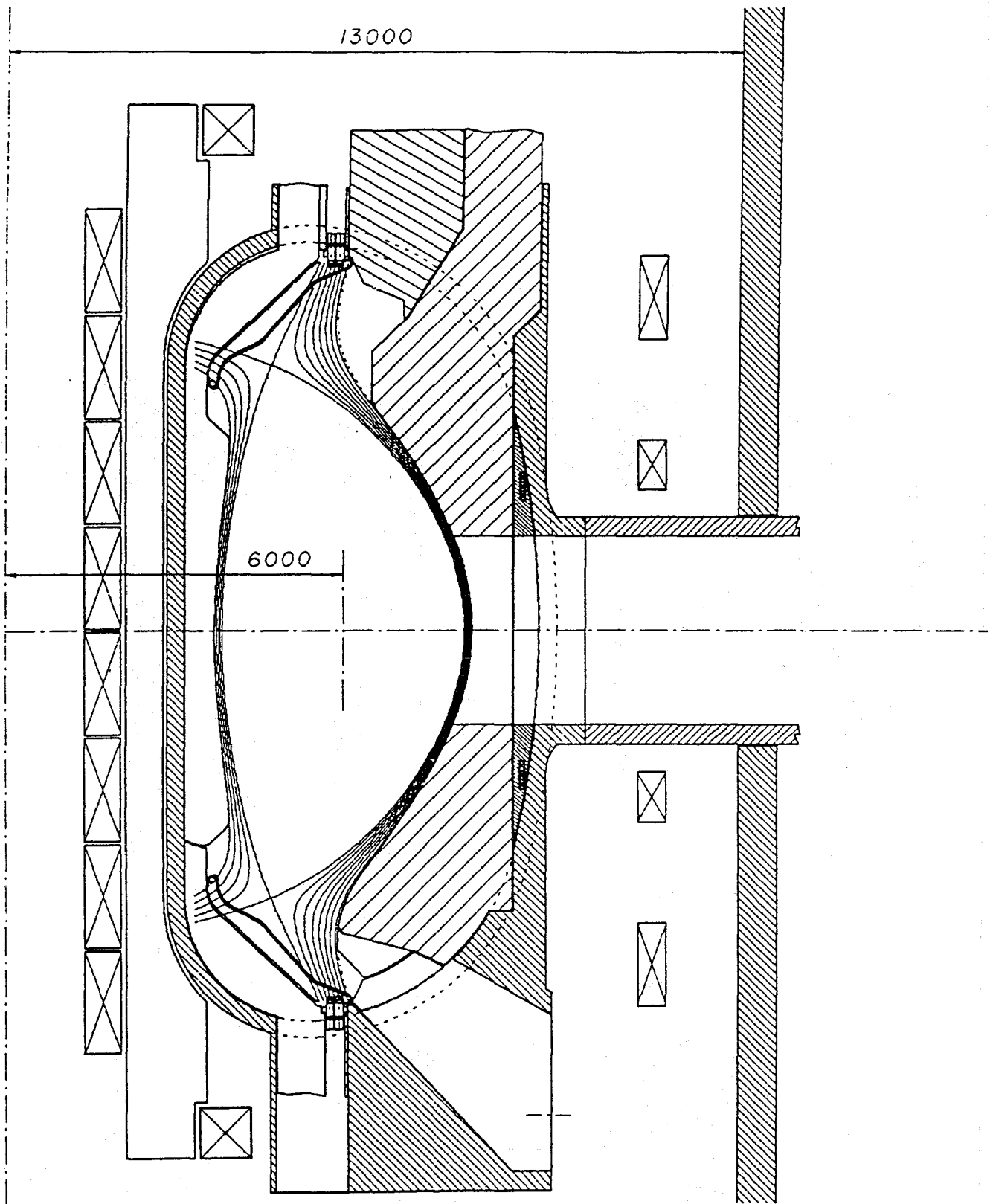
Fig. 3.1-1   Blanket test port in ITER

cryostat wall

shield

plug box

test
module

vacuum vessel
wall

adapter box
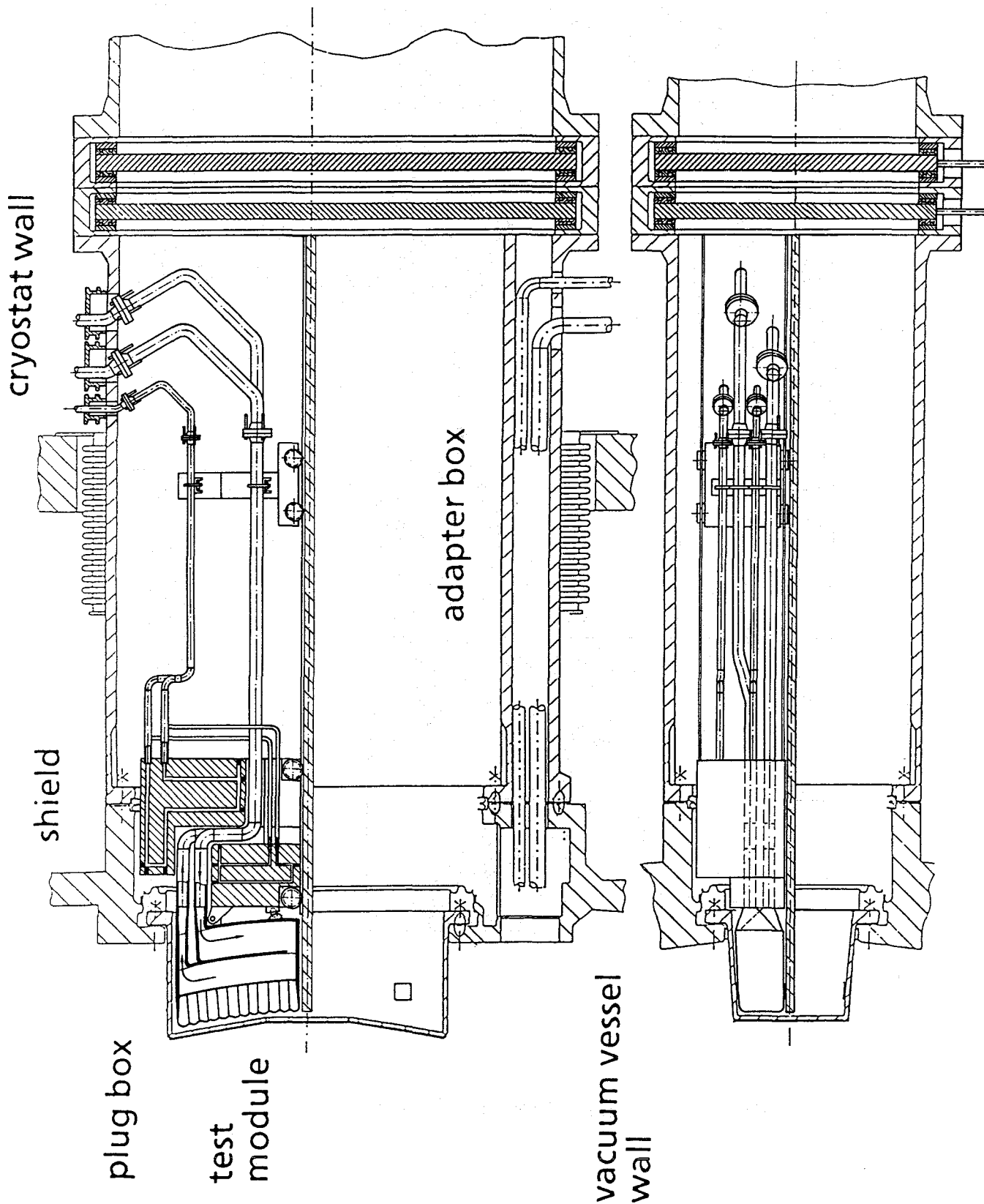
Fig. 3.1-2   Quarter-sized blanket test modul

108

3.2   Ancillary loop system
3.2.1   Loop concept of test module

The goal of the NET/ITER ancillary loop system is the cooling of the test module and the removal and recovery of the bred tritium. In contrast to DEMO (section 2.3) only the one test plug has to be maintained instead of the 80 blankets and no power conversion station is foreseen. Fig. 3.2-1 shows the schematic of the NET/ITER-ancillary loop system.

Because NET/ITER will be the first fusion plant with a burning plasma the operational risk of the ancillary loops should be as low as possible. Conventional and well approved components therefore are chosen for the use in these loops. More advanced designs as the double walled steam generator are foreseen for the next step of fusion reactors, for DEMO.

Two heat exchangers of the KNK type with an intermediate NaK loop are the central components of this loops. These components with a long time operation experience are promising a good reliability of the loop system.

The liquid lead lithium is circulated with a one stage free surface circulation pump (like DEMO section 2.3) through the test plug, the first heat exchanger and the purification system. The heat and the tritium are passing the pipe wall of the heat exchanger (2.9 mm) from the Pb-17Li to the NaK of the intermediate loop. The intermediate NaK-loop is necessary here in contrast to DEMO due to the division of the heat exchanger in 2 components. An electromagnetic pump is circulating the NaK flow between both heat exchangers. The second heat exchanger is releasing the heat flow to the site cooling water system without steam production. To prevent freezing of the lead lithium flow, the second heat exchanger has a NaK bypass and a temperature controlled valve. For the same reason, and particularly for bridging the off-burn time and for preheating before filling with Pb-17Li a heater is installed in the intermediate NaK loop.

The tritium removal and recovery system is described in section 3.2.2.1.

3.2.2   Conceptual design

The most important design details of the NET/ITER ancillary loop system comprising the Pb-17Li - the NaK - and the cooling water loop are described in this section. In the section 3.2.3 a room layout for this loop system is presented.

Fig. 3.2.-2 shows the two heat exchangers, which are modifications of the well approved KNK type. They consist of double tubes components which are arranged in parallel and surrounded by a casing. Pb-17Li, NaK or water are introduced in the direction of the expected natural circulation flow through the inner tube and the annular gap between the inner and outer tube. The tubes are bent into a meandering shape and they are inclined so that a complete draining is possible. At the Pb-17Li/NaK heat exchanger a trace heating is provided on the outside for preheating before filling with Pb-17Li, and the insulation on these sides is arranged with a space between casing and insulation material. The space allows air cooling of the casing if decay heat removal is required. Table 3.2-2 shows the main data of the heat exchangers.

A single stage radial centrifugal pump with vertical shaft designed for a pressure difference of about 22 bar, which has a free surface covered with cover gas (He), is proposed for the Pb-17Li pump, like DEMO (Section 2.3.2.1). The bottom of the vertical pump shaft is borne in a hydrostatic bearing with Pb-17Li as the working substance. The covergas shaft sealing is performed by means of two mechanical shaft seals. An improvement of the sealing concept may be necessary in the view of possible tritium contamination of the oil lubricant and the detriation of cover gas containing oil impurities.

An electromagnetic induction pump designed for a pressure difference of 4 bar was chosen for the NaK pump. On account of its closed design, the EM pump displays a number of advantages over pumps with free surfaces as regards possible tritium leakages. Only the pressure difference in the NaK-loop which is low compared with the Pb-17Li-loop permits the use of an EM pump in the NaK loop. The small NaK flow through the tritium extraction system in a parallel loop is forced by this pump too (Section 3.2.2.1).

A purification system to hold back corrosion products and other contaminants of the Pb-17Li flow in order to reduce radioactive contamination and to prevent plugging of the components, has still to be developed as already outlined in Section 2.3.2.1 for DEMO.

As necessary for each liquid metal loop two dump tanks (for Pb-17Li and NaK), two expansion tanks, two covergas systems (He and Ar) and several valves, filters, steam traps etc. are provided as can be seen in Fig. 3.2.-1.

3.2.2.1 Tritium extraction system (NaK)

The system for tritium removal and recovery for NET/ITER principly works as described for DEMO (Section 2.3.2.3). The main difference between both systems is that at NET/ITER only the tritum production of a 5 MW test plug has to be removed and recovered but at DEMO a 4 resp. 6 times higher tritum rate at each of the 80 blanket segments exists. Moreover, the NaK loop at NET/ITER has a relativ high mass flow rate due to the additional heat transportation function. The tritum extraction system only uses a small branch flow of the intermediate loop. As listed out in Table 3.2.-1 this mass flow rate branching to the tritium extraction system is only 0.15 kg/s which is about 0.2% of the intermediate loop NaK flow. The volume of one corresponding cold trap (for precipitation only) is 0.05 m^3 roughly resulting in the dimensions of 0.2 m diameter to 1.6 m length. This dimensions are basing on the assumption that no extra tritium permeation resistance in the NaK/water heat exchanger is provided and a tritium loss into the site water cooling system of 4.5 Ci/d is tolerated.

3.2.3   Room layout of system components

Fig. 3.2-3 shows an arrangement of the components of the NET/ITER ancillary loops in a room with an area of about 75 m^2 on two levels and a height of about 11 m. This arrangement is tentative of course because the exact location in the reactor site is not defined till now. Several small components like valves, control facilities, the cover gas system and compensators of the piping system are omitted in this drawing.

References to section 3.2:

[1]   INTERATOM, contract for development of the cooling circuits for the liquid metal cooled blankets, Kernforschungszentrum 1990, unpublished.

Table 3.2.-1 Thermal data of the NET/ITER ancillary loops

Thermal Power [MW]	5
Pb-Li-loop:	
Mass flow rate [kg/s]	351
Temperatures [°C] Blanket outlet	350
Blanket inlet	275
Pressure loss [bar]	~ 22
Total volume (PbLi) [m³]	~ 5
Nom. diameter (main pipe) [mm]	200
NaK-loop:	
Mass flow rate [kg/s]	76
Temperatures [°C]	
Heat exchang. PbLi/NaK, inlet:	240
outlet:	315
Heat exchang. NaK/Water, inlet:	315
outlet:	240
Total volume (NaK) [m³]	~ 2
Nom. diameter (main pipe) [mm]	150
NaK-tritium-loop:	
Mass flow rate [kg/s]	0.15
Volume of 1 cold trap [m³]	0.06
Water-loop:	
Mass flow rate [kg/s]	16
Temperatures [°C]	
Heat exchang., inlet:	120
outlet:	195

Tab. 3.2.-2   Design data of the 5 MW NET/ITER heat exchangers

	Pb-17Li/NaK Heat Exchanger	Nak/H$_2$O Heat Exchanger
Temperatures [°C]		
Inlet (prim./sec.)	350/240	315/120
Outlet (prim./sec.)	275/315	240/195
Number of tubes	35	16
Dimensions		
Outer tube [mm]	60.3 x 2.9	60.3 x 2.9
Inner tube [mm]	42.4 x 2.9	30 x 2.6
Annular gap [mm]	6.05	12.25
Heating surface [m^2]	36	10.5

He-Inlet

PbLi-expansion vessel

PbLi-pump

NaK-expansion vessel

Heater

Testplug

PbLi/NaK-
heat exch.

NaK/H₂O-
heat exchanger

Cooling water

PbLi-purificat.

NaK-pump

Filter

He-Outlet

Steam trap

PbLi-dump tank

Economiser

114

Ar-Inlet

Ar-Outlet

Vac.-pump

Ar-pump

Tritiumgetter

Cold trap

Heater
Cooler

Cold trap

Buffer for
trit. contain. Ar

NaK-dump tank
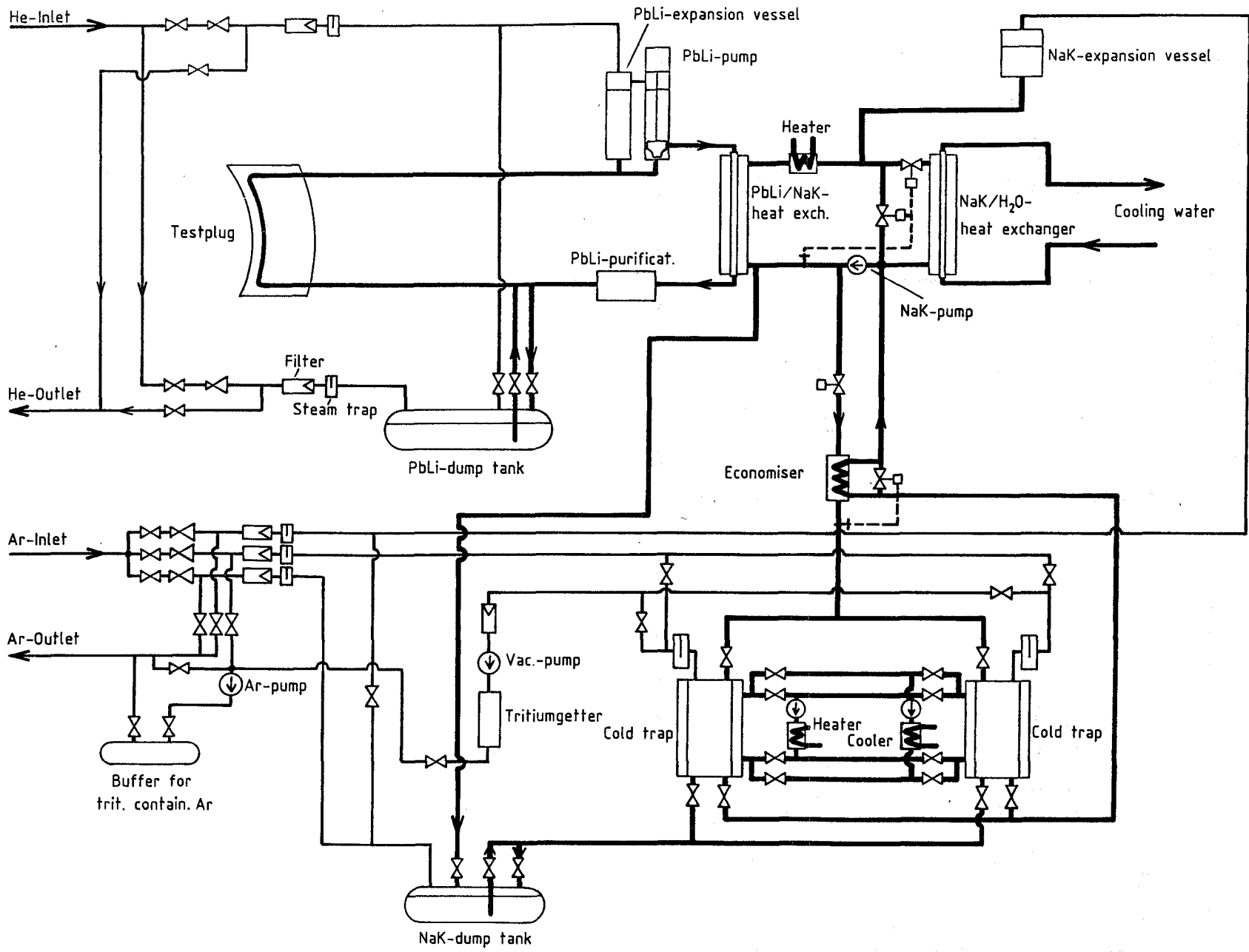
Fig. 3.2-1   NET/ITER ancillary loop system
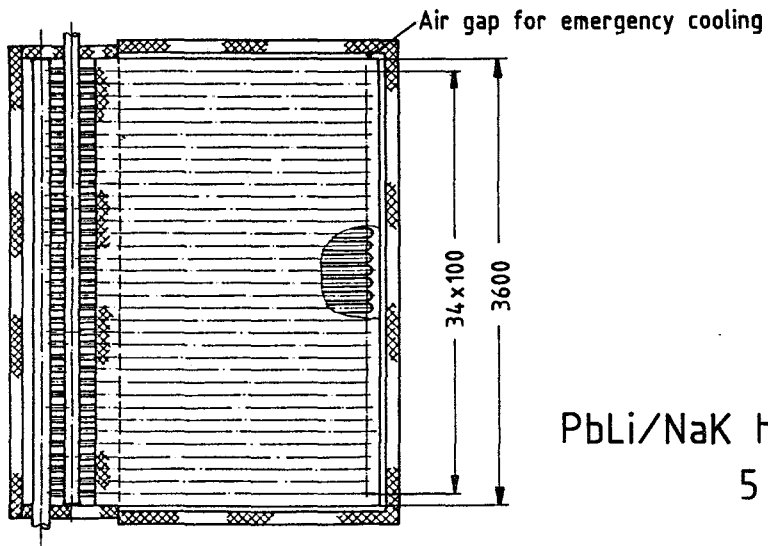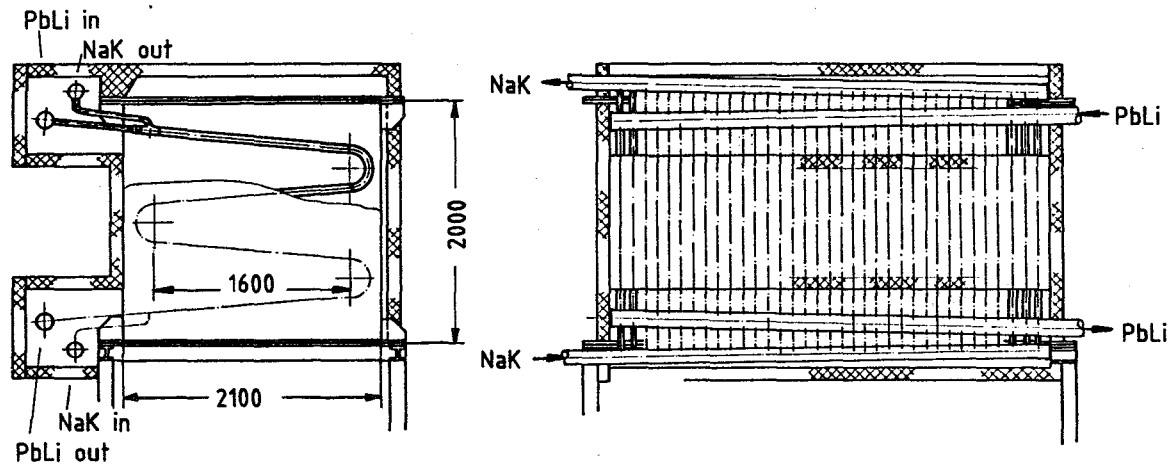
PbLi/NaK heat exchanger
5 MW
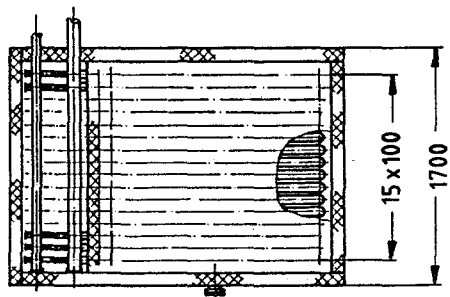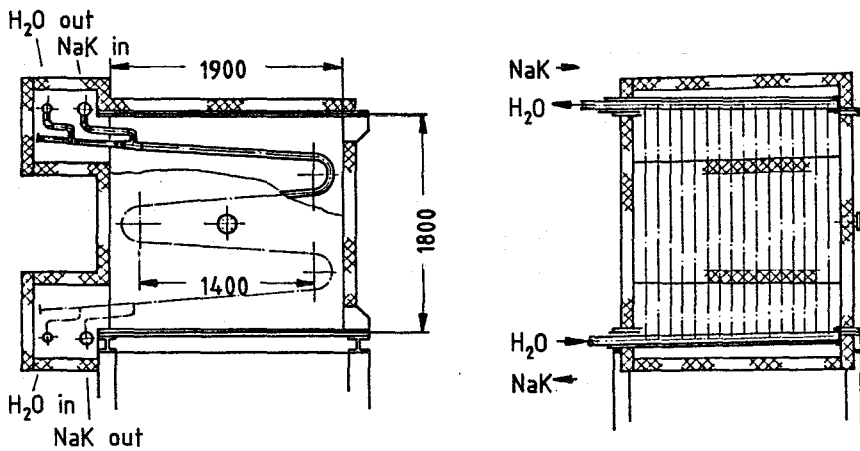
NaK/H₂O heat exchanger
5 MW

Fig. 3.2.2   NET/ITER heat exchangers

115

Section A-A

PbLi-Exp.-Tank

PbLi-NaK-HTX

PbLi-Purification

NaK-Pump

NaK-Water-HTX

Cooling-Water

PbLi-Pump

Section B-B

PbLi-Tank

Economiser

Cold-Traps

Tritium-Extr. System

NaK-Tank

PbLi-Pump

NaK-Exp.-Tank

NaK-Water-HTX

PbLi-NaK-HTX

NaK-Pump

PbLi-Purification

Section C-C

PbLi-Exp.-Tank

Tritium Extr.System

PbLi-Tank

Cold-Trap

NaK-Tank

Economiser

PbLi-Tank

1 m
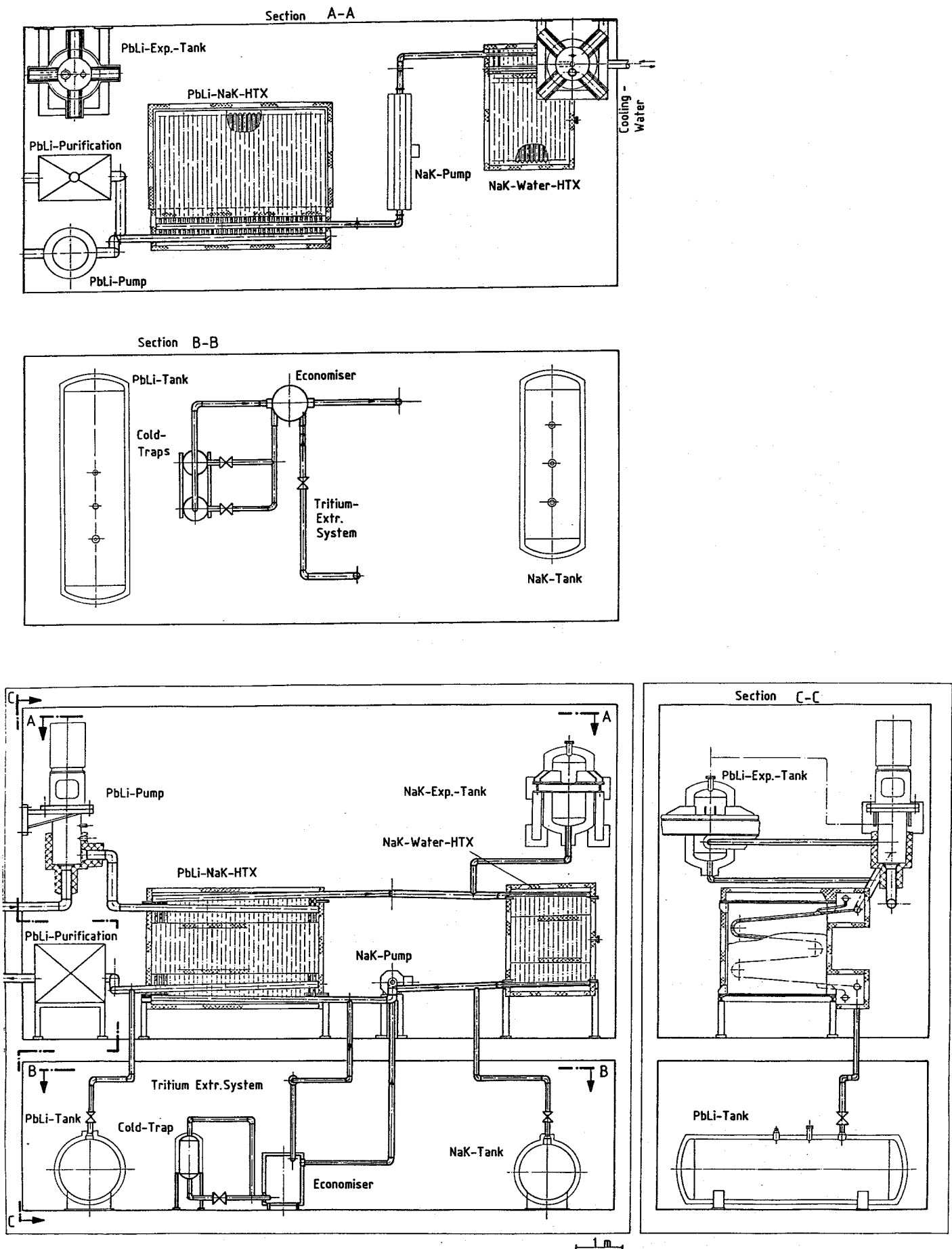
Fig. 3.2-3   NET/ITER Room layout of system components

116

3.3 Tritium build up in the NET/ITER test object system

Equilibrium measurement conditions must be reached to test tritium transport, inventory and removal efficiency, therefore, the fusion reactor has to operate for a certain time period to build up the required tritium concentrations in the NET/ITER test object and the ancillary system. Calculations were performed in order to determine the time dependent tritium concentrations in the primary Pb-17Li loop, the secondary NaK-loop and the structural materials, compare Fig. 3.3-1. As tritium source term only tritium production in the Pb-17Li was considered; plasma-driven permeation through the first wall was neglected. Due to the cyclic NET/ITER operation the tritium build up shows a sawtooth-type dependency. This sawtooth structure is not modeled but averaged values are used. With further simplifications coupled ordinary differential equations are finally obtained, for details see [1].

Table 3.3-1 contains characteristic values used in the calculations. Compared to this table, the present maximum dimensions of the test object and ancillary circuits are increased by a factor of about 1.5. Because the tritium generation rate is increased in the same way the time dependent tritium concentrations are not changed significantly. The presented values for the tritium inventories are valid for the new values.

Figure 3.3-1 shows results for the case that the permeability of the ferritic heat exchanger material is the same as measured recently for MANET [2]. (This assumption does not imply that MANET is recommended outside of the blanket but points out the sensitivity of the calculations in respect to permeability data as shown below). Steady-state conditions are then reached approximately after 100 hrs. A final tritium inventory in the liquid metals and structural materials of about 1.8 g is obtained. The additional tritium inventory in the cold traps during the testing period is about 0.5 g (assuming two recovery cycles per day).

One method to save operational time of the reactor is to start cold trap operation only when the steady-state concentration in the secondary loop is reached. With this, the required time period then becomes about 20 hrs, compare Fig. 3.3-2.

If it proves that the permeability of conventional ferritic steels is about a factor of 7 higher than that of MANET (as measured by [3]), then the required reactor operation period is reduced to about 20 hrs, see Fig. 3.3-3 (and can be further reduced

with a delayed start of the cold trap operation). An additional favourable feature due to the higher permeability is the decreased tritium inventory which becomes about 0.5 g compared to 1.8 g. These calculations show the importance of the accurate knowledge of permeation data (including permeation barriers) for technical systems.

Another method to save reactor operation time would be to add tritium to the liquid metal loops (essentially to the NaK-loop) by permeation through a special permeator unit. This could be done by heating electrically the circuits without reactor operation at all. Then, reactor operation would be mainly required only for the testing period.

References to section 3.3:

[1]   J. REIMANN, "Tritium Inventory and Recovery for a Self-cooled Pb-17Li Blanket", Fusion Engng. and Design 14 (1991) 413-425.

[2]   K.S. FORCEY, D.K. ROSS, J.C.B. SIMPSON and D.S. EVANS, "Hydrogen Transport and Solubility in 316L and 1.4914 Steels for Fusion Reactor Applications", J. Nucl. Mater. 160 (1988), pp. 117-121.

[3]   T.A. RENNER and D.S. RAUE, "Tritium Permeation through Fe-2 1/4 Cr-1Mo Steam Generator Material", Nuclear Technology 22 (1979), 312-319.

Table 3.3-1 Characteristic values for the NET/ITER test object and ancillary components

plasma burn time	t_{burn} = 800 s
plasma off time	t_{off} = 200 s
permeation time per cycle	t_{perm} = 720 s
actual time	$t' = 1.38 \cdot t$
blanket tritium production rate	$\dot{m}_B$ = 0.75 g/d
blanket outlet temperature ($t \to \infty$)	T_{1o} = 350°C
blanket inlet temperature	T_{1i} = 275°C
NaK-heat exch. inlet temp.	T_{2i} = 240°C
NaK-heat exch. outlet temp.	T_{2o} = 315°C
mean permeation temperature	T_{perm} = 298°C
permeation factor	$\varnothing = 1.15 \cdot 10^{-14}$ (kg/s mPa$^{0.5}$)
Sievert constant K_1 for T_1 = 313°C	$K_1 = 3.05 \cdot 10^{-10}$ w.fr./Pa$^{0.5}$
Sievert constant K_2 for T_2 = 277.5°C	$K_2 = 3.44 \cdot 10^{-6}$ w.fr./Pa$^{0.5}$
Sievert constant K_M for T = 313°C	$K_M = 6.11 \cdot 10^{-10}$ w.fr./Pa$^{0.5}$
cold trap mass flow rate	$\dot{m}_2$ = 0.1 kg/s
cold trap outlet saturation concentration	$c_{CTo} = 1.05 \cdot 10^{-7}$ w.fr.
Pb-17Li/NaK heat exchanger surface	A = 25 m^2
NaK/water heat exchanger surface	A = 7.5 m^2
heat exchanger wall thickness	s = 2.9 mm
mass of NaK	m_2 = 1000 kg
mass of Pb-17Li	m_1 = 25000 kg
mass of structural material	m_M = 3000 kg

$$\frac{c_1}{c_{1\infty,\dot{m}_p=0}}$$

$$\frac{c_2}{c_{2\infty,\dot{m}_p=0}}$$

"2"

"1"

$\dot{m}_p = 0$: $c_{1\infty} = 3.63\cdot10^{-8}$ w.fr.; $I_{PbLi_\infty} = 1.15$ g

$I_{M_\infty} = 0.30$ g

$c_{2\infty} = 2.34\cdot10^{-7}$ w.fr.; $I_{NaK_\infty} = 0.35$ g

"1" Pb-17Li "2" NaK H_2O

$\dot{m}_P \sim B_1$

$\dot{m}_B$

$\dot{m}_{HX}$

$\dot{m}_2$

$\dot{m}_{CT}$

t'(h)
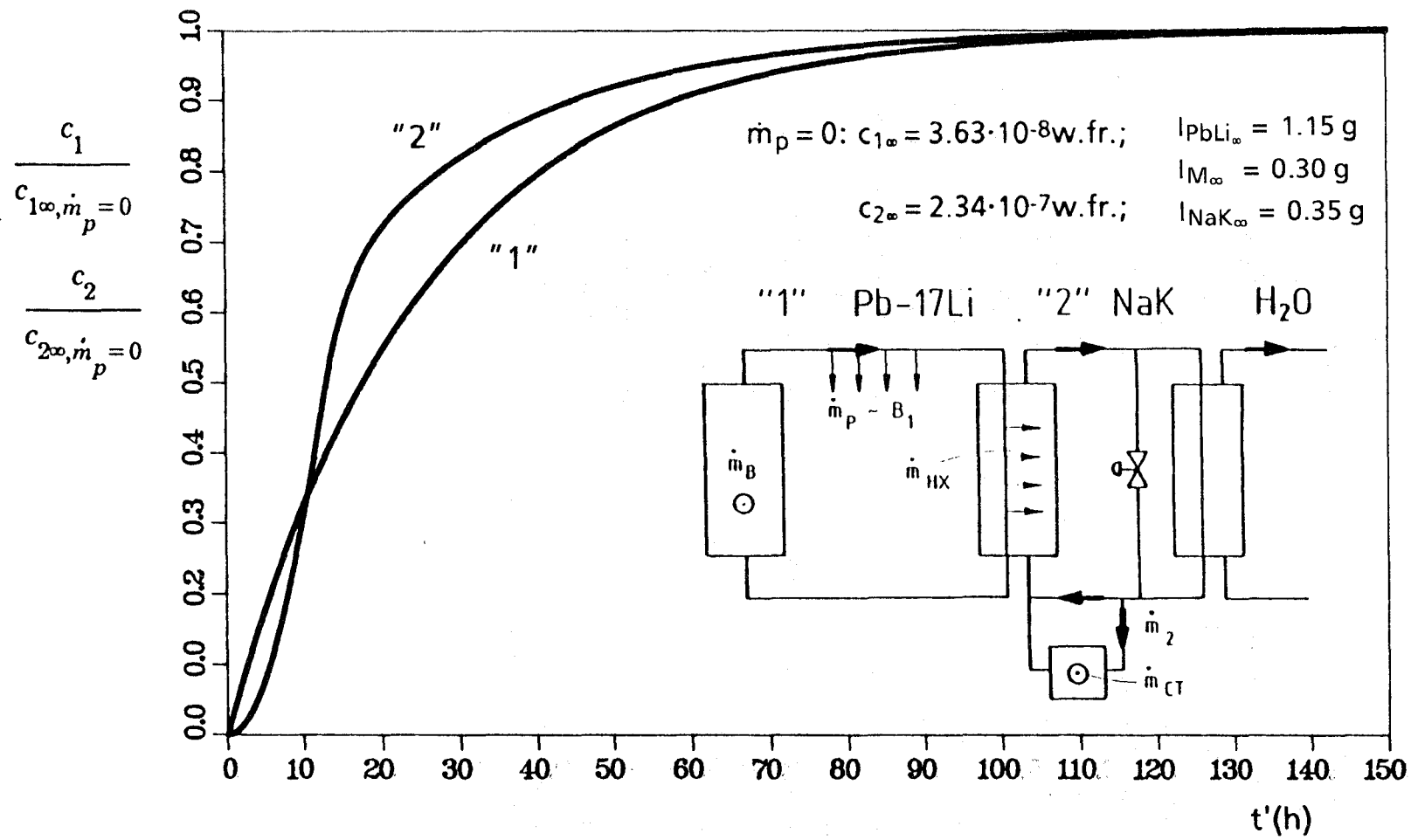
Fig. 3.3-1 Tritium Concentrations and Inventories

(Tritium Permeability from [2])

121

$$\frac{c_1}{c_{1\infty,\dot{m}_p=0}}$$

$$\frac{c_2}{c_{2\infty,\dot{m}_p=0}}$$

"2"

"1"

no tritium removal by
cold trapping

t'(h)
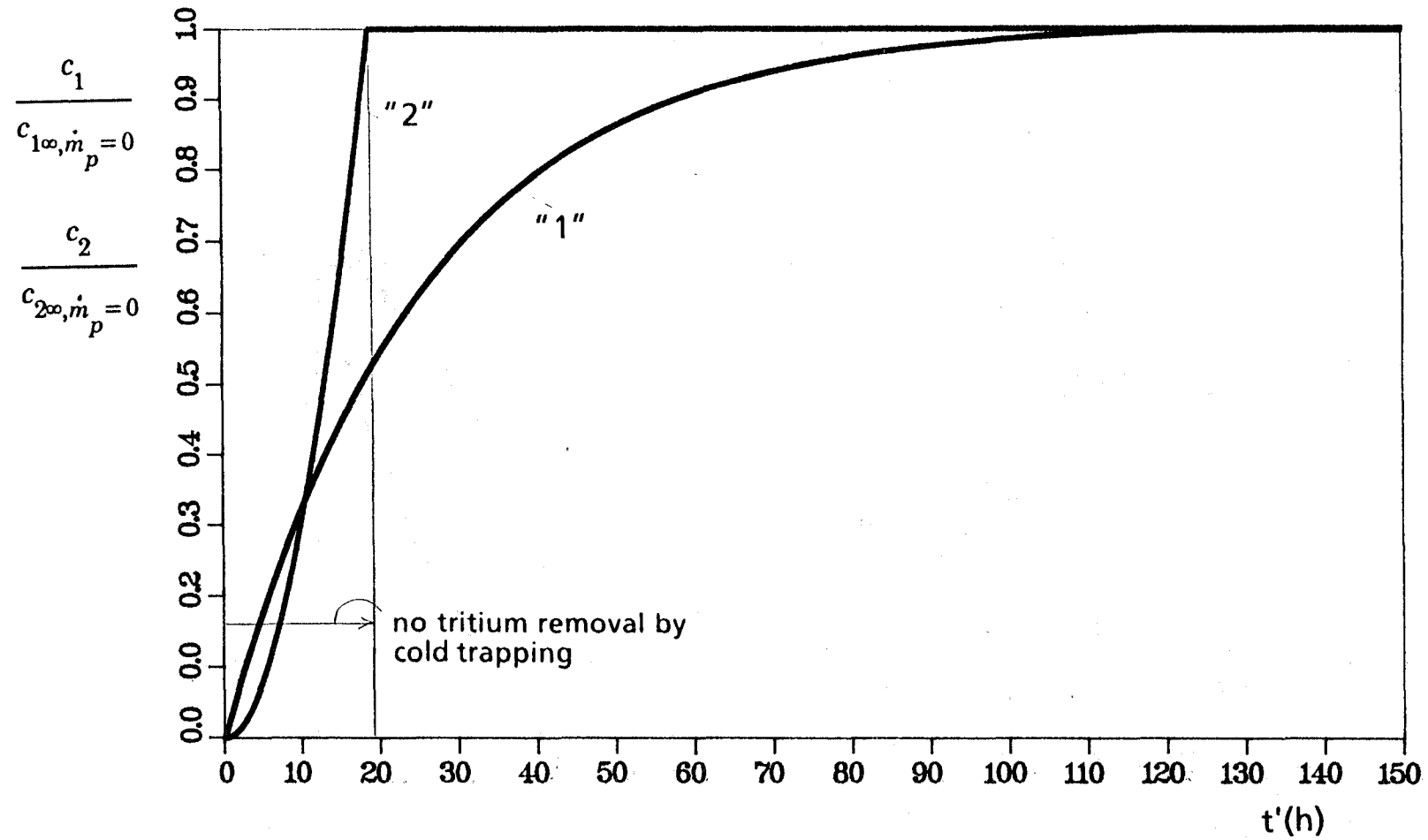
Fig. 3.3-2 Tritium Concentrations and Inventories (Tritium Permeability from
[2] (no Tritium Removal by Cold Trapping for the first 18 hours)
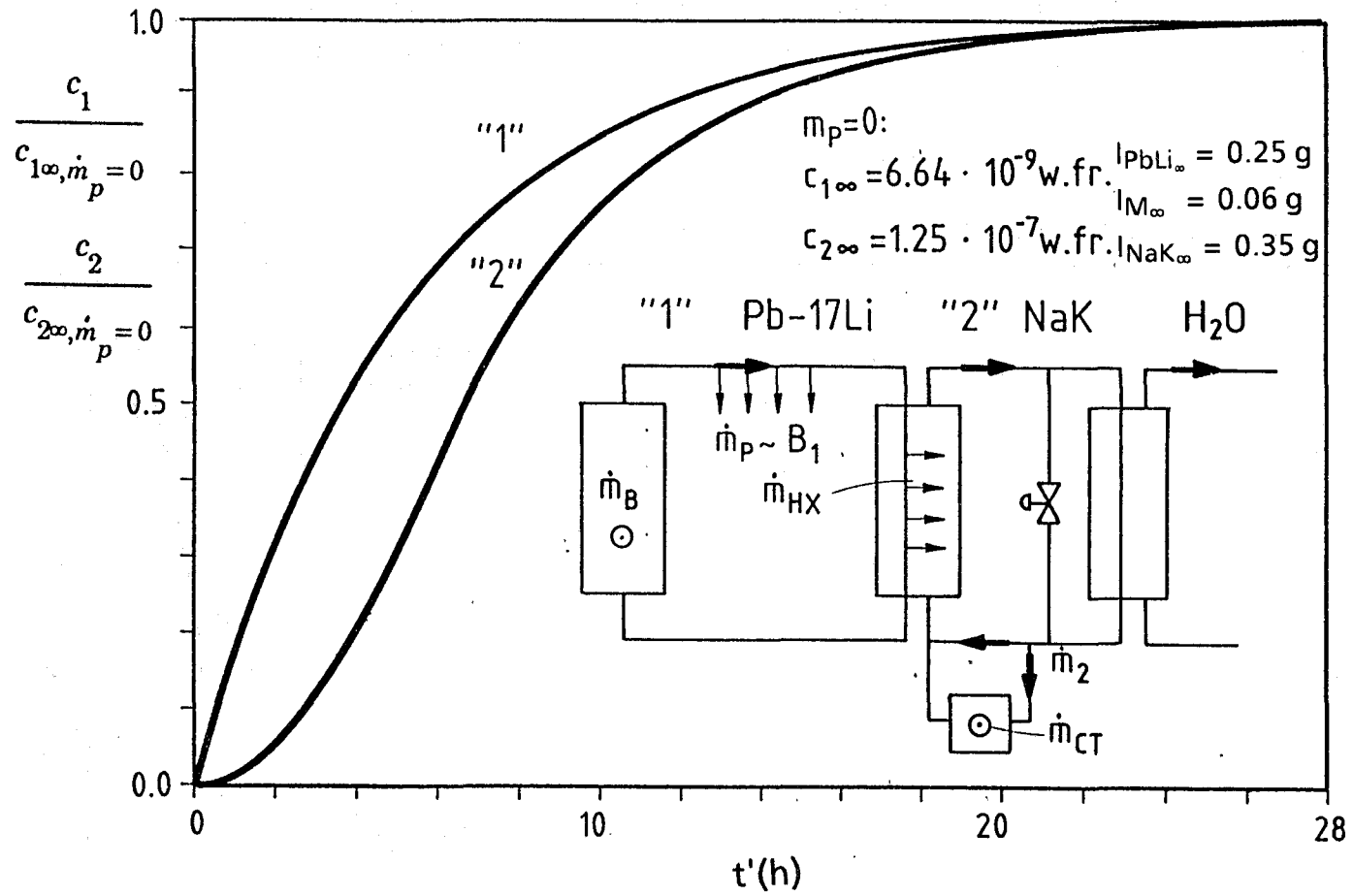
Fig. 3.3-3 Tritium Concentrations and Inventories
(Tritium Permeability from [3])

3.4 Safety

As described in section 3.1 and 3.2 a test plug requires three separate circuits coupled with two heat exchangers. The plasma-near test module and primary circuit respectively uses Pb-17Li as coolant, the intermediate circuit NaK and the third circuit water.

The possible interaction of liquid metals with water, concrete or air are similar to those mentioned in section 2.5. However, a Pb-17Li/NaK or a NaK/water heat exchanger is simpler and more reliable than the three component heat exchanger foreseen for the DEMO. For sodium water heat exchangers experimental experience is available from the fast breeder projects of different countries. Besides this, the amount of liquid metals involved are less than for a DEMO even if we refer to one blanket segment only.

Irradiation concerns are also expected to be of less concern because of lower neutron fluxes and shorter exposure time. However the concern with respect to polonium is similar because of its low acceptable release rates.

Thus, the safety aspects of a test modul for NET/ITER are mainly seen in the field of operational safety and reliability. With respect to accidents no severe problems are expected. However, a definitive statement requires a much more detailed design both for the test plug and for the NET/ITER machine.

3.5 Building, heat sink and handling requirements of the blanket test program

Blanket testing will be performed through horizontal access ports around the torus. There will be a separate heat extraction system for each test module. This implies that, if for example a test port is shared by four sub-modules, space has to be provided for a number of independent heat- and tritium extraction systems. It has been estimated [1] that the space requirement for four sub-modules amounts to 300 m$^2 \times 11$ m. This space has to be provided as close as possible to the test ports in order to minimize the length of liquid metal pipes between test module, primary heat exchanger, and secondary heat exchanger. Short connecting pipes are necessary to minimize the liquid metal inventory for safety reasons and to reduce the time required to achieve tritium equilibrium conditions. Space allocation close to the test port is of less importance for gas- or water-cooled blanket test modules.

The heat and tritium extraction systems for the self-cooled blanket test module are described in section 3.2. The main data of the systems for a full-sized test module are listed in Tab. 3.2-1 and 3.2-2. An important issue is the tritium permeation rate to the cooling water in the secondary heat exchanger. The present estimate is, that this permeation loss will be limited to a value below 20 Ci/day for a 5 MW test module. This value may be tolerable since a closed water loop is required in any case. Tritium recovered during regeneration of the cold traps is of high purity. It can be transferred to storage getters without any additional interface system.

The handling equipment has to be designed for a frequent exchange of test modules having a weight of up to 10 tons. Test port design and handling equipment should allow for replacement of one sub-module without interfering with the neighbouring sub-modules. Double doors between test port and transfer flask as shown in Fig. 3.1-2 will facilitate the module exchange without opening the test port to the building hall. This is especially important for modules exposed to the plasma.

References to section 3.5:

[1]   M. Tillak et al., ITER Test Program, ITER Document Series, No. 24, International Atomic Energy Agency, Vienna 1990.

4. STATUS OF THE R + D PROGRAM

The sections "Blanket Design for a DEMO-Reactor" and "Test Object Design for NET/ITER" concentrated on selected design aspects. These aspects, however, are based on an extensive R + D effort to provide the theoretical and experimental base. Additionally the scope of the R + D is much more comprehensive and allows alternatives which are also described in the sections 4.1 to 4.8 giving the state of the art. Section 4.9 adds short descriptions of the main KfK experimental facilities.

4.1 Neutronics: Methods and data
4.1.1 General aspects

The neutronic calculations for the blanket layout are performed with the Monte Carlo transport code MCNP and nuclear data from the European Fusion File EFF-1 (see section 2.1.2). The application of the Monte Carlo transport procedure allows to model the geometrical arrangement of the blanket segments in the three-dimensional configuration of the Demo reactor. This is possible as the Monte Carlo procedure does not solve a transport equation, but it rather simulates individual neutron histories. Actually the Monte Carlo procedure is an appropriate description of the microscopic neutron transport phenomenon, which on principle is a stochastic process, where the interaction probability of a neutron and an atomic nucleus is described by means of the underlying nuclear cross-sections. Anologous to the physical reality the Monte Carlo procedure follows a neutron history from its birth in a (d, t)-fusion reaction to its death in an absorption reaction in the reactor components or by leakage out of the reactor system. All stochastic events (neutron birth, nuclear interaction processes, generation of secondary particles etc.) are simulated by sampling random numbers and taking into account the governing physical laws with their associated data.

In principle there are no restrictions imposed on the quality of this computational procedure: the accuracy of a specific calculational quantity depends on the number of events contributing to this quantity and, of course, on the involved nuclear cross-section data. In practice this means that a large number of neutron histories has to be followed in order to minimize the statistical uncertainty; thereby use is made of the fact that for a large number of neutron histories on average the behaviour of a statistical ensemble of neutrons in reality is approached. On modern large computers this is not a serious limitation for the accuracy; this even holds for

"deep penetration problems", e.g. shielding calculations, if sophisticated variance reduction techniques are applied (see section 2.2.1).

Therefore, the accuracy of the calculated quantities (reaction rates, flux densities, power densities etc.) mainly is limited by the accuracy of the applied nuclear cross-section data. Considerable effort is being spent on improving the nuclear data base for neutronic calculations. Within the European Fusion Technology Programme this is performed in the EFF (European Fusion File)-project, on a supranational level this is performed in the FENDL (Fusion Evaluated Nuclear Data Library)-project under the auspices of the IAEA.

With regard to tritium breeding in the Pb-17Li liquid metal blanket, the most important nuclear data are those of ^{6}Li and Pb: ^{6}Li acts as tritium breeding material (enriched to 90 atom %), Pb serves as neutron multiplier. Thus the most important nuclear interaction processes are the ^{6}Li (n, α)t- and the Pb (n, 2n)-reaction. Furthermore, the elastic scattering process of Pb plays an important role: it dominates all other competing nuclear reactions in the high energy range. However, elastic scattering is a well known nuclear process; but care must be taken of the angular dependence of the elastic scattering cross-section at high neutron energies and its adequate description in the transport calculation. Actually this is not a problem for the Monte Carlo transport technique using angle-dependent scattering intervals, but it may be a problem for deterministic computational procedures using truncated Legendre polynomial series expansions of the scattering kernel (see below).

The nuclear cross-section of the ^{6}Li (n, α)t-reaction is of the well known 1/v-type with a broad resonance at 0.25 MeV neutron energy; its accuracy surely is sufficient. The (n, 2n)-cross-section of Pb therefore is the main source of data uncertainties with respect to the uncertainty of the TBR-calculation in the Pb-17Li blanket. In the past considerable effort has been spent on improving the knowledge of the neutron interaction processes in lead: integral 14 MeV neutron multiplication experiments in spherical geometry have been performed [1 − 7] and have been analysed by using various computational approaches and data evaluations [1,8,9]. The lead spherical shell experiment performed at the Technical University of Dresden (TUD) has been the subject of an extensive benchmark task organized by the IAEA in the framework of the FENDL-project [10]. As a result of all these activities it can be stated that satisfactory agreement

between experiments and calculations has been achieved for the neutron multiplication factors of lead.

4.1.2 Neutron multiplication of lead

In the past decade there had been a serious discrepancy between calculated and measured neutron multiplications factors: in integral experiments about 10% more neutrons had been observed than had been predicted by the calculations (see, for instance, the experimental data points TUD 87 and Takahashi et al. 85 in Fig. 4.1-1). This discrepancy had been observed in all calculations, independent on the computational procedure and the data evaluation used [9] (see, for example, Table 4.1.1). Actually the Pb (n, 2n)-cross section at 14 MeV agreed fairly well in all of the data evaluations, the EFF-1-evaluation inclusively. As a result of the benchmark analyses it had been concluded, that there is a need for increasing the 14 MeV (n, 2n)-cross-section of Pb in EFF-1 [9]. This conclusion meanwhile also has been drawn by the nuclear data evaluators: Vonach et al. recommend a 14 MeV (n, 2n)-cross-section of 2.193 ± 0.07 barn [11], which means an increase of about 4.4% with respect to EFF-1. This value will be used in the forthcoming EFF-2 evaluation of lead. The calculated neutron multiplication factor for the TUD lead spherical shell thereby would increase from 1.76 (EFF-1) to about 1.80 (EFF-2). It is obvious from Fig. 4.1-1, however, that the discrepancy between experiments and calculations rather is due to the large uncertainties of the integral experiments than due to data uncertainties: the more recent multiplication experiments give considerable lower multiplication factors than the former ones (see Fig. 4.1-1). This also holds for the remeasurement of the TUD lead spherical shell performed at the Kurchatov Institute of Atomic Energy (KIAE 89) with the more accurate "boron tank method". Taking into account the increased (n, 2n)-cross-section of 2.193 barn, the calculated neutron multiplication factor agrees with the experimental one within its uncertainty margin. The same behaviour can be observed in case of the older KIAE-experiments (KIAE 88) and the more recent experiments of the Osaka University (Yamamoto et al. 88). In view of the fact that the 14 MeV (n,2n)-cross-section is rather well established now and, furthermore, the sensitivity of the neutron multiplication factor on the (n,2n)-cross-section is rather moderate, no further improvement can be expected from the calculational side; however, this could be expected from more accurate integral experiments. Despite the fact, that the Pb (n,2n) cross-section is well known at 14 MeV neutron energy, there are serious doubts about the shape of its excitation function, i.e. the energy-dependent (n,2n)-cross-section between the reaction threshold and 14 MeV. Actually this has

a significant impact on the neutron multiplication power of a liquid metal Pb-17Li blanket, as the neutron spectrum in the blanket is degraded. Therefore, new (n, 2n)-measurements between 7 and 14 MeV are strongly recommended [12].

4.1.3 Lead DDX-data and their use in transport calculations

The Pb (n, 2n)-reaction is a three-particle process which requires the use of correlated energy-angle emission cross-sections, i.e. double-differential (DDX) data, for the description of its kinematics. Actually, the lead evaluation performed at ECN Petten for the European Fusion File EFF-1 [13] was the first one taking fully into account the energy-angle correlation of the Pb (n, 2n)-reaction. For processing the lead DDX-data, which are stored in the ENDF/B-VI-format (MF6-file) on EFF-1, a special processing code GROUPXS had been developed [14]. In its original version GROUPXS generates conventional scattering matrices of Legendre order ℓ for use in conventional S_N-transport codes applying the Legendre approximation of the scattering kernel (S_N/P_ℓ-procedure). Accordingly the angular dependence of the scattering process is described by means of a truncated Legendre series expansion in the transport calculation, although the angle-energy correlation of the scattered neutrons is taken into account.

At KfK a completely different approach has been chosen: following a theory proposed by Takahashi et al. [15], a computational procedure has been developed that avoids the Legendre approximation of the scattering kernel through the use of novel angle-dependent scattering matrices. In this case the scattering integral can be evaluated by numerical integration. In a first step this rigorous method has been implemented into the well established S_N transport code ONETRAN [16] for treating one-dimensional problems in spherical and plane geometry [17]. A special processing code system has been developed to enable the generation of angle-dependent scattering matrices [18]: it consists of a special version of the GROUPXS-code for treating DDX-data, coupled with a special version of the NJOY83 processing code [19] for treating single-differential (SDX)-data. In both cases use is made of the fact that the underlying cross-section data are given in the Legendre approximation in the centre-of-mass system. The transformation to the laboratory system is performed pointwise in energy and angle taking into account the proper energy-angle correlations. Thus the angular dependence due to the transformation from the centre-of-mass system to the laboratory system is taking into account rigorously, whereas the angular dependence of the scattering process itself again is restricted by the use of the Legendre approximation for the SDX-

and DDX-data in the centre-of-mass system. For lead this is not really a restriction, as the angular dependence of the scattering processes is rather weak.

4.1.4 Lead benchmark calculations

For the validation of the rigorous S_N-method and its related data processing system the TUD lead spherical shell has been used. This experiment is sensitive to transport effects due to the large shell thickness of 22.5 cm corresponding to about 4.1 mean free paths of the 14 MeV neutrons. Rigorous ANTRA1-calculations are benchmarked against S_N/P_ℓ-calculations with the ONETRAN-code and Monte Carlo calculations with the MCNP-code. Fig. 4.1-2 shows the neutron leakage spectra obtained with the different computational approaches using the same underlying nuclear cross-sections from the EFF-1 file. Obviously there is perfect agreement between rigorous ANTRA1-calculations and approximative ONETRAN S_N/P_ℓ-calculations. This agreement is due to the fact that the underlying DDX-data are given in the Legendre approximation on the EFF-data file and, furthermore, the anisotropic neutron transport is very weak in lead. Actually the P_1-approximation is sufficient in this case, it agrees already with the rigorous ANTRA1-calculation (see Fig. 4.1-2). The rigorous S_N-procedure therefore is validated for the description of the 14 MeV neutron transport in lead and, moreover, it can be used for benchmarking the approximative S_N/P_ℓ-procedure. The leakage spectrum calculated with the MCNP-code and EFF-1 lead data largely agrees with the spectra calculated by ANTRA1 and ONETRAN, respectively (Fig. 4.1-3). There is, however, a significant difference in the high energy region (see Fig. 4.1-2): around 10 MeV and in the region 3 − 6 MeV the MCNP-calculation gives significantly less neutrons than the S_N-calculations. This difference is due to the energy-angle coupling of the secondary neutrons which is taken fully into account in both S_N-calculations but not in the MCNP-calculation. In other words, both S_N-calculations make use of the DDX-data, but the MCNP-calculation does not, although it is based on the same EFF-1 lead evaluation. This is due to the fact that the MCNP-code presently is not able to handle DDX-data; therefore the EFF-1 lead DDX-data have been processed into SDX-data [20], i.e. uncorrelated energy-angle distributions. The information on the correlation consequently is lost in the processing procedure. Actually this leads to an underestimation of the high energy neutron emission spectrum of the lead (n, 2n)-process.

4.1.5 Comparisons to measurements of the neutron leakage spectrum

Comparisons to measurements of the neutron leakage spectrum of the TuD lead spherical shell are shown in Figs. 4.1-2 and 4.1-3 using a linear and a logarithmic energy scale, respectively. It is seen that the leakage spectrum calculated with ANTRA1 and EFF-1 DDX-data agrees rather well with the measured spectrum nearly over the whole measured energy range. This also holds for S_N/P_ℓ-calculations with the ONETRAN-code and EFF-1 data. Actually this agreement reflects the quality of the underlying EFF-1 DDX-data. The MCNP-calculations using EFF-1 SDX-data, on the other hand, give a less good reproduction of the measured high energy spectrum. In fact it is very similar to the spectrum obtained with ENDF/B-IV lead data (not shown), neglecting also the angle-energy correlation of the lead (n, 2n)-process. Thus there is a need for using DDX-data in the transport calculations and the Monte Carlo code MCNP should be enabled to handle DDX-data as it is the main computational tool for the neutronic blanket layout.

References to section 4.1:

[1] A. Takahashi, Integral Measurements and Analysis of Nuclear Data Pertaining to Fusion Reactors, in: Proc. Int. Conf. Nuclear Data for Basic and Applied Science, Santa Fe, New Mexico, USA, May 13 - 17 (1985), pp. 59 - 70

[2] L.F. Hansen et al., The Transport of 14-MeV Neutrons Through Heavy Materials 150 < A < 208, Nucl. Sci. Eng. 92 (1986), 382 - 396

/3/ T. Elfruth et al., The Neutron Multiplication of Lead at 14 MeV Neutron Incidence Energy, Atomkernenergie-Kerntechnik 49 (1987), 121 - 125

[4] O.P. Joneja, V.R. Nargundkar, T.K. Basu, 14-MeV Neutron Multiplication Measurement in Lead, Fusion Technology 12 (1987), 114 - 118

[5] J. Yamamoto, A. Takahashi, M. Izumi, K. Sumita, Determination of Tritium Breeding Ratio in a Pb-Li Spherical Blanket by Leakage Neutron Spectra, Proc. First Int. Symp. on Fusion Nuclear Technology, Tokyo, Japan, April 10-19 (1988), Part C, 169 - 174

[6]   V.A. Zagryadskii et al., Calculated Neutron Transport Verification of Integral 14 MeV Neutron Source Experiments with Multiplying Assemblies, Proc. First Int. Symp. on Fusion Nuclear Technology, Tokyo, Japan, April 10-19 (1988), Part B, 353 - 358

[7]   S.I. Bessonov et al., Measurement of a Total Flux of Leakage Neutrons from a Lead Sphere Using the Total Absorption Method, IAEA-Advisory Group Meeting on the Nuclear Data for Neutron Multiplication in Fusion Reactor First Wall and Blanket Materials, Chengdu, P.R. China, November 19 - 21, 1990

[8]   M. Segev, Analysis of the Multiplication of D-T Neutron Sources in Blanket Materials of Fusion Reactors, Kernforschungszentrum Karlsruhe, Report KfK-3620 (May 1984)

[9]   U. Fischer, A. Schwenk-Ferrero, E. Wiegner, Neutron Multiplication in Lead: A Comparative Study Based on a New Calculational Procedure and New Nuclear Data, Proc. First Int. Symp. on Fusion Nuclear Technology, Tokyo, Japan, April 10 - 19 (1988), Part C, 139 - 144

[10] V. Goulo, J.J. Schmidt, Memorandum on the IAEA Fusion Evaluated Nuclear Data Library (FENDL), INDC/P (89) - 16, 9 June 1989

[11] H. Vonach, A. Pavlik, B. Strohmaier, Accurate Determination of (n, 2n) Cross-Sections for Heavy Nuclei from Neutron Production Spectra, Nucl. Sci. Eng. 106 (1990), 409 - 414

[12] H. Gruppelaar, K. Sumita, Workshop Report on Differential Data and Evaluation, IAEA Advisory Group Meeting on the Nuclear Data for Neutron Multiplication in Fusion Reactor First Wall and Blanket Materials, Chengdu, P.R. China, November 19 - 21, 1990

[13] H. Gruppelaar: Status of the European Fusion File, Int. Conf. on Nuclear Data for Science and Technology, Mito, Japan, May 30 - June 3, 1988

[14] H. Gruppelaar, D. Nierop, J.M. Akkermans, Processing of Double-Differential Cross Sections in the New ENDF-VI Format-GROUPXS Code Descrip-

tion and Users' Manual, Netherlands Energy Research Foundation, Report ECN-182 (April 1986)

[15] A. Takahashi et al., Method for Calculating Anisotropic Neutron Transport Using Scattering Kernel Without Polynomial Expansion, Journal of Nuclear Science and Technology 16 (1979), 1 - 15

[16] T.R. Hill, ONETRAN, a Discrete Ordinates Finite Element Code for the Solution of the One-dimensional Multigroup Transport Equation, Los Alamos National Laboratory, Report LA-5990-MS (1973)

[17] A. Schwenk-Ferrero, GANTRAS-A System of Codes for the Solution of the Multigroup Transport Equation with a Rigorous Treatment of Anisotropic Neutron Scattering - Plane and Spherical Geometry, Kernforschungszentrum Karlsruhe, Report KfK-4163 (November 1986)

[18] U. Fischer, E. Wiegner, Kernforschungszentrum Karlsruhe 1986, unpublished

[19] R.E. MacFarlane, D.W. Muir, R.M. Boicourt, The NJOY Nuclear Data Processing System, Vol. I, II, Los Alamos National Laboratory, Report LA-9303-M (May 1982)

[20] P. Vontobel, Generation of an EFF-1 Based Monte Carlo Neutron Library for MCNP, Paul Scherrer Institut Villigen, Switzerland, 1990, unpublished

Table 4.1-1: Osaka lead sphere experiment: Comparison of the total neutron multiplication factors obtained with different calculational methods and data evaluations

Data Base	EFF-1		ENDF/B-IV		ENDF/B-V	ENDL85	Takahashi 85 [1]
Transport Code	ANTRA1[a]	ONETRAN[b]	ONETRAN[c]	MCNP	MCNP[d]	MCNP	
shell thickness							
3 cm	1.20	1.19	1.20	1.20	1.20	1.20	1.34 ± 0.08
6 cm	1.35	1.35	1.37	1.36	1.36	1.37	1.54 ± 0.09
9 cm	1.48	1.47	1.49	1.49	1.49	1.50	1.69 ± 0.10
12 cm	1.57	1.57	1.59	1.58	1.58	1.60	1.80 ± 0.11

a)   rigorous method (30 energy groups/S_8-segmentation)

b) P_4-approximation (30/S_8)

c) P_3-approximation (25/S_8)

d)   performed by E.T. Cheng, General Atomics

neutron multiplication factor

lead spherical shells

TUD 87 /3/

KIAE 89 /7/

MCNP/ENDF|B-IV

Takahashi et al. 85 /1/

ANTRA 1/EFF-1

Yamamoto et al. 88 /5/

KIAE 88 /6/

shell thickness [cm]
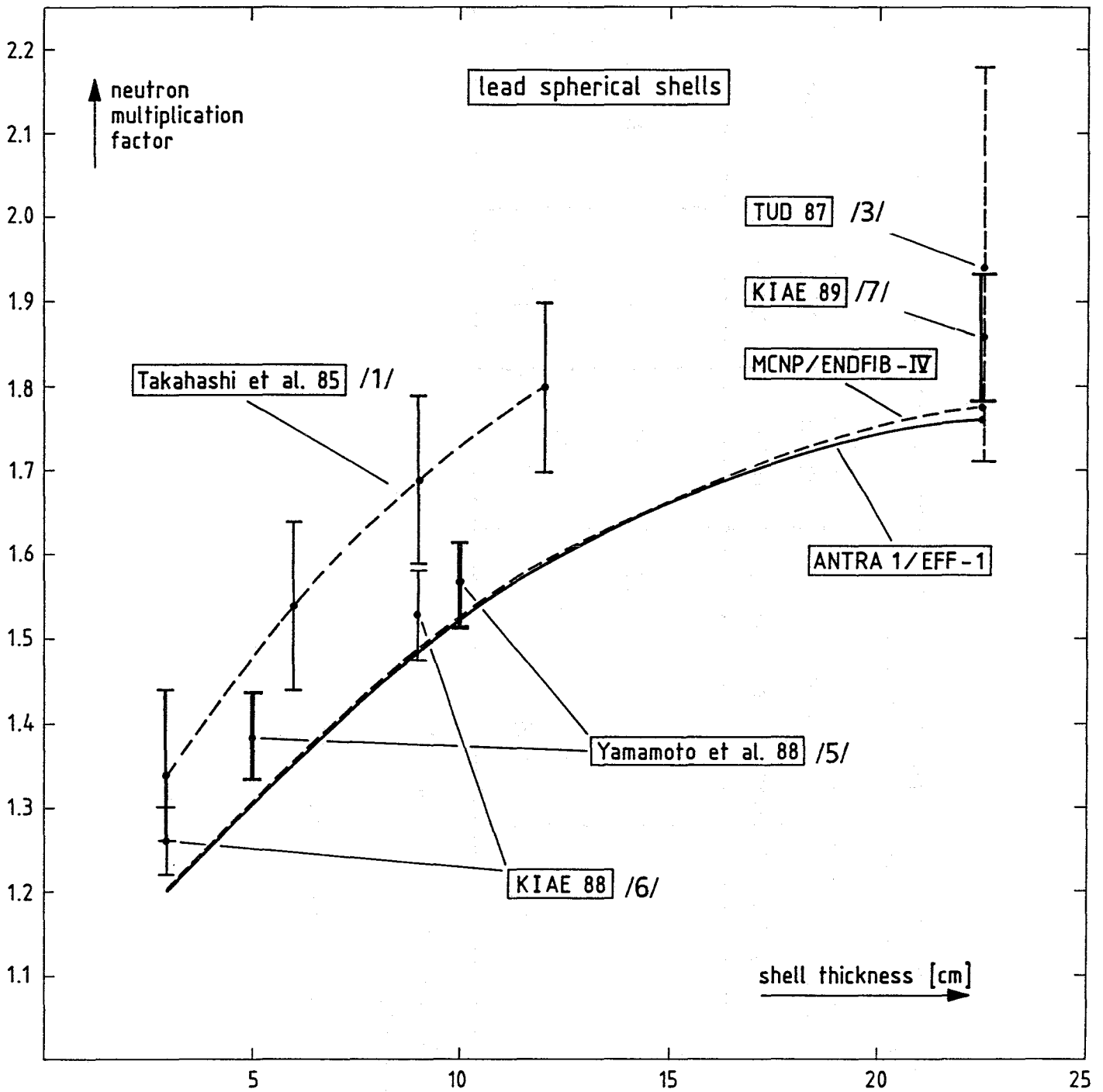
Fig. 4.1-1   Neutron multiplication factors of lead spherical shells with a central
14 MeV neutron source

134
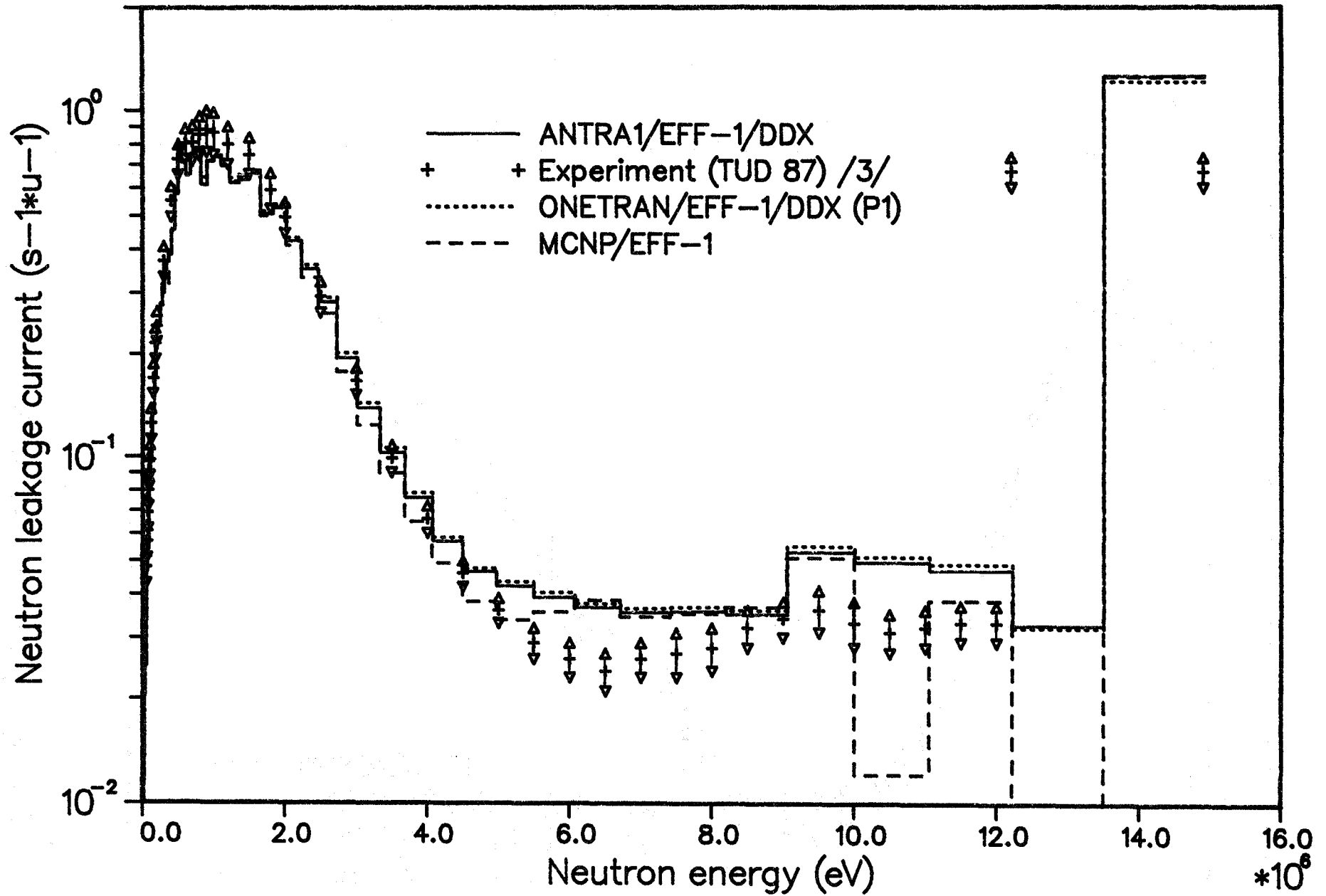
Fig. 4.1-2   Neutron leakage spectra of the TUD lead spherical shell: comparison
between different computational techniques using EFF-1 cross-section data and experimental data (linear energy scale)
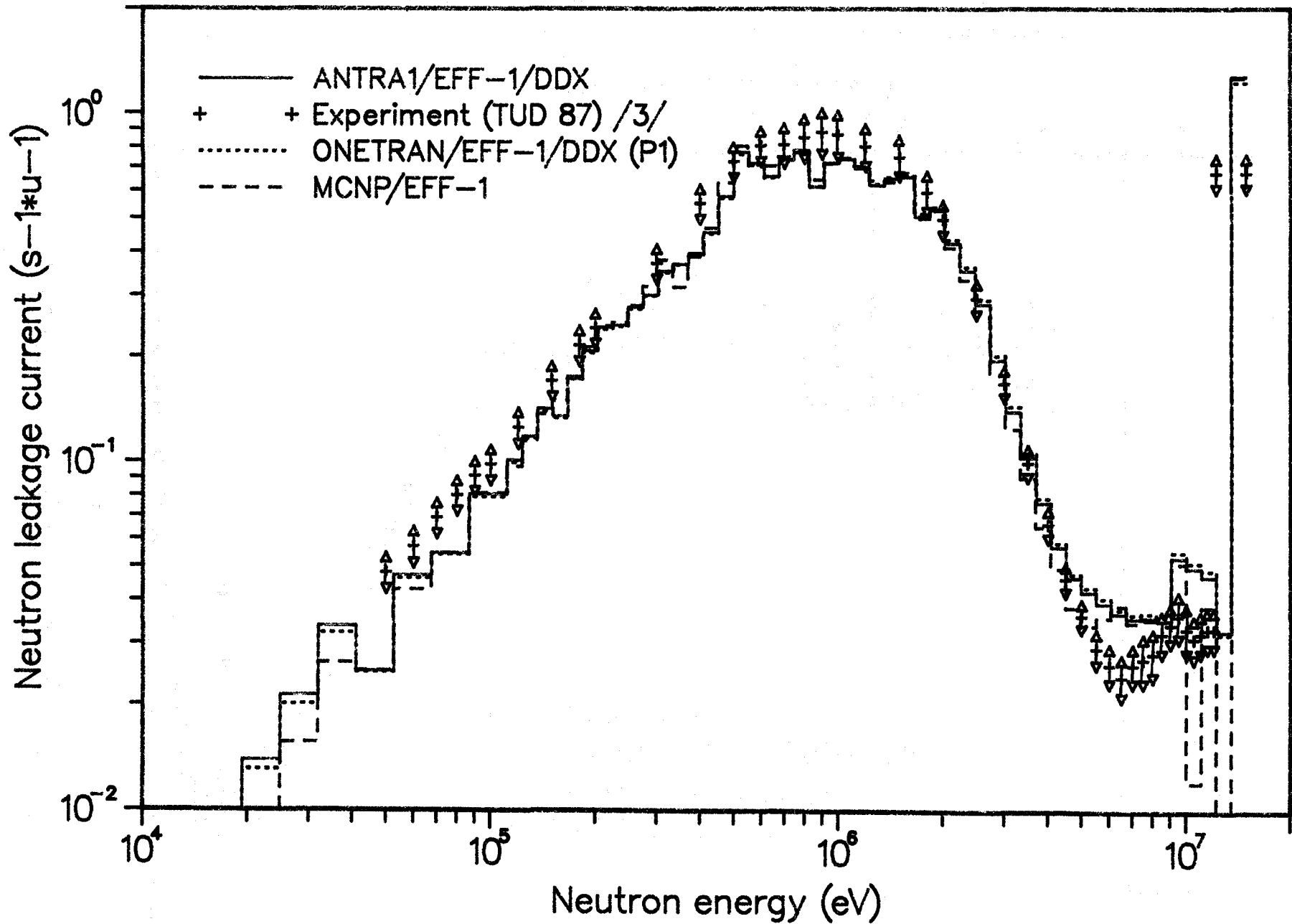
Fig. 4.1-3   Neutron leakage spectra of the TUD lead spherical shell: comparison between different computational techniques using EFF-1 cross-section data and experimental data (logarithmic energy scale)

4.2 Magnetohydrodynamics in self-cooled liquid metal blankets

The design of liquid metal cooled blankets is dominated by MHD-considerations. Liquid metal flow perpendicular to the strong magnetic field in a tokamak is accompanied by a high MHD pressure drop which can be a feasibility issue because it may result in mechanical stresses beyond the allowable limits of the structural material.

The magnetic field also influences the flow partitioning in parallel channels and causes velocity profiles in channels completely different from "usual" viscous flow. Velocity profiles in cooling ducts influence the heat transfer from the wall into the bulk flow which is in any case degraded by the suppression of turbulence in the magnetic field.

All three MHD problems - pressure drop, flow partitioning, and heat transfer reduction - are crucial issues for self-cooled liquid metal breeder concepts.

The MHD-issues encountered in designing self-cooled liquid metal breeder blankets can be divided into five groups:

a) Pressure drop in single ducts caused by two-dimensional flowing electrical currents.

b) Velocity profiles and additional pressure drops caused by three-dimensional flowing electrical currents in the regions of bends, expansions/contractions, manifolds, locally variable magnetic fields and so on. Generally, these currents flow inside the liquid metal and occur therefore in ducts with conductive and non-conductive walls as well.

c) Multi-channel effects caused by electrical currents flowing across the walls of parallel ducts. These "leakage currents" can cause large additional pressure drops and influence the flow partitioning in parallel channels.

d) Heat transfer from a heated duct wall to the flowing liquid metal. This heat transfer is determined by the velocity profiles and the turbulence near the wall.

4.2.1 Heat transfer and pressure drops in MHD channel flow

The flow velocity v of the liquid metal in the front cooling channel of a selfcooled liquid metal blanket must be sufficiently high to withdraw the heat generated by the fusion process deposited in the first wall and in the liquid metal without over-heating the first wall.

For all design considerations up to now pure conducting heat transfer from the first wall into the liquid metal was assumed. This assumption was chosen because full suppression of turbulence under fusion relevant conditions was predicted by many investigators [1 to 7].

Therefore in the considerations discussed below turbulence-free slug flow is assumed. The arguments for the existence of slug flow will be given later. Neglecting at first the small contribution of the heat up caused by the volumetric heat source q_{LM} (Fig. 4.2-1) the temperature rise ΔT_w of the liquid metal at the heated first wall is approximated [8] by:

$$\Delta T_\omega = 2 j_0 \left(\frac{L}{\pi v_w \lambda \rho c_p} \right)^{1/2} , \qquad (4.2.1.1)$$

where

$$\Delta T_w = T_1 - T_0 \qquad (see\ Fig.\ 4.2-1). \qquad (4.2.1.2)$$

j_0 is the heat flux density from the first wall to the fluid; v_w is the local velocity at the first wall, λ the thermal conductivity of the liquid metal and c_p the specific heat. At conditions relevant for a self-cooled liquid metal fusion blanket this approximation holds as long as the channel depth 2b (Fig. 4.2-1) is equal or greater than 2 cm.

In the case of fully wetted surfaces there is no temperature jump at the interface between the heated wall and the liquid metal so that the temperature of the liquid metal at the wall is equal to the wall surface temperature.

The efficiency of a power reactor essential relies on the mean liquid metal outlet temperature. Assuming the total energy flow j_{tot} to be converted in the fluid, and the backward and front channels to be series-connected, the rise of the bulk temperature ΔT_B is determined by the following equation

$$\Delta T_B = \frac{P_{tot}}{\dot{m}\,c_p} \qquad\qquad (4.2.1.3)$$

where P_{tot} is the total power converted in the fluid and $\dot{m}$ the mass flow rate.

If an electrically conductive fluid, in our case the liquid lithium-lead alloy Pb-17Li, is flowing at a velocity v in a channel perpendicular to a magnetic field whose magnetic flux density is B electrical currents are induced (Fig. 4.2-2).

The electric currents induced in the fluid are short-circuited by conducting walls or by slower flowing liquid metal in boundary layers. The interaction between the electric currents and the magnetic field creates a Lorentz force causing a pressure drop along the flow channel. The Lorentz forces (full arrows in the upper part of Fig. 4.2-2) flatten the velocity profile of the flow (see lower part of Fig. 4.2-2). Therefore, in the presence of a strong magnetic field, there is almost laminar slug flow except for thin boundary layers. Depending on the conditions prevailing, jets can develop in the boundary layers at walls parallel to the magnetic field, causing velocity fluctuations under certain conditions [9].

For fully developed slug flow perpendicular to the magnetic field, MHD pressure drop is described using the simplified equation [3]:

$$\Delta p = v \cdot L \cdot \sigma \cdot B_\perp^2 \left(\frac{1}{M} + \frac{C}{1+C} \right) \qquad\qquad (4.2.1.4)$$

with

$$M = B_\perp \cdot a \sqrt{\frac{\sigma}{\eta}} \quad \text{dimensionless Hartmann number} \qquad\qquad (4.2.1.5)$$

and

$$C = \frac{\sigma_w \cdot t_w}{\sigma \cdot a} \quad \text{wall conduction ratio} \;, \qquad\qquad (4.2.1.6)$$

where v is the velocity of the liquid metal flow, L is the length of the channel, $B_\perp$ the magnetic flux density perpendicular to v, a the half width of the duct in $B_\perp$ direction, σ the electric conductivity, η the dynamic viscosity, ρ the density, and t_w the wall thickness with w denoting the wall. For fusion reactors, M is on the order of 10^4, and C on the order of 10^{-3}. In the case of thin conducting walls $1/M \ll C \ll 1$, eq. (4.2.1.4) applies in its simplified form

$$\Delta p = v \cdot L \cdot B_\perp^2 \cdot o \cdot C = v \cdot L \cdot B_\perp^2 \cdot \sigma_w \cdot t_w / a \quad \text{thin conducting walls} \qquad (4.2.1.7)$$

For non-conducting or insulated walls with $C = 0$, one obtains

$$\Delta p = \frac{v \cdot B_\perp^2 \cdot L \cdot o}{M} = v \cdot L \cdot B_\perp \cdot \sqrt{(\eta\sigma)}/a \quad \text{non-conducting walls} \qquad (4.2.1.8)$$

The advantages resulting for MHD flows in non-conducting channels are evident from pressure drop equations (4.2.1.7) and (4.2.1.8) showing that

- pressure drops are smaller by a factor of C x M in the case of insulated walls. Blankets based on this technique would exhibit pressure drops which would be one order of magnitude smaller than those in the case of thin conducting walls.

- pressure drop, is only linearly proportional to the strength of the magnetic field ($\Delta p \sim B$).

The above equations are valid only for electrically uncoupled straight channels perpendicular to the magnetic field. Additional pressure drop (see chapter 4.2.3) occurs in the case of three-dimensional and multichannel flows in blankets of the type described in in this report. The currents induced in one channel are then short-circuited by the liquid metal itself, by walls or adjacent channels.

Since MHD pressure drops are by several orders of magnitude higher than those caused by viscous forces, the latter are of negligible relevance for liquid metal flow in blankets of fusion reactors.

The entrance length of MHD flow is defined as the distance needed for hydraulic velocity profiles to develop into MHD velocity profiles; it considerably depends on the axial electric potential difference in the liquid metal and therefore on the wall conduction ratio C. The entrance length is proportional to $1/\sqrt{C}$. For fusion blankets with $C \simeq 10^{-3}$ it can be in the order of magnitude of meters. Within the entrance length, MHD pressure drops exceed the values given above.

For slug flow, the velocity v_w at the first wall can be replaced by the mean velocity v. Resolving by the velocity and entering the latter into the pressure drop equa-

tion valid for thin conducting walls (4.2.1.7), the pressure drop of the front channels turns out to depend on design and material parameters only

$$\Delta p = \frac{4 j_0^2 \cdot L^2 \cdot B_\perp^2}{a \Delta T_w^2} \cdot \frac{\sigma_w \cdot t_w}{n \cdot \lambda \rho c_p} \qquad (4.2.1.9)$$

The design of a blanket must take aim to minimize the pressure drop Δp and to achieve a rise of the bulk temperature ΔT_B as high as possible. Low pressure drop is required by limits of material strength and safety considerations. High rise of bulk temperature ΔT_B enables a high thermal efficiency of a power plant.

From the equations (4.2.1.9) essential design guidlines can be derived:

- The first wall heat flux j_0, the total power P_{tot} and the channel length L are predetermined by the respective fusion reactor concept.

- The component $B_\perp$ should be as small as possible. The field component can be eliminated for the front channels if they are parallel to the magnetic field.

- The channel half width a should be as large as possible. It is however restricted by the strength of the structure.

- The temperature rise ΔT_w of the liquid metal at the heated wall should be large, but it is limited by corrosion and strength of the first wall and by the melting temperature of the liquid metal.

- The effective wall thickness t_w of the flow channels should be as small as possible. Its lower limit is given by the strength of the structural material.

- A further reduction of the wall thickness can only be achieved by separating the load-carrying from the conducting walls. Direct insulation, the liner technique, or the flow channel inserts (FCI) described in section 4.3 are solutions to be investigated.

- The electrical conductivity of the wall σ_w is determined by the structural material selected. At this time there seems no technology available for fabricating a non-conducting wall. Work on insulating coatings has been started.

- The product of $\lambda\rho c_p$ of the liquid metal should be large. It is determined by the choice of the coolant. Pure Lithium would be preferable. Its value of $\lambda\rho c_p$ is by a factor 4 higher than that of Pb-17Li which was selected for the European concept with respect to safety considerations.

- The mass flow rate $\dot{m}$ of the coolant through the blanket has to be kept low to achieve a high rise of the bulk temperature ΔT_B. The demand of a low mass flow rate together with the restrictions for the coolant velocity v_w in the channels at the first wall given by equation 2.6 prescribes the depth 2b of the channels.

The KfK reference concept fullfills in essence these design criteria by choosing

- toroidal flows (parallel to the magnetic field) at the first wall, where for heat removal reasons high velocities and small channel dimensions are required.

- poloidal flows in the larger rear channels where velocities can be kept low.

- radial flows to connect toroidal and poloidal flow channels.

When designing a self-cooled liquid-metal blanket it is not always possible to strictly follow the rules for low pressure drops given above. Also drawbacks and additional problems arise from the concept of bending the liquid metal flow from poloidal to radial and to toroidal and vice versa, which are described later.

Other flow concepts which may also fulfill this design criteria under certain circumstances are described in section 4.2.6.

4.2.2   Velocity profiles

The magnetic field not only causes high pressure drops in liquid metal flow but also influences the velocity profiles in channels as already mentioned before. This influence is especially difficult do describe in regions where the flow is not fully developed, i.e. in bends, expansions, contractions, and zones of variable magnetic field strength. In these regions, three-dimensional currents flow mainly inside the liquid metal, and interact here with the magnetic field. The influence of the three-dimensional flowing currents on the velocity profile is of special importance for the poloidal-radial-toroidal flow concept where they can obstruct first wall cooling

at the radial-toroidal bend because they may cause locally stagnant zones and/or velocity distributions, which may result in inhomogeneous temperature distribution on the first wall. Fig. 4.2-3 illustrates the current loop and the velocity profile in such a bend.

On the other hand, it is possible to design liquid metal ducts in a way to obtain a positive influence of the magnetic field on the velocity profiles ("flow tailoring" [10,11]) by creating high velocity ("flow jets") at the first wall of a blanket.

The investigation of the velocity fields in liquid metal flowing in a strong magnetic field - both experimental and theoretical - is a very ambitious task but the results are essential for all liquid metal cooled blanket designs.

4.2.3 MHD key problems of the KfK reference concept

In the reference concept two groups of MHD problems arise. Group one comprises single-channel effects, group two effects of multi-channel interaction. Fig. 4.2-4 gives a schematic representation of the two groups. Group one comprises:

- straight channels with constant and with locally variable magnetic fields (perpendicular to the flow),
- expansions and contractions,
- straight rectangular channels in constant, slightly inclined magnetic fields,
- hairpin-shaped bends (magnetic field perpendicular to the flow),
- radial-to-toroidal bends.
- toroidal-to-toroidal hairpin-shaped bends

In straight channels MHD pressure drop and velocity distribution for homogeneous and inhomogeneous magnetic fields perpendicular to the flow, are well known. This is especially true for high Hartmann numbers and typical fusion reactor interaction parameters [12,13]. For the regions of fully developed flow the eq. (4.2.1.7) may be used for the pressure drop calculation as a good first approximation. In slowly changing magnetic fields a mean field strength has to be used.

Phenomena ressembling those observed in the flow within a spatial variable magnetic field also occur as the liquid metal flows through spatial variable cross sections perpendicular to the magnetic field. The changing velocities affect potential differences in the flow direction. The wide-ranging short-circuit currents effect ad-

ditional pressure drops. This was verified in the joint ANL/KfK experiment on "MHD Flow Tailoring" [11]. The resulting 3-dimensional effect may be minimized even in the case of expansion or contraction perpendicular to the magnetic field if the channel width 2b(x) (perpendicular to the field) and the mean velocity v(x) at each cross section along the channel are correlated according to:

$$v(x) \cdot b(x) = K_1 .$$

(4.2.3.1)

The characteristic length a(x) is then determined due to mass conservation by

$$a(x) = \frac{K_2}{b(x)}$$

(4.2.3.2)

with K_1 and K_2 being constant.

Pressure drops and flow distribution in rectangular straight channels in constant and slightly inclined magnetic fields may be calculated similar to flow perpendicular to the magnetic field using the respective field component. According to the theoretical results obtained by Walker [14], the three-dimensional flows occurring in bends in a plane perpendicular to the magnetic field exhibit retarding effects on one side and stimulating effects on the other. For a bend with bending radius larger than the channel diameter additional three-dimensional pressure drop was found to be small. A similar approach may be used to investigate the pressure drop and the flow distribution in the sharp bended hairpin at the bottom of the blanket (Fig. 4.2-4). In the case of radial-to-toroidal bends, the electric potentials induced in the radial domain are short-circuited by the enclosing channel wall, and, more important, by the toroidally flowing liquid metal. The short-circuit current produces an additional pressure drop in the radial domain which can neither be avoided by reducing the thickness of channel walls nor by insulated walls. Similar phenomena arise in the toroidal-to-toroidal hairpin-shaped bend of the meander-shaped front channels.

The additional pressure drop of expansions, poloidal-toroidal bends etc., caused by these 3-dimensional short circuits, called 3-dimensional pressure drop can be described by the general expression:

$$\Delta P_{3D} = K \ b \ \beta^{-1} C^* \sigma \, v B_0^2$$

(4.2.3.3)

144

where K is a factor which is dependent on the geometry, the aspect ratio a and the wall conduction ratio and the wall conduction ratio C^*. b is the half distance between the sidewalls, a the half distance between the Hartmann walls (walls perpendicular to the magnetic field), $\beta = a/b$ the aspect ratio of the channel and $C^* = \sigma_w \cdot t_w / \sigma \cdot b$ the wall conduction ratio related to b.

For the radial-toroidal bend the factor K is taken from theoretical work by Th. Hua and J. Walker [15]. The experimental verification of equation 4.2.3.3 is only available for one aspect ratio [16] and only in the form of the total pressure drop over the whole bend. Experiments to validate the above equation are described in 4.2.5.

Nevertheless essential conclusions concerning the reference design may be drawn.

- For a given wall conduction ratio C^* of the radial channels the aspect ratio β has to be kept high.
- The parallel radial channels has to be separated electrically otherwise they would behave like a channel with a very low aspect ratio resulting in a high 3-dimensional pressure drop according to equation (4.2.3.3).
  This is fulfilled by outfitting the radial channels with flow channel inserts or by direct insulation of the duct walls.

Group two:

Since the flow of the liquid metal in the magnetic field must be diverted from poloidal to toroidal with radially arranged connection ducts, three-dimensional flows and the interaction of channels among each other are posing additional problems. The key problems of group two become clearer to understand explaining the flow characteristics of the KfK reference concept: flowing downwards in the two backward poloidal channels (channel type I, Fig. 4.2-4), the fluid is diverted at the foot of the blanket. Entering six parallel poloidal distributing channels it is caused to flow upwards (channel type II, Fig. 4.2-4). All walls separating these channels run parallel. They are inclined relative to the side walls of the blanket. Fig. 4.2-5 shows a poloidal cross section of the distributing/collecting channels. It reveals their inclined position and connections with the numerous radial channels running parallel. It is due to the inclination that the upward flowing fluid is displaced from the respective left-hand distributing channel to the radial channels. Flowing through the radial channels and the downstream toroidal channels, it passes the

radial channels on the left side of the blanket to again reach the right-hand front collecting channel. The radial channels and the interconnected toroidal channels are arranged over the total height of the blanket in parallel. The poloidal/radial/toroidal flow in parallel channels gives rise to additional MHD interactions.

- As the fluid leaves the respective distributing channel to enter the radial channels, a radial velocity component starts acting on the distributing channel. This velocity component is perpendicular to the magnetic field (the same is true for the fluid leaving the radial channels). It creates a poloidal electric potential difference which short-circuits in the fluid of the distributing and collecting channels, respectively. The short-circuits produced lead to additional pressure drops. As is evident, they cannot be reduced by isolating the channel walls. As the radial entrance flow is not guided by walls but self-adjusts, the extent of these MHD pressure losses can only be approximated at present. Assuming a slug flow at the entrance of the radial channels an approximate correlation is derived for the 3-dimensional pressure drop:

$$(\Delta P_{3D})_{poloidal-radial} \simeq K_3 \cdot L_{ng} \sigma \cdot B^2 \tag{4.2.3.4}$$

where the constant K3 is of the order of 1 and the length L_{ng} of the non guided entrance flow is of the order of the characteristic length a of the radial channels.

Given the inclined position of the distributing/collecting channels, the flow providing the short-circuit link is of different resistivity in the different poloidal positions. This could cause different inlet/outlet losses for different channels which would result in nonuniform flow partioning in the parallel front channels.

- The radial channels arranged in parallel are perpendicular to the magnetic field. Therefore, an electric potential difference is induced again. Since left-hand radial channel flows are in foreward (towards the first wall) and right-hand ones are in backward direction, both channel arrays are of opposite electric polarity. With no electrical insulation between the radial channels, the potentials add up to induce wide-ranging electrical short-circuit currents flowing through the blanket and causing additional MHD drop (Madarame effect [17]). Conducting radial channels would lead to unacceptably high pressure drops. In

addition, this effect causes nonuniform flow rates in different channels. Flow in the mid-blanket channels is slower than those in channels at the top or foot of the blanket. The Madarame effect can be reduced only by insulating the radial channels, but it cannot be avoided completely; the relatively short radial channels ($L \approx 0.3$ m) are electrically connected by the first wall, the toroidal channels, and other structures even when they are insulated.

The feasibility of a blanket concept with three-dimensional flow will essentially depend on the successful solution of the key problems assigned to group two.

In order to get experimental data on problems related to MHD-flow of group 1 (single channel) and group 2 (multichannel) flow the program MEKKA was initiated, described in section 4.2.5.

4.2.4 Analysis

To analyse the MHD flow in a SCLMB two numerical methods are developed to solve the MHD basic equations.

The hydrodynamic motion of the liquid metal is affected by additional electrodynamic interactions between velocity, electric current density and the applied strong magnetic field. Especially for fusion relevant parameters (Hartman number $M \approx 10^4 - 10^5$, interaction parameter $N \approx 10^3 - 10^5$ and wall conductance ratio $c \approx 0.01 - 0.05$) the electromagnetic force is the dominant one, that determines pressure drop and velocity distribution of magneto hydrodynamic (MHD) channel flow.

Basic equations:

To describe the motion of an electrically conducting fluid in a strong magnetic field B, the ordinary hydrodynamic equations (conservation of mass and momentum) have to be suplemented by equations describing the electrodynamic interaction.

Hydrodynamic equations:

If we assume an incompressible fluid with constant mass density ρ the equation of mass conservation gives:

$$\nabla \cdot v = 0 \tag{4.2.4.1}$$

with the velocity vector v. In the classical Navier-Stokes equations for Newtonian fluids with constant dynamic viscosity η, additional terms are introduced, describing the electromagnetic interaction (Lorentz - force).

$$\rho \left| \frac{\partial v}{\partial t} + (v \cdot \nabla)v \right| = -\nabla p + \eta \nabla^2 v + \rho_{el} E + j \times B, \tag{4.2.4.2}$$

with pressure p, electric charge density ρ_{el}, electric field E, magnetic field B and electric current density j.

Electrodynamic equations

Electrodynamic phenomena are described by Maxwell's equations, where ε is the dielectric coefficient and μ the magnetic permeability in the considered fluid region.

$$\varepsilon \nabla \cdot E = \rho_{el} , \tag{4.2.4.3}$$

$$\nabla \cdot B = 0 \tag{4.2.4.4}$$

$$\nabla \times E = -\frac{\partial B}{\partial t} , \tag{4.2.4.5}$$

$$\nabla \times B = \mu (j + \varepsilon \frac{\partial E}{\partial t}) . \tag{4.2.4.6}$$

Ohm's law gives for a fluid with electric conductivity σ, moving with velocity v.

$$j = \sigma (E + v \times B) . \tag{4.2.4.7}$$

Nondimensional parameters and assumptions

All physical MHD conditions can be quantified by the following nondimensional coefficients [15]:

Hartmann-number
(electromagnetic force/viscous force)$^{1/2}$

148

$$M = a B_0 \sqrt{\sigma / \eta} \ ,$$

<div align="right">(4.2.4.8)</div>

Interaction parameter
(electromagnetic force/inertia force)

$$N = \sigma a B_0^2 / \rho v_0 \ .$$

<div align="right">(4.2.4.9)</div>

In addition to material properties, a characteristic length a and a suitable velocity v_0 is needed to normalize the basic equations. Electrically conducting channel walls of conductivity σ_w and thickness t are characterized by another nondimensional parameter:

Wall conductance ratio
(electric resistance fluid/electric resistance wall)

$$c = \frac{\sigma_w t}{\sigma a} \ .$$

<div align="right">(4.2.4.10)</div>

The ratio of induced magnetic field/applied magnetic field is given by $c^{1/2} R_m$ with R_m called

Magnetic Reynolds number

$$R_m = \mu \sigma v_0 a \ ,$$

<div align="right">(4.2.4.11)</div>

Especially for blanket relevant conditions the following simplifications are justified:

$c^{1/2} R_m \ll 1$ The magnetic field is dominated by the applied field B_0. Induced fields are neglected.

$M \gg 1$ Negligible viscous effects except in very thin shear layers. They do not affect the mean flow quantities.

$N \gg 1$ Inertia forces are negligible compared to electromagnetic forces.

Full solution

With the assumption $R_m \ll 1$ a code has been developed at KfK [18,19] which is capable of simulating the MHD flow in a straight duct of constant rectangular cross

section. This code is called "full solution", because viscous and nonlinear inertial effects are included. Three-dimensional effects caused by arbitrary spatial variation of the magnetic field or the wall conductance ratio can be analysed.

The Navier-Stokes equations are solved in time by an ADI method until steady state is reached. At each time step, two Poisson equations for pressure and electrical potential are solved by the Fast Poisson Solver H3D (Schumann and Sweet [20]). Spatial discretization is done on a three-dimensional staggered grid.

With $34 \times 34 \times 34$ grid points the typical cpu time on a Siemens computer 3090 for a Hartmann number $M = 50$ is 1 hour, rising to 15 hours for $M = 300$.

As an example, Fig. 4.2-6 shows the development of the velocity profile along the channel perpendicular to the magnetic field. The field is given by $B = (0, B_y, 0)$, $B_y = 1/(1 + e^{x/x_0})$, $x_0 = 0.15$, as a function of the duct's axis x. The plots show the x-component of the velocity at different positions x. The parameters used are $M = 100$, interaction parameter $N = 10^3$, wall conductance ratio $C = 0.1$.

As the magnetic field starts to increase, the flow is driven towards the side walls, forming the well-known "M-shaped" profile. Most of the mass flux is carried by these side-wall jets. As the flow reaches the constant B-field regime, these jets decay, leading to a slug profile with only a small overshoot close to the side walls. This overshoot is dependent on the wall conductance ratio. For $C = 10^{-3}$, which is a reasonable value for fusion blankets, there is no such overshoot. The M-shape in the fringing field region still exists, because it is caused by axial currents flowing in planes perpendicular to B.

Core flow solution

If negligible viscous effects ($M \gg 1$) and inertia effects ($N \gg 1$) are omitted, the 3D-equations can be reduced to 2D-equations, nevertheless containing the full 3D information. This procedure is known as 'Core Flow Approximation'. The reduced equations are solved on the channel surface. 3D velocity, pressure and potential distributions can be obtained from the surface solution due to special analytical relations.

A lot of work had been done [21,22,23] to predict flow quantities of various channel geometries, channel orientations, magnetic field distributions or wall conductance

150

ratios with the 'Core Flow Approximation'. But all analytical or numerical calculation procedures are restricted to very special geometries or conditions.

Now a method has been developed at KfK [24], capable to treat the MHD core flow equations for a variety of geometries, variable magnetic field, and variable wall conductance ratios. If the channel wall is penetrated by a magnetic field line in only two points a special coordinate transformation transforms each arbitrary channel volume into a standard one for which all calculations are performed. Therefore it is possible to apply this procedure to 3D geometries like bends expansions contractions or helical turned channels in variable magnetic fields.

As a generalization, the nondimensional Core Flow equations are used in their covariant form:

Momentum equation:

$$\partial_i p = \sqrt{g}\, b_{ik} j^k \tag{4.2.4.12}$$

Ohm's law:

$$j_i = -\partial_i \Phi + \sqrt{g}\, b_{ik} v^k \tag{4.2.4.13}$$

Conservation of mass and charge:

$$\partial_i (\sqrt{g}\, v^i) = 0, \quad \partial_i (\sqrt{g}\, j^i) = 0 \tag{4.2.4.14/15}$$

Upper indices denote the contravariant components of a vector, lower indices stand for the covariant components of the same vector. They are related for example by $j_i = g_{ik} j^k$. The covariant derivative of a scalar is expressed by $\partial_i = \partial / \partial u^i$.

Here the influence of the magnetic field B is expressed by the antisymmetric field tensor b_{ik}. The arbirary geometrical conditions are represented by the metric tensor g_{ik} or by $\sqrt{g}$.

Conservation of charge in thin conducting walls with $c \ll 1$ leads to the so called 'thin wall approximation'.

151

If the coordinate u^3 is taken in the magnetic field direction, eq. (4.2.4.12) contains the very important statements:←

→   The pressure is constant along magnetic field lines ($\partial_3 p = 0$).

→   The contravariant components j^1 and j^2 of the current density are independent of the u^3 coordinate ($j^1, j^2 \neq f(u^3)$).

j^3 can be evaluated by integration of eq. (4.2.4.15). The third of eq. (4.2.4.13) gives after integration the potential variation along u^3 The wall.potentials ϕ_t and ϕ_b at the top and bottom are introduced as unknown integration constants. So all electrical properties can be expressed by three scalar unknowns p, ϕ_t and ϕ_b.

The velocity components v^1 and v^2 follow from Ohm's law. An integration of the mass conservation eq (4.2.4.14) gives the change in the velocity component Δv^3. If the integration was performed from the bottom to the top, the left side of eq (4.7) vanishes due to the kinematic boundary condition.

Eq (4.2.4.14) gives a second order partial differential equation for the pressure p, coupled to the wall potentials ϕ_t and ϕ_b in their first derivatives if the v^i are taken from Ohm's law.

A second order partial differential equation for the wall potential $\phi_w = \phi_t$ or ϕ_b can be obtained by integrating the charge conservation eq (4.2.4.15) in the wall along the wall normal direction.

The partial differential equations are solved by a finite difference approximation. A staggered grid between wall potentials and pressure ensures a mass and charge conservative formulation of the problem. The Harwell MA28AD - sparse matrix solver is used to obtain the solution of the resulting linear algebraic system.

Some applications

Some examples are presented to show the various application possibilities of the numerical method. The first one is a fully developed flow in a straight duct with elliptically deformed side walls. Fig. 4.2-7a shows the velocity profile in such a duct cross section.

In the side wall region (walls tangential to magnetic field lines) the flat core velocity matches the side wall jets continuously. A numerical experiment was performed by decreasing the small ellipse axis toward small values. The resulting increasing side wall velocities give nevertheless a finite amount of volume flux in the simultaneously decreasing side wall part of the cross section. The volume flux in the core region (side layers are excluded) compared to predicted values given by Tillack and McCarthy 1989 for rectangular ducts with side walls parallel to magnetic field lines show relative deviations of 0.3%. Fig. 4.2-7b shows the velocity distribution in an square duct, inclined by 10° with respect to the magnetic field direction.

As a 3D-example the problem of MHD flow in the meander shaped front part (see Fig. 4.2-4) of the reference concept was investigated. Because the core flow solution does not allow flow aligned to the magnetic field the meander was deformed by a angle of a few degrees as shown in Fig. 4.2-8. This figure shows also the calculated pressure distribution along the flow path.

From this figure one may distinguish the low pressure drop in the toroidal leg of the meander and the high pressure drops in the toroidal-radial-toroidal bends.

The calculated velocity profile at the toroidal-radial bend is given in Fig. 4.2-9. Liquid metal is driven towards the side wall regions, specially near duct wall opposite to the corner.

4.2.5   MEKKA-program, experimental set-up and experiments

In order to get a better data base, to learn about new physical problems and to verify computer programs used for design calculations the experimental program MEKKA was started in 1985 [25]. Investigations of single-channel effects with the magnetic field being perpendicular or parallel to the flow are planned to be followed by investigations of channel interactions. Fig. 4.2-10 shows a photographic view of the MEKKA test facility.

For the first step of the program involving experiments in straight ducts a normal conducting dipole magnet is used. It has a field strength of 2 Tesla and a test volume of 0.17 m x 0.5 m x 1.5 m.

As the liquid metal for the first step of the program the eutectic sodium-potassium alloy $Na^{22}K^{78}$ is used. The fact that NaK is liquid at room temperature not only simplifies the loop design but most importantly facilitates the operation of the loop and the conduction of the tests and enables the acquisition of data of higher quality and greater variety than would be possible with a higher melting material like sodium, lithium, or lithium-lead. The use of NaK allows thinner tubings for pressure measurement, and the use of rubber and some plastics. To overcome the problem of wetting stainless steel surfaces, the loop is designed to operate also at elevated temperatures (300°C) to accelerate and insure the wetting of all MHD-relevant surfaces. After wetting is achieved once, the experiments are performed near room temperature.

The special features of the NaK loop are described in detail in section 4.9.3. Some of the initial experiments in MEKKA are outlined in the following sections.

Straight duct-effects of flow channel inserts

The first MEKKA experiments was intended to proof the assumption that FCI's can reduce MHD pressure drops [13,25].. By introducing an FCI with an inner wall thickness of 0.5 mm into a straight channel with circular cross sectiom, 130 mm inside diameter, and a wall thickness of 5 mm the wall conduction ratio was reduced from $C = 0.036$ to $C = 0.0039$. Fig. 4.2-11 compiles the results. Together with the analytical prediction $\Delta P/\Delta x = C/(C+1)$ the dimensionless pressure drop is plotted as a function of the interaction parameter N. The experimental results verify the theoretical prediction of pressure drop reduction by a factor of nearly 9.

The 20% deviation of the experimental results with the FCI compared with the slug flow prediction may result from the non fully developed MHD flow (see also section 4.2.1) caused by the final length of the magnet.

Circumferential pressure distribution

In order to test the performance of the core flow model, the circumferential pressure distribution was measured at characteristic points along the axis of the magnet [13]. In Fig. 4.2-12, the measured and calculated pressure differences of the thick-walled round duct are plotted as a function of the axial position in the fringing field. Evidently, there is good agreement between theory and experimental results.

The radial-toroidal bend experiment

The radial-toroidal bend experiment is a joint ANL/KfK project intended to investigate the pressure drop and flow distribution in the bend from radial to toroidal ducts of the KfK reference blanket concept. The experiment will be performed in the magnetic field of a superconducting solenoid magnet. The magnet has a warm bore of 400 mm diameter, a length of 1100 mm, and a maximum field strength of 3.5 Tesla. Fig. 4.2-13 shows the superconducting magnet and the installed test section.

The radial-toroidal multichannel bend experiment

Following the above experiment the multichannel MHD-effects of group 2 in section 4.2.3 will be investigated by an experiment schematically outlined in Fig. 4.2-14.

By connecting or separating the different channels electrically MHD induced alternating effect can be investigated. Additionally the dependence of the 3-dimensional pressure drop on the channel width 2b will be studied.

4.2.6   MHD-features of blanket design with other flow concepts

The quasi-two-dimensional poloidal-toroidal flow concept

Looking for possibilities to avoid or to reduce 3-dimensional MHD effects of the poloidal-toroidal flow of the reference concept a quasi two dimensional geometry for the liquid-metal-blanket duct of a poloidal-toroidal blanket concept was investigated [26]. This concept is an attempt to exclude electric current caused by 3-dimensional effects and integral currents in the blanket module. It opens also the possibility of influencing the flow structure in order to improve the heat transfer. Fig. 4.2-15 shows schematically in a perspective view this flow concept. In the figure the back poloidal feeding channels are omitted for simplicity. Although the main constructive elements of the reference version of a poloidal-toroidal concept remain the same in this new geometry, the local organization of the flow as at the inlet to the radial channels as in the first wall region is changed essentially.

A two dimensional flow in the bend from the poloidal distribution channels (DCH) to the radial channels (RCH) is insured using a slot nozzle (SN) at the inlet of to parallel radial channels. The toroidal channels are divided in sections in the toroidal direction.

In each section the coolant flows upwards (in the poloidal direction).Then the flow is shifted to the next section in a pipe which connects all sections to the central part of the toroidal duct. In the process of shifting, coolant, which is heated up from the first wall will be mixed with coolant not being in contact with the first wall and therefore not being heated up. This improves the heat transfer from the first wall to the liquid metal and allows to reduce the velocity of the coolant at the first wall resulting in a reduced pressure drop.

The poloidal flow blanket concept

As a backup a blanket concept with poloidal flow is investigated at KfK. Two kinds of poloidal front channels were studied: Channels of rectangular cross section with a width of 2 a = 8 cm, comparable to the reference concept and channels with circular cross section and with a helical vane for flattening the temperature distribution (see Fig. 4.2-16) and channels with full and half blanket length. According to equation 4.2.1.9 the governing pressure drop in the front channels is proportional to the square of the channel length L; therefore the reduction of the front channel length will reduce the pressure drop drastically but has also the strongest influence on the design.

The calculations were conducted for Lithium and Lithium-Lead and showed the following results:

. Under the same design constraints as for the reference concept namely Lithium-lead as breeding and cooling material, using an In- and outboard blanket, front channels with supporting walls of 8 cm distance and the use of the FCI-technique the poloidal flow is not possible for DEMO-conditions.

. Using Lithium as coolant a poloidal flow concept for DEMO conditions is possible if both the In- and outboard blanket are divided in halfs.

. If fully electrical insulation of the channel walls could be realized, the pressure drop would be reduced so far, that smaller channel dimensions and higher velocities could be chosen. Herewith the heat transfer could be improved so that a blanket concept with poloidal flow for a full blanket length would become possible not only for Lithium but also for Lithium-Lead.

. For Lithium-Lead the velocity in the front channel would be sufficient high to fullfill the criterion of incipient turbulent MHD-flow.

Whereas the poloidal flow is better understood and 3-dimensional effects are minimized the proof that the pressure can be reduced sufficiently needs a lot of additional effort.

As outlined in section 4.2.1 the pressure losses can be further reduced by the above mentioned reduction of the channel length, by reducing the MHD effective wall thickness for example with the FCI technique or by fully insulating the duct surfaces or by reducing the mean velocity in the front channels. The later may be fullfilled by flow tailoring as shown in [10,11], by enhanced convection or by mechanical mixing. As shown by analytical and additional numerical calculations [24] mechanical mixing by helical vanes in poloidal flow produces strong 3-dimensional pressure drop and complicated flow structure which may reduce the improvement of the heat transfer by mixing. In Fig. 4.2-17 the flow structure in a poloidal channel with a helical vane is shown.

A method to enhance convective heat transfer is shown in Fig. 4.2-18.
By tailoring the flow in the front channel with adjusting the thickness of the wall perpendicular to the magnetic field direction a free shear layer is produced. The effect of MHD flow tailoring was proposed by Walker and Picologlou [10] and was shown experimentally in [27]. This free shear layer is able to promote a two-dimensional turbulence [28] which may increase the heat transfer from the first wall reducing the necessary flow velocity in the front channels and by this the MHD-pressure drop.

To confirm this effect and to study its implication on the MHD design of a self-cooled liquid metal blanket an experiment is prepared at KfK.

References to section 4.2:

[1]   Abdou, M. et al.: Blanket Comparison and Selection Study. ANL/FPP-83-1, Vol. I, 1983, Chapter VII

[2]   Branover, H.H., Suppression of Turbulenc in Pipes with Transverse and Longitudinal Magnetic Fields, Magnetohydrodynamics, 47, 107 (1967)

[3]   Hoffman, M.A., Carlson, G.A.: Calculation Techniques for Estimating the Pressure Losses for Conducting Fluid Flows in Magnetic Fields, UCRL-51010, Lawrence Livermor Laboratory (1971)

[4]   Hunt, J.C.R., Hancox, R.: The Use of Liquid Lithium as Coolant in a Toroidal Fusion Reactor, Part I, CLM-R41,5, Culham Laboratory (1971)

[5]   Hancox, R., Booth, J.A., ibid, Part II, CLM-R116, Culham Lab. (1971)

[6]   Kammash, T.: Fusion Reactor Physics - Principles and Technology, Ann Arbor Science Publishers Inc., Ann Arbor, Michigan (1975)

[7]   Branover, H.: Magnetohydrodynamic Flows in Ducts, John Wiley (1978)

[8]   Carslaw, H.S., Jaeger, J.C.: Conduction of Heat in Solids, 2nd ed., Clarendon Press Oxford (1959)

[9]   Reed, C.B., Picologlou, B.F.: Sidewall Flow Instabilities in Liquid Metal MHD Flow under Blanket Relevant Conditions, Fusion Technology, Vol. 15, March 1989, pp- 707-715.

[10] Walker, J.S., Picologlou, B.F.: MHD Flow Control as a Design Approach for Self-cooled Liquid Metal Blankets of Magnetic Confinement Fusion Reactors, Fusion Technol. 8(1985) 270-282.

[11] Picologlou, B.F., Reed, C.B., Hua, T.Q., Barleon, L., Kreuzinger, H. and Walker, J.S.: "Experimental Investigations of MHD Flow Tailoring For First Wall Coolant Channels of Self-Cooled Blankets", Fusion Technology, Vol. 15, March 1989, pp. 1180-1185.

[12] Reed, C.B., Picologlou, B.F., Hua, T.Q. and Walker, J.S.: "ALEX Results - A Comparison of Measurement from a Round and a Rectangular Duct with 3-D Code Predictions", 12th Symp. on Fusion Eng., Monterey, CA, 1267 (1987).

[13] Barleon, L., Lenhart, L., Mack, K.J., Sterl, A., and Thomauske, K.: "Investigations on Liquid Metal MHD in Straight Ducts at High Hartmann Numbers and Interaction Parameters", Proc. 4th Int. Topical Meeting on

Nuclear Reactor Thermal-Hydraulics, Oct. 10-13, 1989, Karlsruhe, pp. 857-862.

[14] Walker, J.S., "Liquid-Metal Flow Through a Thin-Walled Elbow in a Plane Perpendicular to a Uniform Magnetic Field ", ANL/FPP/TM-204, April 1986

[15] Hua, T.Q., Walker, J.S.: "MHD Considerations for Poloidal-Toroidal Coolant Ducts of Self-Cooled Blankets. Proc. Ninth Topical Meeting on the Techn. of Fuson Energy Oct. 7-11, 1990, Oak Brook, IL

[16] Grinberg, G.K., Kaudze, M.Z., Lielausis, O.A.: "Local MHD Resistances on a Liquid Sodium Circuit with a Superconducting Magnet". Magnituaya Gidrodinamika, No. 1, Januar-March 1985, pp. 121-126

[17] Madarame, M., Taghavi, K. and Tillack, M.S., "The Influence of Leakage Currents on MHD Pressure Drop", Fusion Technology, Vol. 8, 264, July 1985.

[18] Sterl, A., Numerische Simulation magnetohydrodynamischer Flüssigmetall-Strömungen in rechteckigen Rohren bei großen Hartmann-Zahlen, KfK 4504, Jan. 1989.

[19] Lenhart, L., McCarthy, K., Müller, U.: "Comparison of the Core Flow Solution and Full Solution for MHD flow", to be published in Proc. 6th Beer-Sheva Intern. Sem. on MHD-Flows and Turb., Jerusalem, Isr., Febr. 25-March 2, 1990.

[20] Schumann, U., Sweet, R.A., "Fast Fourier Transforms for Direct Solution of Poisson's Equation with Staggered Boundary Conditions", Journ. Comp. Physics, 75, 123, 1988.

[21] Talmage, G., Walker, J., "Three-dimensional laminar MHD flow in ducts with thin metal walls and strong magnetic fields", Proceedings of the 6th Beer Sheva Seminar, March 1987, pp. 3-25.

[22] Hua, T.Q., Walker, J.S., Picologlou, B.F., and Reed, C.B.: "Three-Dimensional MHD Flows in Rectangular Ducts of Liquid-Metal-Cooled Blankets", Fusion Technology, Vol. 14, No. 3, Nov. 1988

[23] McCarthy, K.: Analysis of Liquid Metal MHD Flow Using a Core Flow Approximation, with Application to Calculating the Pressure Drop in Basic Geometric Elements of Fusion Reactor Blankets, PhD-Thesis, University of California, Los Angeles (1989).

[24] Bühler, L., "Liquid Metal Flow in Arbitrary Thin Walled Channels Under a Strong Transverse Magnetic Field", Proc. ISFNT, to be publ. in Fusion Eng. & Design

[25] Barleon, L., Casal, V., Mack, K.J., Kreuzinger, H., Sterl, A. and Thomauske, K.: "Experimental and Theoretical Work on MHD at the Kernforschungs-zentrum Karlsruhe, The MEKKA-Program, Liquid metal magnetohydro-dynamics, Mech. of fluids and Transport processes, Vol. 10, Kluwer Acad. Publ., Dordrecht 1989.

[26] Platnieks, I.: Personal Communications (1991)

[27] Kolesnikov, Yu.B. and Tsinober, A.B.: Magnetohydrodynamic Flow in the Region of a Jump in the Conductivity at the Wall, Magnetohydrodynamics, No. 1, 1972, pp. 61-65.

[28] Rosant, J.M.: "Ecoulements hydromagnétiques turbulents en conduites rectangulaires, Thèse présentée à L'Université Scientifique et Méchicale, Sept. 1976.

Nomenclature:

a   = half width of a duct in B direction

b   = half depth of a duct perpendicular to the B direction

B   = magnetic field strength

c_p = specific heat

$C = \dfrac{\sigma_w \cdot t_w}{\sigma \cdot a}$ = wall conduction ratio

f_p = power multiplication factor

j   = heat flux density

L   = length of the duct

$M = a \cdot B \sqrt{\dfrac{\sigma}{\eta}}$ = dimensionless Hartmann number

$N = \dfrac{M^2}{Re} = \dfrac{a \cdot B^2 \cdot \sigma}{v \cdot \rho}$ = interaction parameter

p   = pressure

P   = Power

t_w = wall thickness

T   = temperature

v   = velocity

η = dynamic viscosity

λ = heat conductivity

ρ = density

σ = electric conductivity

Subscripts:

rad   =   radiation

ss   =   stainless steel (structure)

tot   =   total

w   =   wall

0   =   inlet of cooling channel

1   =   outlet of cooling channel

Temperature distribution in the liquid
metal near a heated wall as a function
of the radial and axial distance

The inset surface plot is labelled:

$\Delta T_W = T - T_0$ (GRAD C) on the vertical axis with values 0., 30., 60., 90., 120., 150., 180.

R (M) on one horizontal axis with values .000, .020, .040, .060

Z (M) on the other horizontal axis with values 0, 2., 4., 6., 8., 10., 12.

$V = 5.4$ (M/S)

Main diagram labels:

q (W/cm^3)

q_{SS} (W/cm^3)

$q_{LM} = f(R)$

$\overline{v}_{FK}$

$\otimes$ B

T_1

$j_{surf} \Rightarrow$ $\Rightarrow j_0$

j_{tot}

front-channel

rear channel

$z, q(z)$

v

$2b$

0

R axis: 0, 10, 20, 30, 40, 50, R (cm)

$$\Delta T_W = 2 j_0 \left(\frac{L}{\pi \cdot v_w \cdot \lambda \, \rho \, c_p} \right)^{1/2}$$

$$\Delta p = \overline{v} \cdot L \cdot B^2_{\perp} \frac{t_W \cdot \sigma_W}{a}$$

$$v_w = \overline{v} \quad \text{"Slug flow"}$$

$$j_0 = j_{surf} + q_{SS} \cdot t_{SS}$$

$$\overline{\Delta T}_{Ges} = \frac{L \cdot j_{tot}}{\overline{v} \cdot 2b \cdot \rho \, c_p}$$

Fig. 4.2-1   Heat transfer in a self-cooled liquid-metal blanket
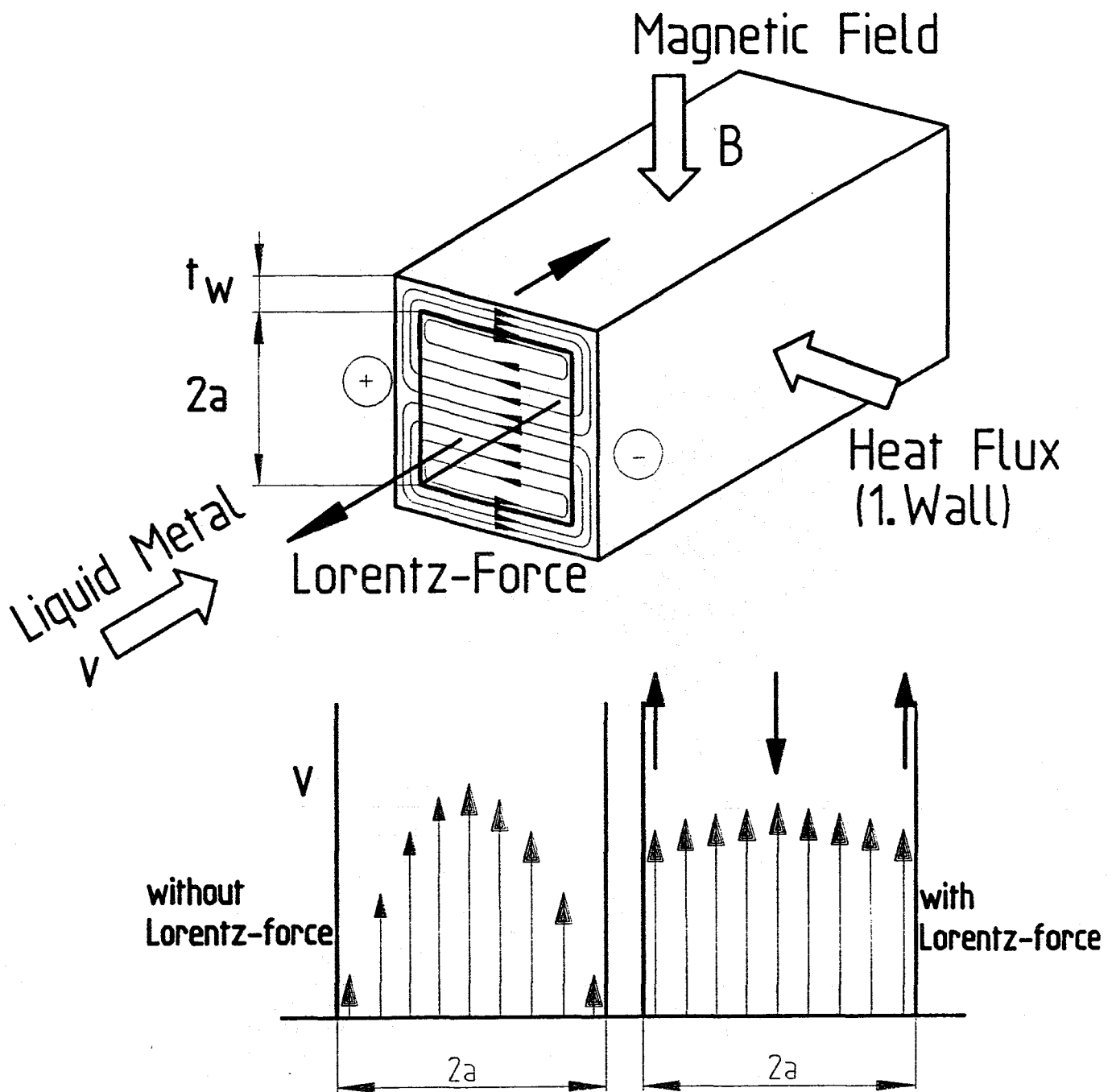
Fig. 4.2-2   Magnetohydrodynamics of liquid metal flow in channels

163
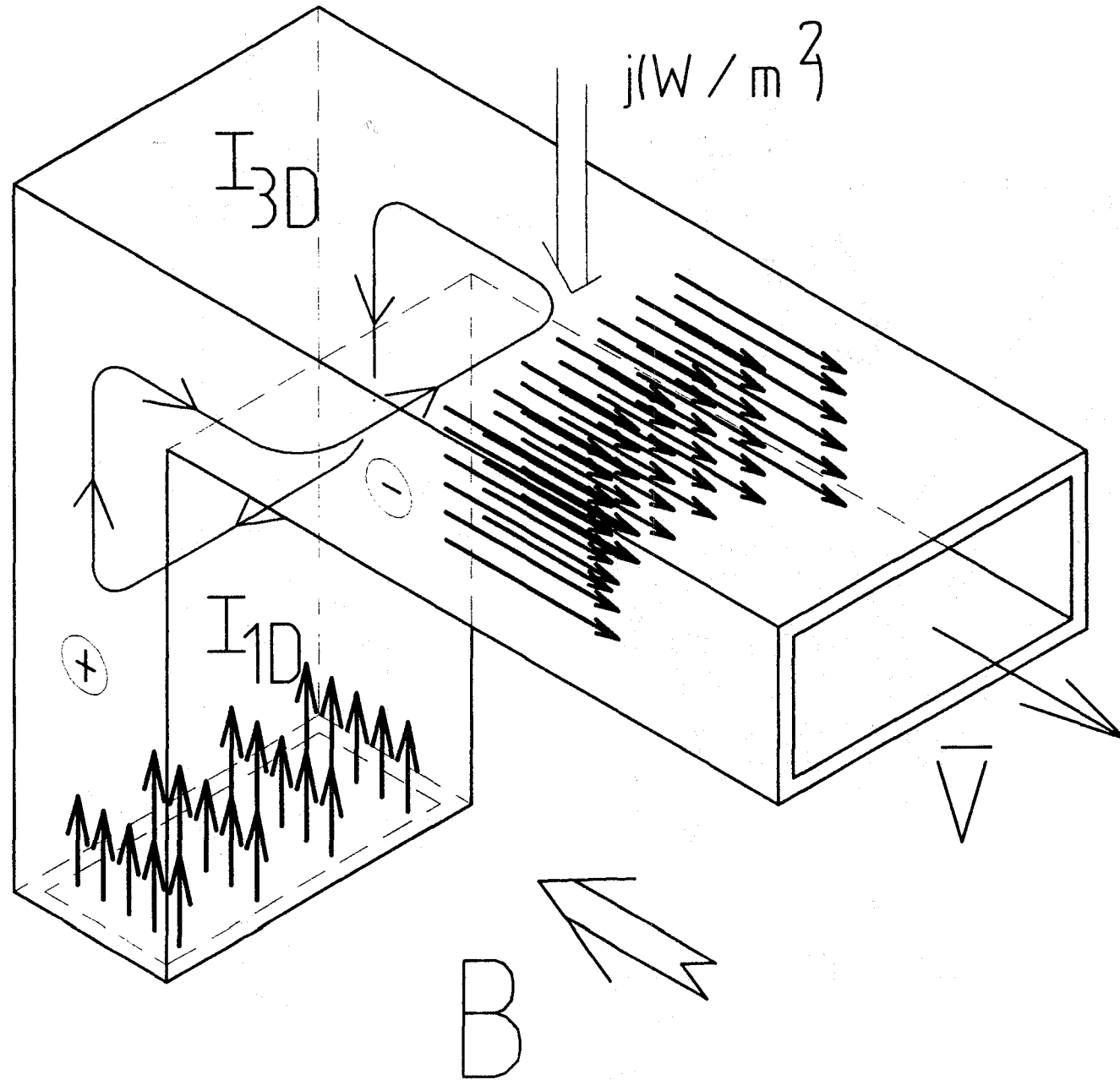
Fig. 4.2-3   Electrical current and velocity profiles in a radial-toroidal bend
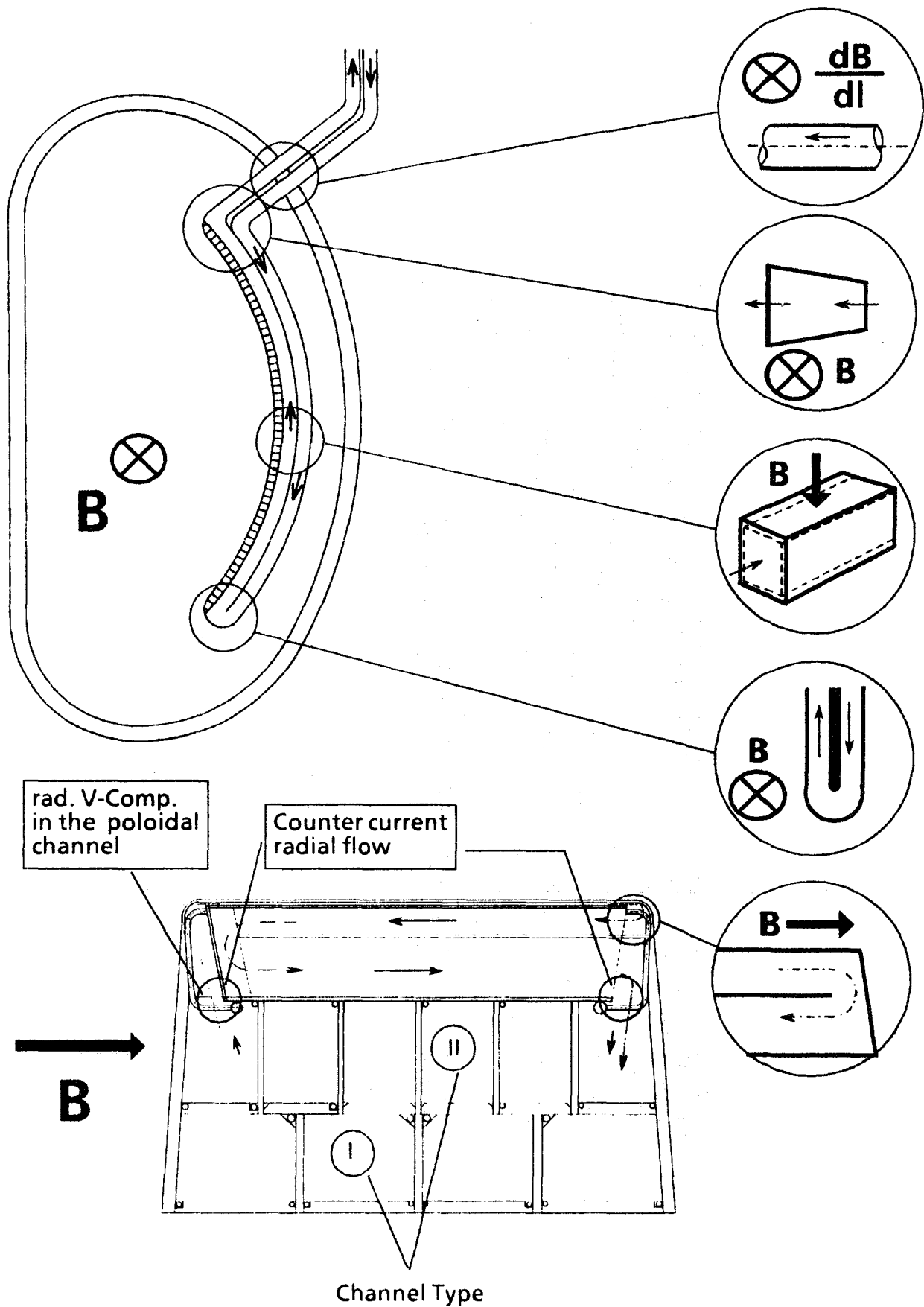
Fig. 4.2-4   MHD-key problems of the self-cooled liquid-metal blanket

radial
channels

poloidal
distribution-
collection-
channels
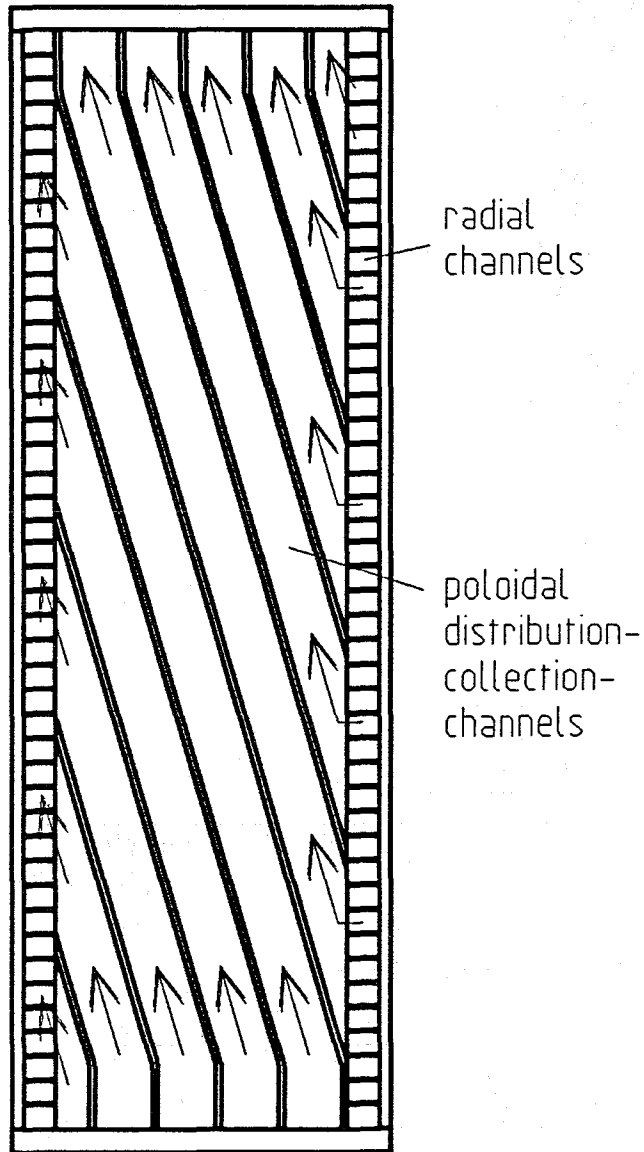
Fig. 4.2-5   Poloidal cross section through the distributing/collecting poloidal
   channels

166
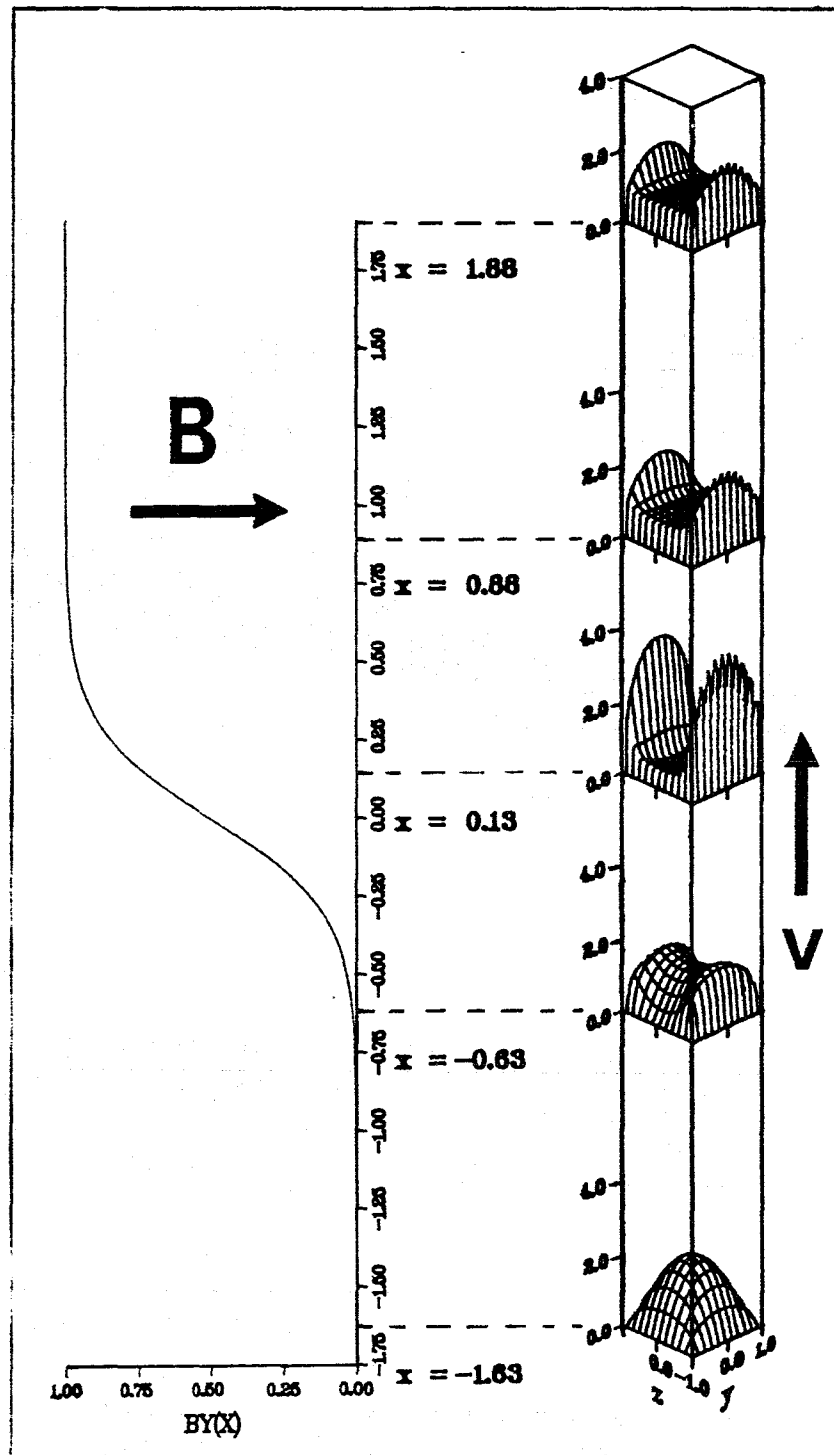
Fig. 4.2-6   Development of the velocity profile in the entrance region of a magnet
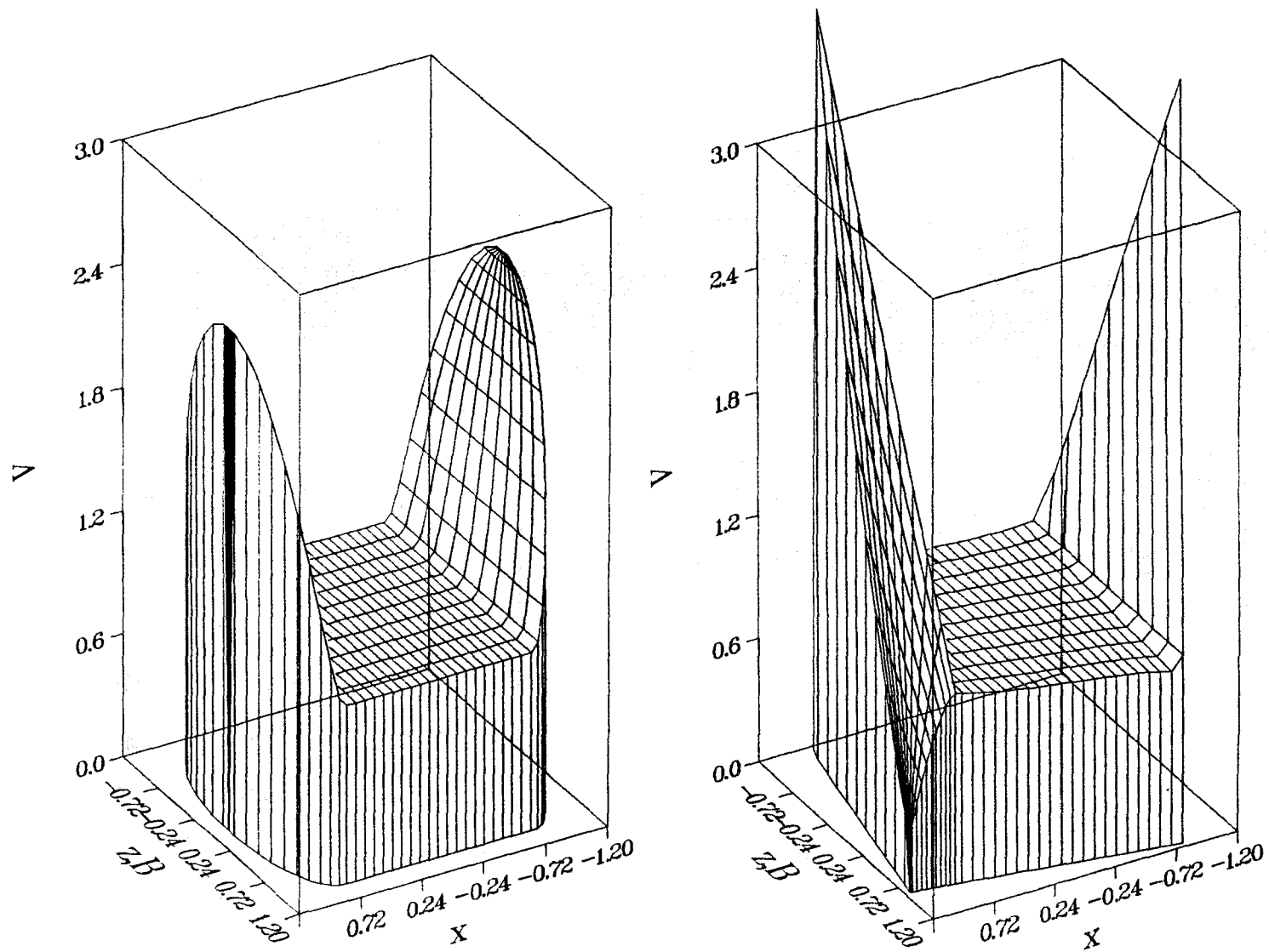
Fig. 4.2-7   Velocity profiles in a) a duct with elliptically shaped sidewalls and
b) in a square duct with inclined magnetic field

MHD − Core − Flow
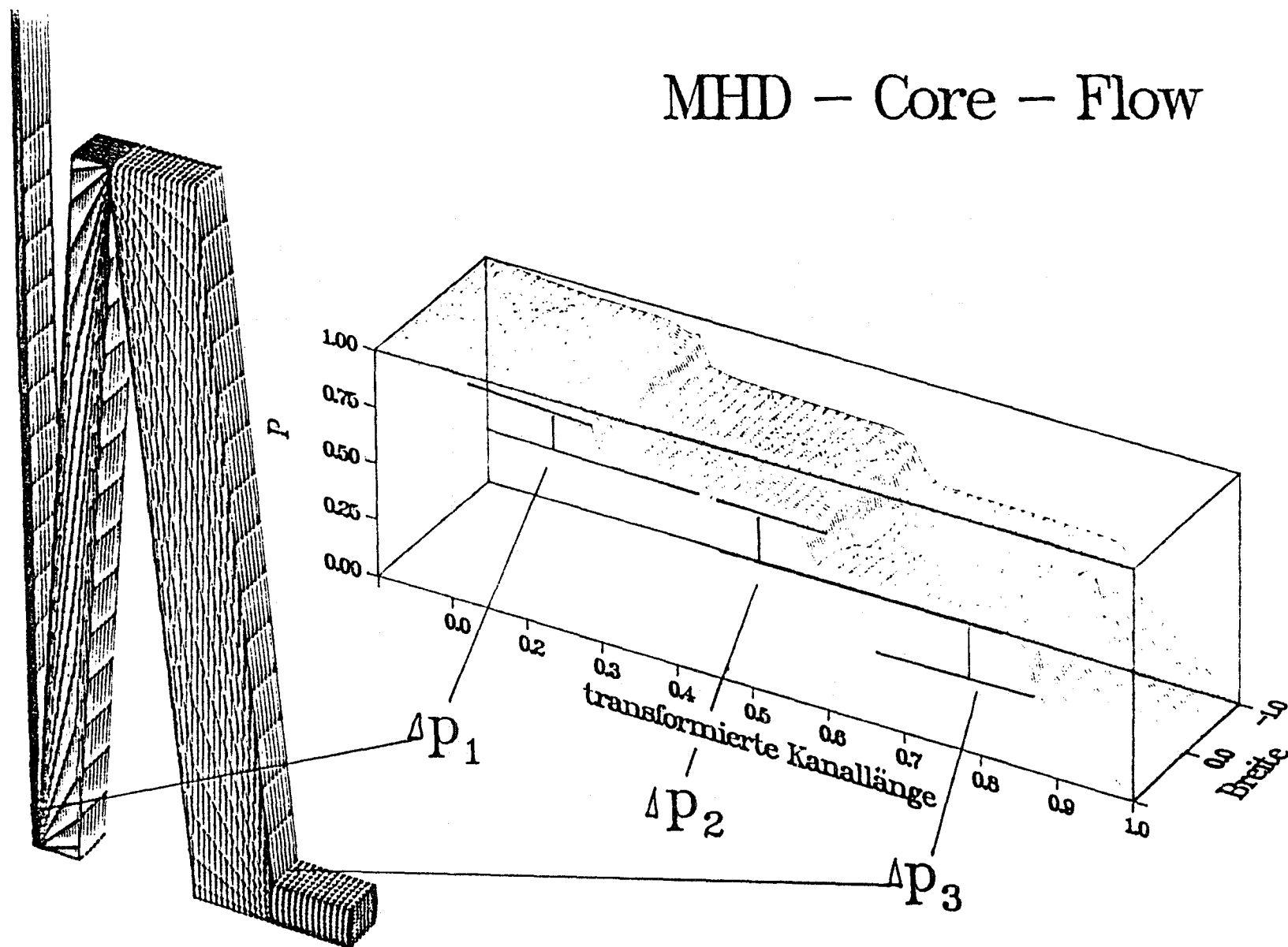
Fig. 4.2-8   MHD-flow in a meander shaped duct, pressure distribution
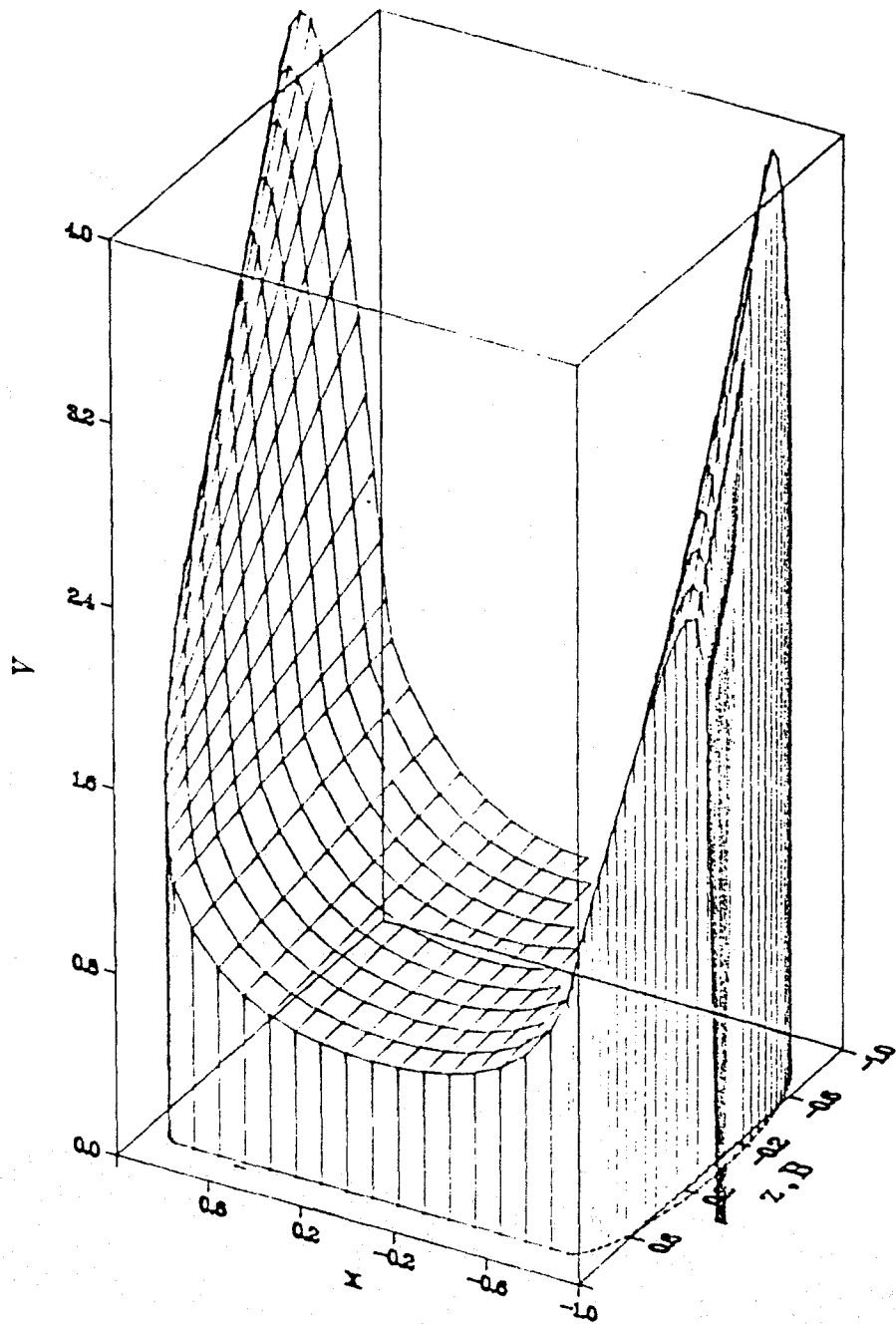
Fig. 4.2-9   MHD-flow in a meander shaped duct, velocity profile in the 3. bend
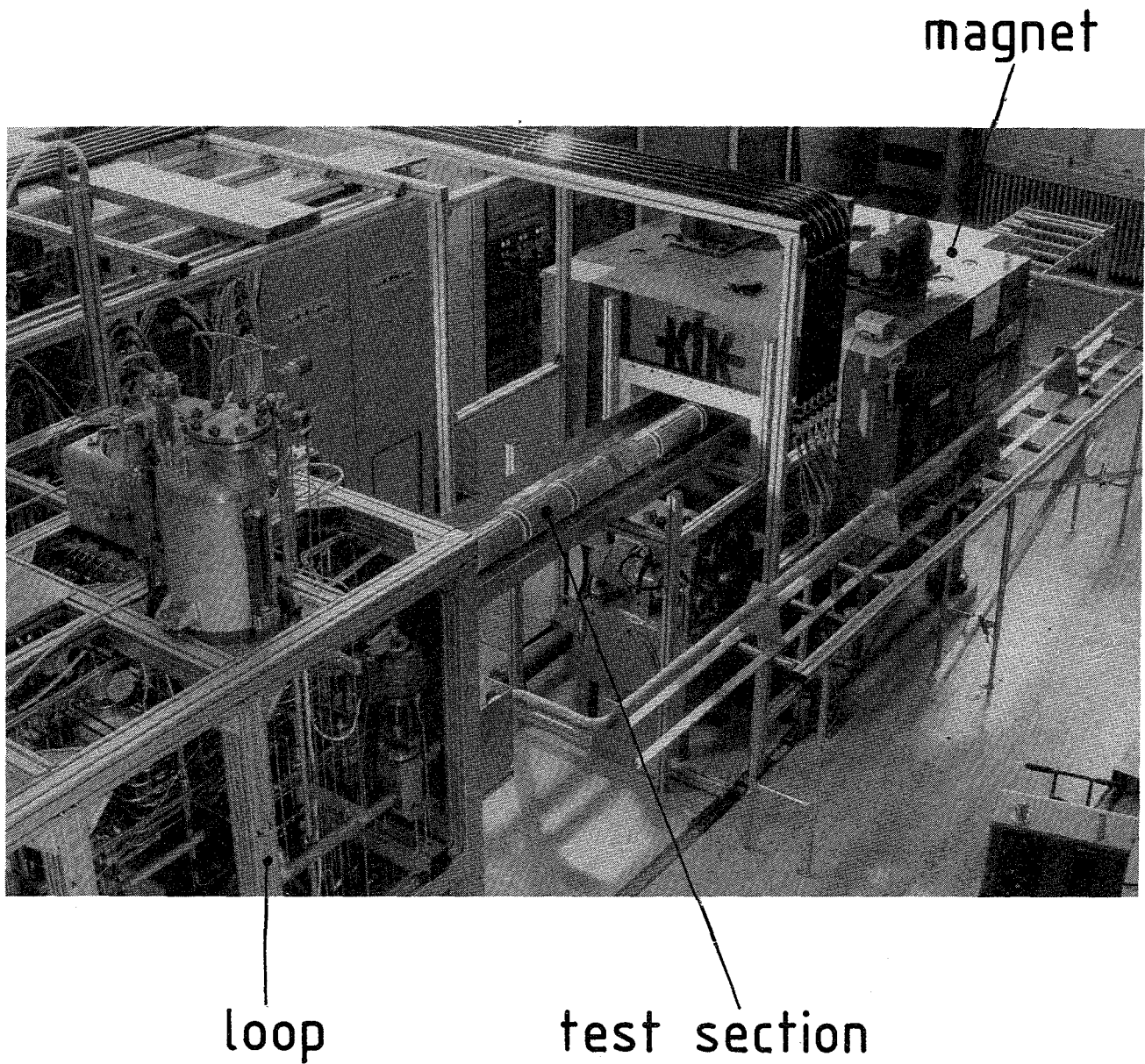
Fig. 4.2-10   The MEKKA experimental installation
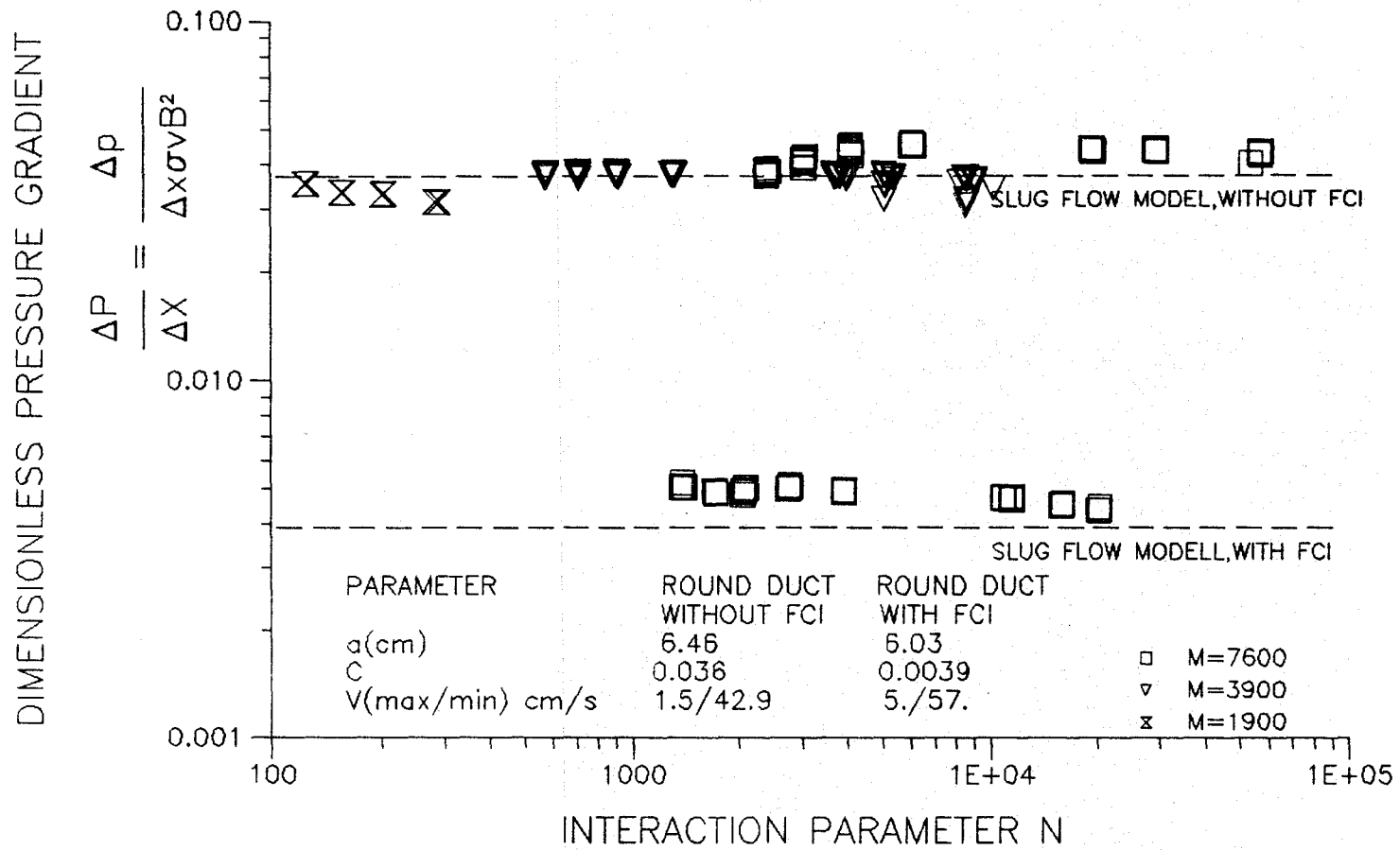
Fig. 4.2-11   MHD pressure drop experiment in a round duct

MHD DUCT FLOW

## circular pipe - conducting walls - variable magnetic field
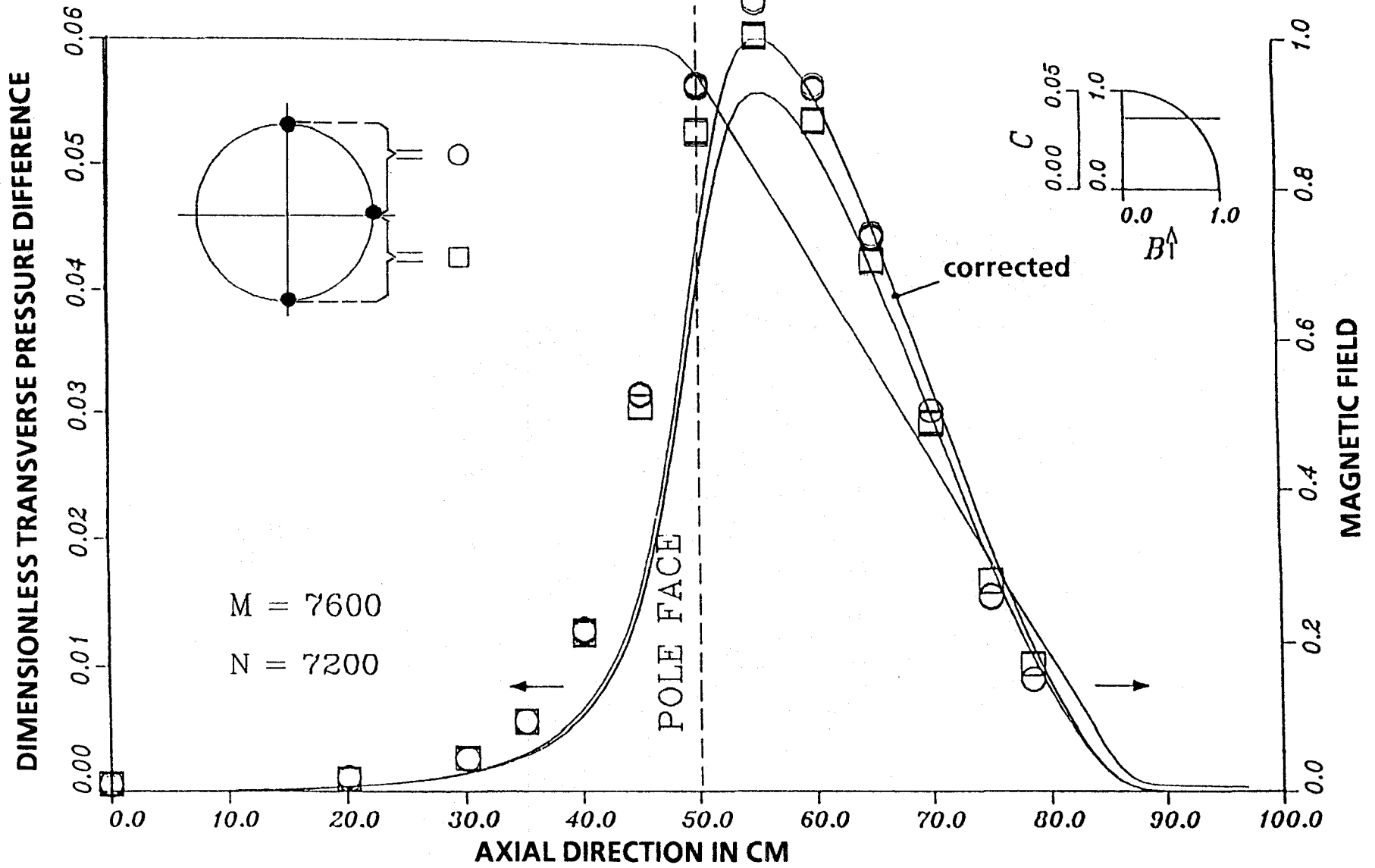
Fig. 4.2-12   Dimensionless pressure difference in a round duct
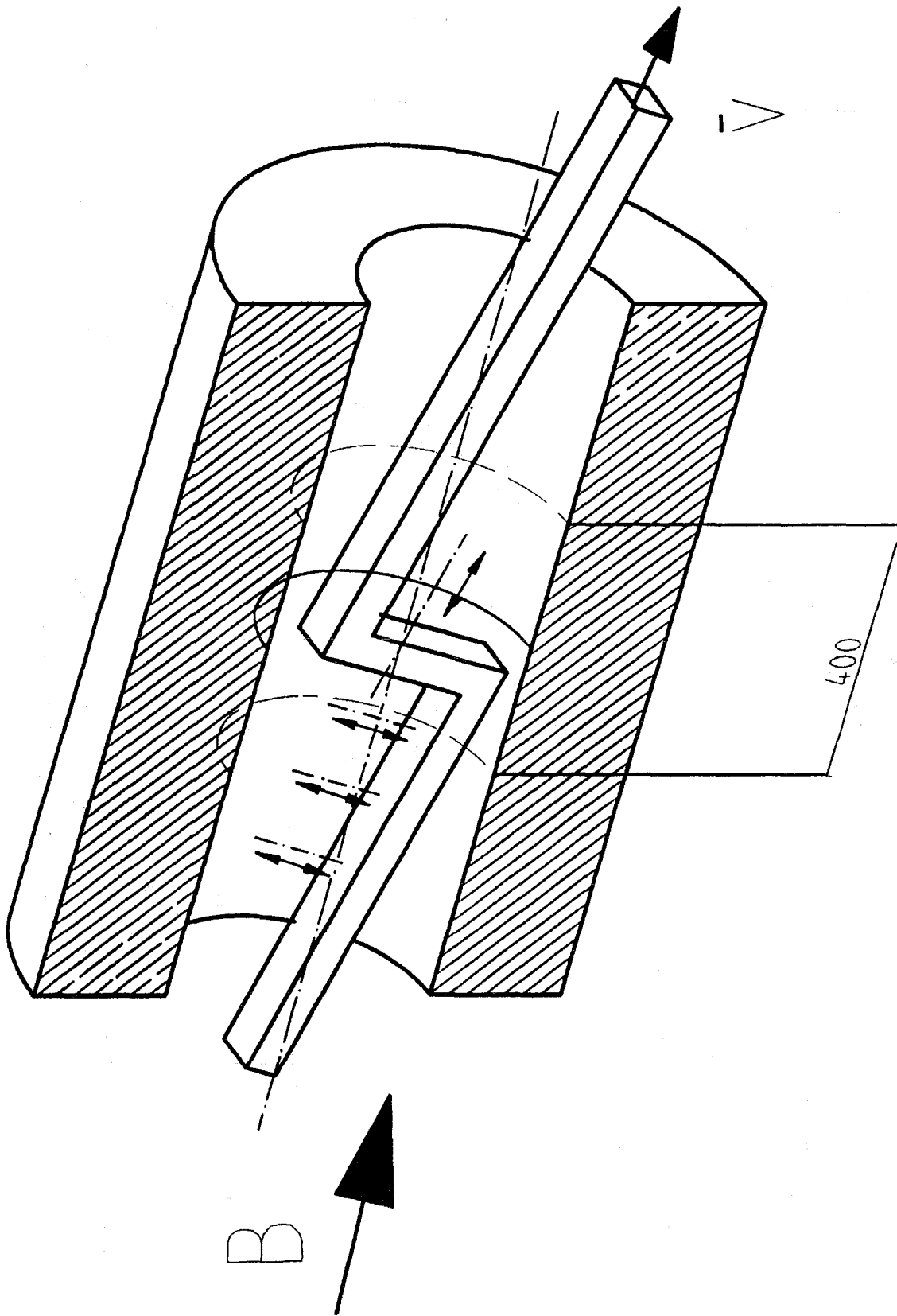
Fig. 4.2-13   Radial-toroidal bend experiment

400

B
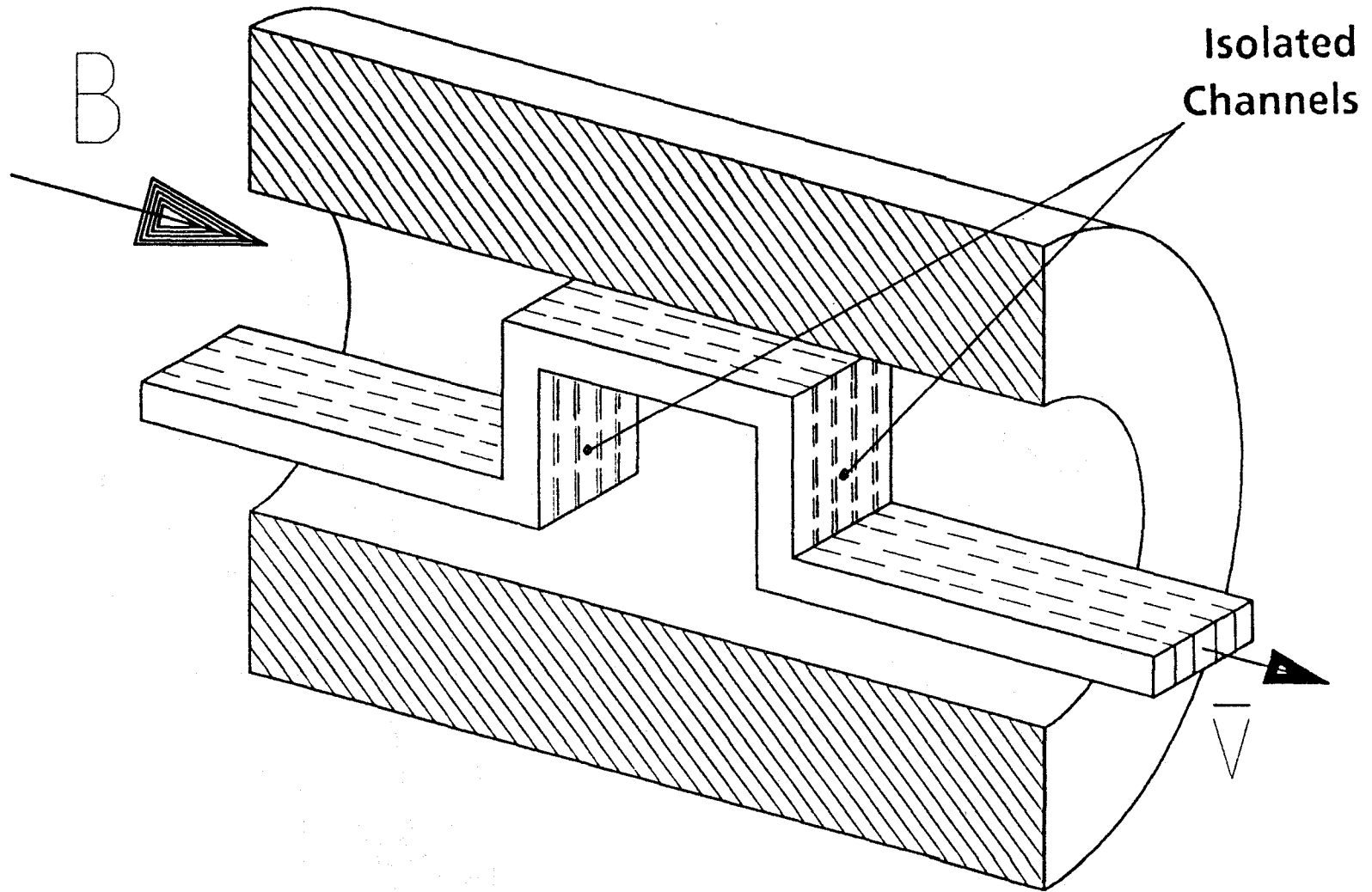
Fig. 4.2-14   Multichannel U-bend test section with countercurrent poloidal flow
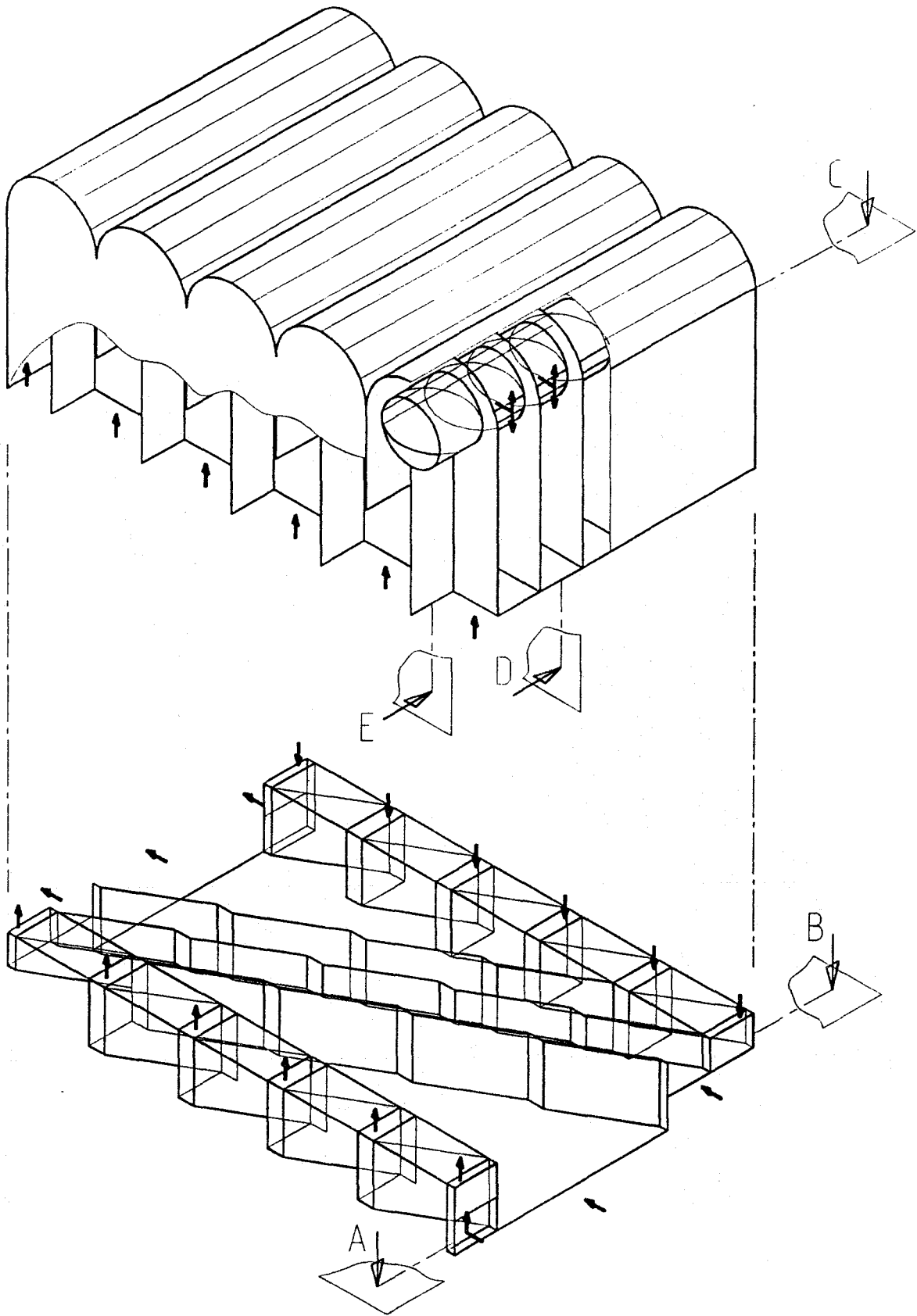
Fig. 4.2-15   The quasi-two-dimensional poloidal-toroidal flow concept, total view
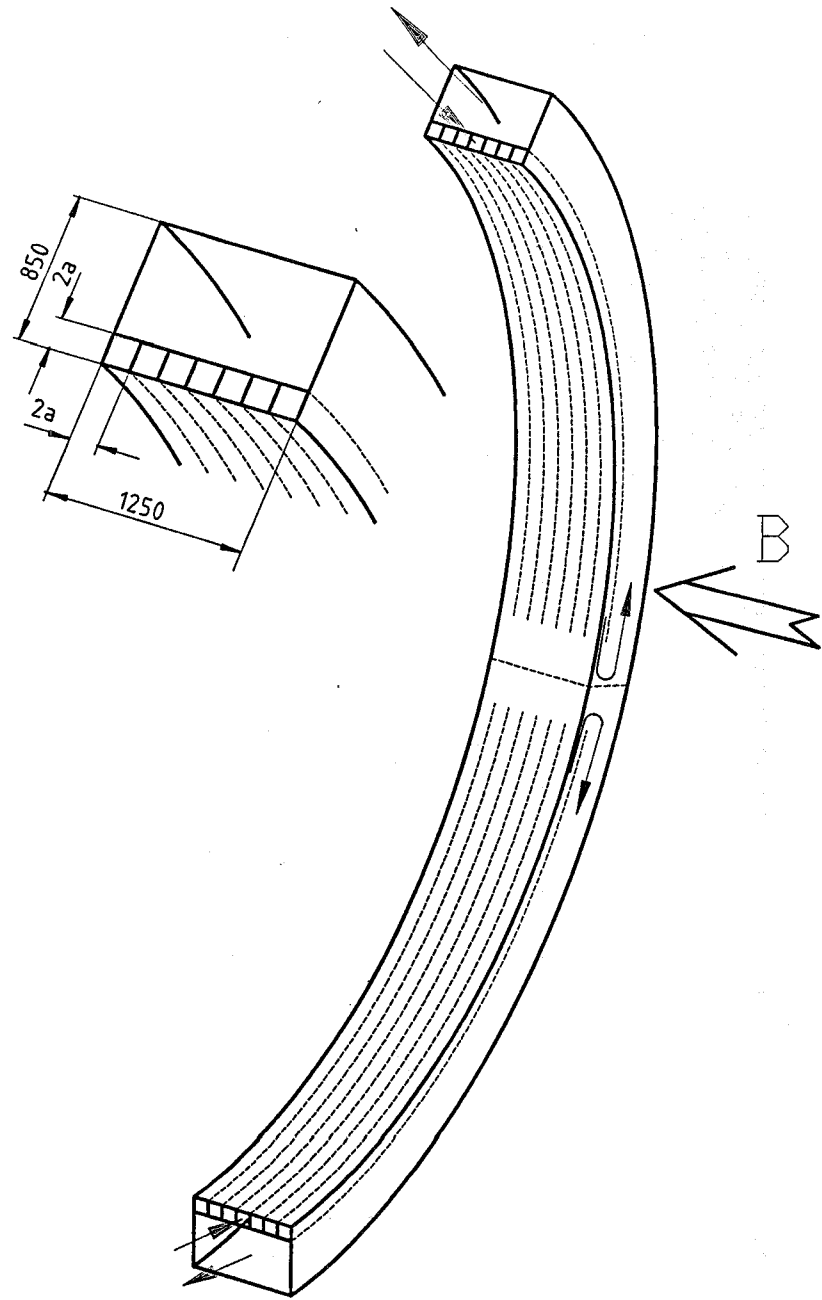
Fig. 4.2-16a   Blanket concept with poloidal flow and
rectangular shaped front channels
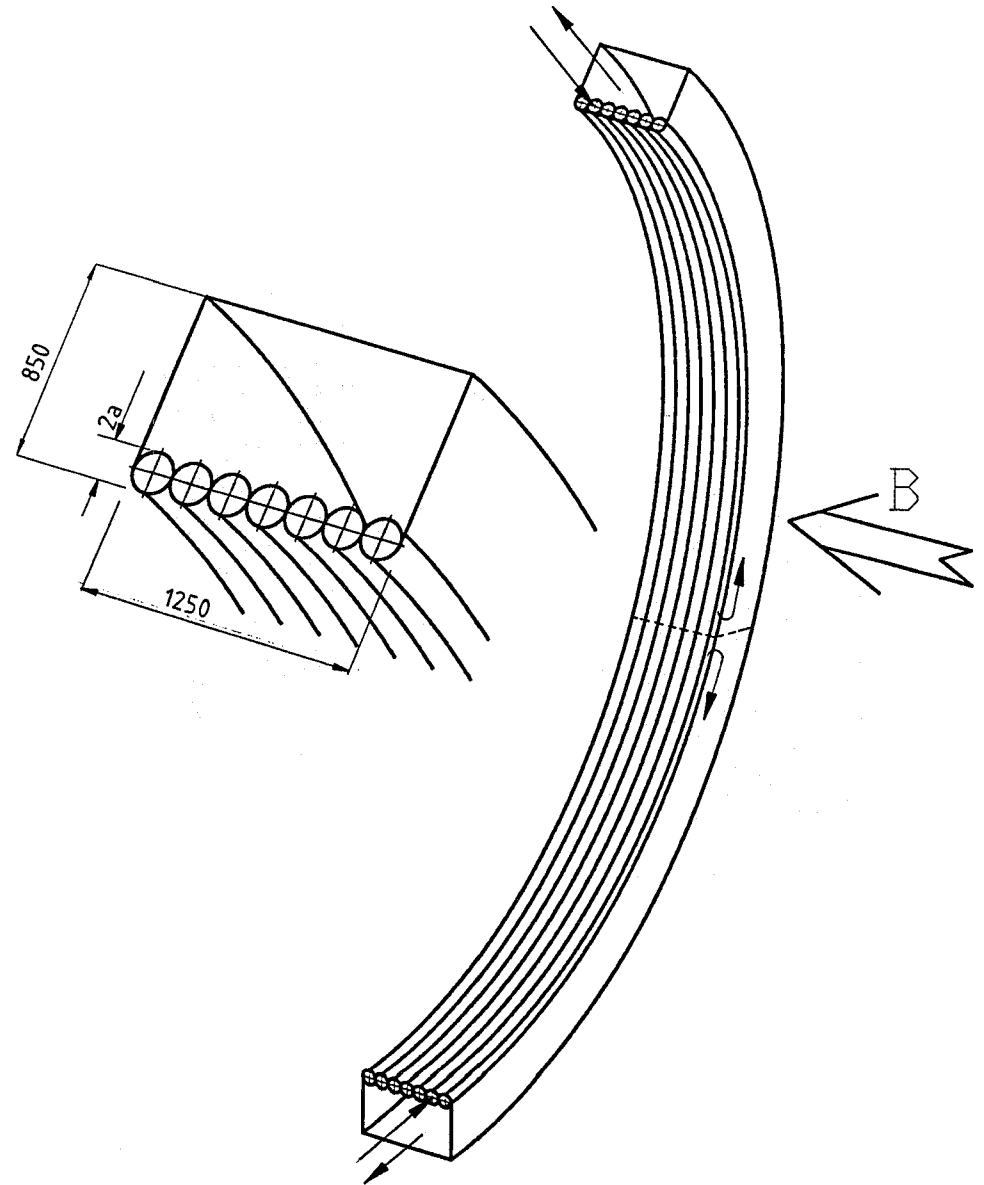
Fig. 4.2-16b   Blanket concept with poloidal flow and
round front channels

B

Lines of constant Potential
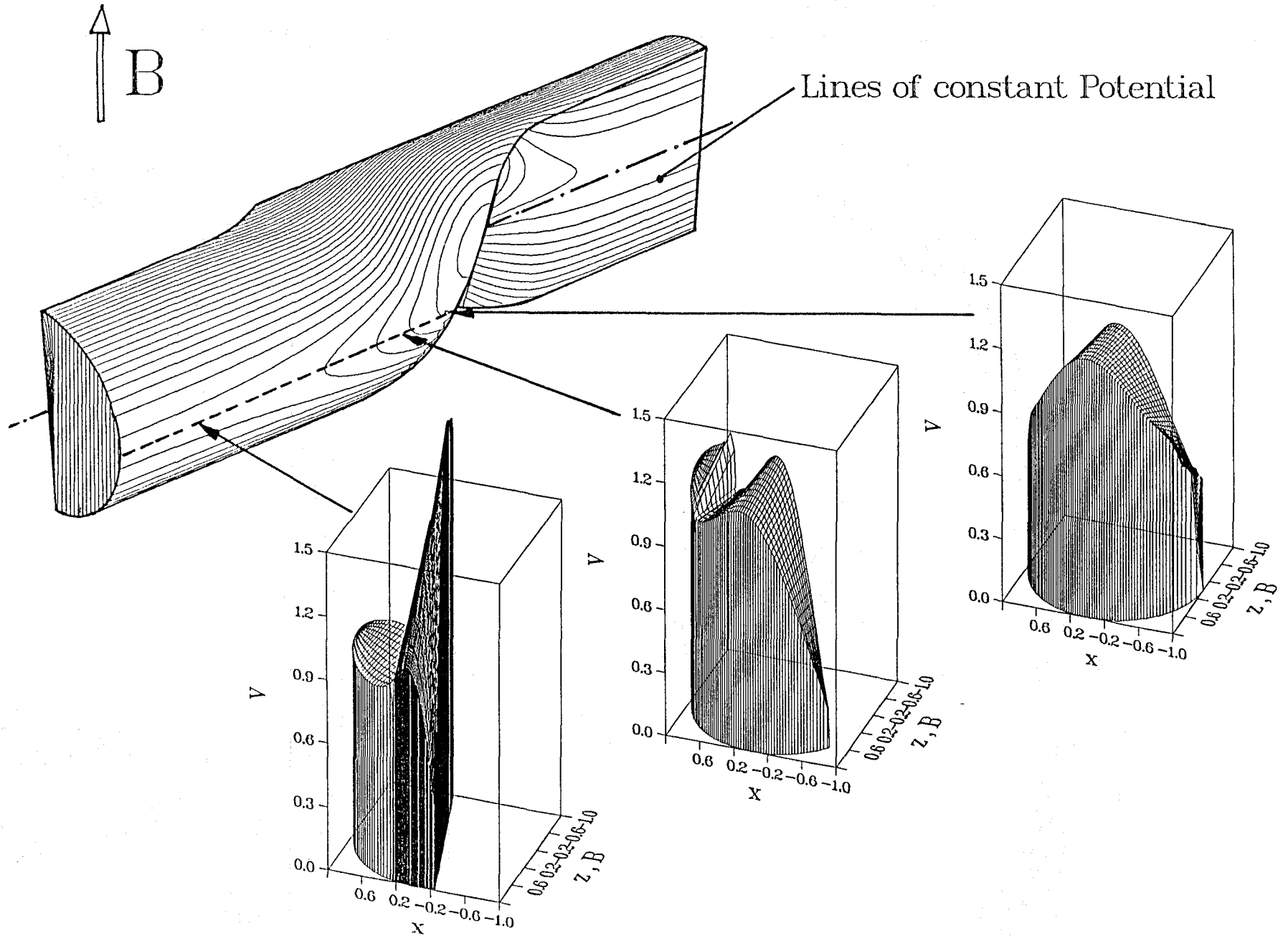
Fig. 4.2-17   Potential and velocity distribution in a round duct with a helical vane
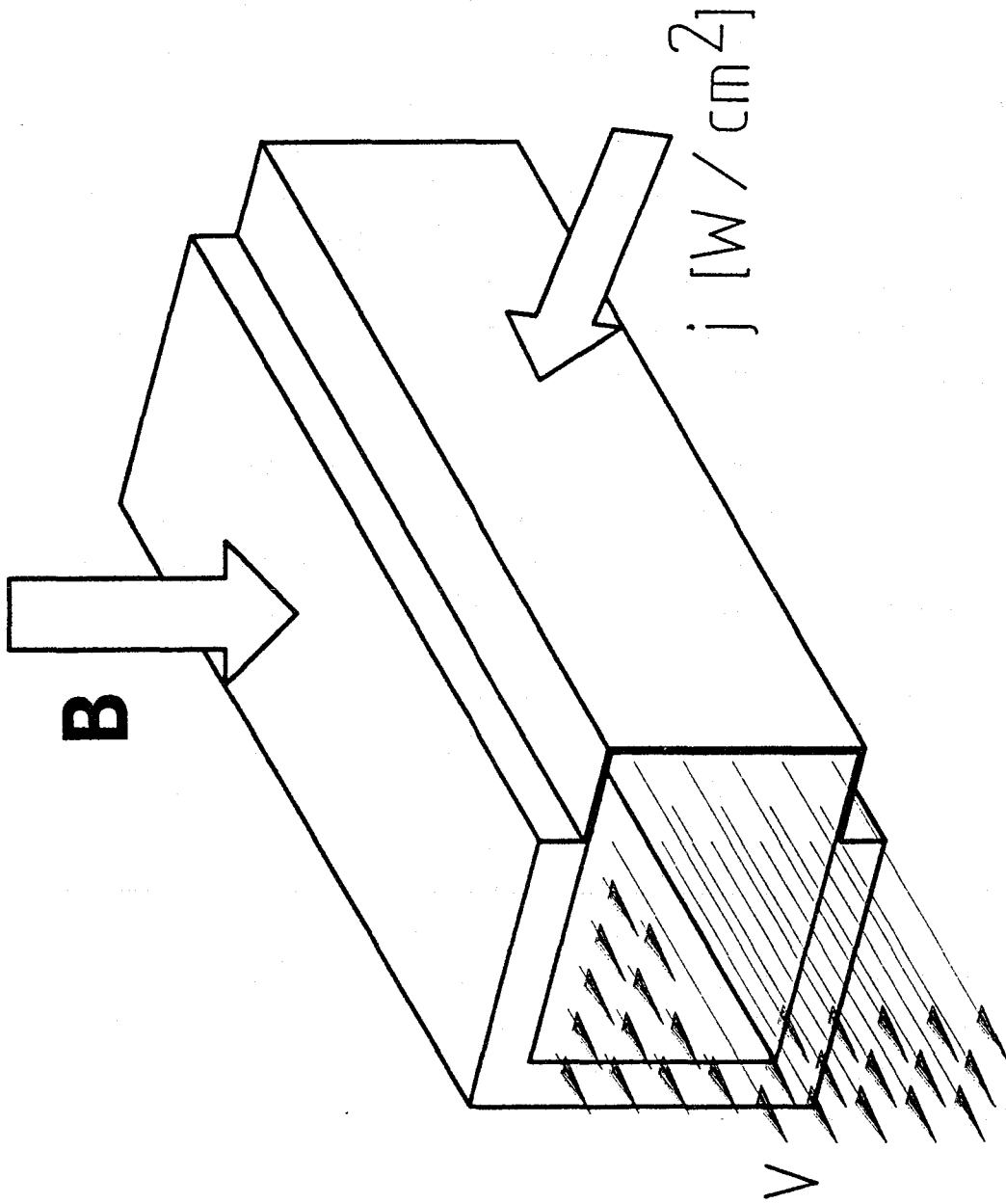
Fig. 4.2-18   Enhance of convection by free shear layers.

179

4.3   Electrical insulation by flow channel inserts
4.3.1. Introduction

An electric potential is induced in an electric conductor moved perpendicular to a magnetic field. This happens in a blanket of a fusion reactor cooled with liquid metal. The induced potential drives an electric current through conducting parts not being in motion perpendicular to the field. These comprise conducting structures of the blanket and stagnant coolant. The first short circuit can be avoided by electric insulation, the latter by a proper design. The power of the short-circuit must be produced as additional pumping power. In a blanket with uninsulated steel structures, the additional pumping power would cause mechanical stresses in the structure which could not be controlled.

Therefore liquid-metal cooling requires strong reduction of the electric short-circuit. One way to minimize them would be a direct electric insulation of the inner surface of all flow ducts. This insulation is exposed to combined attack of corrosion, thermal stresses, and neutron-flux at elevated temperatures (400°C).

Materials to insulate the flow ducts at the inner surface are not available. Therefore we develop so-called flow channel inserts (FCI), a separate component to prevent the short-circuit. They consist of two thin metal sheets with an insulating ceramic layer between them. The sheets are welded together at the edges. The laminated sheets are formed to the shape of the flow channels. They are inserted loosely into the ducts of the blanket. A longitudinal slot in the FCI ensures pressure equalization between the main stream inside the FCI and the liquid metal in the slot between FCI and channel structure. Fig. 4.3-1 shows the mode of operation of an FCI. The electric potential induced in the fluid finds a short-circuit through the thin inner sheet of the FCI, only.

4.3.2   Design of flow channel inserts

The following designs were considered for FCI:

a)   Two metal sheets with a ceramic fleece in between; no mechanical bonding between the ceramic and the two metal sheets. This design can be realized without any effort for the development of fabrication methods. But heat transfer through the FCI and its stability will be low. The behaviour of the

FCI in vacuum is difficult to predict. Vacuum might be necessary before filling of the blanket with the coolant.

b) Coating of a metal sheet with a ceramic layer. Second metal sheet without mechanical bonding to the ceramic; the second plate is only welded at the edges to the ground sheet. This design can be assessed like design a).

c) FCI with mechanical bonding of the ceramic layer to both sheets. This design guarantees a good heat transfer through the FCI and it has a good stability; but the fabrication of FCI is complicated.

It has been decided to develop FCI with mechanical bonding of the ceramic layer to both metal sheets.

4.3.3   Load on flow channel inserts

During operation FCI have to withstand the following loads:

- Pressure of $3 \div 6$ MPa acts from all sides; it does not produce considerable load. In contrary the pressure helps to reduce the effect of shear stresses caused during thermal cycling.

- Pressure gradients in downstream direction cause low tensile stresses. Pressure gradients perpendicular to the flow direction may occur when the magnetic field is changing. The FCI have to be installed in such a way into the channels that these gradients create always the lower pressure at the longitudinal slot of the FCI. Then the FCI is pressed against the channel walls.

- Operation temperature of 400°C is rather moderate. But it can influence the choice of material selection for the insulator. Some types of glass-ceramic do not permit such temperatures. Temperature changes of 100°C occur at the beginning and the end of a heat pulse. They give rise to thermal stresses, creating compressive stress, tensile stress, and shear stress. The first two types of stress can be kept low in the ceramic layer, when both steel sheets have the same thickness, and when the ceramic layer is thin. The shear stress has its maximum in the ceramic layer. It has a discontinuity at the edges of the FCI in case of different thermal expansion of ceramic and steel. This discontinuity is the most serious mechanical load of the FCI.

- Electrical potential of 0.3 V can be induced in the channels. This voltage has to be insulated.

- Neutron flux exposure will create in the steel of the FCI 10 DPa in case of NET, and 70 DPa in a demo-plant. The first load is considered to be low, the second is considerable high.
- Under the combined loads the effect of temperature, electric potential and neutron-flux have to be investigated. As measured by [1] Al_2O_3 for example becomes an electrical conductor within hours, when a voltage of 1300 V/cm and irradiation is superimposed. This result will affect the choice of the insulation material and the dimensioning of its thickness.

From these considerations the following dimensions were chosen:

Thickness of the outer steel sheet: $\sim$ 1 mm
Thickness of the insulation layer: $\sim$ 0,1 mm
Thickness of the inner steel sheet: 0.5 $\div$ 1 mm

4.3.4   Choice of materials and fabrication methods

The material selected for NET and a DEMO-plant is stainless steel 316L or a martensitic steel, similar to 1.4914. In principle for the steel sheets of the FCI a different material could be selected. Low mechanical strength is required, but the material must have sufficient corrosion and irridiation resistance. The selection of an other material would require additional corrosion experiments. Table 4.3-1 shows thermal expansion and electric conductivity of some ceramics. The corresponding values for stainless steel (316 L) and martensitic steel (1.4914) are included.

For a laminated element (steel-ceramic-steel) with mechanical bonding at the inter-phases materials should be selected with equal thermal expansion. From this point of view martensitic steel and glass should be the best choice. After consideration of all parameters (material properties, fabrication methods, and the mechanical and chemical behaviour) stainless steel and Al_2O_3 were selected as first choice. The possibility to develop FCI with martensitic steel will be investigated in a second step.

Fabrication methods consist of two major step:
- Coating of the basic steel sheets with ceramic,
- diffusion welding of the top steel sheet to the ceramic layer and welding of the steel sheets at the edges.

The coating process of the basic steel sheet with ceramic could be carried out by one of the following processes:

- Plasma spraying,
- chemical vapour deposition (CVD),
- physical vapour deposition (PVD),
- brazing of the two steel sheets with a glass as brazing material,
- diffusion welding of a thin-wall ceramic sheet to the two steel sheets.

In an assessment, at the beginning of the development of FCI it has been decided to select plasma-spraying as coating process. CVD and PVD were considered to be not very suitable when rather thick layers (100 μm) are required. Glass-brazing was rejected because of low resistivity against neutron irradiation of many glasses. Application of thin-wall ceramic sheets would require ceramic layers thicker than 100 μm, maybe 500 μm.

4.3.5 Development of fabrication methods

The development of fabrication methods has been carried out until now in industry (MBB). This work was performed in the years 1986 to 1990. Steel sheets of 1 mm thickness were taken. As material 1.4544, a material which has a similar composition as SS.316.L. As bonding material (under the ceramic) the following plasma-sprayed materials were applied: NiCrAl (Metco 443-powder), Cu, CuTi (90/10), FeCr (88/12). As insulation material the following ceramics were investigated: Al_2O_3, $Al_2O_3 + TiO_2$ (3/13/40%), $MgAl_2O_4$. In some cases the ceramic layer was metallized by plasma-spraying with: Ni, Cu, NiCr (80/20), 70 ($Al_2O_3 + TiO_2$) + 30 (NiCrAl).

As bonding materials for diffusion-welding the materials listed in table 4.3.2 were examined.

The coated basic sheets were diffusion welded with the top sheets at temperatures between 550°C and 1200°C and with pressures between 3 and 120 MPa. The temperature was kept below the melting temperatures of the metal; diffusion welding takes place between solids. Metallographical investigation carried out by [2] showed in many specimens good bonding between the ceramic and the metals; but very often cracks in the ceramic layer parallel to the sheets could be detected . A photo of a typical specimen is shown in Fig. 4.3-2.

With many specimens uni-axial tensile tests were performed. Many samples dismantled already during machining them out of a larger element. Different methods were tested for cutting them out. Table 4.3-3 presents results from the uniaxial tensile tests. One realizes large scattering of the results. But additionally it has to be mentioned that these results were not reproducible. At this moment we have no technique to fabricate a laminated element with mechanical bonding and good electrical insulation as well.

Investigations of the structure of the plasma-sprayed ceramic layers, carried out by [3], show a rather amorphous structure which results in a reduced strength. In uni-axial tensile tests of stainless steel sheets plasma-sprayed with Al_2O_3 ultimate strength of about 25 MPa was measured. One has to consider, the laminated element (steel-ceramic-steel) undergo high shear stresses at the interfaces, due to differences in thermal expansion between stainless steel and the ceramic. They are produced by joining the metal and ceramic at high temperature and cooling them down. These shear stresses are not uniform. For an elastic case they create infinite tension at the edges of the sample, and zero shear stresses in its middle part. Reason of the failure of many samples during cutting them may be caused by this non-uniform stress distribution.

In an FCI - with the metal sheets welded together at the edges - this discontinuity of tension will be located in the welding region. There the infinite tension will be reduced by plastic deformation. Therefore new specimens for tensile tests are in preparation. Bottom sheets coated with ceramic will be cut off by laser to round disques. On top of each of them a top sheet will be diffusion welded by hot isostatic pressing. During the welding process the specimen is enclosed in a thin wall gastide container. It is made of stainless steel and has a thickness of a tenth of a millimeter; this thin steel sheet will seal the edges of the ceramic, the area with discontinuity in shear stresses. The uni-axial tensile tests will be carried out without dismantling this metal wrapping. These tests with specimens specially manufactured shall give the answer whether FCI can be fabricated with stainless steel and coating by plasma-spraying. The results initially expected from the work performed in the last 4 years were not achieved. Therefore additional work has been initiated to investigate the applicability of other materials and of other fabrication methods to fabricate FCI.

As the first alternative it will be investigated to produce FCI with martensitic steel and plasma- sprayed ceramic. This possibility has become more interesting, since martensitic steel has been selected as design material for a DEMO-reactor. For FCI martensitic steel has two major advantages compared with stainless steel. Its thermal expansion fits better to those of oxid-ceramic; and martensitic steel will allow a heat treatment of the coated element at least at 1150°C. Already at 1240°C amorphous plasma-sprayed Al_2O_3 is transformed to the a-phase which has the better mechanical properties. Corresponding work has already been started.

As second alternative work has been initiated to fabricate FCI with glass as insulating material. In combination with martensitic steel it is an interesting material. Glasses with identical thermal expansion like martensitic steel are available (see table 4.3-1). However, their behaviour in a high neutron flux has not yet been investigated. Fig. 4.3-3 shows a photo of a metallurgical cut through a FCI-probe with glass as insulation layer (Schott glass 8470); good bonding can be observed. The glass has no cracks. The black circles in the glass layer are quartz spheres. They were added to the melt to achieve a defined thickness of the insulation layer. In the probe shown, the quartz spheres have a diameter of 150 µm and smaller.

As a third alternative coating of the martensitic steel by chemical vapour deposition (CVD) with aluminia or with silicium-nitride will be investigated; corresponding work has been initiated. The problem with CVD is that this coating method is normally achieved to produce very thin ceramic layers (a few µm). Thicker layers tend to split off during cooling them down from the hot fabrication process. Basing on the knowledge of the change of electric resistance of alumina when both electric tension and radiation are superimposed, a thickness of the insulation layer of at least 10 µm will be required. In the moment it is discussed how to realize thick layers (≥ 10 µm) by providing additional sublayers.

References to section 4.3:

[1]   E.R. Hodgson: High Temperature Irradiation of Fusion Materials. Cristal Lattice Defects and Amorphous Materials, Vol. 18 (1989), p. 169

[2]   B. Bennek-Kammerichs: unpublished work

[3]   W. Schneider: private communication.

Table 4.3-1: Material properties

Material	Melting Point	Thermal expansion	Specif.el.resist. at 20°C	radiation resistance
	°C	10^{-6}/K	Ω cm	
Al_2O_3	2047	8.4	10^{14}	good
Al_2TiO_5	1894	9.7	10^{10}	
TiO_2	1867	9.0		
MgO	2827	13.0	10^6	
$MgAl_2O_4$	2135	9		excellent
Si_3N_4	1900	2.5	10^{12}	
AlN	2250	5.7	10^9	
SiO_2	1650	0.6	10^{14}	
ZrO_2	2980	6.5	10^9	
Glass (Schott 8470)	~ 680	10.5 ÷ 11.5	10^8	
SS 316L		~ 17		
1.4914		~ 11		

Table 4.3-2: Bonding material for diffusion welding

Type	Composition	melting temp. °C	thickness μm	deliverer
L-Ni2	Ni82.6 Cr7 Fe3 Si 4.5 B 2.9	970 - 1000	50/100	Degussa
L-Ni6	Ni 89 P 11	875	35	Degussa
TiCuNi	Ti 70 Cu 15 Ni 15	910 - 960	70	GTE Wesgo
Cu-Folie	99.9 Cu	1083	80	-
Incusil 15-ABA	Ag 41 Cu 23 In 14 Ti 1.25	605 - 730	100	GTE Wesgo
SCP-2	Ag 58 Cu 32 Pd 10	824 - 852	100	Degussa
SCP-5	Ag 95 Pd 5	970 - 1010	100	Degussa
SCP-6	Cu 82 Pd 18	1080 - 1090	100	Degussa
6009	Ag 60 Cu 30 Sn 10	600 - 720	100	Degussa
5603	Ag 56 Cu 26 In 14 Ni 4	620 - 730	100	Degussa
Cu	99.9	1083	50 - 100	plasma-sprayed
Ni	99.5	1452	50 - 100	plasma-sprayed
CuTi	Cu 90 Ti 10	1038	50 - 100	plasma-sprayed
FeCr	Fe 88 Cr 12	1510	50 - 100	plasma-sprayed

Table 4.3-3 Strength of FCI with stainless steel sheets in uniaxial tensile tests

| speciment No.	under-coating	insulation material	surface layer	strength [MPa]	
x 7	NiCrAl	Al_2O_3 +	Ni/TiCuNi	3.2	↑
x 8	"	13 % TiO_2	Ni/Cu	1.7/9.4	
x 10	"	"	Cu-Glass/Cu	3	
x 11	"	"	Ni	2	
x 12	"	"	Ni/Incusil	5.6	
x 13	"	"	Cu/Incusil	3.2	
x 14	"	"	Cermet/Incusil	4.0	
x 15	"	"	Incusil	1.0	
x 21	"	"	Ni/SCP 5	0.6/1.6	
x 22	"	"	Cu/SCP 5	5.5/2.5	
x 24	"	"	Ni/SCP 6	7.6/4.8	no electric
x 28	"	"	Cu/Cu	4.5/12.6	insulation
x 29	"	"	Ni	2.3/7.7	of specimen
x 30	"	"	Cu/Incusil	16/17.5	
x 31	"	"	-/Incusil	9.4/20.2	
x 32	"	"	Ni/5603	12.5/19.1	
x 33	"	"	Cu/5603	25.5/26.7	
x 34	"	"	-/5603	14.1/17.9	
x 36	"	"	Cu/6009	8.1/9.2	
x 37	"	"	Ni/SCP 2	8.7/10.5	
x 38	"	"	Cu/SCP2	5.2/8.2	
x 39	"	"	C/SCP2	2.8/5.43	↓
5	Cu	spinel	Cu	2.6	a ceramic
7	"	"	Cu	4.8	was pene-
8	"	"	Cu	7.3	trated by
9	"	Al_2O_3	Cu	6.8	under-
24	"	"	Cu	47.9 a	coating/sur-
28	"	"	Cu	46.4 a	face layer
29	"	"	Cu	16.9 a	material
30	CuTi	Al_2O_3 + TiO_2	CuTi	4.2	
31	"	"	"	18.4 a	
32	"	"	"	36.8 a	
33	"	Al_2O_3	"	68 a	
34	"	"	"	67 a	
35	"	"	"	72 a	
36		spinel		5.1	
37		"		0	
38		"		0	
26	FeCr	spinel	FeCr	0	
27	"	spinel	"	0	
39	Cu	Al_2O_3	Cu	0	
40	"	"	"	8.4	
41	"	"	"	0	
43	"	"	"	0	
51	FeCr	Spinel	FeCr	0.8	
52	"	"	"	0.4	
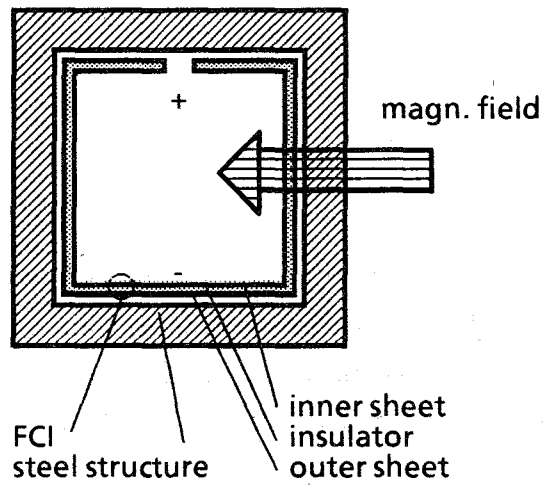
Fig. 4.3-1   Function of an FCI
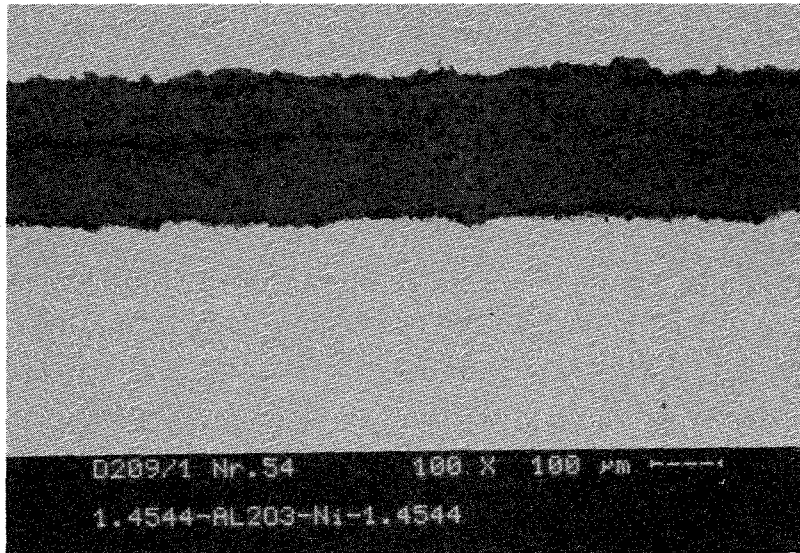
Fig. 4.3-2   Metallographical cut through an FCI with alumina as insulator
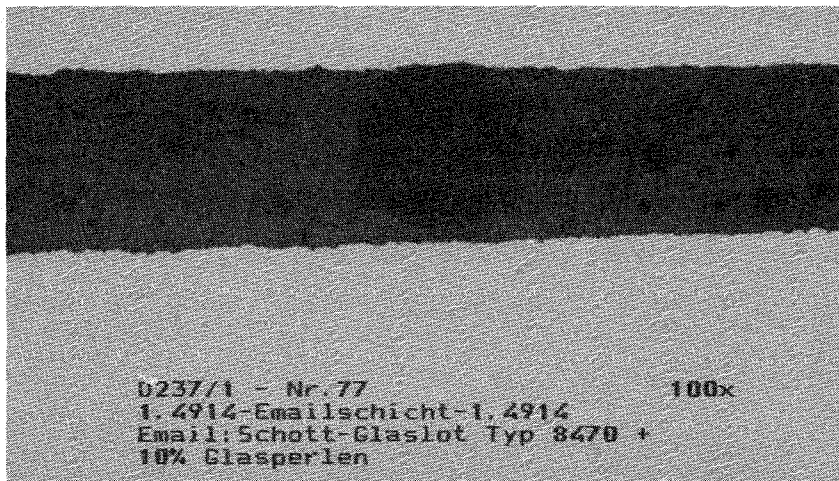
Fig. 4.3-3   Metallurgical cut through an FCI with glass as insulator

4.4 Tritium extraction and recovery
4.4.1 Permeation/Cold trapping

The favourized tritium removal and recovery technique is based on tritium permeation from Pb-17Li through the ferritic wall of the double-walled heat exchanger into the NaK-filled gap, tritium removal from NaK by cold trapping as tritide and tritium recovery by thermal decomposition of the tritide, compare Fig. 4.4-1.

4.4.1.1 Tritium transport from Pb-17Li into NaK

In the heat exchanger piping tritium diffuses from the bulk Pb-17Li flow through the liquid metal boundary layer to the wall surface, dissolves in the ferritic material, diffuses through the wall, dissolves at the NaK-wall interface, diffuses through the NaK-boundary layer and is transported in the liquid metal bulk flow to the cold trap. In all metals tritium exists in atomic form and no recombination process to T_2 (or HT if protium coexists) is involved. Therefore, permeation is rather facilitated [1,2] compared to permeation from a gas phase through a metal wall. However, the above description is only correct if surface layers due to impurities do not exist which otherwise would give rise to an permeation barrier.

Surface layers, especially oxide layers can drastically reduce permeation. In Pb-17Li the oxygen solubility is very small [3] so that oxygen is scarcely transported from a potential oxygen source (for instance the cover gas system in the expansion vessel) to the heat exchanger. Furthermore, corrosion experiments have shown that initial oxide layers are dissolved, compare Section 4.5.1. In the NaK system, the chemical activity of NaK towards oxygen is also higher than that of the ferritic wall material and oxide layer cannot build up and will be dissolved if they exist initially. Therefore, surface layers are not likely to occur on both sides of the heat exchanger wall. An engineering assessment shows that the tritium concentration difference across the liquid metal boundary layers is also small compared to the bulk concentration.

Therefore, no serious difficulties are expected due to the permeation process which require specific investigations in an early stage.

4.4.1.2 Tritium removal by cold trapping

Fig. 4.4-2 explains the principle of hydrogen removal by cold trapping in a graph with the square root of the tritium partial pressure and the tritium concentration as coordinates. For a given temperature a nonsaturated solution occurs at low concentrations (Sievert's range) and a saturated solution (coexistence between dissolved hydrogen and hydride precipitations) at higher values (horizontal curve). Cold trapping is based on the fact that the saturation concentration c_{sat} decreases with decreasing temperature.

When a liquid metal entering the cold trap with a temperature T_i and concentration c_i (Sieverts range) is cooled down, hydride crystals start to form below the corresponding saturation temperature T'. Ideally, the liquid metal leaves the cold trap with the concentration c_{osat}, corresponding to the saturation concentration for the cold trap outlet temperature T_o. In practice, this equilibrium is not reached due to nonideal mass transfer and the difference between the actual cold trap outlet concentration and the equilibrium value, c_o-c_{osat}, is of main importance.

Fig. 4.4-3 (from [4]) shows characteristic solubility data for different liquid metal-hydrogen systems. The term hydrogen is generally used if it is not differentiated between the different isotopic species. If concentrations are defined with atomic fractions then the Sieverts constants K and saturation concentrations c_{sat} are approximately equal for all isotopes.Tritium removal by cold trapping from Pb-17Li is not favourable due to the high value of the minimum achievable saturation pressure leading to heigh permeation losses. This would result in a high tritium pressure and tritium permeation losses would be large. Compared to Na, NaK is more favourable due to the higher Sieverts constant and the fact that much lower cold trap outlet concentration may be achieved due to the low melting point (-12°C). The latter point, however, must be experimentally verified.

Presently, a heterogeneous nucleation mechanism is assumed for the system H-Na [5] which means that the hydride nuclei are generated on solid surfaces in the cold trap (mainly on the large surface of the cold trap inserts). Then, these crystals grow and precipitation rates are governed by growth kinetics.

Local mass transfer is often described by the sum of two deposition mechanisms

$$\dot{m} = \dot{m}_N + \dot{m}_G \quad , \tag{1}$$

with

$$\dot{m}_{N,G} = A_{N,G} \cdot k_{N,G} \, (c - c_{sat})^{n_{N,G}} \qquad (2)$$

where A is the surface of the cold trap inserts, k is the mass transfer coefficient, n is the order of reaction, c_{sat} is the saturation concentration, and c is the local concentration. The indices N and G denote nucleation and growth of crystals, respectively. Experiments with sodium [5] have shown that the mass transfer coefficient and the order of reaction are very different for the two processes. In previous modeling attempts for the H-Na system the nucleation process is often neglected. For crystal growth n should be unity for diffusion controlled mass transfer and k should be calculated by appropriate Sherwood number correlations. If the mass transfer rate is governed by the integration of molecules in the hydride crystals, n is expected to be between 1 and 2 and the dependence of k on the operational parameters should be different.

The question which process is dominating is of special importance for the fusion blanket cold trap. Because of the operation at very low concentrations, cold trap volumes can become quite large assuming mass transfer coefficients used for the cold trap design for conventional applications. These cold traps are designed such to ensure a large loading capacity (long-term operation without plugging). Premature plugging is no critical problem of the present cold trap due to frequent cold trap regeneration. If it proves that mass transfer is diffusion controlled, then, the mass transfer coefficients can be increased considerably by increasing the NaK velocity through the cold trap, which - in total - results in a decreased cold trap volume.

To determine the mass transfer characteristics two kinds of experiments are performed

a) the cold trap outlet concentration c_o is measured as a function of time during hydrogen loading at constant operating parameters (mass flow rate, cold trap inlet concentration, inlet and outlet temperatures).For presentation of these results, often, the cold trap efficiency η is used, defined by

$$\eta = \frac{c_i - c_o}{c_i - c_{osat}} \qquad (3)$$

b)   after termination of this experiment the axial distribution of the deposited hydrogen in the cold trap is determined.

Compared to sodium cold traps for fast breeder applications the operation of the fusion blanket cold trap differs by:

-       hydrogen removal at a low concentration level
-       small loading times (typically less than one day instead of several months).

In this case the nucleation process may become more important than in previous applications.

First experiments have been performed in the WAWIK-facility. Protium is used to simulate tritium. The test facility is shown schematically in Fig. 4.4-4, for details see [6]. The hydrogen is permeated into the NaK through a coiled nickel tube. Hydrogen concentration are measured at the cold trap inlet and outlet. After loading the cold trap with hydride the drained cold trap is either transferred to a glove box or hydrogen is recovered directly, compare Section 4.4.2.3. In the former case the cold trap is demounted, probes for further analyses are taken from the wire mesh packings and, finally, the hydrogen mass of the single packings is determined.

Fig. 4.4-5 shows the experimental cold trap which consists of a vertical pipe (inner diameter: 100 mm) filled with up to 9 wire mesh packings (total length 450 mm, specific surface 1000 m^2/m^3). There is a cooling zone where the liquid metal is countercurrently cooled by air, followed by an isothermal zone without cooling.

First results on cold trap efficiencies as a function of loading time are shown in Fig. 4.4-6. For comparison, the results from a sodium cold trap is also shown. Both experiments were performed at similar hydrogen concentrations; the specific wire mesh surface of the Na cold trap, however, was about one third of that used in the present experiment.

At the beginning of an experiment only mass transfer due to nucleation can occur and the efficiency is lowest. The mass transfer by crystal growth starts and becomes finally the dominating process. For the Na cold trap the nucleation process seems to dominate during the first several hours whereas the crystal growth process is dominant after about 20 hours. For the NaK cold trap the efficiencies are

considerably higher, even shortly after starting the hydrogen loading. This indicates that nucleation is much faster in NaK than in Na. The final efficiency is considerably higher for the present NaK cold trap. For the same specific wire mesh surface as used in the Na cold trap a final efficiency of 85% is estimated. Corresponding experiments will be performed in the near future.

First measurements of the axial hydrogen distribution in the cold trap are shown in Fig. 4.4-7 together with the results of a one dimensional calculation. In this calculation only mass transfer due to crystal growth was considered. The best agreement with the experimental values was obtained for $n = 1$ and $k = 4 \cdot 10^{-5}$ (m/s) These values correspond fairly well to those assessed for diffusional mass transfer.

The question is if the one dimensional model is sufficient for mass transfer modeling. For the low liquid metal velocities of interest in the cold trap the influence of natural convection cannot be excluded. Calculations for Na and NaK as liquid metal were performed for the cold trap geometry used in the experiments.

Constant inlet conditions were assumed and linear wall temperature decrease in the cooled zone and a constant wall temperature in the isothermal zone, compare Fig. 4.4-5. The calculations were done on the basis of the quantities summarized in Table 4.4-1. Two flow directions of the liquid metal were considered a) vertical upward and b) vertical downward (cold trap with cooling rotated by 180°). A detailed description of the physical correlations and mathematical procedure is given in ref. [7].

Figure 4.4-8 contains for Na as liquid metal radial distributions of the normalized temperature (T), velocity (v), concentration (c), and deposition rate (s) for different values of the dimensionless axial coordinate z/r indicated in Fig. 4.4-5. A characteristic velocity of $V = 4$ mm/s was assumed.

Without natural convection, $Gr = 0$ (results not shown), the internal friction due to the packing forces a nearly constant radial velocity distribution except close to the cylinder walls. For $Gr = 6 \cdot 10^7$, the profile differs significantly: the wall gradients become smaller for upward flow and larger for downward flow; in the latter case the developed velocity distribution has its maximum close to the wall. The flow field is already developed at $z/R \approx 2$.

The temperature distribution is merely influenced by the velocity distribution because heat transfer by heat conduction is the dominating process (small Prandtl number). For the local deposition rate, it was assumed that diffusion is the dominating mechanism. The radial deposition rate is then of similar type as the velocity distribution and, therefore, is influenced by natural convection.

These numerical results show that natural convection effects are not limited to unpacked cylinders (compare [7]). Further experimental and theoretical work is required in order to develop a reliable mass transfer model.

For NaK as liquid metal the natural convection effects are even more pronounced mainly due to the lower thermal conductivity ($\lambda_{NaK} = 0,3\ \lambda_{Na}$ for $T = 120°C'$). Fig. 4.4-9 shows corresponding results [8] for the upward flow direction: The radial dependency of temperature and velocity is stronger than for Na and with this the radial dependency of the concentration and local deposition rate. The characteristic maximum of the local deposition rate close to the wall at low distances from the inlet was also observed experimentally.

Fig. 4.4-10 shows hydride crystals in different enlargements obtained by optical microscopy and electron microscopy. The crystals are of the octahedral type but are less regular than observed in sodium experiments [5]. By means of the EDAX method (Energy Dissipative X-Ray Analyses) it was found that the crystals consist of pure potassium hydride. This fact was already suspected previously [1] but not experimentally verified yet.

4.4.1.3 Tritium recovery from cold traps

In the experiments again protium was used to simulate tritium. First experiments to investigate hydrogen release by thermal decomposition were performed with commercial fine NaH-powder [9]. In a part of these experiments Na_2O powder was added. The release coefficient k was defined as

$$\dot{m} = km^n \tag{4}$$

where $\dot{m}$ is the hydrogen mass flow rate, m the actual mass of hydrogen in the reaction vessel, and the exponent n characterizes the reaction order. The experiments were fitted assuming first order reaction ($n = 1$). No influence of oxygen on the release rate was found. Fig. 4.4-11 contains the mean curve of the

experiments in an Arrhenius plot which is in excellent agreement with previous data [10,11].

In a next step, NaH-crystals were generated in a Na filled vessel where hydrogen was absorbed at the top of the Na interface and hydride crystals precipitated at the cooled bottom of the vessel. This experimental set-up was then also used with NaK instead of Na [12]. Fig. 4.4-11 shows that for NaH crystals the release coefficient is significantly lower than for NaH-powder which is due to the considerably smaller specific surface of the crystals. The release mechanism was clearly dominated by hydrogen bubble formation and transport in the Na pool.

The release coefficient for KH crystals is significantly larger than for NaH-crystals as long as release by hydrogen bubble formation prevails. However, hydrogen release without hydrogen bubble formation in the NaK pool occurs at low release rates. Then, the release coefficients become considerably lower because diffusion in the liquid pool and desorption mechanisms at the free surface become rate determining. The practical consequence from these experiments is to drain the cold trap from NaK before heating up the cold trap.

Fig. 4.4-12 contains new results where either the hydrogen from the single cold trap packings was determined or the hydrogen content from a complete cold trap was released [12]. In the former case the hydrogen loading was quite large whereas in the latter case the cold trap were only loaded for some hours which is characteristic for the anticipated application. The release coefficients are slightly higher at lower temperatures than for the crystallizer experiments. No significant difference is observed for high and low loading.

For a release temperature of 400°C, 99% of the tritium would be released in about three hours which is a very favourable result. Two regeneration cycles per day could be feasible; the tritium inventory in the two cold traps (batch operation) would be about 0.5 tritium productions per day.

4.4.1.4 Requirements for processing tritium recovered from the self-cooled Pb-17 Li blanket: The blanket interface

The aim of the blanket tritium recovery system (BTRS), in our case the cold trap system, is to recover the tritium bred in the blanket. However, not only gaseous tritium may leave the BTRS but, depending on the blanket concept, also protium,

tritium carrier gas and various impurities. An additional tritium processing system (TPS) may be required to obtain pure T_2 gas. The boundary between these two processing systems was called Blanket Interface [14].

For ceramic breeders, tritium is very diluted in a He stream, and the protium concentration is higher by several orders of magnitude due to isotope swamping in order to obtain a small tritium inventory in the breeder. For water-cooled Pb-17Li blankets, tritium purification of the water loop is required. For self-cooled Li blankets various impurities are carried over into the TRS.

The specific features of the BTRS for the self-cooled Pb-17Li blanket are:

- No carrier gas is required for tritium recovery (small volume flow rates have to be processed).
- Tritium is recovered in gaseous form (HT) (no processing of HTO required).
- The blanket tritium recovery system (BTRS) is disconnected from the neutron field (no loading of the BTRS with radionuclides besides tritium).
- The BTRS is disconnected from the Pb-17Li loop (much lower corrosion in Na or NaK which results in very low impurity levels).

An estimation of impurity source terms in the intermediate loop showed that besides protium and tritium no significant amounts of other species leave the BTRS. This flow can then be processed in the system required for fuel clean up without any significant modifications.

4.4.2 Getter

In order to use getter metals or alloys in contact with the liquid metal for tritium extraction, two requirements have to be fulfilled besides a large hydrogen solubility:

a) The metal or alloy must have a very low corrosion rate, otherwise mass transfer processes will transport the getter to unwanted places of the liquid metal system. Furthermore because of the risk of embrittlement, the getter metal should not show phase transformations during loading and degassing.

b) The kinetic of tritium absorption must be fast enough to be useful for its extraction. Also the recovery of tritium should be possible at moderate temperatures.

197

Compatibility

Screening tests in static Pb-17Li were performed with 35 metals and alloys, some also with coatings [15].

The typical tritium getters U and Y dissolve even at moderate temperatures completely [16].

Ti, Zr and its alloys could be used at lower temperatures. Above 450°C Ti forms an intermetallic compound Ti_3Pb_2, which destroys the metal. With alloys Ti/Zr a larger fraction of the Ti in the compound can be replaced by Zr [17]. Recovery of tritium has to be done at temperatures above 700°C. Phase transformations as well as corrosion with adhering Pb-17Li destroy these metals.

Vanadium was proposed sometimes as a structural material. This metal can also be used as a getter [18]. It is very stable in the LM [15,16], and shows no phase transformation in the range of interesting temperatures up to 700°C.

Transport of deuterium

For easier handling and analysis deuterium was used instead of tritium in most of the experiments. All results could be confirmed with normal hydrogen. Experiments with tracer amounts of tritium are under preparation.

Deuterium (Tritium) extraction experiments have to be performed with circulating Pb-17Li. Dissolution, transport and degassing/desorption behavior of deuterium in the facilities have to be known before extraction experiments can be done. Two kinds of facilities were used.

Austenitic steel thermal convection loops proved very usefull [19,20]. The deuterium behavior was investigated between 300 and 610°C, the partial pressure in the gas phase was between 1 and 1000 mbar, the equilibrium partial pressure of deuterium in the liquid metal was between 0.05 and 15 mbar.

It was found, that the transfer of deuterium through a liquid metal/cover gas interface is controlled by diffusion through a liquid metal boundary layer. Only a small temperature dependence was observed (Fig. 4.4-13). The transfer rate was

always proportional to the square root of the partial pressure of deuterium. This boundary layer was also effective for the transfer of deuterium from a gas phase through a Fe-membran into the liquid metal, and from the liquid metal through a membran into the gas phase.

Loading and degassing of the liquid metal with deuterium was always a two step process, having half lives in the range of 0.1 to 1 hours, and in the range of 2 to 60 hours. Always exponential functions were found; 'half lives' are given in this paper instead of time constants. We assume that the faster process reflects deuterium behavior in the liquid metal, while the slower process is connected with deuterium in structural materials.

TRITEX [21] is a pumped ferritic steel loop. All transport processes observed with thermal convection loops could be proved. The half lives for loading and degasssing were found to 0.4 to 2 hours, and 20 to 150 hours. A third time constant appears sometimes in fit functions (using IMSL-routines). So far this is not well understood.

Gettering of deuterium with vanadium

Most of the experiments were done with vanadium. Again thermal convection loops were used [22]. Vanadium is a good getter metal. Deuterium uptake from molten Pb-17Li is shown in Fig. 4.4-14. The rate can be expressed by the function

$$\ln(R) = -14.0 - 2167/T$$

Here the rate is given in (Mol $D_2/m^2 \cdot s \cdot mbar^{0.5}$), T in K. The heat of absorption is -18 kJ/Mol D_2. This function is nearly the same as found for permeation through an iron membran [20]. Again the rate controlling step is diffusion through the liquid metal boundary layer.

The absorption of deuterium is a reversible effect. After loading a V foil for 76 hours at 315°C, 90% of the deuterium was released within 10 hours at 460°C, and 99% within 20 minutes at 850°C. During this degassing there was still Pb-17Li at the surface of V. Degassing was faster than the loading because of a reduced influence of the boundary layer.

Other getter metals

Because the rate controlling step is diffusion through a liquid metal boundary layer, Ti, Zr, Fe and even Mo (quickly saturated) showed the same rate for deuterium uptake as V. However these metals do not fulfill the other requirements to be used as getters [22].

Technical aspects of getters

A first study of technical aspects of getters for tritium extraction was published in 1990 [23]. Generally gettering is possible and only simple facilities are needed. The absorbers will become large under conditions of a self cooled blanket, when used in the main flow (high flow rates), and if the permeation barrier factor is small. However even in this case getters could be advantageous compared to extraction with NaK because of safety aspects.

Influence of oxides

No influence of an oxide layer at the surface of the molten eutectic has been detected. This can be explained by the very low oxygen solubility in Pb-17Li and a porous layer. So far it was however not investigated if oxygen can be transported from the surface to a getter metal.

Transport of helium

The transport of helium and other rare gases from one covergas space to the other in thermal convection loops was investigated at temperatures up to 700°C. The He solubility in the molten eutectic at 1 bar was evaluated to be only in the range of 10^{-6} appm, five orders of magnitude smaller than this of tritium [19,20]. Helium and tritium are formed in the blanket with equal amounts. Tritium will be extracted contineously. Helium will be always supersaturated with the risk of bubble formations. If such bubbles have an impact on blanket operation has to be evaluated.

Evaporation and transport of aerosols

From observations at the facilities, and with some special experiments during studies of the behavior of Po-210, information were obtained about evaporation

rates and transport of aerosols [24]. Evaporation rates of Pb + Li at 400°C in helium were only 10^{-6} (mg/cm²·h). The aerosol concentration at the outlet of experimental facilities was as low as 10^{-9} g/m³ (for comparison: in sodium systems up to 70 g/m³ were observed !). Therefore no aerosol problem will exist with normal blanket operation.

Pb and Li evaporate independent on each other and show different transport and deposition behavior. Usually deposits of evaporated metal contain 40 to 60 at % lithium. However concentrations as low as 0.2 at.% and as high as 98 at.% were also measured. Because of the low total evaporation rate, this will have no influence on blanket operation.

References to section 4.4:

[1]   H.W. SAVAGE, E.L. COMPERE, B. FLEISCHER, W.R. HUNTLEY, R.E. MacPHERSON, and A. TABAODA, "SNAP-8 Corrosion Program", Summary Report, ORNL-3898, Oak Ridge National Laboratory (1965).

[2]   M. HISHIDA, K. SANOKAWA, M. OUCHI, T. TAKIZUHA, S. NEKOYA, M. OGAWA, and K. EMORI, "Versuche zur Reduktion der Wasserstoffpermeation (II)-Calorized Coating Methode" (Übersetzung aus dem Jap.), Japan At. Energy Soc. Japan, Vol. 22(4), p. 251-263, (1980).

[3]   N.P. BHAT, C. ADELHEIM, and H.U. BORGSTEDT, "Oxygen measurements in liquid Pb-17Li eutectic", Fourth Int. Conf. Liquid-Metal Eng. and Techn., Avignon, France, Oct. 17-21, Vol. 3(1988), 623/1-9.

[4]   J. REIMANN and S. MALANG, "A study of tritium separation from LiPb by permeation into Na or NaK and cold trapping", Kernforschungszentrum Karlsruhe, KfK-4105 (Oct. 1986).

[5]   C. SAINT MARTIN, C. LATGE, P. MICHAILLE, and C. LAGUERIE, "Mechanism and kinetics of crystallization of sodium hydride in cold traps", Fourth Int. Conf. Liquid Metal Eng. and Techn., Avignon, France, Oct. 17-21, Vol. 3, (1988), 617/1-10.

[6]   J. REIMANN, "Tritium inventory and recovery for a self-cooled Pb-17Li blanket" to be published in Fusion Engng. & Design.

[7]   L. BÜHLER and J. REIMANN, "Mass transfer at mixed convection in vertical cylinders", VII Symp. Heat & Mass Transfer, Jadwison, Poland, Oct. 23-26 (1989), 57-69.

[8]   J. REIMANN, R. KIRCHNER, M. PFEFF, and D. RACKEL, "Tritium removal from NaK-cold traps: First results on hydride precipitation kinetics", Fourth Top. Meet. Tritium Techn., Albuquerque, USA, Oct. 1991.

[9]   J. REIMANN and H. JOHN, "Tritium separation from Pb-17Li by permeation into NaK and cold trapping: First experiments on hydrogen recovery", Fourth Int. Conf. Liquid Metal Eng. and Techn., Avignon, France, Oct. 17-21, Vol. 3 (1988), 621/1-8.

[10]   C.C. McPHEETERS, S.B. SKLADZIEN, D.J. RAUE, "Experiments on cold-trap regeneration by NaH decomposition", ANL-79-100, Argonne National Laboratory, Argonne, Illinois 60439 (June 1980).

[11]   R.S. FIDLER and A.C. WHITTINGHAM, "A comparison of alternative methods for in-situ sodium cold trap regeneration", Liquid Metal Eng. and Techn., BNES, London (1984), 413-417.

[12]   J. REIMANN, H. JOHN, and S. MALANG, "Tritium separation and recovery from NaK by cold traps: Results on hydrogen recovery from Na and NaK"; Fusion Technology 1988, Elsevier Science Publishers (1989), 1306-1311.

[13]   J. REIMANN, R. KIRCHNER and D. RACKEL, "Tritium recovery from NaK-cold traps: Investigation of hydrogen release kinetics", ISFNT 2, Karlsruhe, Germany, June 2-7, 1991.

[14]   D.K. SZE, P. FINN, R. CLEMMER, J. ANDERSON, J. BARTLIT, Y. NARUSE and H. YOSHIDA", The role of a blanket tritium system on the fusion fuel cycle", Fus. Eng. and Design 10(1989), 203-207.

[15]   H. Gräbner, J. Oschinski and H. Feuerstein, Compatibility of 35 Metals and Alloys with Static Pb-17Li, KfK-report (1991), to be published

[16]   H. Gräbner, H. Feuerstein, J. Oschinski, Compatibility of Metals and
         Alloys in Liquid Pb-17Li at Temperatures up to 650°C, J. Nucl.Mater.
         155-157 (1988) 702

[17]   H. Gräbner, H. Feuerstein and J. Oschinski, Behavior of Titanium and its
         Alloys in Molten Lead and Molten Pb-17Li, Proc. of the 4th International
         Conference on Liquid Metal Engineering and Technology, Vol. 3, p. 524,
         Avignon (France), Oct. 17-21, 1988

[18]   D.L. Smith, Vanadium Base Alloys for Fusion Reactor Applications, A
         Review, J. of Nucl. Materials 135 (1985) 125-139

[19]   H. Feuerstein. H. Gräbner, S. Horn and J. Oschinski, Transport of
         Deuterium and Rare Gases by Flowing Molten Pb-17Li, 4th International
         Conference on Fusion Reactor Materials, Kyoto,Japan, Dec. 4-8. 1989

[20]   H. Feuerstein, H. Gräbner, S. Horn and J. Oschinski, Behavior of
         Deuterium and Rare Gases in Thermal Convection Loops with Molten Pb-
         17Li, Fusion Engineering and Design 13 (1991), to appear

[21]   H. Feuerstein, H. Gräbner, G. Kieser, TRITEX, a Forced Convection Loop
         with Pb-17Li, J. Nucl. Mater. 155-157 (1988) 520

[22]   H. Feuerstein, H. Gräbner and S. Horn, Extraction of Tritium from Molten
         Pb-17Li by Use of Solid Getters, 16. SOFT Conference, London, Sept. 3-7,
         1990

[23]   J. Reimann and H. Feuerstein, Gettering and/or Cold Trapping for
         Tritium from a Self Cooled Pb-17Li Blanket, 16 SOFT Conference,
         London, Sept. 3-7, 1990

[24]   H. Feuerstein, H. Gräbner, J. Oschinski, S. Horn and S. Bender,
         Evaporation of Lead and Lithium from Molten Pb-17Li, Transport of
         Aerosols, ISFNT-2, Karlsruhe 1991, to be published
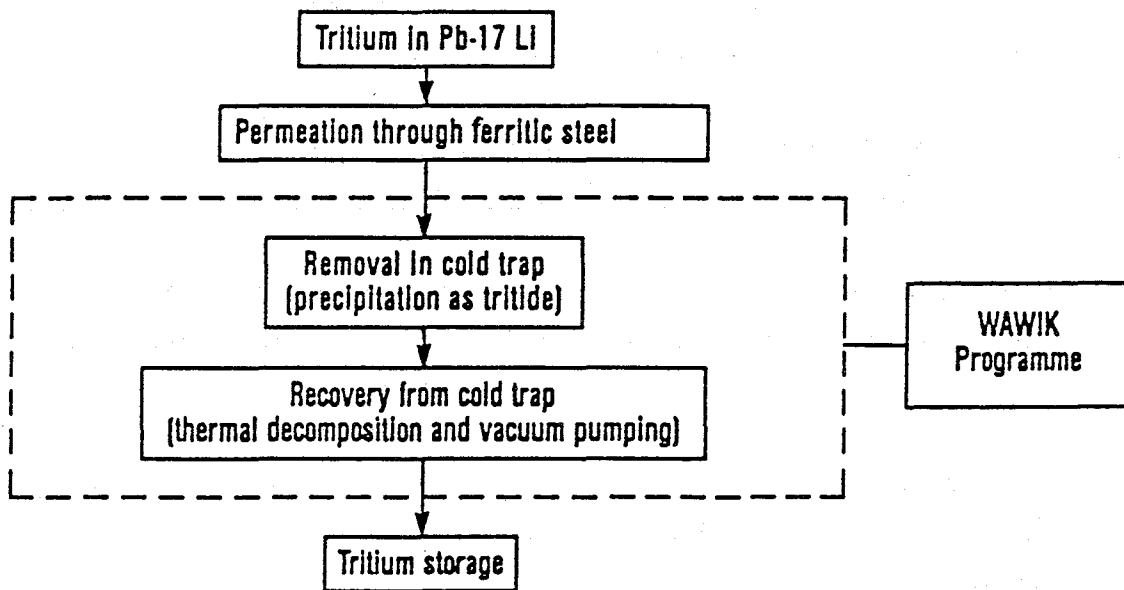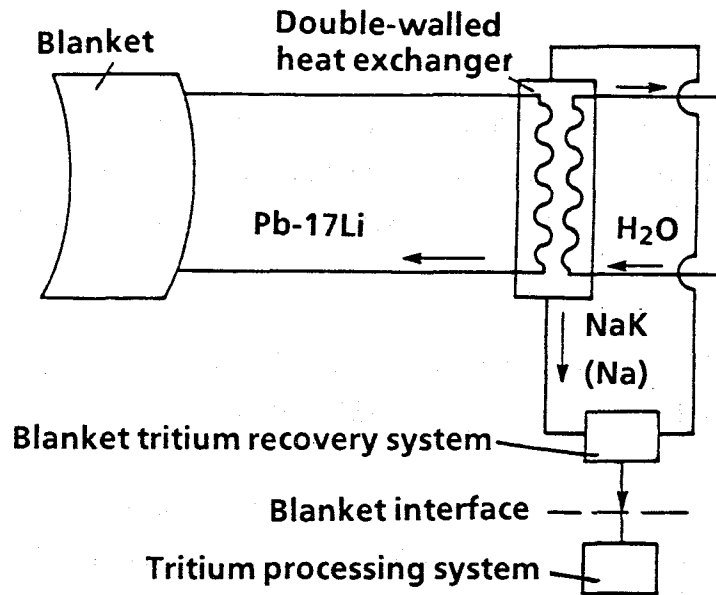
Fig. 4.4-1:   Flow sheet for tritium removal and recovery by cold trapping

$\dot{m}_{NaK+H}$

T_i, c_i

T'

coolant

wire mesh

T_o c_o

tritium partial
pressure $\sqrt{p}$

T_i

T'

ideal
precipitation

real
precipitation

T_o

$c_{o\ sat}$ c_o c_i $c_{i\ sat}$ concentration c
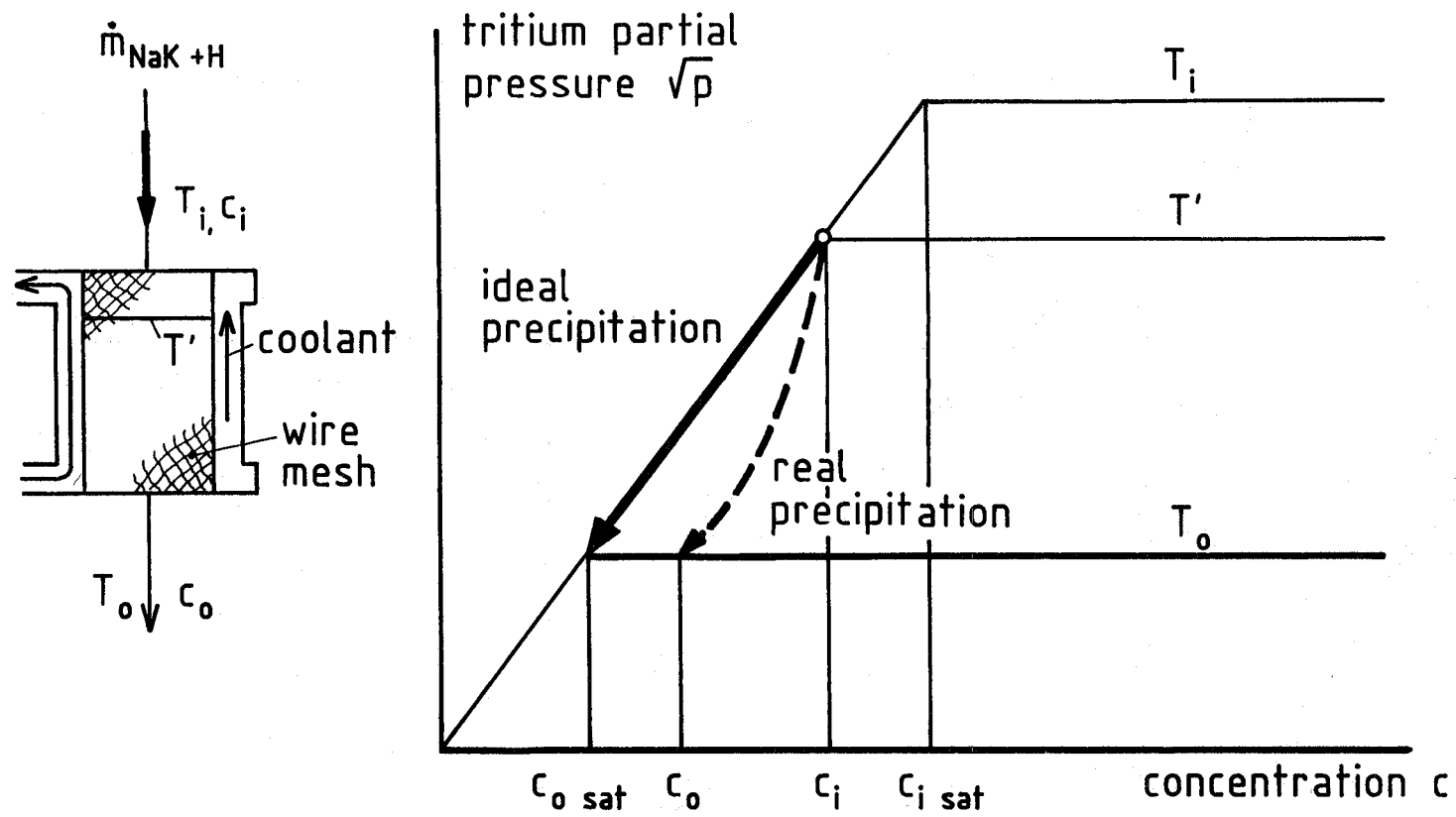
Fig. 4.4-2:   Principle of hydrogen removal by cold trapping
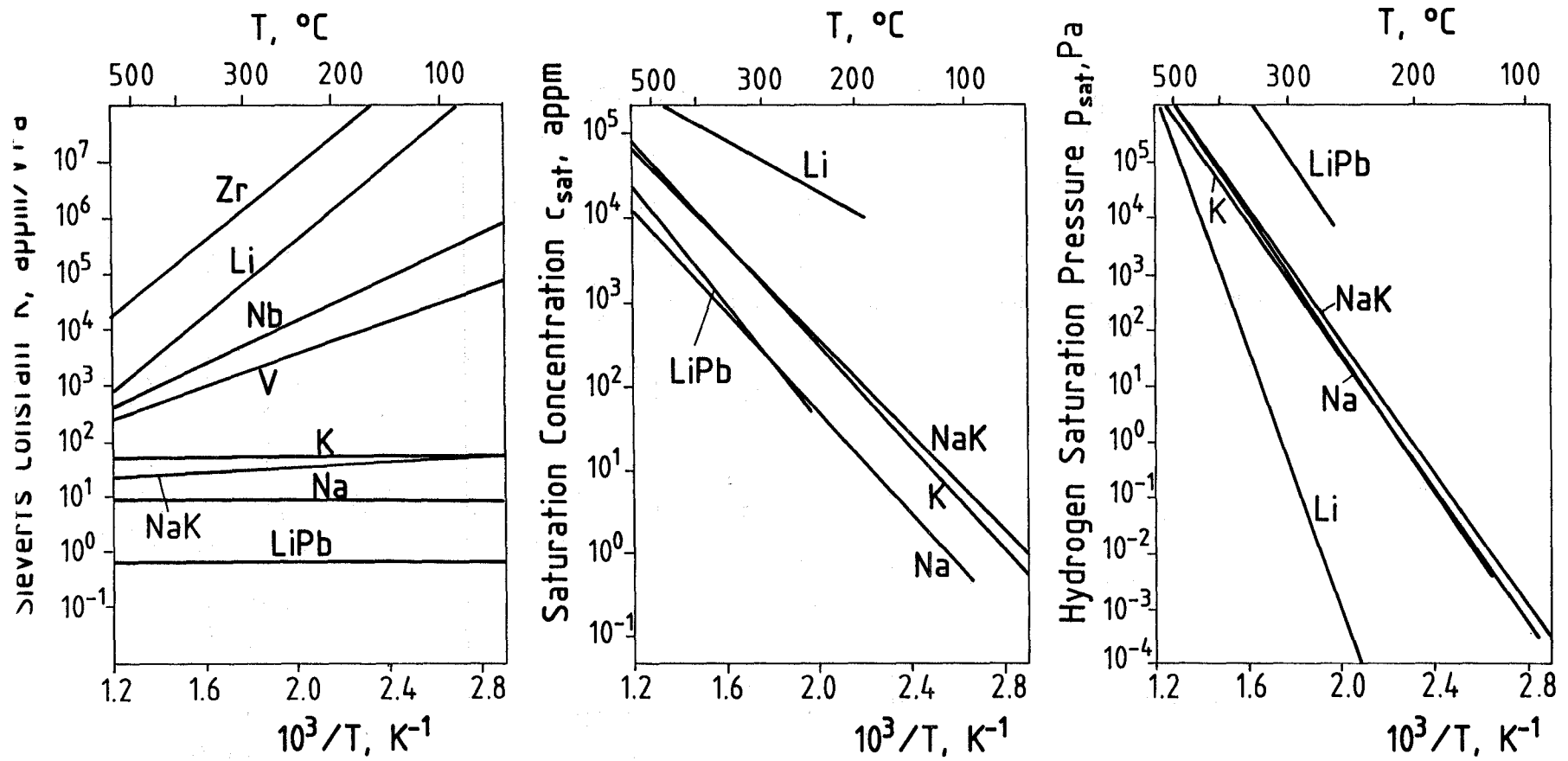
Fig. 4.4-3:   Hydrogen solubility characteristics for different metals
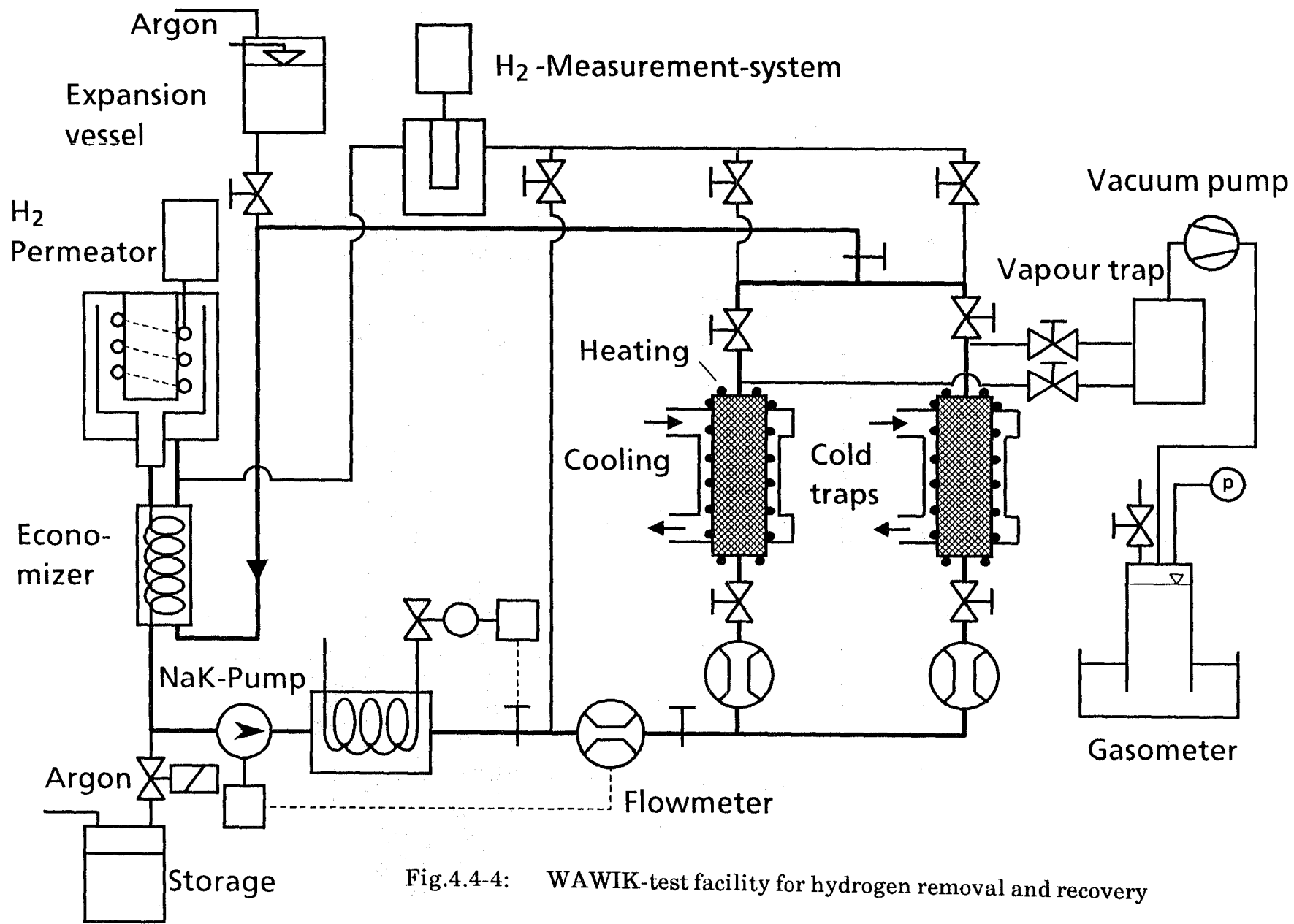
Fig.4.4-4: WAWIK-test facility for hydrogen removal and recovery
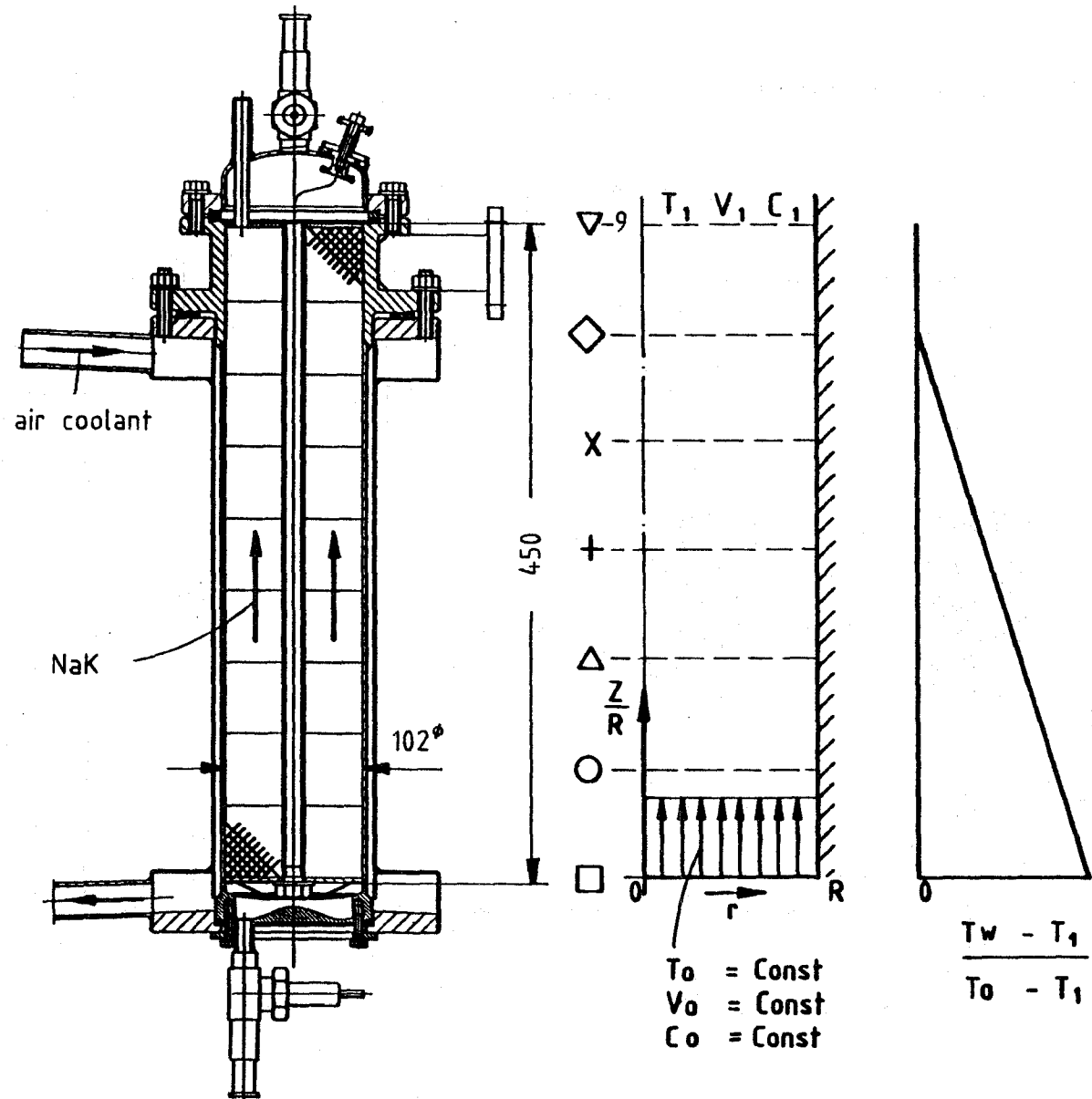
Fig. 4.4-5:   Experimental cold trap and assumption for the calculations

η (%)

100

0

NaK cold trap:

A_{spez} = 980 m²/m³

T_i = 136° C; T_o = 103° C

C_i = 0.73 wppm; C_o = 0.19 wppm

Na cold trap:

A_{spez} = 340 m²/m³

T_i = 185° C; T_o = 150° C

C_i = 0.73 wppm; C_o = 0.20 wppm

$$\eta = \frac{C_i - C_o}{C_i - C_{osat}}$$

0   10   20   30   40   50   t (h)   60
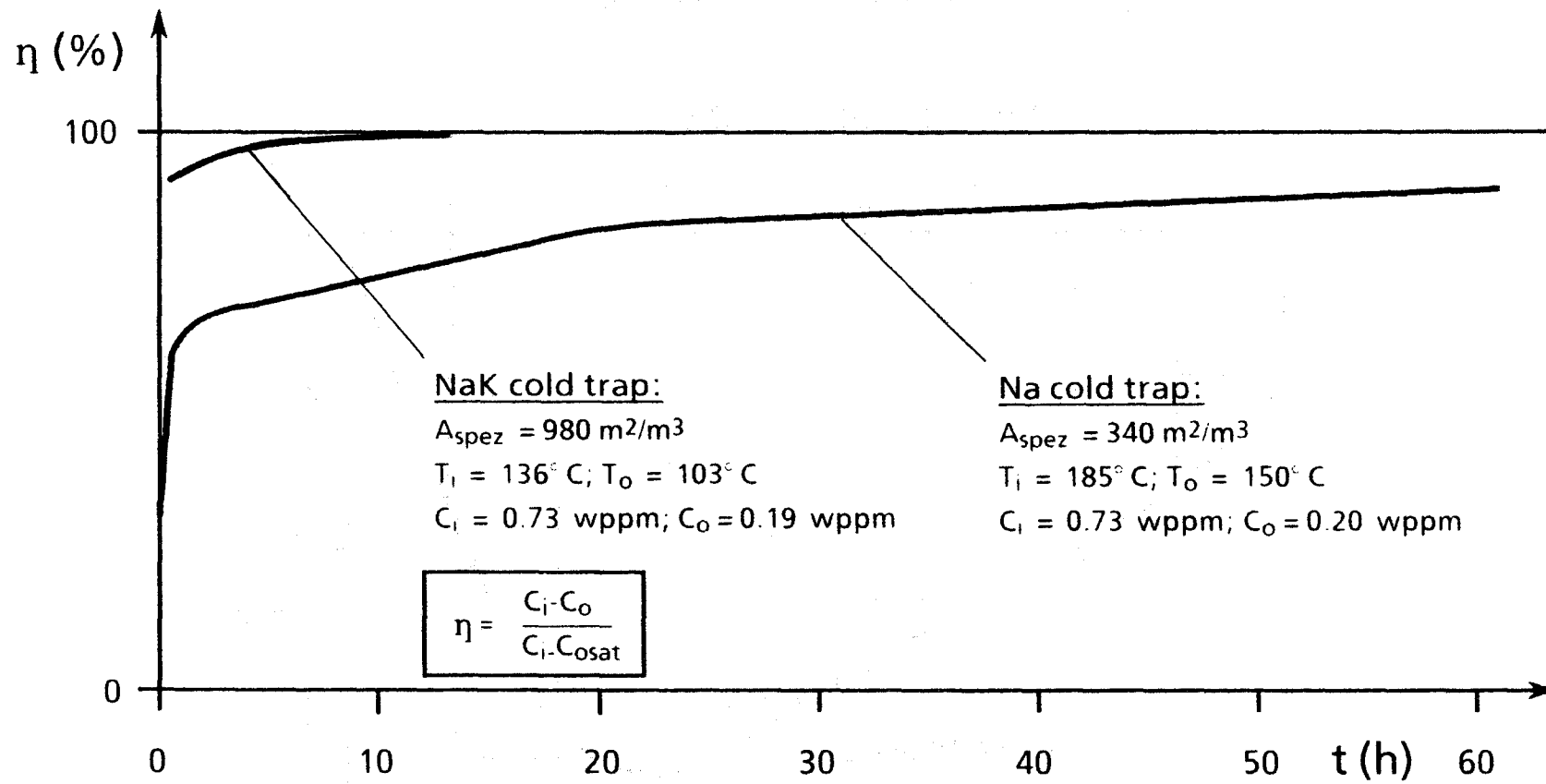
Fig. 4.4-6:   Cold trap efficiency as a function of hydrogen loading time
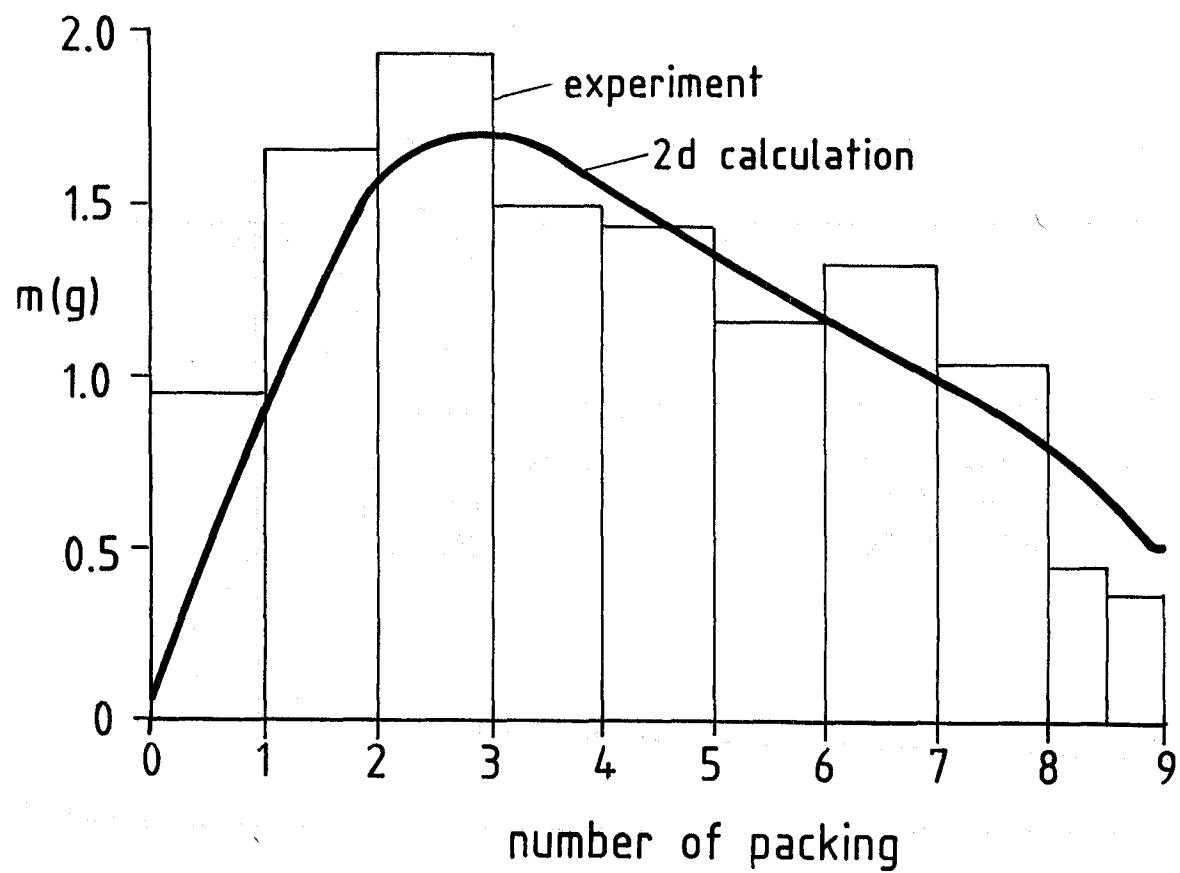
Fig. 4.4-7:   Axial distribution of hydrogen in the cold trap
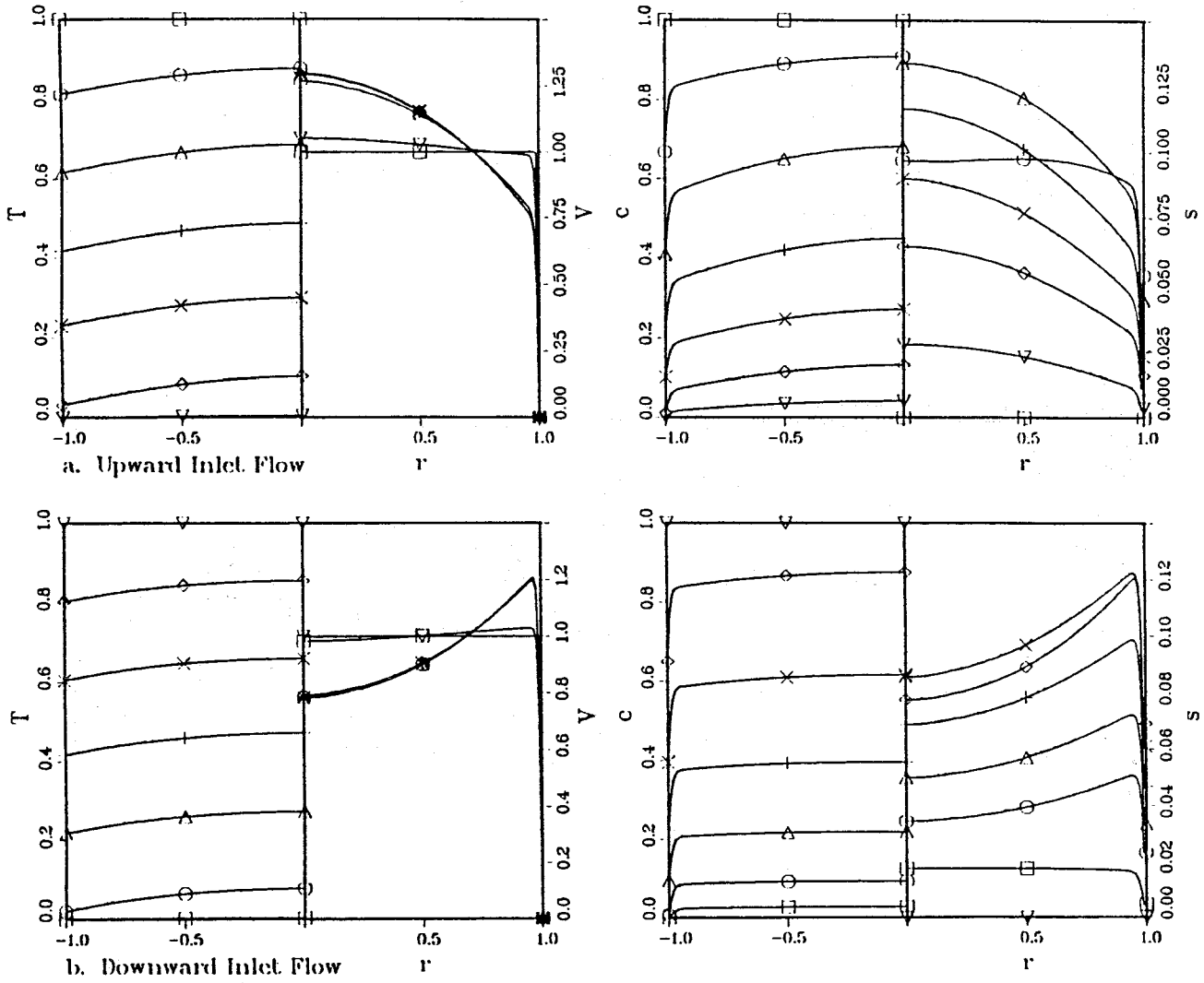
Fig. 4.4-8: Radial distributions of normalized temperature T, velocity v, concentration c and precipitation rate s for different axial locations for the system Na-H
a) upward, b) downward flow

211

Fig. 4.4-9: Radial distributions of T, v, c and s for different axial locations H and axial distribution of cross section averaged distribution S'
(NaK-H-system, upward flow, $T_i = 135$ °C, $T_o = 100$ °C, $v_{NaK} = 4$ mm/s, $A_{spez} = 1050$ m²/m³)
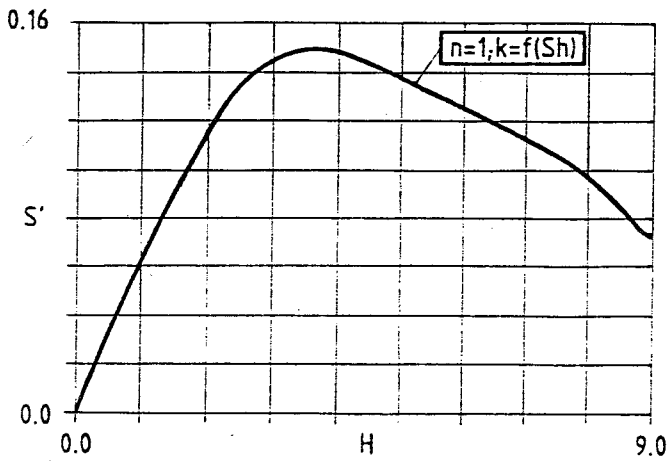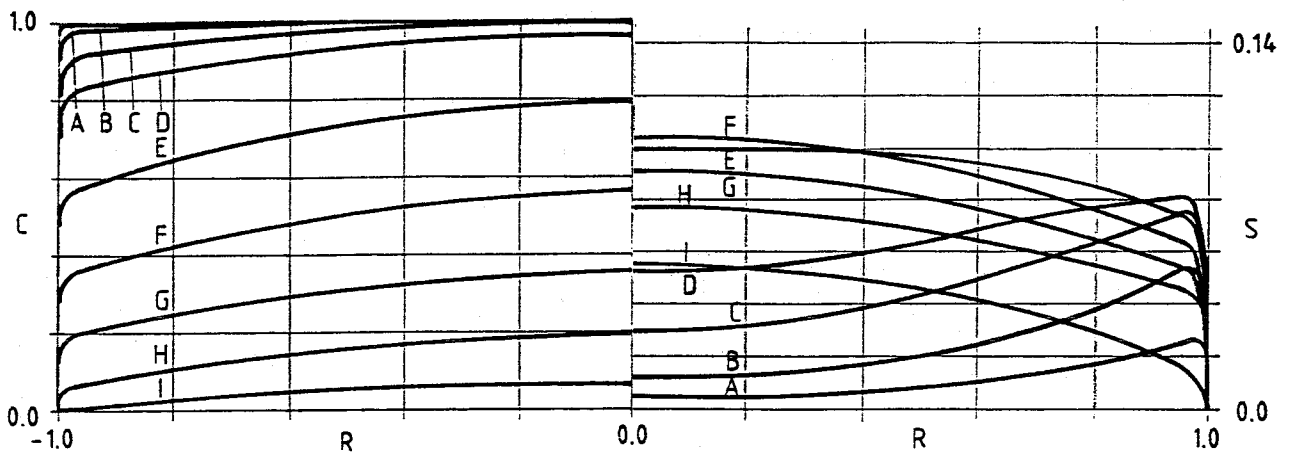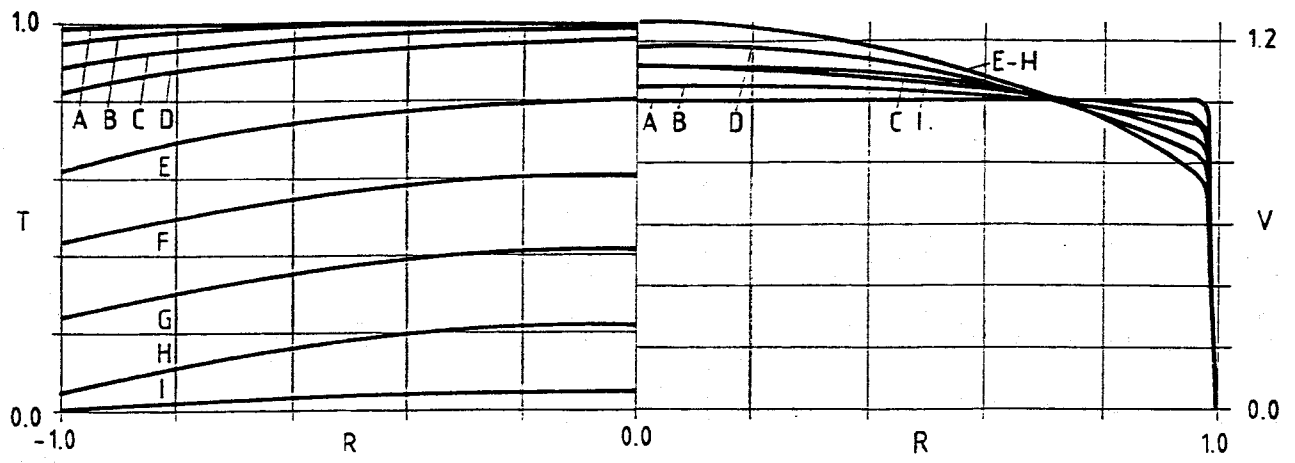
curve	height H
I	9.0
H	7.5
G	6.0
F	4.5
E	3.0
D	1.5
C	1.0
B	0.5
A	0.0

212
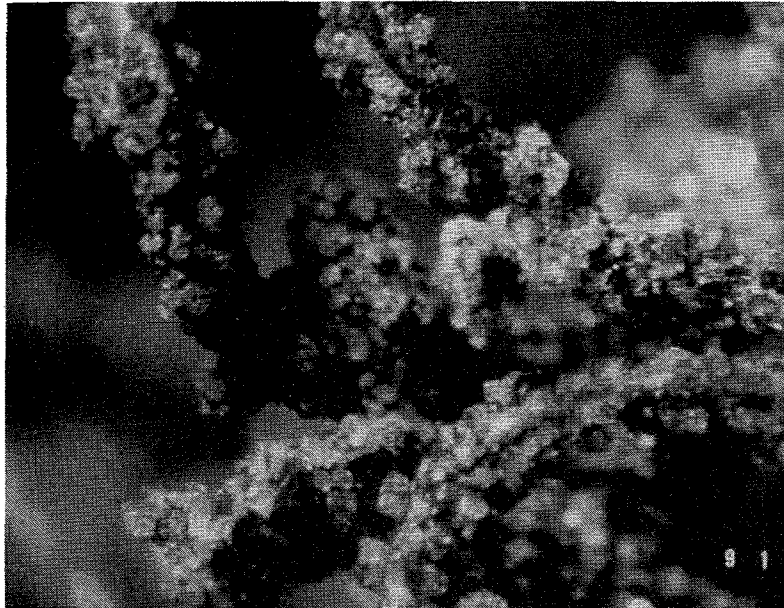
Fig. 4.4-10: Octahedral crystals on wire mesh

T (°C)

400   350   T (°C)   300   280

$k(s^{-1})$

Na-H	--- NaH-particles (+Na$_2$O-particles)
	--·-- NaH-crystals+Na (crystallizer)
NaK-H	--···-- KH-crystals+NaK (crystallizer)
	—— KH-crystals (drained cold trap)

10^{-2}

fine NaH-particles
coarse NaH-particles

$\dot{m} = k\, m$

10^{-3}

10^{-4}

KH-crystals
(crystallizer exps.)

NaH-crystals
(crystallizer exps.)

KH-crystals
(cold trap exps.)

10^{-5}

1.5   1.6   1.7 $10^3/T$(K)
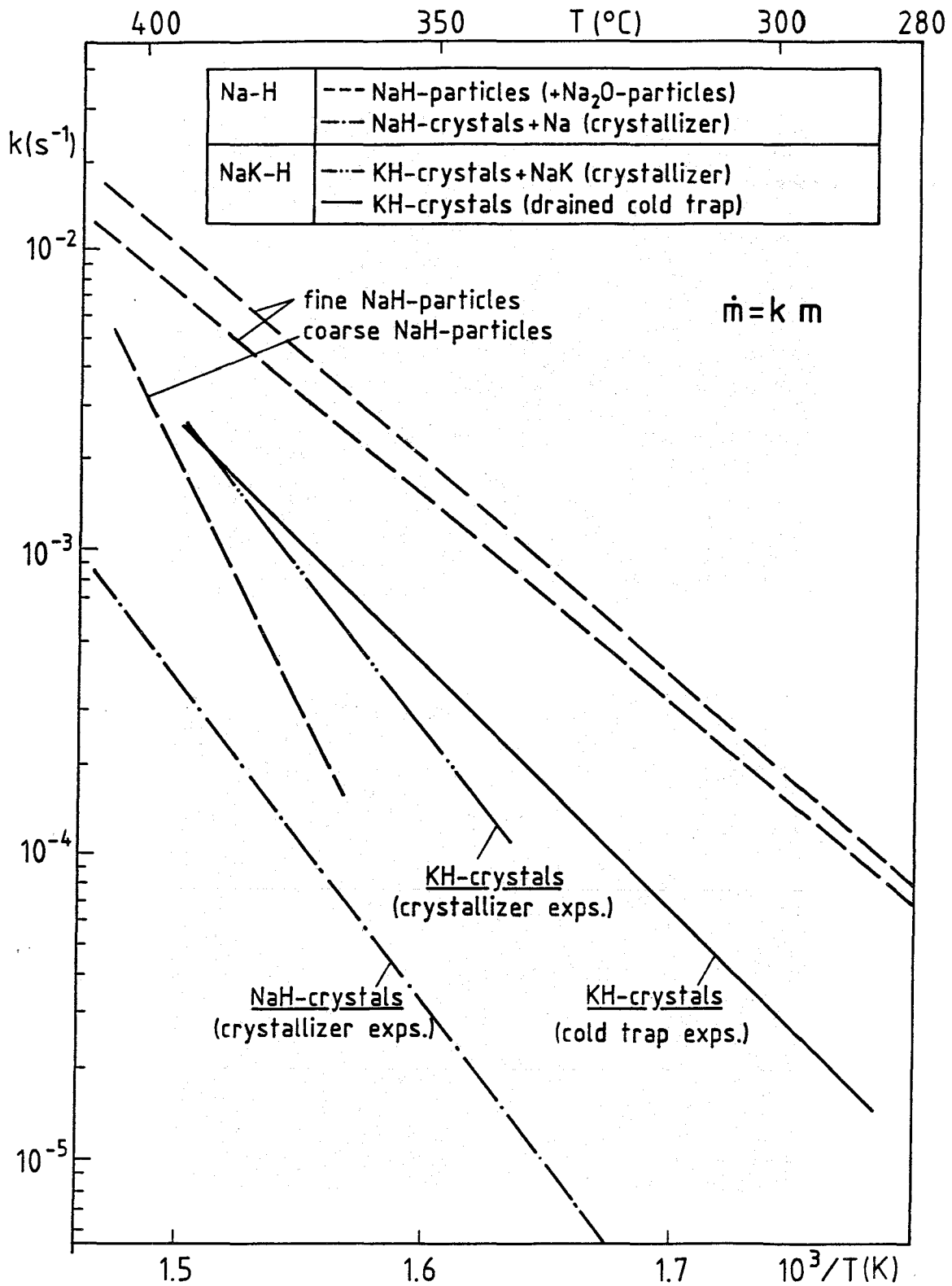
Fig. 4.4-11: Hydrogen release coefficient k as a function of the reziprocal temperature (mean curves)

214
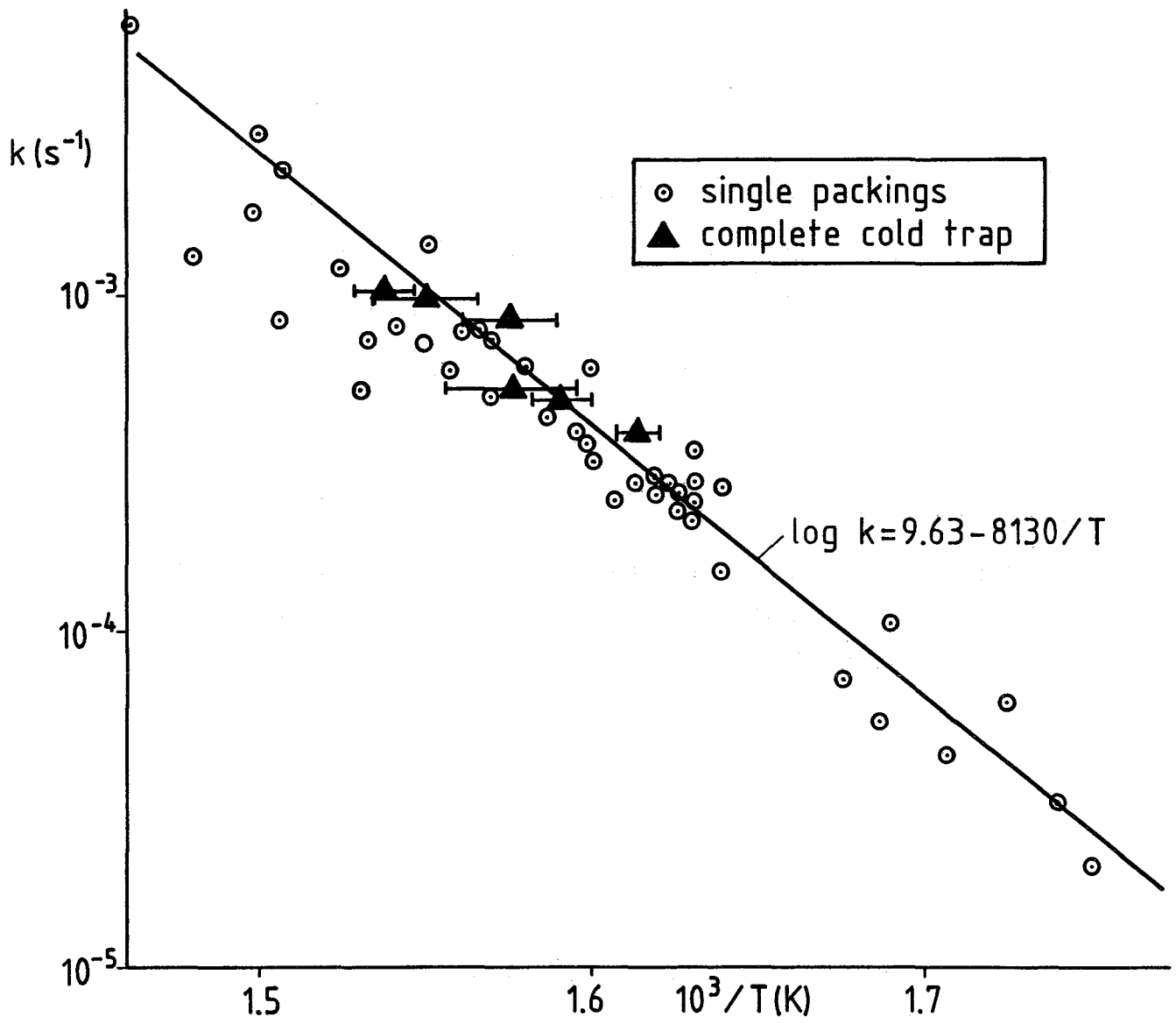
Fig. 4.4-12: Hydrogen release coefficients for NaK cold traps
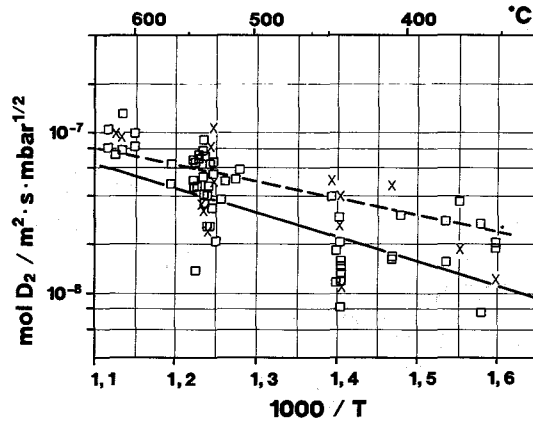
Fig. 4.4-13: Dissolution and desorption rates of deuterium by Pb-17Li.
Dashed line = permeation through a 0.5 mm Fe membran.
Solid line = dissolution and esorption form a gas phase.
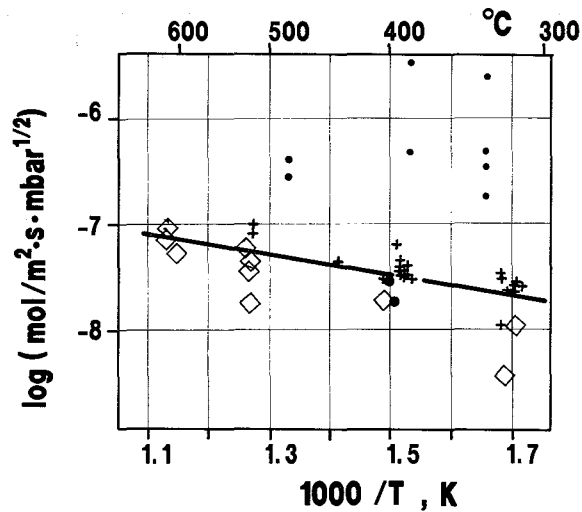
Fig. 4.4-14: Rate of deuterium uptake by vanadium getter from Pb-17Li.
(small dots from measurements without Pb-17Li)

4.5   Compatibility, liquid metal purification
### 4.5.1   Compatibility

The corrosion of the martensitic steel X18 CrMoVNb 12 1 (MANET) in flowing liquid Pb-17Li was studied at 823 and 773 K at a flow velocity of 0.3 m/s and a temperature difference of 240 and 190 K. The cylindrical specimens of 50 mm length and 8 mm diameter were centrally placed in a tube of 14 mm diameter. The test section and the other high-temperature components of the PICOLO loop [1] were fabricated of ferritic steel. The low-temperature components were of austenitic steel, since an electromagnetic pump and flow meter and a magnetic trap for particles were placed in this part. The corrosion effects were determined by means of weighing the specimens and measuring their diameters before and after exposure in PICOLO. Additionally, metallographic studies were performed in order to evaluate the corrosion effects on the bulk of the material.

The measurements of changes of the weight and diameters of the specimens resulted in fairly well agreeing results. All specimens indicated that the steady state corrosion followed a period of initial corrosion. The rates of diameter changes were much slower in this initial phase, they did not exceed one tenth of the steady state reaction rates [2,3]. The losses of diameter are shown in Fig.4.5-1 as a function of time for the two testing temperatures.

The material losses shown in Fig.4.5-1 are mean values which are in fair agreement with the measured weight losses. The changes of diameter are, however, unequal distributed around the cylindrical surface of the specimens. The losses of material measured as changes of the diameter around the specimens scatter by 50% of the average. Thus, maximum corrosion has to be considered as 50% larger than the value indicated in Fig.4.5-1. Furthermore, a small degree of local scatter of material losses is due to the structure of the martensitic material. Material between the bundles of martensite needles seems to be preferentially dissolved.

The metallographic examinations do not indicate any selective corrosion of one of the alloying elements, since the surface layers show the same microstructure as the bulk of the specimens. The corrosion in flowing Pb-17Li does not create any grain boundary grooving. The leaching of minor alloying elements as carbon has not yet been detected. The surfaces of the specimens have a metallic appearance, oxide layers do not cover the solid material.

The steady state corrosion rates are calculated as $r_1 = 0.13$ [mm/a] at 773 K and $r_2 = 0.91$ [mm/a] at 823 K. The temperature dependence of the rate constants can be expressed by an Arrhenius law. The rate constants r_n of the linear corrosion equation

$$\Delta R = r_n \cdot t$$

are related to the hydraulic parameters of the test section of the loop. It can be calculated on the basis of the relation $r_n = \beta(x_s - x_0)$, in which β is the mass transfer coefficient and x_s the saturation concentration of the material in Pb-17Li, x_0 its concentration in the bulk flow of liquid metal. x_0 is small compared to x_s and can be neglected [3].

The mass transfer coefficient is related to hydraulic parameters according to the equation [Gleichung:beta] $= (Sh \cdot D)/d$ with Sh as SHERWOOD number, D as diffusion coefficient (of iron in Pb-17Li) and d as hydraulic diameter of the test section. For developed turbulent flow, Sh can be calculated from the simplified equation $Sh = 0.037 \cdot Re^{0.75} \cdot Sc^{0.42} \cdot 1.3$. Re is the REYNOLDS number of the tests section for the given flow velocity, $Re = (v \cdot d)/v$ (v is the kinematic viscosity of the liquid metal). The value of Sc is received from $Sc = v/D$. The rate constants r_n are calculated based on the data taken from tables for the liquid metal and calculated for the dimensions of the loop and the parameters of tests. We receive $r_1 = 0.37$ [mm/a] at 773 k and $r_2 = 1.47$ [mm/a] at 823, in good agreement with the measured values.

The agreement of measured corrosion rates with values calculated on the basis of the hydraulic model indicates that the corrosion mechanism is a dissolution of the solid metal in the liquid metal, and a precipitation of the dissolved material in the low temperature branch of the loop. The metallic nature of the precipitates in the magnetic trap is the second argument for the mechanism of metallic dissolution [4,5].

The hydraulic model can be applied to calculate the corrosion in flow channels (with turbulent flow) of the blanket for which the hydraulic parameters are known. For example, the corrosion in a channel of a cross section of 9 cm^2 in which the liquid alloy flows with a rate of 2 [m/s] at a temperature of 400°C was calculated as $r = -0.055$ [mm/a]. This corrosion rate is significantly higher than rates which are measured at 400°C in corrosion loops with small tubes and low flow velocities. The model can also be applied to the liquid metal flow in the blanket. It

has, however, to be taken into account that the magnetic field suppresses the turbulence and causes the formation of a thin boundary layer.

The very low concentration of oxygen in Pb-17Li and its comparably high chemical activity [6-8] support the assumption of the mechanism based on the dissolution of metals, since the formation of complex oxides as in the case of sodium corrosion is unlikely under these conditions. The formation of nitrides as in liquid lithium seems also to be not favoured due to low solubility and instability of compounds under these conditions. On the other hand, the solubility of metals is higher than in the alkali metals [7].

The chemical activity of oxygen in Pb-17Li is favourable for the chemical stability of several oxides which may be used as electrical insulating layers. While Al_2O_3 is not stable against liquid lithium and reacts thoroughly at temperatures above 350°C [9], it should be compatible with Pb-17Li at moderately elevated temperatures. The verification of this assumption by means of experimental studies is still open.

The influence of the eutectic alloy Pb-17Li on the mechanical properties of the MANET steel was studied in stagnant medium. The creep-rupture behaviour at 500°C did not show a significant influence of the environment. At a temperature of 550°C and above the corrosion influences the creep life of the steel at higher levels of stresses. Very low stresses do not seem to superimpose with the corrosive action of the liquid metal [5,10-12]. The influence of Pb-17Li on the creep-rupture life of MANET steel at 550°C is shown in Fig. 4.5-2.

There was no apparent influence of the liquid alloy in tests of short duration, as was seen in some low-cycle fatigue and tensile tests. The tensile tests clearly demonstrated that there was no tendency for a liquid metal embrittlement in the system MANET steel - Pb-17Li at temperatures in the range 250 to 300°C [12].

4.5.2   Purification

The development of purification methods for Pb-17Li has just started. Three kinds of impurities are of special concern.

Impurities undergoing mass transfer will be mainly studied in the facility TRI-TEX. First results were obtained also from thermal convection loops. It was found that particles from different parts of the loop had different composition. Most amazing was an intermetallic phase between Mn and Ni, inspite of low Mn concentration in the Pb-17Li. Particles of this were found in the coldest area of the cold spot. The results were not published so far, but reported during an international workshop at Nottingham in 1990.

Radioactive impurities are often in very low concentrations, some even as tracers. Po-210 is alway in tracer concentrations. In sodium cooled reactors such impurities show different behavior than expected from larger concentrations [13,14]. The investigation of the behavior of Po-210 is under way [15]. It was found that Po-210 is enriched in oxide layers, but it is not clear so far if Po-210 can be separated completely from the Pb-17Li by oxidation. Currently a study of the volatility of Po-210 from the molten eutectic has started.

The third kind of impurities are interstitial elements of the steels. Will there be a transport of carbon and other elements in Pb-17Li as known from sodium systems, and will such elements have an impact on blanket operation?

So far in all observations never any influence was seen of oxide layers on results, neither on deuterium behavior nor in compatibility tests. Like in sodium systems methan was seen in TRITEX covergas at higher temperatures. Probably some residues of lubricants had reacted with Pb-17Li. Oxides from thermal convection loops contained some elemental carbon.

References to section 4.5:

[1]   G. Frees, G. Drechsler, Z. Peric, Dynamische Korrosionsuntersuchungen in der eutektischen Blei - Lithiumschmelze Pb-17Li, Werkstoffe und Korrosion 40 (1989) 593-598

[2]   Z. Peric, G. Drechsler, G. Frees, H.U. Borgstedt, The corrosion of steels in liquid Pb-17Li alloy. 4th Internat. Conf.on Liquid Metal Engineering and Technology, Avignon, France, Oct. 17-21, 1988, Vol 2, paper 511

[3] H.U. Borgstedt, H.D. Roehrig, Recent results on corrosion behaviour of MA-NET structural steel in flowing Pb-17Li eutectic. 4th Internat. Conf. on Fusion Reactor Materials, Kyoto, J., Dec. 4-8, 1989; J. Nucl. Mater. 179 (1991) 596-598

[4] H.U. Borgstedt, Corrosion of Austenitic Stainless Steel in Liquid Metals. 11th Intern. Corrosion Conf., Florence, 2-6 April 1990, Proceedings, Vol. 4, 186/191

[5] H.U. Borgstedt, G. Frees, M. Grundmann, Z. Peric, Corrosion and Mechanical Properties of the Martensitic Steel X18CrMoVNb 12 1 in Flowing Pb-17Li, Fusion Engng. Design 14 (1991) 329-334.

[6] N.P. Bhat, Ch. Adelhelm, H.U. Borgstedt, Oxygen measurement in liquid Pb-17Li eutectic. 4th Internat. Conf. on Liquid Metal Engineering and Technology, Avignon, France, Oct. 17-21, 1988; Proc. Vol. 3, paper 623

[7] H.U. Borgstedt, Chemische Eigenschaften des flüssigen Blanketstoffs Pb-17Li, KfK - Bericht 4620, Aug.1989

[8] Ch. Adelhelm, H.U. Borgstedt, Löslichkeit und Bestimmung von Sauerstoff in der eutektischen Schmelze Pb-17Li. Nichtmetalle in Metallen, Münster, 14-16 March 1990; Nichtmetalle in Metallen '90, Ed. D. Hirschfeld, DGM Informationsgesellschaft - Verlag, Oberursel 1990, 17-22

[9] J. Konys, H.U. Borgstedt, The product of the reaction of alumina with lithium metal. J. Nucl. Mater. 131 [1985] 158-161

[10] H.U. Borgstedt, M. Grundmann, The Influence of Liquid Pb-17Li Eutectic on the Mechanical Properties of Structural Materials, Fusion Engineering and Design 6, (1988) 155-158

[11] M. Grundmann, H.U. Borgstedt, M. Schirra, The creep-rupture behaviour of the martensitic steel X18 CrMoVNb 12 1 (Werkstoff-Nr. 1.4914) in liquid Pb-17Li at 550 and 600 °C, 4th Internat. Conf. on Liquid Metal Engineering and Technology, Avignon, France, Oct. 17-21, 1988; Proc. Vol 2, paper 510

[12] M. Grundmann, Strukturmechanische Untersuchungen am 12% Cr-Stahl

X18CrMoVNb 12 1 (1.4914) im flüssigen Pb-17Li Eutektikum, Bericht KfK 4703, Kernforschungszentrum Karlsruhe 1990

[13] H. Feuerstein, A.J. Hooper and F.A. Johnson, Mechanism of release of radioactive products into liquid metal coolants, Atomic Energy Review 17, 3 (1979)

[14] H. Feuerstein and A.W. Thorley, IAEA-IWGFR Specialists' meeting on Fission and Corrosion Product Behavior in Primary Circuits of LMFBRs.KfK-4279/IWGFR-64 (1987) .

[15] H. Feuerstein and J. Oschinski, Behavior of Po-210 in molten Pb-17Li. To be presented at the Fifth International Conference on Fusion Reactor Materials, ICFRM-5, Nov. 17-22, 1991, Clearwater, Florida, USA
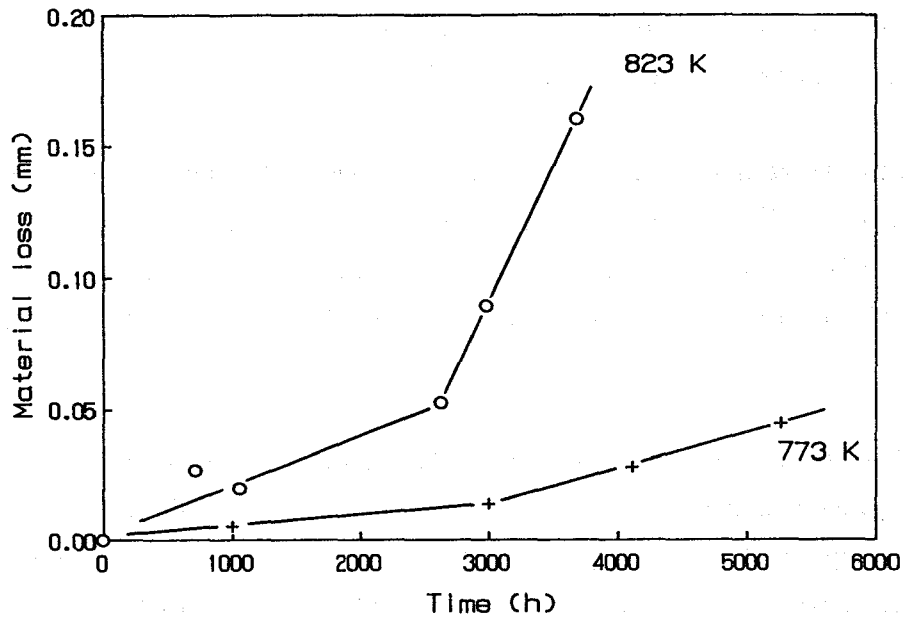
Fig. 4.5-1: Material losses of MANET steel in the PICOLO loop at 773 and 823 K
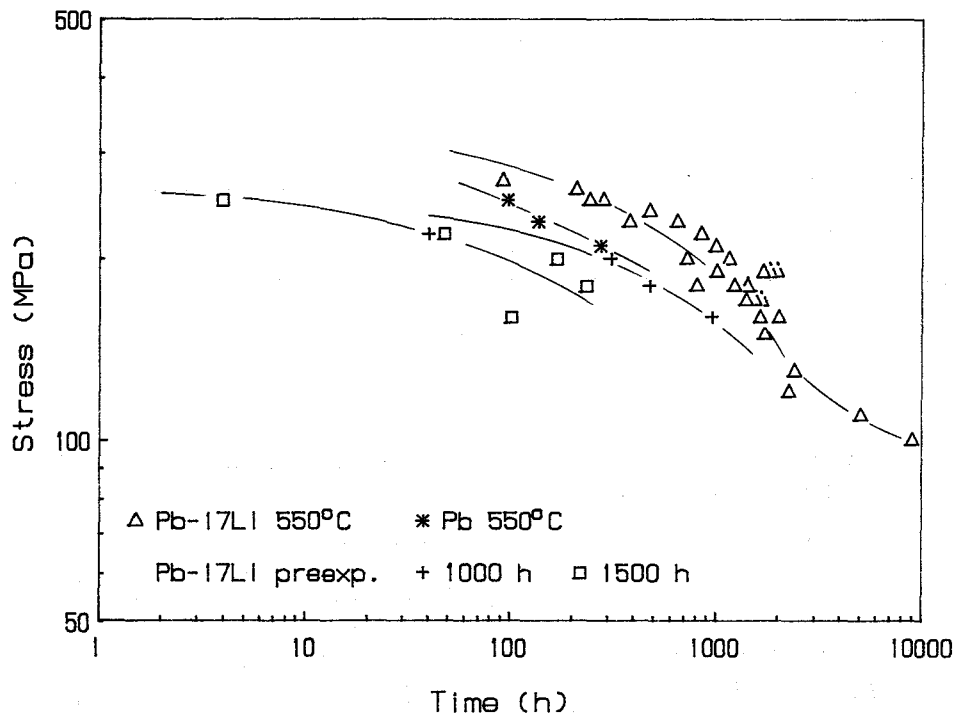
Fig. 4.5-2: Creep-rupture life of MANET steel in Pb-17Li at 550°C

4.6 Ancillary loop system, components
4.6.1 Main heat exchanger (Pb-17Li, NaK, H₂O) study

The first concept of a PbLi-heated steam generator for DEMO was based on a straight double-wall-tube design with NaK flowing slowly inside the gap between the two concentric tubes. In order to provide a more profound basis for that design, alternative steam generator designs with and without double-wall tubes were investigated [1].

Designs without double-wall tubes were soon eliminated mainly because they require a complete secondary liquid metal loop and investigations showed too the necessarily large NaK inventory in the steam generator combined with a high tritium content, a great disadvantage compared to the double-wall design.

Steam generator designs with double-wall tubes which were considered in more detail, can roughly be divided into the following categories according to their tube designs

- Bajonet tubes
- Tubes with a 90° elbow (J Tubes)
- Tubes with a 180° elbow (U-tubes)
- Helical tubes

Table 4.6-1 summarizes basic data of these designs in comparison to the straight-tube steam generator.
The dimensions in the table are basing in contrast to the actual design of 40 MW on 52 MW, which was previously investigated.

Table 4.6-1   Comparison of Double-Wall Steam Generator Designs (52 MW) (water inside inner tubes)

	Straight Tube	Bajonet Tube	J-Tube	U-Tube	Helical Tube
Number of Tubes	331				63
Height [m]	21	20-25	22	12-14	14
Vessel diam. [m]	1	1.5-2	1	2-3	1.6
PbLi volume [m³]	8	10-12	10	10-12	13.5
NaK volume [m³]	1.1	1.5-2	1.5	1.4	0.8

Among these variations only the helical-tube design seems to be a promising alternative solution to the straight-tube design. In particular it offers a smaller construction height and the possibility to identify faulty outer tubes, too, a problem which can hardly be solved in the straight-tube steam generator. Two design options of a helical-tube steam generator were considered, PbLi inside the inner tubes and H_2O in the vessel and vice versa. A common design feature is the individual penetration of double-wall tubes from the tube bundle through the steam generator vessel wall and the outside separation of H_2O or PbLi and NaK-tubes thus avoiding tube plates (Fig. 4.6-2). The H_2O-inside-inner-tube option (Fig. 4.6-1) seems more favourable due to the lower number of double-wall tubes resulting in less welds and wall penetrations. Fabrication possibilities and consequenses of possible NaK-H_2O-reactions were investigated in comparison to the straight-tube steam generator. With respect to fabrication, the helical-tube steam generator will be feasible, but although very costly to fabricate.

Helical-tube designs will eliminate NaK collectors between two tube plates. Therefore significant possibilities of NaK-H_2O-reactions will be eliminated and special structures to avoid consequential damages in adjacent tubes are not necessary. With respect to detection of NaK-H_2O-reactions, there are no differences to be seen in comparison with straight-tube steam generator.

However, mainly due to the very cost-intensive fabrication of the helical-tube design, the straight-tube double-wall steam generator is considered as the reference version and the helical-tube design as a realistic alternative approach.

4.6.2   DEMO steam generator accident study (NaK-H_2O-reactions)

If NaK comes into contact with water/steam it will react under formation of hydroxides, oxides and gaseous hydrogen at a high temperature level. Consequences of such a NaK-H_2O-reaction mainly depend on the leak rate and on the geometrical conditions in the leak area.

In case of small leaks (H_2O-leak rate some g/s) and a sufficient free volume of NaK a so-called reaction flame will be formed. Due to the high temperatures and the high velocities of hydroxide-particles neighboured tubes may be damaged in relatively short times by an effect called wastage; the accident is escalating. To minimise the escalation of a wastage, several design precautions can be taken, as these

are: protection sleeves around the inner tubes in the NaK collector area, reliable detection systems, adequate design of the liquid metal system. But nevertheless the definition of a design basis accident and the consequences is necessary.

In the following is described the:

Definition of the Design Basis Accident (DBA):

The definition of DBA's of liquid metal heated steam generators depends upon which types of leak escalation have to be covered within the design. The leak-before-break criterion cannot be claimed for small heat exchanger tubes. So at least the sudden guillotine rupture of a tube has to be taken into account.

DEMO-steam generators exclude by design the possibility of a simultaneously multi-tube rupture during a NaK-H_2O reaction due to the double-wall concept and additional wastage protection tubes in the NaK collector area (Fig. 4.6-3). Therefore, the DBA for this type of steam generator is the assumption of a sudden guillotine fracture of one tube.

Pressure Load Calculations:

Pressure load calculations have been performed with the ROLAST code with the following adaptions to DEMO-conditions:

Due to the wastage protection over the whole length of the tubes (Fig. 4.6-3) the water leak rate is not given by the cross-section of both open ends of the broken tube but limited by the cross-section of the bores located at the end of the tubes (to allow NaK flow in the gap of the double-wall tubes). For the calculation four bores with 5 mm in diameter have been presumed (plus a 0.5 mm gap between the wastage protection tube and the sliding plate). Water conditions are: $T_{H_2O} = 250°C$, $P_{H_2O} = 70$ bar.

Additionaly assumptions had to be made to modelize the NaK-system. Pipe length, heat exchanger, cold trap and expansion tank dimensions had been deduced from comparable liquid metal loops; changes have only minor influence on the pressure build-up.

A simplified flow scheme and the pressure development at different points of the NaK system is shown in Fig. 4.6-4. The rapid pressure increase in the reaction zone (outlet of the gaps at the wastage protection plate) is mainly due to the small volume of the NaK collector area. This high pressure transient provokes pressure waves with maximum values at about 100 bar (heat exchanger and cold trap). Because the NaK system is designed for this pressure and no depressurization of the NaK system via bursting discs has taken into account, the overall pressure reaches after about 3 s the water side pressure of 70 bar and the water leak flow is stopped.

4.6.3 Pipe concept

For the PbLi-piping system a design can be chosen similar to that of liquid metal cooled fission reactors. The main pipes for the DEMO blanket cooling system of DN 400 nominal diameter for the present design are equipped with trace heating, leak detection and thermal insulation (200 mm). The trace heating system is an electrical heating system with wires around the pipe.

A local leak detection system by short circuit measuring was selected as reference concept. The reference leak detection system consists of an electric conductor enclosed in a woven ceramic tube.

Due to the large specific weight of PbLi, special attention has to be paid to support concepts. Taking into account static and dynamic loads, a maximum distance of 6 m between supports of horizontal piping was calculated. The calculations also showed that most of the pipe clamps for static load dissipation (hangers) may be combined with dynamic load dissipation (shock absorbers or pendulum supports). Fixed points, hangers or plain bearings were investigated and found to be feasible as supports.

4.6.4 Main circulation pump

A single-stage, single-flow radial centrifugal pump is proposed as reference concept for the main PbLi circulation pump. It has a free surface with helium as cover gas. The PbLi-pump is arranged in the cold leg of the PbLi-loop providing a pressure increase from about 18 bar to approx. 50 bar. The design mass flow rate amounts to approx. 1700 kg/s corresponding to 40 MW per loop. The bottom of the vertical pump shaft is borne in a hydrostatic bearing with PbLi as working sub-

stance. A conventional axial/radial roller bearing is used at the shaft top. The cover gas sealing to the outside is performed by means of two mechanical shaft seals. It may be necessary to improve the sealing concept due to possible tritium contamination of the oil lubricant and the detritiation of cover gas containing oil impurities.

Reference to section 4.6:

[1]   INTERATOM, contract for development of the cooling circuits for the liquid metal cooled blanket, Kernforschungszentrum 1990, unpublished.

228
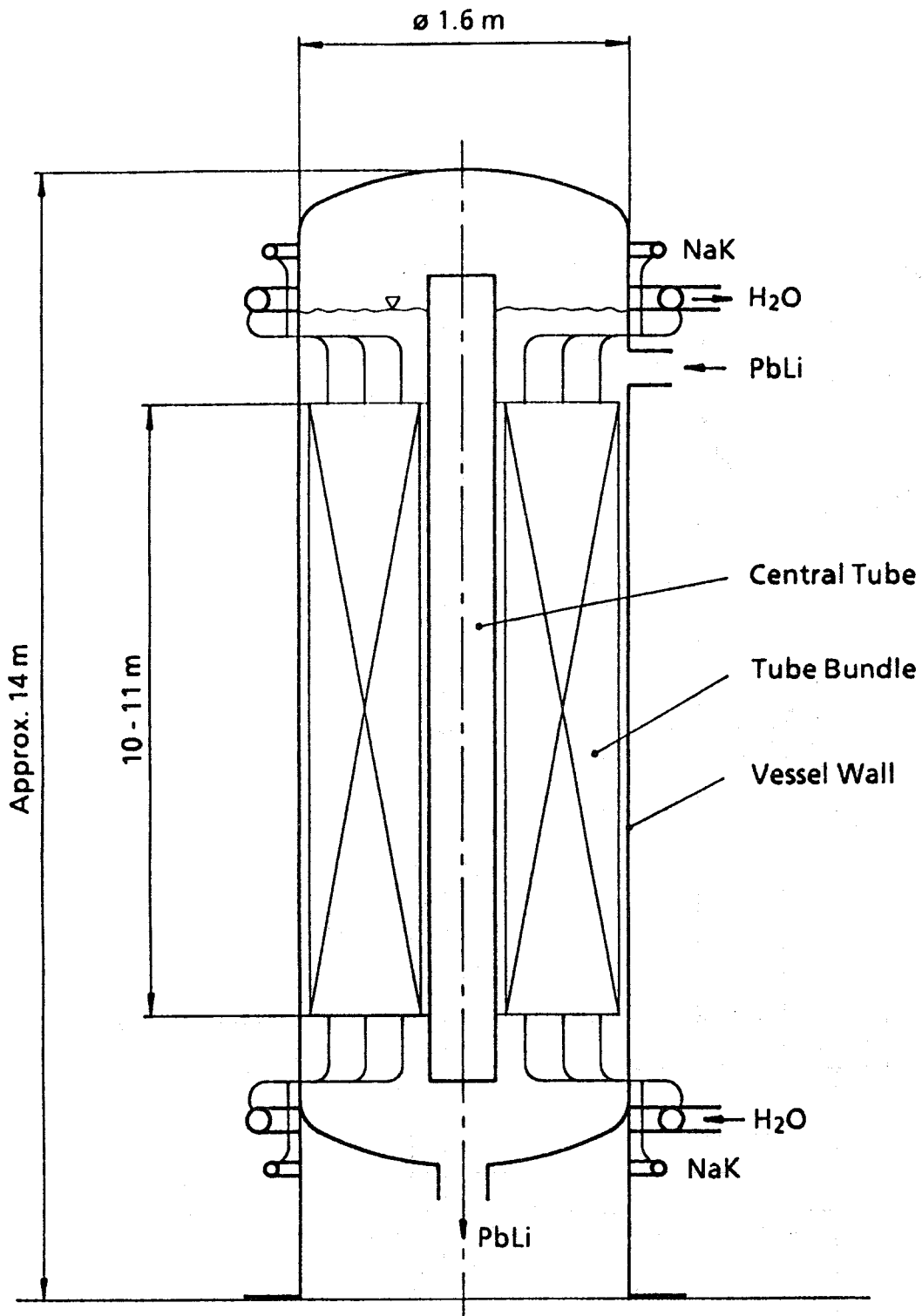
Fig. 4.6-1   Steam generator for DEMO. Helical double-wall tubes (H_2O inside inner tubes)

Ø ca.2,1m

Ø1950

30

H₂O

H₂O

NaK

PbLi

16x1,8mm

34x2mm

Air

40x2mm

34x2mm
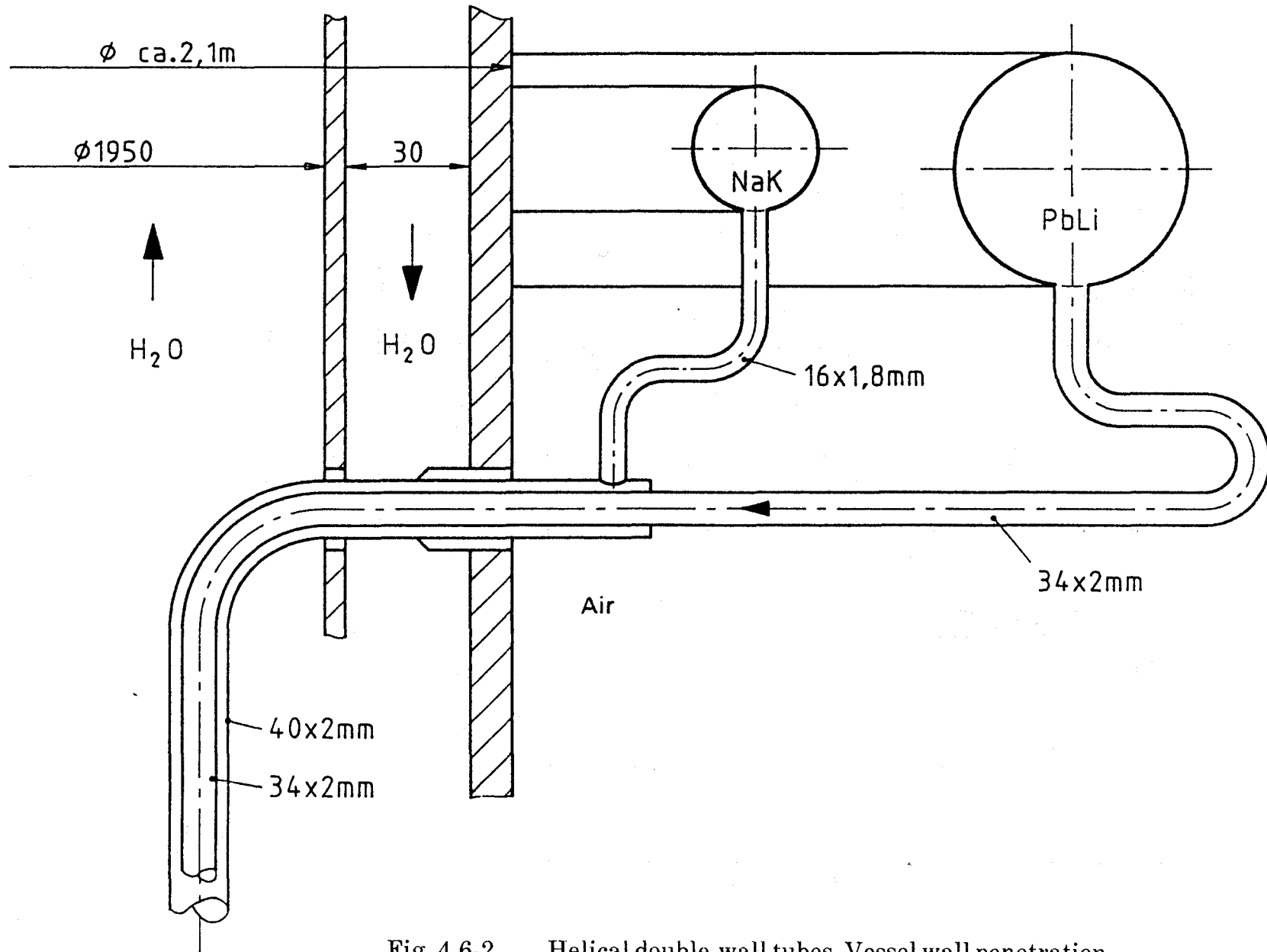
Fig. 4.6-2   Helical double-wall tubes. Vessel wall penetration

PbLi

Thermal
Schock-plate

PbLi/NaK -
Tubeplate

Sliding-
plate

Wastage
protection
tube   (31 x 2mm)

NaK

Bores

Wastage
protection
plate

NaK/H_2O -
Tubeplate

H_2O
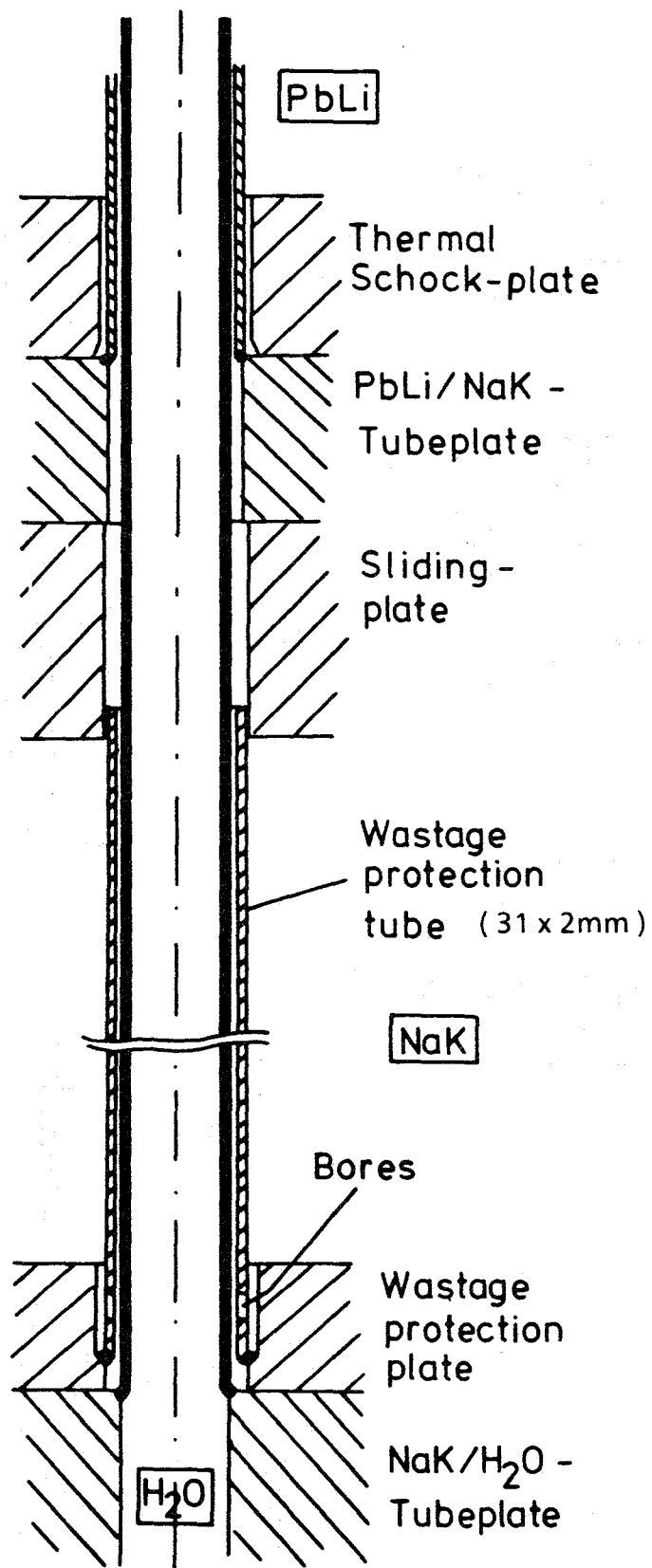
Fig. 4.6-3   Wastage protection tube
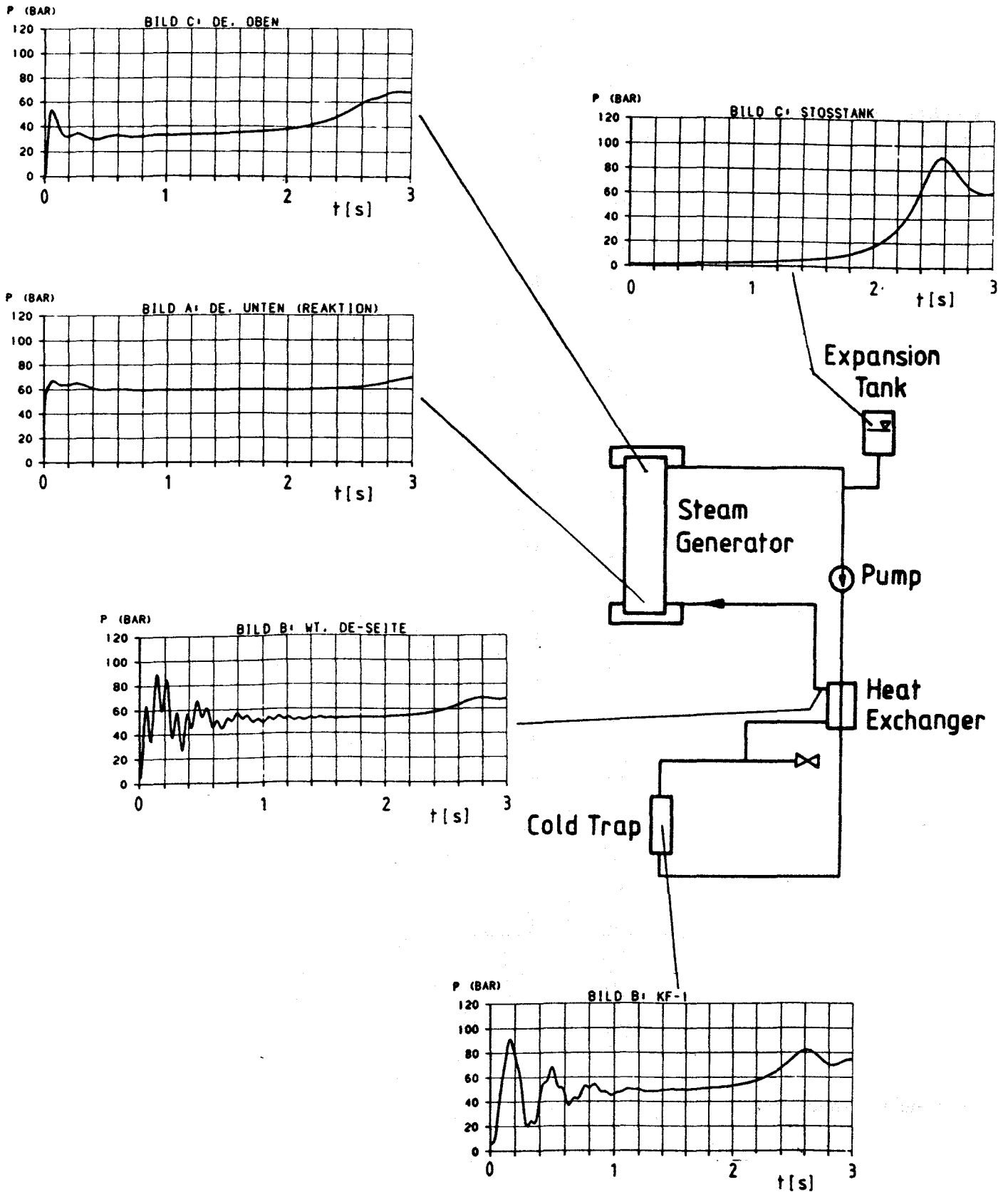
Fig. 4.6-4   Pressure pattern in different components of the NaK-loop after NaK-
H₂O reactions (design basis accident)

4.7   Safety and reliability

With respect to safety the potential hazards resulting from the use of liquid metals seem to be of most concern. These materials imply the possibility of chemical reactions if leaks occur. Application of the general safety objectives:

- Minimizing of facility damage, this means avoiding of failure propagation, and

- Minimizing of radioactivity mobilization

leads to the demand of minimizing possible reactions by reduction of reactive inventories and separating the reaction partners. To avoid release of aerosols into the environment confinement buildings and filtering systems are recommended.

Three different chemical reactions have to be considered for both Pb-17Li and NaK: Liquid metal/gas, liquid metal/water, and liquid metal/concrete reactions. The reaction severity depends on different variables, e.g. the temperature and pressure of the reactants. Table 4.7-1 gives a qualitative picture about the behaviour of the different reactants. The information is based on [1, 2 and 3]. For more details and more design and safety related recommendations, see these references.

In the case of water the distinction between liquid and steam and the type of the contact mode are important. Experiments indicate that both the energetics of liquid metal/water interactions and the long-term chemical reaction with hydrogen generation depend on the degree of fragmentation and mixing. For example, experiments with the injection of subcooled water into a stagnant pool of Pb-17Li indicate that the chemical reaction is self-limiting due to crust formation [4].

The reliability assessment is of increasing importance in the early conception and design phase. The recognition that by early and adequate conceptional and design precautions the risk of bad developments can be reduced, is based on the experience with the first results. The problem of missing or insufficient operating experience and therefore the lack of reliable data must be passed by an appropriate safe design, as demonstrated on the example of the blanket cooling system. This experience suggests, especially for the relatively complicated blanket components, a partition or reduction to the elementary components as there are welds, screws, tubes, plates etc., and the consideration of these parts separately in view of reliability. Then the individual reliability results will be combined to the complete blanket element, a procedure as practised in electrical or electronical equipment, where operating experience for the whole component is not available. The quality of the results is very much dependent on the degree of detailability of

the lay-out. The consequence is a close connection between design and reliability. Reliability assessment becomes, and is to see, as a permanent and accompanying part of the design from the early conceptional phase until the operating of the complete equipment. This procedure in view of a permanent reliability assessment is only practicable if adequate assessment methods are available, e.g. as successfully used for years in the KfK, which are able to deliver reliability results in an uncomplicated and clear manner.

A more detailed description of the safety related tasks to be performed in the future KfK R + D programme are given in chapter 5.6.

References to section 4.7:

[1]   S.J. Piet et al.,
        Liquid Metal Chemical Reaction Safety in Fusion Facilities,
        Fusion Eng. and Design 5 (1987), 273 - 298

[2]   O.J. Foust, Ed.,
        Sodium-NaK Engineering Handbook, Vol. III,
        Gordon and Breach, Science Publishers, Inc. New York (1978)

[3]   H.U. Borgstedt and C.K. Mathews,
        Applied Chemistry of the Alkali Metals,
        Plenum Press, New York 1987

[4]   C. Savatteri,
        Lithium-Lead/Water Interaction
        Large Break experiments, ISFNT2, Karlsruhe, June 2-7, 1991

[5]   D.F. Holland et al.,
        Fusion Safety Program Annual Report, Fiscal Year 1990, EGG-2631,
        March 1991

Table 4.7-1: Chemical reactions

	Pb-17Li	NaK
Gas (air, N_2, CO_2)	No significant temperature increase in air or nitrogen. Rapid temperature increase in CO_2. Here mobilization of radioactive aerosols and hydrogen seems possible. More recent investigations [5] indicate that the peak reaction rate (g-Li/min ⋅ cm^2) of Pb-17Li with air is higher than that of Pb-17Li with steam. This means that Pb-17Li may react more violently and liberate more heat in an air environment than in a steam environment.	No reaction with nitrogen and the noble gases. Reaction with carbon dioxide producing highly caustic oxide and poisonous carbon monoxide.
Water (steam, liquid)	Reaction with steam significant, producing some aerosols. Hence, mobilization of activation products possible. Reaction with liquid appears to result in lower temperatures, however, in higher pressurization than in the case of steam. Injection mode seems to be of most concern. The potential for Pb-17Li/Water reactions to mobilize large amounts of radioactivity within the containment is largely unknown. Since the self-cooled blanket does not contain water this question is of concern within the vacuum vessel only for a simultaneous leak of a blanket segment and a leak in another in-vessel component being water-cooled. However, failure in the steam generators with possible liquid metal/water reactions need special attention. In principle, efforts to remove routinely activation products, especially the more volatile isotopes mercury, polonium incl. bismuth, and thallium, should be enhanced (see chapter 4.5 and 5.4).	Violent exothermic reaction with water. If an oxigen atmosphere is available a secondary explosive reaction is possible between the liberated hydrogen and the oxygen.
Concrete	Mild reaction, with hydrogen production and mobilization of radioactive aerosols. Concrete protection by a steel liner is standard practice.	NaK spilled onto concrete may react with water or chemicals in the concrete. To prevent reactions and protect the surface steel liners are normally used.

235

4.8 Electromagnetic forces

The existing code CARIDDI which allows to compute the eddy currents and electromagnetic forces in toroidal structures has been improved. By introduction of the extended memory option the number of degrees of freedom which can be considered could be increased significantly. This is an essential condition for the treatment of complex, asymmetric structures with internal walls and electrically conducting fluids. Also the reduction of the computing time is mandatory for solving large problems. This could be achieved by optimization of the data processing and introducing more suitable routines for the inversion of the system matrix which take advantage of its symmetry. The improved capability of CARIDDI was tested by application to rather realistic blanket models (water cooled and self-cooled liquid metal blanket). Fig. 4.8-1 shows a mesh of the liquid metal blanket built up of 8-node bricks, the elements used in CARIDDI.

It turned out that the solution of problems with a large number of degrees of freedom has a tendency to instability. Two reasons for this behavior were detected. In the first place the original numerical integration scheme used a too coarse distribution of the Gaussian integration points. This leads to ill-conditioned inductivity and system matrices with even negative eigenvalues. Therefore a different procedure for a more appropriate arrangement of the Gaussian points necessary for the integration has been developed.

Secondly the inversion of these matrices suffers from numerical inaccuracies. Furthermore, these inaccuracies accumulate during the iterative solution. So depending on the available precision beyond a certain number of degrees of freedom the inverted matrix becomes useless for the transient analysis. To avoid this difficulty it is necessary to drop the inversion and solve the system of linear equations for each time step.

It is state-of-the-art that the forces calculated by eddy current codes, i.e. CARIDDI, are used as input to carry out structural dynamics analyses. To transmit the results of CARIDDI to the finite element code ADINA a FORTRAN program has been developed and tested.

Usually the feedback of the structural deformations on the electromagnetic behavior and thus on the resulting forces is neglected. Detailed investigations of this feedback revealed that the coupled treatment of the phenomena leads to differen-

tial equations of third order. Assessments showed that for most cases and approximation by differential equations of second order is possible. Here the feedback is represented by an additional damping which often is quite significant and can be calculated using the results of CARIDDI. For stiff structures like the blankets, however, damping was found to be of minor importance to the maximum stresses. Whether consideration of the interaction with the fluid (undergoing larger deflections) will be more important needs to be investigated.
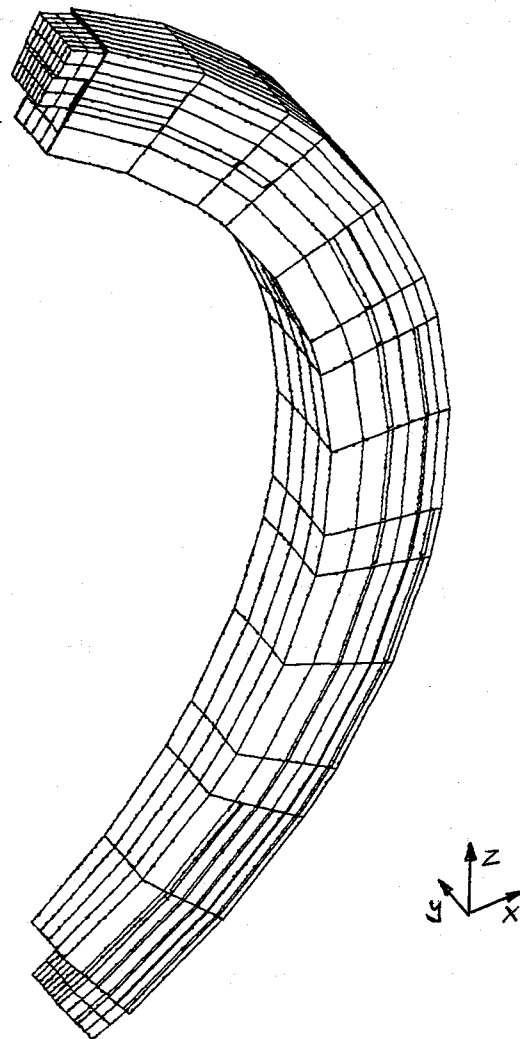

Fig. 4.8-1   Mesh of the DEMO-relevant liquid metal blanket model with transversal internal walls (not visible here)

4.9   KfK-test facilites

In support of design requirements and to establish a data base and to validate theoretical findings KfK has constructed and operates several experimental facilities:

The key problems investigated experimentally are

- compatibility, corrosion of materials in Pb-17Li (PICOLO)
- kinetics of tritium transport, absorption and desorption (removal and recovery) in Pb-17Li and NaK (TRITEX, WAWIK)
- purification of Pb-17Li (TRITEX)
- MHD effects in flowing NaK, simulating Pb-17Li (MEKKA)
- 1. Wall behaviour under high heat flux (FIWATKA).

Sections 4.9.1 to 4.9.6 give a short description and Tables with the main characteristics of the experimental facilities.

4.9.1   Thermal Convection Loops [1,2]

Thermal convection loops were built always for the specific requirements of Pb-17Li experiments and as complementary investigations of the pumped loop experiment TRITEX. So far four loops were operated, loop 4 over a period of 7000 hours. This loop is shown in Fig. 4.9-1.

The loops were fabricated from stainless steel 4571. Table 4.9-1 lists the main parameters of the loops.
4.6 kg Pb-17Li were circulating (26.9 mol). Typically with a temperature gradient of 150°C the flow rate was 0.24 l/min (5 cm/s) in the main pipe. The flow rate was calculated and confirmed by measurements.

About 800 cm^2 stainless steel were wetted by the liquid metal. The mass of this steel was 1.25 kg (about 23 mol).

In two expansion volumes 33 cm^2 of liquid metal surface were in contact with covergas. Furthermore pure iron membranes (55 cm^2, 0.6 mm wall) were submerged in the liquid metal. Therefore there were four gas flows, two going to the mem-

branes, and two going to the liquid metal-gas interface. Gas flow rates were varied between 0.5 and 200 cm^3/min.

One expansion volume in loop no. 4 was equipped with an observation window of quartz. For tests with getter metals a special device was installed on top of the other expansion volume.

All used gases were of high purity, further purified with OXISORB (Messer Griesheim). The Pb-17Li was obtained from Metallgesellschaft Frankfurt, Germany. The surface was scrapped away. Then the metal was purified by remelting in an inert atmosphere and cast into an ingot. This was quickly transferred into the filling tank of the loop.
The whole facility was then degassed at temperatures up to 650°C for 35 hours at a final pressure of 10^{-4} mbar. The loop was filled, leaving about 1 kg of the alloy with floating impurites in the filling tank. Freezing the liquid metal in the area of the cold spot sealed the loop.

A background of hydrogen could always be observed. It caused an equilibrium partial pressure of 0.5 mbar in the liquid metal at a temperature of 500°C. Therefore deuterium was used in experiments instead of normal hydrogen.

The gas flows were analyzed using a HP5890 gas chromatograph with two columns, one operating with argon, the other with hydrogen carrier gas. The detection limits were 1 ppm H$_2$ and He with argon carrier gas, and 5 ppm D$_2$ with hydrogen carrier gas. The equilibrium partial pressure of deuterium in the bulk liquid metal was measured by an accumulation method using the membranes.

The last step of operation of a loop before dismanteling was always oxidation of the Pb-17Li surface in one of the expansion volumes. Then the influence of the oxides on deuterium behavior was investigated. Finally the loop was cut in pieces and corrosion as well as transport of corrosion products was studied. Also deposits in covergas spaces were analyzed in order to get information for aerosol transport of Pb and Li.

Table 4.9-1: Main parameters of the Thermal Convection Loop No. 4

Structure material	austenitic steel 1.4571
Main pipe inner diameter	10 mm
Covergas (in special experiments	Ar-6.0 He, Ne, Kr, Xe)
Total inventory of Pb-17Li	5.5 kg
Circulating Pb-17Li	4.6 kg
Total wetted surface	800 cm^2
Temperature	280°C to 700°C
Flow rate at a temperature gradient of 150°C	0.24 l/min

4.9.2 TRITEX

The TRITEX facility was built 1987 to 1989 for the study of tritium extraction by solid getters [3]. In the meantime the loop is also used to study purification methods and other effects of a Pb-17Li system. The loop has operated so far in four runs for 6200 hours, the longest run lasting 3100 hours. For several thousand hours the cold trap was kept at 260°C, while the loop temperature was varied between 280 and 500°C.

TRITEX is a pumped loop with circulating Pb-17Li. It is a flexible tool and can be adopted to the requirements of experiments. It allows experiments between 250 and 550°C, with flow rates up to 2.5 l/min. With the exception of the cold trap it is an isothermal system.

Fig. 4.9-2 shows a flow sheet, the main parameters are given in Table 4.9-2. TRITEX is build from the ferritic steel 1.4922, with some smaller parts made from molybdenum. Several cover gas spaces are separated from each other and operated with argon.

For experiments with deuterium and tritium the circulating liquid metal can be loaded through a 1000 cm^2 iron membran in the expansion volume. Equilibrium partial pressures in the eutectic between 0.05 and 20 mbar D_2 can be established. The transport of the gas around the loop can be followed by analyzing the different gas flows using a HP-5890 gas chromatograph. Gettering experiments are performed in the test section. This is located in an argon filled glove box and can be

opened without draining the loop. For analytical purposes there is a smaller permeation membrane in the test section.

As in case of the thermal convection loops a background of hydrogen was observed.

TRITEX is equipped with several devices for the investigation of purification methods. The loop has a main flow magnetic trap, a bypass flow cold trap, and the option for mechanical filters. For visuell inspection there is an observation window (quartz) on top of one sampling section. Also distributed along the loop are samples for the study of corrosion of loop materials and for deposition of impurities. Last not least the facility TRITEX is inside of a radiation controlled area and allows the use of radioactive tracers.

Table 4.9-2: Main parameters of TRITEX

Structure material	ferritic steel 1.4922
Main pipe inner diameter	15 mm
Circulating material	Pb-17Li
Covergas	Ar-6.0
Total inventory of Pb-17Li	120 kg
Circulating Pb-17Li	80 kg
Total wetted surface	1.2 m^2
Temperature	250 to 550°C
Flow rate main loop	0.1 to 2.5 l/min
Flow rate cold trap	adjustable

4.9.3 The MEKKA facility

A main issue involved in designing a selfcooled liquid metal blanket is the strong magnetic field which causes high pressure drop of the liquid metal flowing through the cooling channels and the degradation of the heat transport by the liquid metal due to changed velocity profiles and the reduced turbulence.

In order to get a better data base, to learn about new physical problems and to verify computer programs used for design calculations the experimental program MEKKA (Magnetohydrodynamik Experiment in Natrium-Kalium Karlsruhe) was started in 1985.

To conduct fusion relevant MHD-experiments magnets with high field strength and testing volumes and a liquid metal loop with a high flow through are necessary.

For the first step of the program this means for the experiments with restricted testing volumes three magnets are available which cover different items of the step of the MHD-program:

A normal conducting dipole magnet is used for the first experiments in straight ducts. It has a field strength of 2 Tesla and a test volume of $0.17\,m \times 0.5\,m \times 1.5\,m$.

A superconducting Solenoid-Magnet with 3.5 Tesla field strength, a warm bore of 40 cm diameter, and a length of about 1 m is foreseen to investigate all kind of 3-dimensional MHD-flow problems, especially the radial to toroidal bend. Fig. 4.9-3 shows this magnet with the installed radial-toroidal bend test section.

Additionally a superconducting dipole magnet is available but not yet in operation which has a field strength of 4.5 Tesla, a warm bore of 6 cm diameter and a length of 1 m will provide a tool to investigate the extrapolation to high field strength and high flow velocities in small, presumably insulated flow ducts, discussed for alternative flow concepts.

The eutectic Sodium-potassium alloy $Na^{22}K^{78}$ is used as the liquid metal for the first step of the program. The fact that NaK is liquid at room temperature not only simplifies the loop design, but, most importantly facilitates the operation of the loop and the conduct of the tests and enables the acquisition of data of higher quality and greater variety than would be possible with a higher melting material like Sodium, Lithium or Lithium-lead. Thinner tubings for pressure measurement can be used, the use of rubber and some plastics became possible. To overcome the problem of wetting stainless steel surfaces, the loop is designed to operate also at higher temperatures ($300°C$) in order to accelerate and insure the wetting of all MHD relevant surfaces.

The NaK loop (Fig. 4.9-4) was designed and built at KfK. There are some special features not widely used in liquid metal technology up to now:

A canned motor pump with a maximum pressure head of 9 bars at a flow rate of 25 m3/h circulates the liquid metal at lower temperatures ($<250°C$). An additional

242

electromagnetic pump is used to circulate the NaK during the high temperature wetting phase. All the heat dissipated in the loop and in the test section is removed by an oil cooled double tube heat exchanger. The oxygen content in the NaK is controlled by an oil cooled cold trap. The flow through, the most important value is measured by a gyrostatic flowmeter with an accuracy of 0.5%. The pressure in the loop and the pressure differences in the test section are measured by pressure transducers. The entire loop is built up in a rack which can be moved on rails along the axis of the magnet. Using ducts much longer than the magnet and with constant cross section along its length, this method allows for local pressure and velocity distribution measurements at different regions of the magnet only by traversing the loop with a hydraulic piston. The position of the test section relative to the magnet is measured by an ultrasonic ruler.

The operation of the loop and the magnet is controlled by a programmable logical controller; the relevant data are recorded. All the experimental data are collected in a 96 channel data logger connected to a personal computer system, which allows to process the data acquisition and to make a data reduction.

4.9.4 PICOLO

The PICOLO [PbLi Corrosion Loop] facility was designed in 1985 for corrosion tests of ferritic steels in flowing liquid Pb-17Li alloy [4]. The loop has a capacity for about 10 l (100 kg) of the eutectic alloy. It is provided with an electromagnetic pump and flow meter to generate and to measure a turbulent flow in the test section by means of a sufficiently high flow velocity. The need for the electromagnetic pump is the reason to fabricate the low temperature section of the loop of austenitic steel (X10 CrNiMoTi 18 10; no. 1.4571). The electromagnetic flow meter, a magnetic trap for corrosion products and the main cooler are also placed in this section of the loop. In addition to the magnetic trap two mechanical traps are placed in series between the cooler and the pump.

The hot section of PICOLO is constructed of a ferritic steel which is available in the needed dimensions (X10 CrAl 7; no. 1.4713). The main components of this section are the test tube, the electrical heater of a capacity of 6 kW, and the recuperative heat exchanger. The test section is a tube of 14 mm diameter in which cylindrical specimens of 8 mm diameter are inserted in the central position. The loop is connected to the bottom of an inert atmosphere glove box which allows the open-

ing of the test section to the atmosphere in order to change the specimens or to take analytical samples of the liquid metal.

The parameters of the flowing liquid alloy which are maintained for corrosion tests are listed in Table 4.9-3. The flow diagram of the PICOLO facility in its present shape is shown in Fig. 4.9-5. The loop is in operation since 1985, the accumulated time of operation exceeds 10000 hours, half of the time with a maximum temperature of 550 °C. The magnetic trap was twice renewed during the operation periods, since precipitates plugged the system after the operation at 550 °C in the test section. The liquid alloy was also renewed twice. This was necessary because of losses of Li from the alloy due to oxidation.

Table 4.9-3:   Parameters of operation of the PICOLO facility in 1986 to 1990

Component	Parameter	Value	Dimension
Loop	Volume of Pb-17Li	10	[l]
	Flow of liquid	120	[l/h]
	Temperaturegradient	200	[K]
	accumulated operation time	> 10000	[h]
Test tube	max. temperature	550; 500; ± 3	[°C]
	flow velocity	0.30 ±0.02	[m/s]
	Reynolds number	20000	
Pump channel	Temperature	310 ± 5	[°C]

4.9.5   WAWIK, Wasserstoff-Abscheidung und Wiedergewinnung in Kalt- fallen (Hydrogen Removal and Recovery in Cold Traps) [5]

Facility description

The facility is used to investigate a) the kinetics of hydrogen removal from NaK by hydride precipitation in cold traps, b) the kinetics of hydrogen recovery from the cold trap by thermal decomposition of the hydride and vacuum pumping.

Fig. 4.9-6 shows the flowdiagram: Two experimental cold traps are used in parallel to precipitate the hydrogen dissolved in the NaK. The hydrogen is permeated

244

into the NaK through a coiled nickel tube. Hydrogen concentrations are measured both upstream and downstream of the cold traps by means of a nickel membrane and an ionic getter pump. The cold traps consist of countercurrently cooled vertical cylinders filled with wire mesh packings.

Hydrogen is recovered by electrically heating up the wire mesh packings and measuring the hydrogen gas flow rate with a gasometer. This is done either directly using the complete cold trap or with single mesh packings after demounting the cold trap in a glove box.

<u>Characteristic features</u>

liquid metal	NaK (if required: Na)
maximum loop temperature	$T_{max} = 450\,°C$
maximum liquid metal flow rate	$V_{max} = 60\,cm^3/s$
cold trap diameter, height	$D = 100\,mm, H = 600\,mm$
measurement techniques for	temperature, pressure, flow rates, hydrogen partial pressure and concentration
glove box	impurity controll (O_2, H_2O) working volume $\approx 3m^3$

<u>Current (and future) use</u>

Development of a tritium removal and recovery technique for a self-cooled Pb-17Li blanket (permeation of tritium through the heat exchanger into the intermediate NaK loop and cold trapping).

(Development of efficient purification techniques for Na or NaK liquid metal loops for fast breeder and non nuclear applications).

4.9.6   FlWATKA - FIrst WAll Test KArlsruhe -a first wall thermal fatigue test facility [6]

<u>Testing Needs</u>

The First Wall (FW) of a fusion device receives thermal loads in cycles. Thermal load cycles cause material fatigue and limit the life time of the cooled steel structure and its protection tiles including attachment devices, if any. Experiments

with FW components are needed to verify life-time prediction tooles and to learn about components integral behavior under cyclic thermal loads.

Facility Description

The specimens will be tested under mechanical boundary conditions and thermal loads close to those of fusion machines except for internal heat sources in the specimens and for disruption forces. Two FW sections of up to 0.25 m^2 each will be positioned in a vacuum chamber (Fig. 4.9-7); they will be actively cooled with water and will be heated by thermal radiation in a cyclic manner. A resistance heater made of graphite hanging from the top will serve as a heat source. It will radiate heat for a few minutes onto the surfaces of two specimens, tile protected or bare, placed on both sides of the heater plates at a distance of two or three centimeters at the edges the room around the heater is closed by a water-cooled housing, framing the specimens. The vacuum atmosphere protects the bare graphite heater elements and protection tiles at high temperatures from oxidation; it also guarantees purely radiative heat transfer to the specimens as well as between the protection tiles and the steel structure, as in the fusion device not overlaid by condution and convection mechanisms. The electrical power to the heater of up to 500 kW will be turned down periodically for one or two minutes to change the temperature distribution in the specimens with time.

The maximum heat flux from the heater to a specimen being on a high temperature level of 1800°C is on the order of 80 W/cm^2; it is much higher at lower specimen temperatures. Other characteristic features are given in Table 4.9-4. Control and safety features provide a safe shutdown even in the cases of water or air breaking into the vacuum vessel.

Status

Construction of the facility including supply units and basic measuring equipment is finished and test runs of the components have been performed. The vessel internals for the first test series are being manufactured. The uniformity of the heat flux from the heater will be determined with movable heat flux sensors. The first specimen will be an instrumented and tile protected FW test section supplied by the NET-Team.

Table 4.9-4: Characteristic Features of FIWATKA Main Components

Vacuum Vessel	
Pressure, max.	-0.1/ + 0.1 MPa
Temperature, max.	120°C
Volume	4.5 m³
Radiative Heater	
Temperature, max.	2200°C
Power, max.	500 kW
Area, each of two faces, on the order of	0.25 m²
AC Power Supply (3 Phases) to heater	
Voltage, max.	180 V
Current per phase, max.	3500 A
Power per phase, max.	167 kW
Cooling Water Circuit II	
Pressure, max.	1,4 MPa
Temperature, max.	120°C
Flow rate at pressure head of 0.75 MPa	100 m³/h
Power, max.	500 kW
Cooling Water Circuit II	
Pressure, max.	0.7 MPa
Temperature, max.	50°C
Flow rate at pressure head of 0.35 MPa	4.5 m³/h
Power, max.	90 kW
Vacuum Pump	
Turbo Pump	500 ℓ/s at < 0.2 Pa
Backing Pumps	400 m³/h at 1.0 Pa

References to section 4.9:

[1] H. Feuerstein, H. Gräbner, S. Horn and J. Oschinski, Transport of Deuterium and Rare Gases by Flowing Molten Pb-17Li, 4th International Conference on Fusion Reactor Materials, Kyoto, Japan, Dec. 4-8, 1989

[2] H. Feuerstein, H. Gräbner, S. Horn and J. Oschinski, Behavior of Deuterium and Rare Gases in Thermal Convection Loops with Molten Pb-17Li
Fusion Engineering and Design 14 (1991) 261

[3] H. Feuerstein, H. Gräbner, G. Kieser, TRITEX, a Forced Convection Loop with Pb-17Li, J. Nucl. Mater. 155-157 (1988) 520

[4] G. Frees, G. Drechsler, Z. Peric, Dynamische Korrosionsuntersuchungen in der eutektischen Blei - Lithiumschmelze Pb-17Li, Werkstoffe und Korrosion 40 (1989) 593-598

[5] J. Reimann, "Tritium inventory and recovery for a self-cooled Pb-17Li blanket", Fusion Engineering and Design 14 (1991) p. 413.

[6] G. Hofmann, E. Eggert; FIWATKA - A first wall thermal fatigue test facility - Proc. of 2. Intern. Symp. on Fusion Nuclear Techn., Karlsruhe (June 1991).
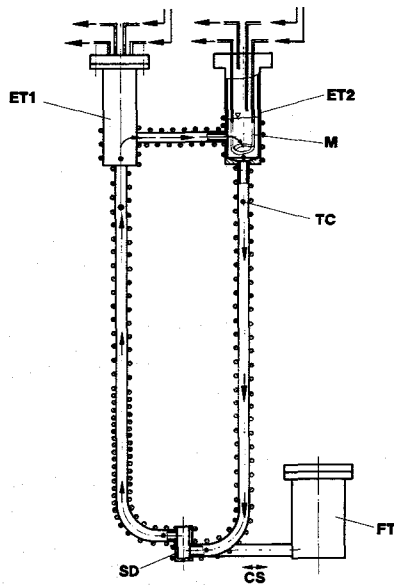
Fig. 4.9-1: **Thermal convection loop 4**
ET = expansion volumes, M = permeation membranes,
TC = thermo couples, FT = filling tank, CS = area of the cold
spot, SD = special device for measurements of the flow rate.
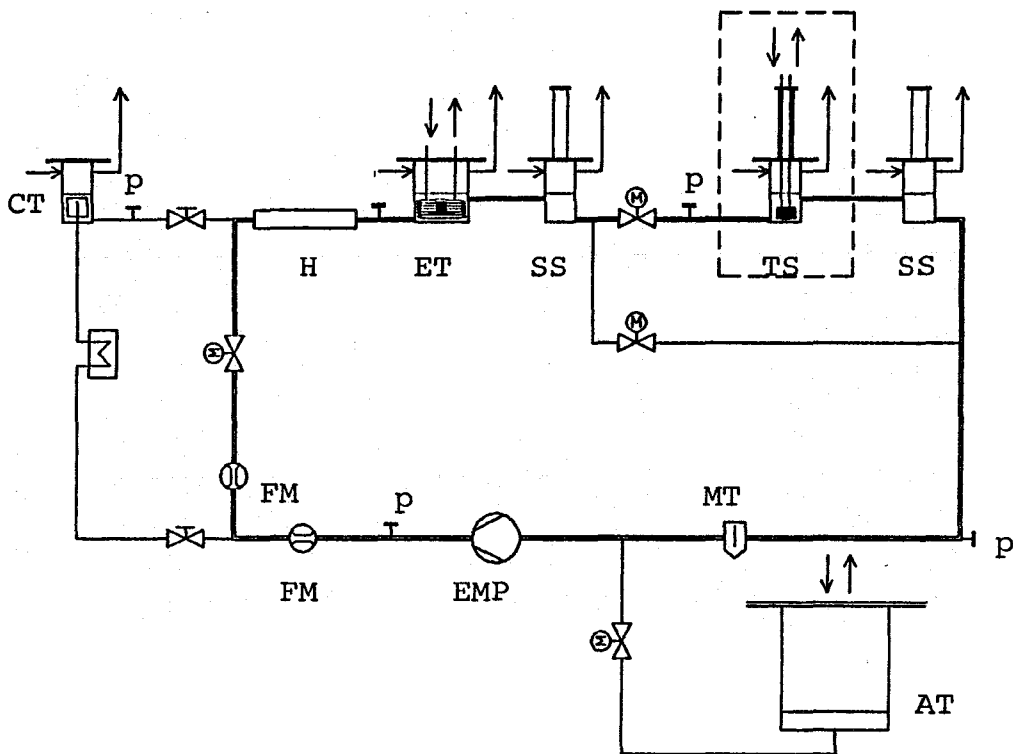
Fig. 4.9-2: **Flow diagram of the loop TRITEX**
EMP = electro magnetic pump FM = flow meter
H = main heater ET = expansion volume
SS = sampling sections TS = test section
MT = magnetic trap CT = cold trap
DT = drain tank p = positions for deposition

249
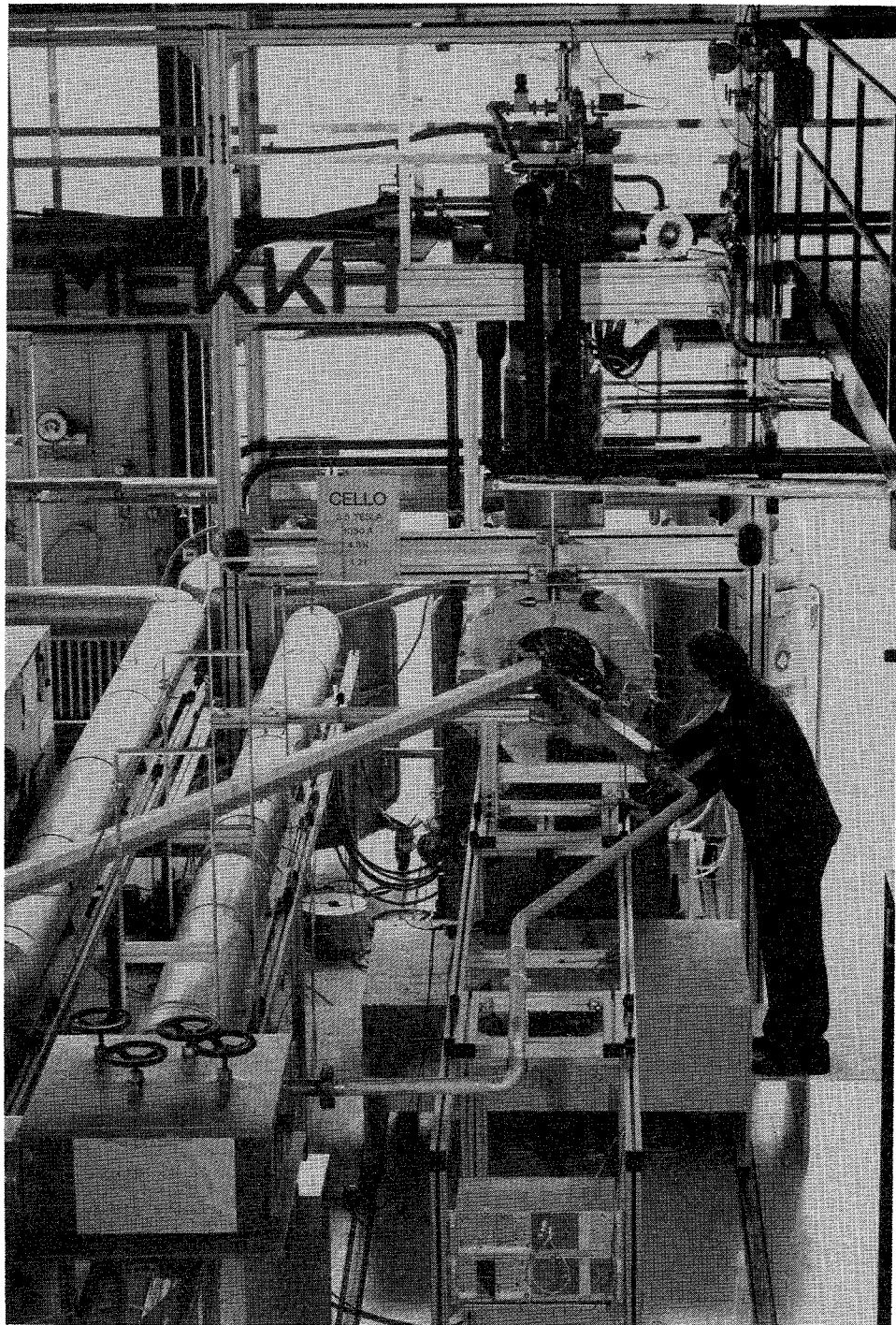
Fig. 4.9-3:   The superconducting solenoid magnet

MAGNET

Expansions
tank

KARLSRUHE

MEKKA

Flow meter

Cold trap

Pump I

Pump II

Dump tank

Argon
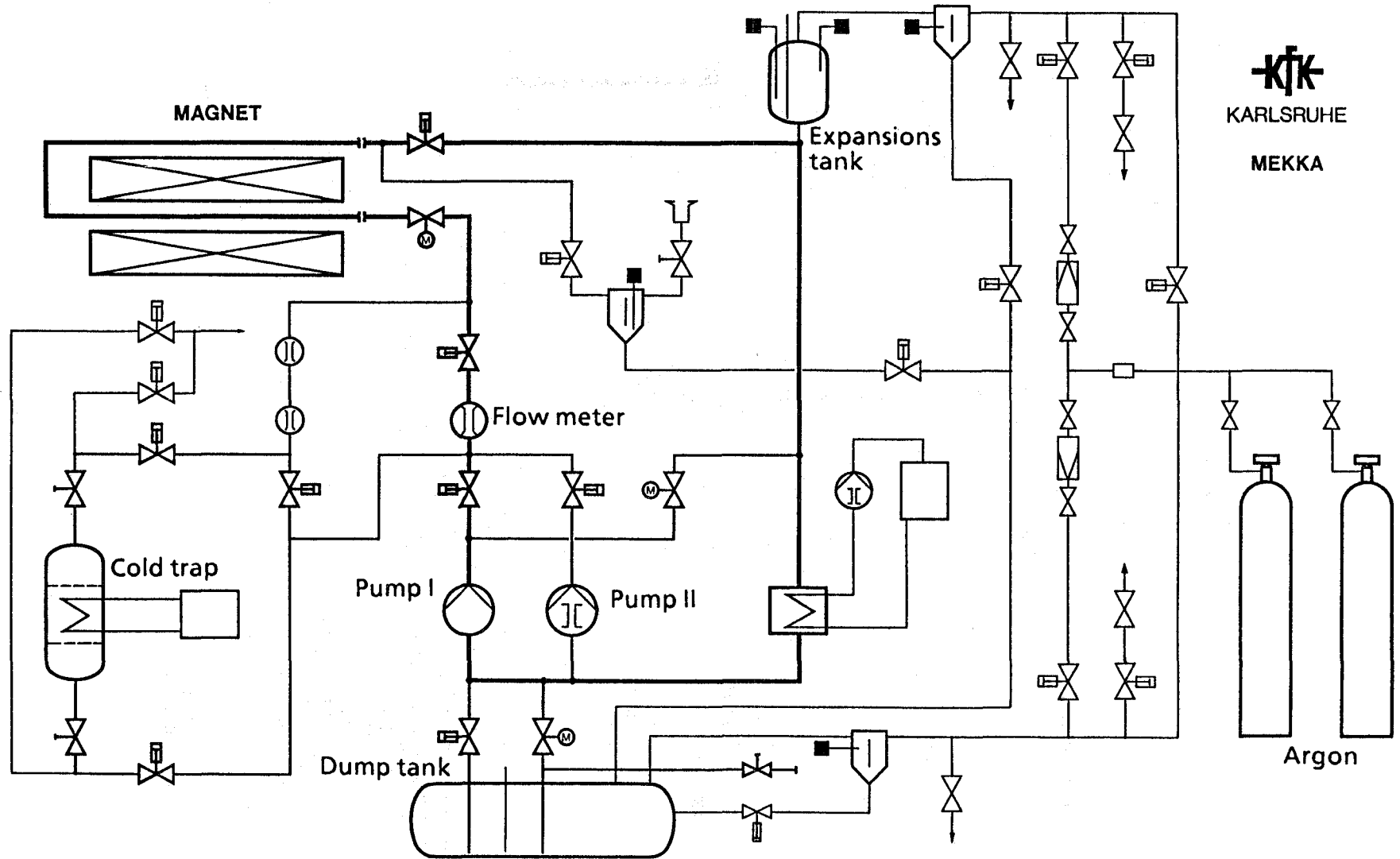
Fig. 4.9-4:   The NaK1 sodium-potassium loop
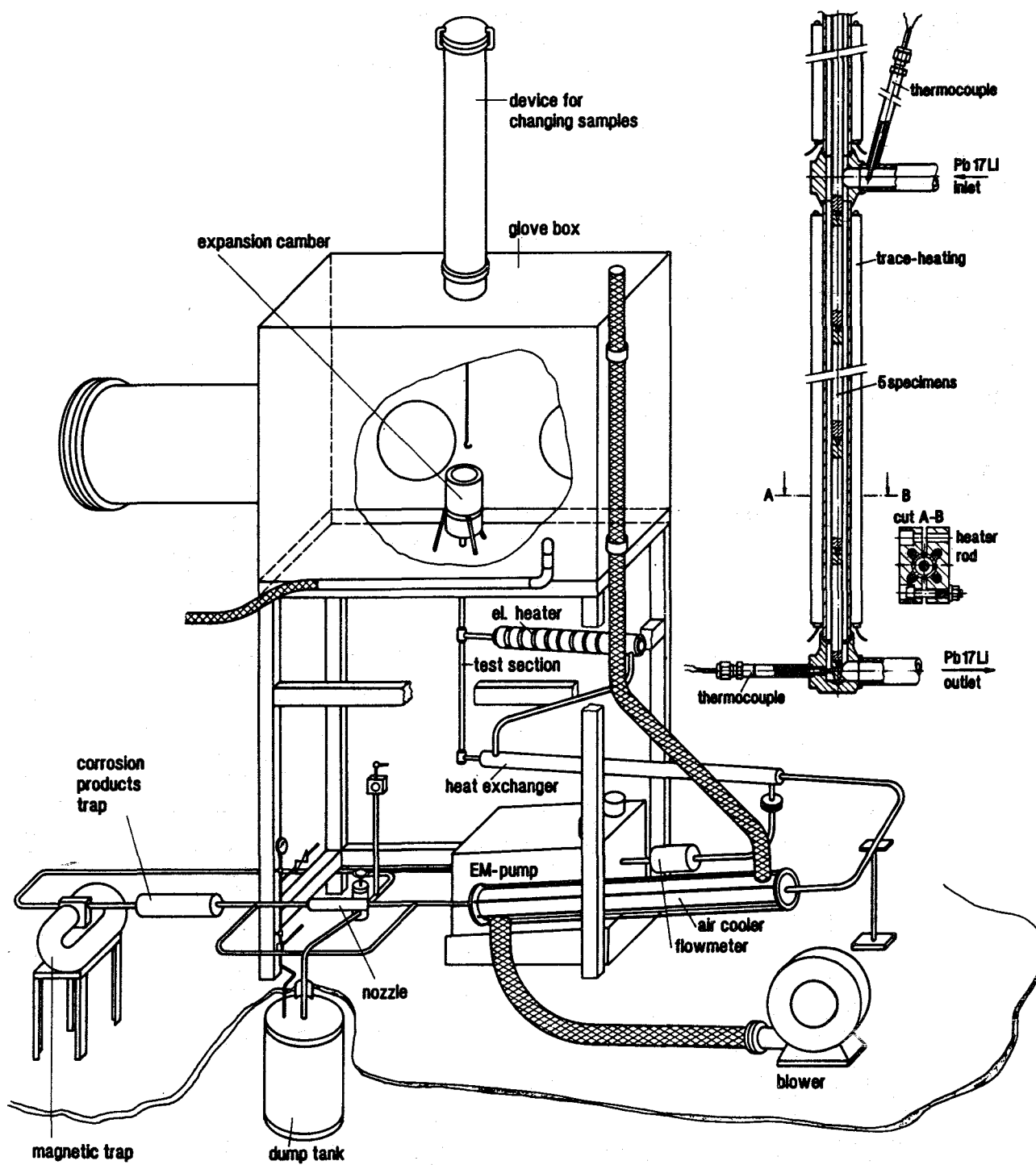
Fig. 4.9-5:   Flow diagram of the PICOLO facility

252
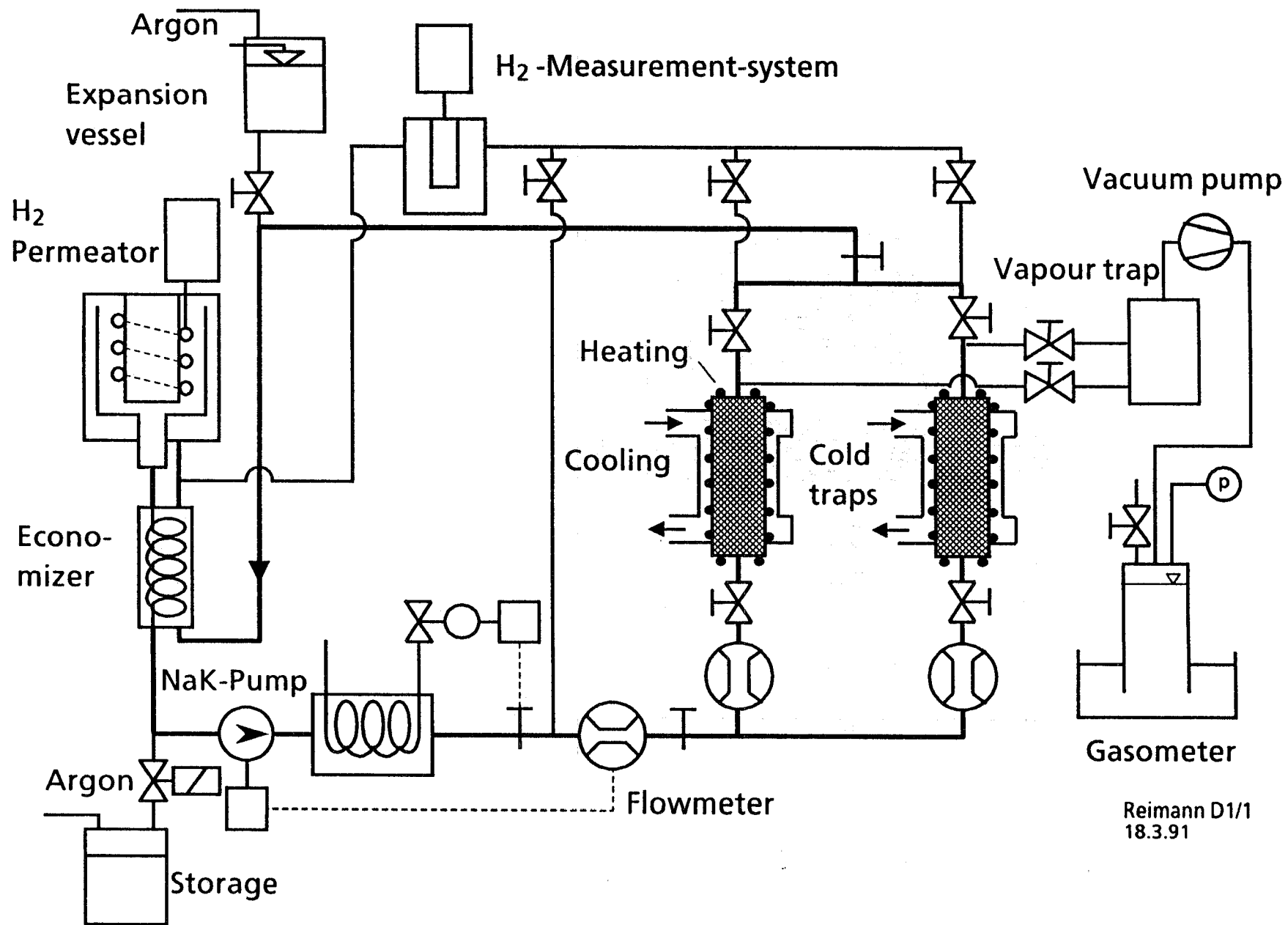
Fig. 4.9-6   WAWIK-test facility for hydrogen removal and recovery

253
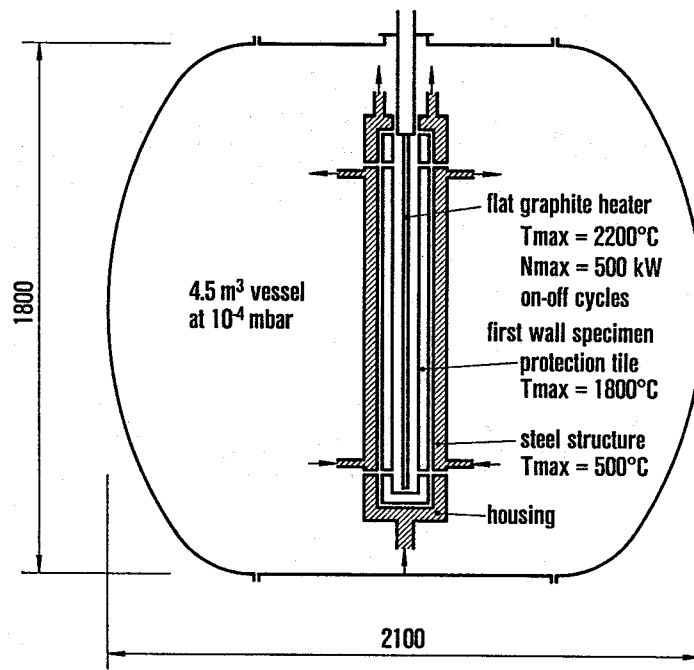
Fig. 4.9-7:   FIWATKA test arrangement (schematic)

254

5.   REQUIRED R + D PROGRAM 1992 – 1994

This status report has been prepared at the end of the first three year R + D period of the European DEMO-relevant blanket program. A second three year period will now follow up to the year 1995 at which date a selection among the European liquid metal blanket alternatives will take place. The selected blanket will be designed in detail and large scale experiments are envisaged. Consequently the coming R + D program described here is limited to key problems and small scale experiments. Section 5.1 to 5.7 and the time schedules (Table 5-1) summarize the R + D tasks foreseen. The blanket design will be modified if required by the results.

Table 5-1 Time Schedule of KfK R&D Programme up to 1995

Activity/Milestones	1989	1990	1991	1992	1993	1994
1. Design						
1.1 DEMO blanket conceptual design						
- Reference-concept			▼			
- Modification due to the results of investigations alternative concepts						
1.2 Test module design						
- Principle design		—				
- Module design for specific tests						
1.3 External loop systems for heat- and tritium extraction						
- Conceptual design for DEMO			▽			
- Conceptual design for NET/ITER		—				
- Modifications due to the results of investigations, alternative concepts						△
1.4 Independent after heat removal system						
- Conceptual design for DEMO, thermal analysis				▽		
2. Physico Chemistry						
2.1 Compatibility, Electrically insulating coatings						
- Corrosion of MANET in flowing Pb-17 Li (PICOLO-loop)					▽	
- Selection study of electrically insulating coatings				▽		
- Testing of electrically insulating coatings in flowing Pb-17 Li (PICOLO-loop)						▽
- Fatigue tests of structural materials in Pb-17 Li		▽				

ITER conceptual design report △

Final report

256

Activity/Milestones	1989	1990	1991	1992	1993	1994
2.2 Removal of impurities from Pb-17 Li (Tritex-loop,thermal convection loop)						
- Corrosion products					▽	
- Polonium, Bismuth, Mercury						▽
3. Tritium extraction						
- Experimental investigation of tritium removal from Nak by cold trapping and tritium recovery by thermal decomposition (WAWIK-loop)				▽		
- Modeling of tritide deposition in a Nak-cold trap				▽		
4. MHD Investigations						
4.1 Experiments						
- Basic experiments		▼				
- Key problems of the poloidal-radial-toroidal flow concept (reference design)						
• single channel tests					▽	
• multi channel tests						▽
- alternative concepts						▽
4.2 Analysis and code development						
- full numerical solutions					▽	
- core flow solutions					▽	

conceptual design of a fusion relevant cold trap, decision on an integral permeation experiment (Pb-17Li/ferritic steel/Nak)at the end of 1992

Activity/Milestones	1989	1990	1991	1992	1993	1994

5. Safety

5.1 Safety and Reliability

- Functional analysis of blanket system
- Reliability of external loops
- Reliability of blanket segments
- Investigations of hazard potential and possible accident sequences

5.2 Electromagnetic forces

- Model and code development for the analysis of forces and stresses on the blanket structure during plasma disruption
- Application to design relevant elements

6. Components

6.1 Flow channel inserts

- Development of fabrication technology
- Thermal-mechanics tests
- Irradiation experiments

6.2 Pb-17 Li components

- Development and small scale testing of key components

5.1 Magnetohydrodynamics

As outlined in section 2.1.3 and 4.2 the MHD design considerations of the reference concept are governed by the 3-dimensional and multichannel effects in the front part of the cooling channels. Therefore the experimental program as well as the code development are focussed on these items:

- In the single channel toroidal-radial-toroidal bend experiment TRT1, jointly conducted together with the ANL in the superconducting solenoid magnet of the MEKKA laboratory, potential distributions on the duct walls, pressure differences between different stations and the potential differences in within the liquid metal are measured and compared with theoretical predictions. The experiments have been started in the mid of 91 and will take about one year including the final evaluation.

- The multichannel U-bend experiment is mainly aimed to study the effect of interconnected channels and the dependence of the 3-dimensional pressure drop from the aspect ratio of the cross section of electrically connected parallel channels.
  The experiment will start in 91.

- Code development
  Two kinds of codes are developed at KfK to describe MHD flow in ducts numerically; the "core flow solution" and the "full solution".

  - The core flow solution developed by ANL and the University of Urbana [1] was adopted by KfK. It will be modified and improved for more complex geometries, verified with the above mentioned experiments and then applied for fusion blanket design calculations.

  - The full solution developed by KfK [2] will be further developed to calculate MHD flow in complex geometries (knee) for fusion relevant parameters Hartmann number M and interaction parameter N.

Beside the reference blanket related R + D work specific problems of design concepts with poloidal flow will be investigated.

An experiment is planned to improve the heat transfer from the first wall to the liquid metal and to homogenize the temperature in the high heated front channel. This experiment will be conducted in the normal conducting dipolmagnet of MEK-KA.

References to section 5.1:

[1]   Hua, T.Q., Walker, J.S., Picologlou, B.F., and Reed, C.B.: "Three Dimensional MHD flows in Rectangular Ducts of Liquid-Metal-Cooled Blankets", Fusion Technology, Vol. 14, No. 3, November 1988.

[2]   Sterl, A., "Numerische Simulation magnetohydrodynamischer Flüssigmetall-Strömungen in rechteckigen Rohren bei großen Hartmann-Zahlen, KfK 4504, Januar 1989.

5.2 Electrical insulation in the flow channel

Before flow channel inserts (FCI) can be used in a liquid metal cooled blanket extensive testing both of small specimens (a) and of FCI with prototypical dimensions (b) has to be performed. The required R + D-program will depend on the fabrication methods for FCI which are not yet developed. From the present point of view the following examinations will be required

- Mechanical bonding of the laminated element by mechanical tests (bending and tensile (a) and by thermoshock tests (a) + (b)
- out-of-pile testing of electrical insulation and of break-down potential of voltage (a)
- corrosion tests (a)
- neutron irradiation tests (a) up to a damage rate of 10 (70) dpa to examine mechanical bonding of the laminated structure
- irradiation tests under combined load of electrical potential and ionizing irradiation (a) to examine electrical insulation
- MHD-experiments in prototypical flow channels with transient magnetic field and direction (b) to investigate the stability of shape of the FCI under transient conditions
- investigations of the stability of shape and of electrical insulation of FCI during disruptions (b)

- filling and draining experiments with Pb-17Li of prototypical parts of a blanket to investigate the motion of the liquid metal in the gaps between FCI and channel structure
- investigation of stability of shape of FCI under the combined load of transient temperatures and pressures and neutron irradiation.

5.3 Tritium extraction and recovery
5.3.1 Getter

While the behavior of deuterium and hydrogen in thermal convection loops and the facility TRITEX is generally well understood, a number of items have still to be investigated.

Besides vanadium, some V-alloys and niobium shall be studied in a thermal convection loop. Alloy often have better properties than pure metals. Vanadium alloys were reported to have higher hydrogen solubilities.

The influence of loading/degassing cycles on deuterium uptake shall be investigated. This can be done in both types of facilities.

Getters will be tested in the TRITEX facility. For this a new test section will be installed for the next experimental phase. The main items to be studied are the influence of the liquid metal velocity and the operation of the cold trap on deuterium uptake. In a special part of the new test section it will be investigated if the calculations for a technical system [1] can be confirmed.

All experimental facilities show a hydrogen background. However the tritium concentration in a self cooled blanket will be much smaller [1]. It is planned to use tracer amounts of tritium in both kinds of facilities. With these experiments the whole range of concentrations and influence of other hydrogen isotopes (swamping) will be covered.

5.3.2 Permeation/Cold Trapping

The required R + D program can be divided in the following steps:

A: Investigation of hydride precipitation kinetics:
    Experiments; parameters: cold trap outlet concentration, concentration differ-

261

ence, NaK flow rate, cold trap geometry, permeation time, number of recovery cycles

Theory: one and two-dimensional calculations of velocity, temperature, concentration and precipitation distributions to develop a mass transfer model

B: <u>Investigation of hydrogen removal kinetics:</u>
Experiments; parameters: temperature, hydride loading, number of recovery cycles

C: <u>Design of a cold trap system for NET/ITER</u>

D: <u>Permeation experiment in the system Pb-17Li/ferritic wall/NaK</u>
The decision point for this experiment will be middle of 1992

A time-table of the R + D program is given below

1991	1992	1993
——— A ——————→		
——— B ——————→		
	————————→	C ——→
	? ←———	——— D ——→

References to section 5.3:

[1] J. Reimann and H. Feuerstein, Gettering and/or Cold Trapping for Tritium form a Self Cooled Pb-17Li Blanket, 16th SOFT Conference, London, Sept. 3-7, 1990

5.4 Compatibility, liquid metal purification

5.4.1 Compatibility

Two mayor testing series have to be performed in PICOLO in the next future. One of them is concerned with the MANET steel. Some additional corrosion tests of this material at different parameters (testing temperature, flow velocity, Reynolds number, etc.) should generate data on the basis of a broad field of parameters in order to verify the relation between the corrosion model and the measured corrosion rates. This program will also be used to get more information on the deposition behavior of corrosion products in the cold branch of PICOLO.

The second one is related to the development of an insulating layer on the structural material which should be stable in contact with liquid Pb-17Li alloy. Alumina layers formed on 316 L(N) steel surfaces after alitization of the material will be the first insulators to be tested. In a following step the alitization of MANET steel will be developed and the stability of alumina layers formed on the iron aluminide layers on MANET will be tested. The program includes the development of a method to measure the resistivity of such layers on specimens which are inserted in Pb-17Li molten alloy.

5.4.2 Purification

The development of purification methods for Pb-17Li has just started. Three kinds of impurities are of special concern.

Impurities undergoing mass transfer will be mainly studied in the facility TRITEX. Here different types of cold and magnetic traps will be used. Also there is an access in TRITEX to the liquid metal/cover gas interface at the test section without drain. Here the possibility to remove some impurities (Bi) with oxides will be investigated.

Radioactive impurities are often in very low concentrations, some even as tracers (Po-210 is always in tracer concentrations). In sodium cooled reactors such radioactive impurities show different behavior than expected from larger concentrations [1,2]. The investigation of the behavior of Po-210 is under way. Po-210 will not be used in TRITEX but only in batch type tests and in a thermal convection loop. Other radioactive impurities are also important, especially if they have a high volatility.

The third kind of impurities are interstitial elements of the steels. Will there be a transport of carbon and other elements in Pb-17Li as known from sodium systems? Meters for oxygen, carbon and lithium will be installed in TRITEX.

References to section 5.4:

[1] H. Feuerstein, A.J. Hooper and F.A. Johnson, Mechanism of release of radio-active products into liquid metal coolants, Atomic Energy Review 17, 3 (1979)

[2] H. Feuerstein and A.W. Thorley, IAEA-IWGFR Specialists' meeting on Fission and Corosion Product Behavior in Primary Circuits of LMFBRs, KfK-4279 / IWGFR-64 (1987)

5.5   Ancillary loop system, components

5.5.1   Leak propagation in main heat exchanger and test module configuration for testing the NaK-H_2O reaction

Theoretical evaluations of consequences of NaK-H_2O reactions in the bundle area and in the NaK collector with wastage protection equipment (protective tubes) of double-wall steam generators showed satisfactory results with respect to leak propagation [1]. However, to confirm the safe operability of this steam generator concept even in case of leaks between NaK and H_2O, experimental investigations are proposed.

The aim of these investigations is to prove the mastering of possible NaK-H_2O-reactions after leaks in the bundle area and in the NaK collector by passive means. The primary objective is the exclusion of consequential damage of adjacent tubes.

An experimental configuration essentially consisting of a NaK-loop and a test object is to be proposed. As a possible design to gain all necessary results, the test object consists of a parallel tube arrangement installed inside a pressure vessel for safety reasons. The tube arrangement consists of several testing tubes and an additional tube of larger diameter in parallel. The testing tubes (approx. 1 m length) essentially consist of a water pressurized inner tube and the enclosing tube (same design principle as the double-wall steam generator) with NaK in the gap. The geometrical boundary conditions of the test object such as wall thicknesses or gap width should correspond to original geometry to guarantee a reliable transfer of results.

Pressure and flow rate conditions of the real NaK-loop will be controlled using the tube of larger diameter and a throttle valve. Having different initial leak preparation, series of experiments can be performed depending on the number of testing tubes.

References to section 5.3:

[1]   INTERATOM, Contract for development of the cooling circuits for the liquid metal cooled blankets, Kernforschungszentrum 1990.

5.6 Safety and reliability

R&D work has to be done in different areas: (a) The investigation of the possible interaction of Pb-17Li with different reactants, (b) the chemistry of polonium, and (c) the analysis of accident sequences in order to assess their consequences.

The work for the first area can be started immediately and should be performed with a high priority and with a very wide scope, because it must be ensured that the operation of a loop with such coolants can be licensed. Beside the chemical reactions of the different species the evaporation of e.g. polonium from liquid Pb-17Li into different atmospheres must be investigated. A phase diagram for such three component systems is not available but will be needed, if release rates should be calculated for the licensing procedure. Because of the high volatility and toxicity of polonium investigations of the chemistry of polonium will be necessary. To give an example, the question if polonium is deposited on the steel structure or gets to the gas loops in form of aerosols is of high importance for the release mechanism in the case of maintenance. For possible cleaning processes, see also section 4.5.2 and 5.4.2. To reduce the quantity of polonium produced in the Pb-17Li investigations being performed at JRC Ispra aiming at the on-line separation of bismuth are of high interest.

More detailed analysis of accident sequences requires a fixed design of the test module and its environment in the NET/ITER machine. Only if these data are available additional effort is meaningful. Areas of special interest are the investigation of a loss of coolant accident inside and outside of the vacuum vessel with possible thermal and radiological consequences, and a loss of site power.

As mentioned in section 3.4 operational safety and reliability need special attention. Hence prior to tests in NET/ITER it is recommended to test the module and its loop system out of pile under real thermal conditions and continuous operation. The final design should be based on a reliability assessment taking credit from experimental data from liquid metal fission reactor technology and fusion component failure rate data, e.g. the corresponding US failure rate screening data [1].

KfK tasks as described in the Task Action sheet of the European Fusion Technology Programme for 1992 - 1994 are especially the following ones:

- to investigate the safety implications of chemical reactions between Pb-17Li and different reactants,
- to analyse possible accident sequences and their consequences,
- to assess the reliability of both the blanket segment and the loop system.

References to section 5.6:

[1] L.C. Cadwallader and S.J. Piet, "1989 Failure Rate Screening Data for Fusion Reliability and Risk Analysis", EGG-FSP-8709, Sept. 1989

5.7 Electromagnetic forces

The electromagnetic forces occuring in the blanket will be determined by a 3D eddy current code (i.e. CARIDDI). Mass and stiffness matrices characterizing the structural response of the blanket will be computed by a finite element code (i.e. ADINA) which, however, has to take into account the fluid structure interaction between the liquid coolant and the flexible flow channel walls of the blanket. For solution usual methods can be employed.

Recent investigations have shown that in structural dynamics the feedback of the structural deformations and the corresponding fluid motion on the electromagnetic forces can be represented by an additional damping matrix. A procedure to obtain this damping matrix using results from the CARIDDI code has been developed.

Electromagnetic experiments with a flexible plate carried out by Bialek and Weissenburger [1] showed, that the damping caused by the structural feedback was able to reduce the resulting stresses by a factor of 5. Such effects can be obtained only if the mechanical oscillation period has the same order of magnitude as the electromagnetic decay time and if the same is true for the elastic and electromagnetic forces. Usually this means that the mechanical system must be relatively flexible.

For stiff structures like the blankets damping was found to be of minor importance to the maximum stresses. Therefore, first calculations for the water cooled blanket and for the more complex self-cooled liquid metal blanket will be performed without consideration of the damping effect. The results of these elastic

267

calculations will be used for an evaluation of the maximum stresses occuring in the blanket by a plasma disruption.

As a next step the influence of the interaction with the fluid will be considered. If the fluid deflections turn out to be considerably larger than the structural deflections damping may reduce the maximum stresses remarkably. Therefore, later on, damping will be included, too.

References to section 5.7:

[1]   J.M. Bialek, D.W. Weissenburger: The coupling of mechanical dynamics and induced currents in a cantilever beam. Computational Electromagnetics; Elsevier Science Publishers B.V. (North Holland), IMACS, 1986; pp. 193-203.

6.   TEST PROGRAM IN NET/ITER

6.1   Test strategy

Test in NET/ITER are the last step in the development program of breeding blankets prior to the use in a DEMO power reactor. Keeping this goal in mind it is desirable to perform an extensive blanket test program in NET/ITER covering both multiple test modules and long term performance tests of some modules or better segments. However, testing space as well as total fluence obtainable in NET/ITER are very limited. At the moment, there are up to four blanket test ports and a total burn time of NET/ITER somewhere between 2000 and 10000 h anticipated. These are the boundary conditions for the test strategy to be developed.

The following approach is proposed [1].

Make extensive use of all testing possibilities outside of NET/ITER. Nearly all separate effects relevant to a blanket design can and should be investigated in test loops (out-of-pile as well as in fission reactors) prior to tests in NET/ITER. This is especially true for complicated and highly instrumented MHD tests and long time corrosion tests. End of life tests and even long time performance tests are, in any case, not possible in NET/ITER due to the relatively low fluence.

Perform as many tests as possible during the physics phase. This phase is especially suited for MHD tests and MHD-Thermalhydraulics tests since these tests do not require long, repeated burns and, for some of the tests, no neutrons at all. What is needed is the real geometry and the real distribution of the magnetic field. This means that most of the tests can be performed even without a burning plasma. An important goal of these tests is the measurement of pressure drops and flow distribution through the blanket. For availability reasons, all these tests will be performed with modules which are not exposed to the plasma. It is proposed that electric heaters be installed at the front surface of the modules in order to simulate plasma surface heating. Besides the MHD tests, it is intended to check out the modules including instrumentation as well as ancillary equipment and to obtain some information about the mechanical behavior of the modules and the testing equipment during the technology phase.

Divide the test port into parts in order to conduct parallel tests during the first years of the technology phase. The allocation of submodules is shown in Fig. 6.1-1. It is proposed to test quartersized modules during the first couple of years of the technology phase. Each submodule needs its own ancillary loop system, and all ancil-

269

lary systems will be installed in parallel. It is intended that each system will be designed for the full capacity of a module (5 MW thermal power and about 0.8 g of tritium per full power day) and operate during the submodule testing at partial capacity. In the next step the size of the submodules is increased and they will be exposed to the plasma for the first time. Again short time tests will be performed, and the submodules will be exchanged at least once.

Perform sequential tests with full size modules during the second half of the technology phase. These tests are not high fluence tests, but they should allow the selection of one or two leading designs that have the potential to meet the requirements of the DEMO reactor.

Test segments of one or two blanket designs towards the end of the technology phase. These tests are highly recommended to test the integrated performance of the blankets that could be installed in a DEMO reactor.

6.2   Technical issues and objectives of tests

The technical issues of self-cooled liquid metal blanket concepts are:

- Tritium self-sufficiency
- MHD effects
- Heat transfer
- Materials interactions (e.g. corrosion)
- Structural response in a fusion environment
- Tritium recovery and control
- Components and system interactions.

For liquid metal cooled designs, the issue which tends to dominate most considerations is MHD. Potentially, MHD effects could influence fluid flow, heat transfer, corrosion rates, and stresses (pressure) in the blankets. Therefore, this issue has an important role in the test program. Other issues, although important, do not play as crucial a role in the NET/ITER program. Individual issues which can be studied without a fusion environment, could be investigated separately, outside of NET/ITER. On the other hand, an in-depth investigation of the structural response would require a neutron fluence much higher than the one achievable in NET/ITER. These considerations indicate that the objectives of the test program have to be chosen carefully in order to eliminate tests which can either be per-

formed earlier, better, and cheaper in a non-fusion environment or would produce results of questionable value due to the low fluence in NET/ITER.

Keeping these limitation in mind, the tests cover the following range of objectives

- Tests of the predictive capabilities of engineering codes
- Tests of the engineering performance of particular concepts
- Tests of the engineering reliability of the concepts.

The specific tests are related to the key issues identified earlier. The tests to be conducted in NET/ITER are MHD tests, combined MHD/thermalhydraulic tests, short term and extended term performance tests, and post-test examinations.

MHD tests

Liquid metal flowing in high magnetic fields can result in high pressure drops, high blanket operating pressures, and coolant flow profile modifications which can affect heat and mass transfer in the coolant. Resolution of MHD-related issues requires investigation in two areas: 1) MHD pressure drop, heat transfer, and fluid flow, and 2) electrical insulators for flowing liquid metal systems. NET/ITER provides both the correct magnetic field configuration and blanket test volume needed for testing MHD effects. Since no neutron flux is needed to conduct these tests and the test times needed to achieve equilibrium flow conditions are short (about 100 s), these tests can be conducted in the physics phase of NET/ITER operation. The MHD tests would be aimed at confirming the predictive capability of MHD models and codes.

MHD/Thermalhydraulic tests

Changes in the coolant flow profiles will alter the heat transfer within the blanket. In order to optimize the performance of the blanket, heat transfer within the coolant needs to be thoroughly understood. NET/ITER will be the first facility where both the coolant flow and bulk heating of the blanket will be properly simulated. However, during the physics phase it will not be possible to expose the test module to the plasma. Therefore, meaningful heat transfer tests during this phase require a simulation of the surface heat flux by installing an electrical heating device at the front surface of the test module. The temperature profiles within the blanket will be measured for a variety of mass flow rates, and these results will be

compared with model predictions. The test times involved are relatively short (100's of seconds), and the neutron fluence will be low. Therefore, these tests will be conducted during the last two years of the physics phase.

Short term performance tests

Following confirmation of the predictive capability of MHD and MHD/thermal-hydraulic effects, the high temperature performance characteristics of liquid metal blankets would be explored. These tests represent the first completely integrated tests to be performed. Items to be measured are coolant temperature increase, overall tritium breeding and release, overall pressure drops, coolant impurity levels, etc. In addition the short-term thermomechanical response (stresses, strains) would be determined. These tests would largely cover the engineering performance phase of testing.

Extended performence tests

These tests would help determine the engineering reliability and provide a data base for extrapolation of blanket life time performance. The tests would emphasize the long-term thermomechanical response of the blanket structures. They would be conducted over a period of 1-2 years, after which the module would be removed for destructive examination in the hot-cell. Segment tests could then be performed for 1-2 years to test performance with the actual geometric constraints (including manifolding structural constraints) anticipated for the DEMO.

Post test examinations

Additional information about the performance of the blanket modules can be obtained through post test examinations. There are numerous non-destructive and destructive tests which can be used to characterize the module structure. The information from post test examinations, combined with the operating history of the module, can be used to interpret the thermomechanical response. This approach is similar to that used in fission reactors to study the behavior of fuel pins. The two keys to being able to correctly interpret the results are first that the test assembly must be very well characterized prior to irradiation, and second, that the power history of the module must be well documented. Information gaps in either or will severely limit the utility of the data gathered during the post test examinations.

6.3 Impact of reduced NET/ITER operating time on the blanket test program

There is a strong interaction between the design of NET/ITER and the maximum operating time of the machine. The important issue is the tritium supply. A limited amount of tritium can be obtained from external sources allowing a total burn time of approximately 2000 to 3000 hours. Longer operating times require tritium breeding blankets in NET/ITER. So called "driver blankets" not only add to the complexity and costs of the machine but also can reduce the reliability of the operation because integrated testing of those blankets require the operation of NET/ITER. To avoid these problems, it is highly desireable to limit the total burn time required for blanket tests to a value below 3000 hours. Estimates have indicated, that such a limited time would allow for a minimum test programme only, excluding all extended performance tests. Only with the help of extensive material irradiations programmes and highly sophisticated computer codes an extrapolation to DEMO can be made.

Mandatory for a meaningful blanket test programme is a relatively high availability of the machine because the average time required for a useful single test is in the order of a few days. A mean time between two unscheduled outages lower than this value would require too many attempts for a successful single test, "wasting" too much tritium. The conclusions of these considerations are:

- Blanket tests require a relatively high reliability of NET/ITER.
- Without driver blankets no extended performance tests are possible.
- Reduced operating time of NET/ITER places a high burden on computer codes necessary for the extrapolation to DEMO-conditions.

References to section 6:

[1]   M. Tillak et al., ITER Test Program, ITER Document Series, No. 24, International Atomic Energy Agency, Vienna 1990.

4 sub modules

2 sub modules

full sized module

3,4 m

1 m

no exposure
to the plasma

modules exposed
to the plasma

module exposed
to the plasma
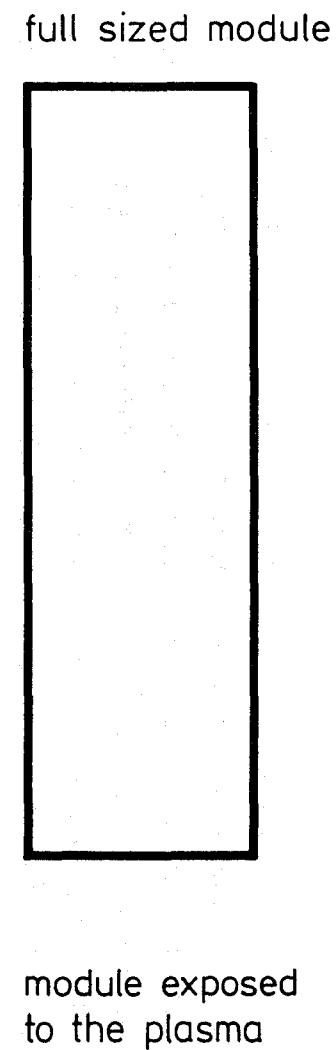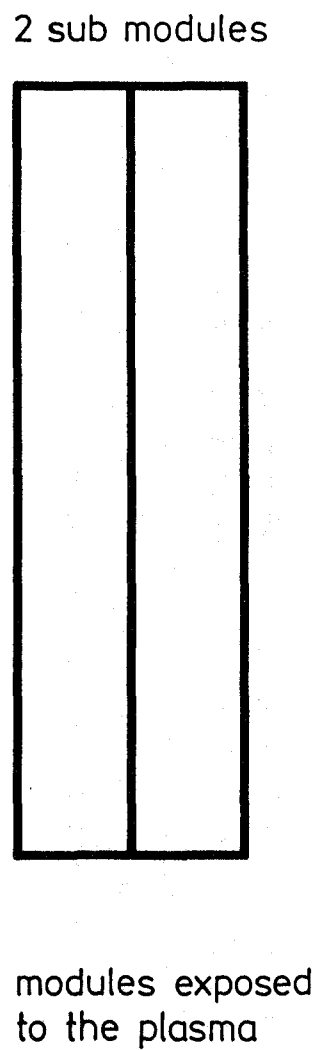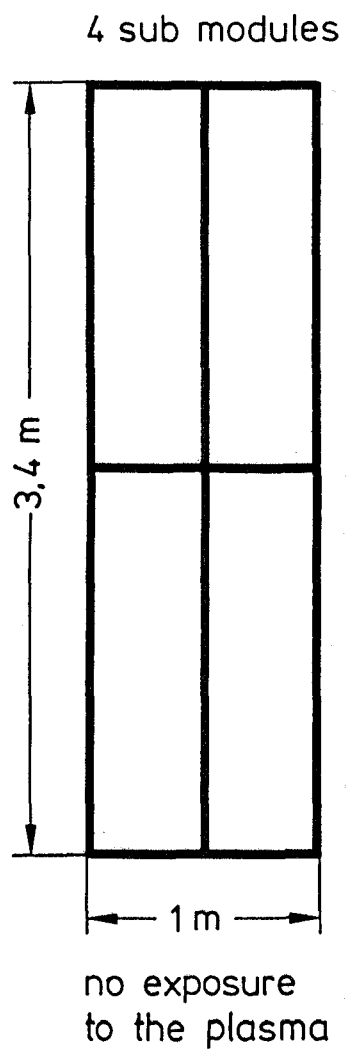
Fig. 6.1-1   Partitioning of the test port